The interaction of β-amyloid model peptides with lipid membranes

Inauguraldissertation

zur

Erlangung der Würde eines Doktors der Philosophie

vorgelegt der

Philosophischen-Naturwissenschaftlichen Fakultät

der Universität Basel

von

Caroline Loew

aus

Mulhouse, Frankreich

Basel, 2011

Genehmigt von der Philosophischen-Naturwissenschaftlichen Fakultät auf Antrag von

Prof. Dr Joachim Seelig

Prof. Dr Dagmar Klostermeier

Basel, den 29.03.2011

Prof. Dr Martin Spiess

(Dekan)

Table of content

I. Introduction

1. Aggregation and disease

Protein or peptide misfolding can be at the roots of various diseases by inducing reduced activity of the involved proteins or peptides. These diseases are referred to as protein misfolding diseases[1]. In most cases, protein or peptide misfolding converts the peptide or protein into an insoluble aggregate usually described as amyloid fibrils or plaques if accumulated outside of the cell[1], or as intracellular inclusions if the accumulation occurs in the intracellular medium[2].

a) A broad range of diseases concerned

The following examples illustrate the various disease areas affected by aggregation but they also illustrate the lack of knowledge with regard to aggregation. It is usually not known whether fibril formation causes the disease or is one of its consequences. In neurosciences, α-synuclein, involved in both Parkinson's disease and dementia with Lewy bodies, is the main component of Lewy bodies, forming insoluble protein-fibrils. These and the loss of dopaminergic neurons are hallmarks of the disease[3], but no direct correlation between the physiological characteristics and the disease symptoms or development could be made yet[4,5]. In the same disease area, Huntington's disease is hereditary and is characterized by aggregated huntingtin expanded with polyglutamine that forms intranuclear and cytoplasmic inclusions[6,7]. The inclusions themselves do not seem to be the cause of the toxicity and the mechanism of polyglutamine expansion remains unclear[8]. In the metabolic diseases area, the insolubilization of human islet amyloid polypeptide (IAPP) progressively forms pancreatic islet amyloids, toxic to the pancreatic β-cells that produce IAPP together with insulin[9]. The cause and mechanism that lead to IAPP aggregation and

hence type II diabetes are not solved yet. However recent findings suggested that IAPP fibril formation is enhanced by dimerization of the protein as α-helices. This discovery induced the search for an aggregation blocker in insulin, that is, a molecule which can interact with the dimerization interfaces[10]. In ophtalmology, α-cristallins helps preventing aggregation of eye lens proteins and thus reduces the scattering on the lens that can in turn interfere with vision[11]. Extensive oxidation of cysteine and methionine residues[12] in α-cristallins sequence is a characteristic of aggregated eye lens proteins; it prevents the protein to play its role as chaperon and could lead to cataract by increased protein aggregation[13,14]. However it is not proven yet whether the aggregates are the cause or the consequence of the disease[14].

b) Alzheimer's disease (AD)

Alzheimer's disease (AD) like other neurodegenerative diseases is characterized, among others, by the formation of plaques, that is, the accumulation of peptides on the neurons[1]. The mechanism of the amyloid peptide toxicity remains unexplained. Currently the most commonly accepted hypothesis is the amyloid cascade hypothesis. It stipulates that the formation of βAP under the action of the secretases is at the origin of AD[15,16]. In parallel, the tau hypothesis is also discussed according to which hyperphosphorylation of the tau protein could be the cause of the disease[17]. But many other hypothesis have appeared over the years, emphasizing alternatively the calcium level[18], metal ions[19], or oxidative stress[20] as important in the development of AD.

The plaques detected in the brain of AD diseased patients are mainly composed by the amyloid peptide βAP, a 39-42 amino-acid peptide[21] (Figure 1).

Figure 1: *One-letter code amino-acid sequence of βAP(1-40) and (1-42). The negatively- and positively-charged residues under physiological conditions are highlighted in pink and orange respectively, while the green amino acids show the intra-membrane part of the peptide.*

The much larger amyloid peptide precursor (APP) can be cleaved by three different secretases, the α-, β- and γ-secretase. βAP(1-40) to βAP(1-42) originate from

the successive cleavage of the amyloid peptide precursor (APP) by the β- and γ-secretase[22-24]. The amyloid β peptides βAP(1-40) and βAP(1-42) have a very low solubility, are highly hydrophobic and neurotoxic[25-27]. The production of βAP(1-40) and βAP(1-42) by the β and γ-secretases is known as the amyloidogenic pathway (Figure 2). In contrast, the cleavage of APP by the α-secretase produces a soluble peptide[28]. This second pathway is named non-amyloidogenic. Figure 2 represents the amyloidogenic and non-amyloidogenic pathways. The accumulation of insoluble βAP(1-40) or βAP(1-42) on the membrane surface leads to aggregation of these molecules, first as small oligomers and eventually as major plaques[29].

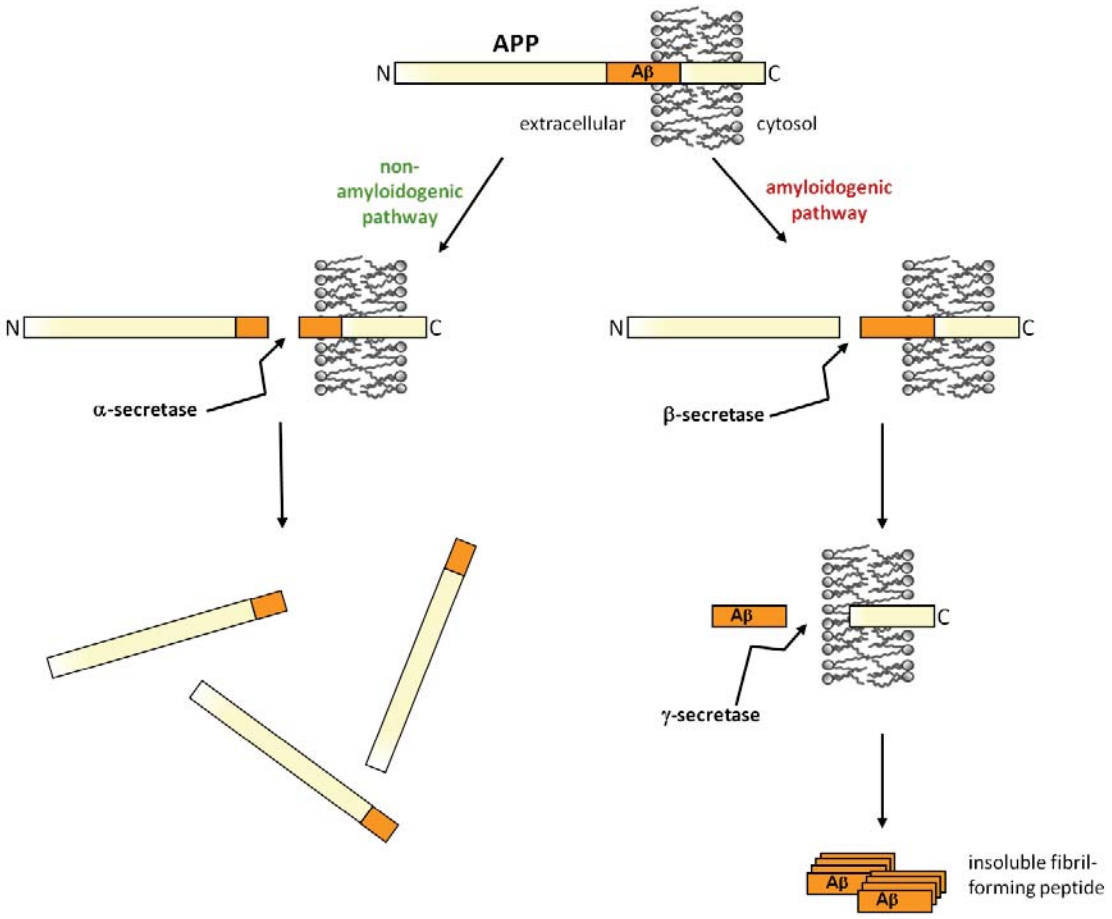

Figure 2: *Schematic representation of the amyloidogenic and non-amyloidogenic pathways of APP processed by the α-, β- and γ-secretases[22].*

c) The seeding mechanism in fibril formation

The reason of amyloid β peptide aggregation is still unclear. Nevertheless a hypothesis describing the various stages of aggregation in a nuclei-seeded manner was

formulated about a decade ago[30]. The nucleation-dependent mechanism involves three steps, namely a slow nucleation step with lag phase, a faster protofibril formation containing a finite number of nuclei, and a thermodynamically favorable fast fibril elongation phase. Finally an equilibrium phase is reached where the soluble peptides coexist with the aggregated species[31]. Nucleus formation is considered to be the kinetic barrier of fibrillogenesis[30]. The period needed for nucleus formation is called lag-phase. It can be considerably shortened or even be nonexistent with the addition of heterogeneous seeds, such as lipids[32] or metal ions[33], or by the presence of a catalytic surface[34]. The presence of the nucleus facilitates further addition of monomers or intermediates that will elongate the nucleus to progressively form protofibrils and then fibrils[30,35,36]. The seeding model is suitable to explain the kinetics of fibril formation, the length of the lag phase, the rate of elongation and the distinct concentration dependence of the aggregation measured by fluorescence techniques[37-39].

The seeding model evolved over the years with the parallel discovery of new types of intermediates and of new rate-influencing factors. More recently, modifications include a rate-limiting step modulated by the peptide concentration[40], a second nucleation step overcoming the nuclei formation when fibrils are formed in sufficient quantities[41], or various intermediate species such as oligomers and protofibrils[31].

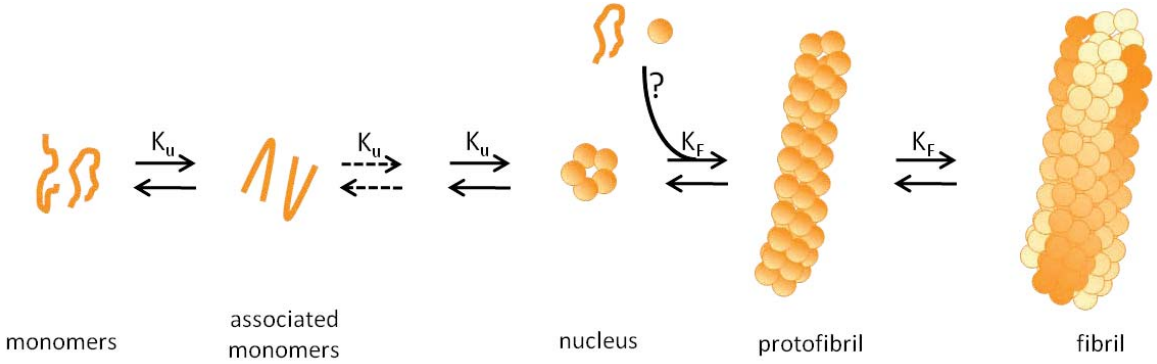

***Figure 3**: Schematic representation of the nuclei-dependent fibrillization. The monomers associate and undergo conformational change to first form aggregates of monomers and then a nucleus after a series of unfavorable equilibrium. Once the nucleus is formed, the quick addition of monomers or aggregates lead to protofibril and then fibril formation[37,40,42].*

Other models exist that try to describe the fibrillization, considering other steps as rate-limiting[43], but the seeding model is able to explain most of the published experimental fibrillogenesis data[44]. It can be represented with the scheme in Figure 3.

2. Toxicity and conformation

a) Origins of toxicity

For a long time, fibrils were thought to be responsible for the observed neurodegeneration, not only for AD, but also for other neurodegenerative diseases[45,46]. More recently the non-fibrillar oligomers of amyloid β peptide, βAP[47,48], α-synuclein, or IAPP were found to be more toxic to neurons[49-52]. Deshpande *et al.* showed that oligomers of βAP bind to the synaptic contact and induce neuronal death, whereas amyloid fibrils need a higher concentration and a longer time span to produce the same toxicity level[29]. The authors also observed various species in an amyloid peptide solution: βAP derived diffusible ligands (ADDLs, from trimer to higher molecular weight complex), βAP oligomers (oligomers composed of 15-20 monomers), Aβ*56 (dodecameric βAP oligomers of 56 kDa)[53], protofibrils (strings of oligomers) and fibrillar βAP. Each of these species has its own specific toxicity on human corticon neurons. Among the oligomeric species, different toxicities can be observed as very small oligomers of mean particle size $z \approx 1\text{-}2$ nm show increased binding to phospholipid vesicles and increased toxicity to neurons compared to those with $z \approx 4\text{-}5$ nm. Monomers and fibrils did not even bind to the membrane[54]. The toxicity of βAP seems to be correlated with the size of the oligomers: dimers are ~ 3 times more toxic and tetramers ~ 13 times more toxic[55] than monomers. In parallel, Aβ oligomers and ADDLs bind with high affinity to neuron cells, whereas much higher concentrations and longer incubation times were needed for Aβ fibrils to lead to the same neurotoxicity[29].

b) Toxicity and structure

Peptide structure appears to be of primary importance. It is directly linked to peptide oligomerization and, in turn, to its toxicity. As was explained above, the

protofibrils and fibrils are not toxic to the cells but rather the small oligomers. Each species has a specific secondary structure: fibrils are mainly composed of cross β-sheets. ADDLs, in contrast, are mostly random-coil[29].

Therefore there could be a link between peptide secondary structure, toxicity and binding to the cell membrane. This hypothesis was expressed already in 1994 by Simmons *et al.*, who could show that β-sheet structure was linked to higher toxicity than random-coil[56]. The recent work of Shtainfeld *et al.* on human calcinotin (hCT), a fibril forming hormone peptide, goes into the same direction[57]. Various mutations in a hCT pentapeptide provided evidence for a correlation between the kinetics of fibril formation, lipid binding and amino-acid sequence. These experiments proved the importance of phenylalanine and methionine residues in lipid-induced fibrillization: a mutation of any of these amino-acids led to a change in the β-sheet organization from parallel to anti-parallel arrangements. However the mechanism of the peptide toxicity is not understood yet.

3. Aggregation model peptides

Research on amyloid peptide aggregation is performed on wild-type peptides but also on models that allow isolation or induction of a specific property of the full-length peptide and hence facilitate the study. Shorter sequences are often used as representations of the full-length peptide behavior and can allow a faster understanding of the studied phenomenon. This is the case, for example, for the human prion protein (PrP). PrP adopts a fibrillar structure whereas a model peptide, containing only 20 amino-acids of the full-length protein, forms stable oligomers. Although similar peptide packing was observed, long-range disorder and increased mobility distinguished the oligomers from the fibrils[52].

a) Designed model peptides

In the past few years, newly-designed peptides were extensively studied as aggregation models. These peptides are able to aggregate or undergo structural changes depending on similar parameters found relevant in fibril formation, such as

pH, salt concentration or the presence of metal ions. Pagel *et al.* conceived a peptide that could adopt either an α-helical or a β-sheet secondary structure[58], similarly to amyloid-forming peptides, as a function of the presence of metal ions[59]. Similar peptides were designed by other groups to examine, for example, the interaction of amyloid peptides with hydrophobic surfaces[60]. The study of a modified amyloid peptide fragment proved that fibrils orient parallel to the membrane surface[61]. The use of a 12-mer peptide, derived from the full-length amyloid β peptide, enabled Makin and coworkers to perform X-rays on the peptide fibers and therefore define characteristics of antiparallel β-sheets in a cross-β arrangement[62]. As a last example the KIGAKI peptide, able to rapidly form β-sheets[63], helped determining the enthalpy of β-sheet formation[64].

b) Amyloid fragments

Shorter sequences of the amyloid peptide are often used as models, as they are sometimes easier to handle than the full-length amyloid peptide. The amyloidogenic βAP(12-28)[65] has the advantage of containing amino-acids supposed to be essential to aggregation[66,67], although its ability to form long fibrils is not certain. βAP(16-22) is one of the shorter fragments that is nevertheless able to form fibrils and is often used as β-amyloid model. Among its 7 residues, it contains the hydrophobic core suspected to be essential for the fibrillization of the full-length peptide[68]. Other fragments comprising various amino-acids of the whole sequence were studied, such as βAP(10-35), βAP(1-28)[69], βAP(10-43), βAP(10-23)[70], βAP(16-35)[71] and many others[72]. All of these fragments possess the ability to form either aggregates or fibrils under specific conditions but usually show a better solubility in aqueous buffers than βAP(1-40) or βAP(1-42).

c) Specific properties of βAP(25-35)

The fragment used throughout this work is βAP(25-35). It contains an intramembrane part as well as an extracellular part. The fragment (25-35) is known to possess many of the characteristics of the full-length amyloid peptide. It has a highly hydrophobic amino-acid sequence, is prone to aggregation and, in contrast to most of

the other fragments studied, shows neurotoxic and neurotrophic activities[73]. Cytotoxicity of the peptide monomers could be proven with its effect on rat mitochondria[74]. This peptide is an attractive model to study not only the biophysical interaction of the amyloid peptide with the lipid membrane but also the physiological effect of amyloid peptide on neuron cells[75-77].

However, the high propensity to quickly form inhomogeneous aggregates in solution is an obstacle for the biophysical description of peptide aggregation, especially at neutral pH. An added difficulty in the study of βAP(25-35) is the absence of a chromophore. This makes the determination of the peptide content difficult. For biophysical studies the precise knowledge of the peptide content is necessary. Once a suitable amyloid model peptide is defined, the membrane behavior itself needs to be understood.

4. Lipids, membranes, and their role in protein aggregation

Although lipid properties are well studied (from the thermodynamics of micellisation[78], to lipid chains structural characterization[79] or membrane curvature[80]), some features of well-known phenomena such as gel-to-liquid-crystal phase transition[81] remain sometimes unexplained. Membrane structure and other properties are part of this study.

a) The biological role of cellular membranes

Biological membranes separate intracellular from extracellular space, but have also additional functional properties. They maintain a constant membrane potential, enable transmembrane ion transport, or allow membrane protein binding. The membrane prevents polar molecules (amino acids, carbohydrates, proteins) to diffuse through the membrane, whereas hydrophobic molecules and water can passively diffuse from the cytosol to the extracellular domain.

Biological membranes are complex and highly structured macromolecular systems composed of a large number of lipid species and proteins. They are formed by a bilayer of amphiphatic phospholipids (glycolipids, steroids and phospholipids) and

contain diverse carbohydrates and proteins. The latter are responsible for the various activities of the cellular membrane. In some cases, the presence of lipids is an absolute prerequisite for the correct functioning of a protein. For example, the family of the protein kinases C (PKC) that play a major role in apoptosis, differentiation, mediation, needs phospholipid (usually phosphatidylserine) in order to phosphorylate diverse proteins[82].

b) Lipid bilayers as a model for the cellular membrane

Phospholipid bilayers have attracted a great deal of interest because of their central role in cellular function and their potential as model bilayer systems in chemical and biological sensing applications. Phospholipids self-assemble spontaneously to form a bilayer structure with their hydrophobic tails directed toward the center, and their headgroups exposed to the aqueous phase[83].

The ability of lipids to self-assemble into fluid bilayer structures is consistent with two major roles in membranes: establishing a permeability barrier and providing a matrix for membrane proteins. Individual lipid components may play specific roles in establishing appropriate permeability characteristics, satisfying insertion and packing requirements for integral proteins, or facilitating the association of peripheral proteins. An intact permeability barrier for ions such as Na^+, K^+, and H^+, is vital for establishing the electrochemical gradients which give rise to a membrane potential and drive other membrane-mediated transport processes. In addition, the lipids surround the membrane protein to seal it into the bilayer so that non-specific leakage is prevented. At the same time they provide an environment necessary for protein activity[84].

c) The importance of anionic lipids

Most lipids present in biological membranes are zwitterionic or uncharged, but the less abundant anionic lipids are of great importance. Indeed a minimal amount of anionic lipids is required for cell growth and various other membrane functions. Van der Goot *et al.* showed the importance of negatively charged phospholipids in the channel formation of colicin A[85]. This pore-forming bacterial toxin kills *Escherichia coli* cells after binding to the specific receptors located in the outer membrane followed by translocation through the outer membrane and the periplasm. *In vitro* studies have

shown that negatively charged phospholipids are an absolute requirement for the channel formation of colicin A[85]. Dowhan and Xia demonstrated that anionic phospholipids are essential for the normal initiation of DNA replication by the DnaA protein[86]. The latter binds to the membrane via interaction with anionic phospholipids[87]. Negatively-charged lipids also play a role in the conversion of the inactive, ADP-bound DnaA protein to the active ATP bound form *in vitro*. It results in regeneration of the initiation activity of the DnaA protein[88].

d) Role of the lipid membrane in amyloid formation

In the case of fibrillogenesis, the role of membranes is controversial. The lipid membrane is described by some groups as a catalyst[32] for fibril formation, or as an obstacle to fibrillization by others[38]. Cell apoptosis could be due to ion channel formation[89] or amyloid formation on the membrane surface disrupting the membrane and leading to lipid uptake involved in amyloid peptides cytotoxicity[90]. Amyloid formation is postulated to either decrease[91] or increase[92] membrane fluidity.

βAP(1-40) was shown to interact with negatively-charged membranes but not with uncharged surfaces[93]. The peptide undergoes a random-coil to β-sheet lipid-dependent conformational transition[93] with the peptide adsorbed to the membrane surface[94].

Structural changes of the amyloid peptide are correlated with fibril formation and contribute to nucleation and aggregate stabilization. A careful thermodynamic study could provide information concerning the parameters controlling the system stability and peptide association. Previous biophysical studies[93-96] established two possible ways of interaction between βAP and the lipid membrane: either the peptide penetrates into the hydrophobic part of the lipid bilayer, or it aggregates at the surface of the bilayer. Following the structural changes of the lipid bilayer could help in understanding the aggregation mechanism and the peptide influence on the cell membrane. The gel-to-liquid crystal transition of the lipid bilayer is also known to influence protein activity[97,98] and is a rather well-described phenomenon[99,100].

5. References

(1) Allsop, D.; Landon, M.; Kidd, M. *Brain Res* **1983**, *259*, 348.
(2) Lundmark, K.; Westermark, G. T.; Nystrom, S.; Murphy, C. L.; Solomon, A.; Westermark, P. *Proc Natl Acad Sci U S A* **2002**, *99*, 6979.
(3) Schulz-Schaeffer, W. J. *Acta Neuropathol* **2010**, *120*, 131.
(4) Weisman, D.; Cho, M.; Taylor, C.; Adame, A.; Thal, L. J.; Hansen, L. A. *Neurology* **2007**, *69*, 356.
(5) Gomez-Tortosa, E.; Irizarry, M. C.; Gomez-Isla, T.; Hyman, B. T. *Ann N Y Acad Sci* **2000**, *920*, 9.
(6) Ross, C. A. *Neuron* **1995**, *15*, 493.
(7) Paulson, H. L.; Fischbeck, K. H. *Annu Rev Neurosci* **1996**, *19*, 79.
(8) Klement, I. A.; Skinner, P. J.; Kaytor, M. D.; Yi, H.; Hersch, S. M.; Clark, H. B.; Zoghbi, H. Y.; Orr, H. T. *Cell* **1998**, *95*, 41.
(9) Kayed, R.; Bernhagen, J.; Greenfield, N.; Sweimeh, K.; Brunner, H.; Voelter, W.; Kapurniotu, A. *J Mol Biol* **1999**, *287*, 781.
(10) Wiltzius, J. J.; Sievers, S. A.; Sawaya, M. R.; Eisenberg, D. *Protein Sci* **2009**, *18*, 1521.
(11) Horwitz, J. *Exp Eye Res* **2003**, *76*, 145.
(12) Truscott, R. J.; Augusteyn, R. C. *Biochim Biophys Acta* **1977**, *492*, 43.
(13) Pang, M.; Su, J. T.; Feng, S.; Tang, Z. W.; Gu, F.; Zhang, M.; Ma, X.; Yan, Y. B. *Biochim Biophys Acta* **2010**, *1804*, 948.
(14) Moreau, K. L.; King, J. *J Biol Chem* **2009**, *284*, 33285.
(15) Hardy, J. A.; Higgins, G. A. *Science* **1992**, *256*, 184.
(16) Hardy, J.; Selkoe, D. J. *Science* **2002**, *297*, 353.
(17) Mandelkow, E. M.; Mandelkow, E. *Trends Cell Biol* **1998**, *8*, 425.
(18) O'Day, D. H.; Myre, M. A. *Biochem Biophys Res Commun* **2004**, *320*, 1051.
(19) Bush, A. I.; Tanzi, R. E. *Neurotherapeutics* **2008**, *5*, 421.
(20) Pratico, D. *Trends Pharmacol Sci* **2008**, *29*, 609.
(21) Masters, C. L.; Simms, G.; Weinman, N. A.; Multhaup, G.; McDonald, B. L.; Beyreuther, K. *Proc Natl Acad Sci U S A* **1985**, *82*, 4245.
(22) Mills, J.; Reiner, P. B. *J Neurochem* **1999**, *72*, 443.
(23) Hussain, I.; Powell, D.; Howlett, D. R.; Tew, D. G.; Meek, T. D.; Chapman, C.; Gloger, I. S.; Murphy, K. E.; Southan, C. D.; Ryan, D. M.; Smith, T. S.; Simmons, D. L.; Walsh, F. S.; Dingwall, C.; Christie, G. *Mol Cell Neurosci* **1999**, *14*, 419.
(24) Kang, J.; Lemaire, H. G.; Unterbeck, A.; Salbaum, J. M.; Masters, C. L.; Grzeschik, K. H.; Multhaup, G.; Beyreuther, K.; Muller-Hill, B. *Nature* **1987**, *325*, 733.
(25) Walsh, D. M.; Klyubin, I.; Fadeeva, J. V.; Cullen, W. K.; Anwyl, R.; Wolfe, M. S.; Rowan, M. J.; Selkoe, D. J. *Nature* **2002**, *416*, 535.
(26) Koh, J. Y.; Yang, L. L.; Cotman, C. W. *Brain Res* **1990**, *533*, 315.
(27) Butterfield, D. A.; Drake, J.; Pocernich, C.; Castegna, A. *Trends Mol Med* **2001**, *7*, 548.
(28) Jager, S.; Leuchtenberger, S.; Martin, A.; Czirr, E.; Wesselowski, J.; Dieckmann, M.; Waldron, E.; Korth, C.; Koo, E. H.; Heneka, M.; Weggen, S.; Pietrzik, C. U. *J Neurochem* **2009**, *111*, 1369.
(29) Deshpande, A.; Mina, E.; Glabe, C.; Busciglio, J. *J Neurosci* **2006**, *26*, 6011.
(30) Come, J. H.; Fraser, P. E.; Lansbury, P. T., Jr. *Proc Natl Acad Sci U S A* **1993**, *90*, 5959.

(31) Roychaudhuri, R.; Yang, M.; Hoshi, M. M.; Teplow, D. B. *J Biol Chem* **2009**, *284*, 4749.
(32) Gorbenko, G. P.; Kinnunen, P. K. *Chemistry and physics of lipids* **2005**, *141*, 72.
(33) Miller, Y.; Ma, B.; Nussinov, R. *Proc Natl Acad Sci U S A* **2010**, *107*, 9490.
(34) Ruschak, A. M.; Miranker, A. D. *Proc Natl Acad Sci U S A* **2007**, *104*, 12341.
(35) Hofrichter, J.; Ross, P. D.; Eaton, W. A. *Proc Natl Acad Sci U S A* **1974**, *71*, 4864.
(36) Ferrone, F. A.; Hofrichter, J.; Sunshine, H. R.; Eaton, W. A. *Biophys J* **1980**, *32*, 361.
(37) Harper, J. D.; Lansbury, P. T., Jr. *Annu Rev Biochem* **1997**, *66*, 385.
(38) Hellstrand, E.; Sparr, E.; Linse, S. *Biophys J* **2010**, *98*, 2206.
(39) Lee, C. C.; Sun, Y.; Huang, H. W. *Biophys J* **2010**, *98*, 2236.
(40) Kelly, J. W. *Nat Struct Biol* **2000**, *7*, 824.
(41) Padrick, S. B.; Miranker, A. D. *Biochemistry* **2002**, *41*, 4694.
(42) Lomakin, A.; Chung, D. S.; Benedek, G. B.; Kirschner, D. A.; Teplow, D. B. *Proc Natl Acad Sci U S A* **1996**, *93*, 1125.
(43) Ecroyd, H.; Koudelka, T.; Thorn, D. C.; Williams, D. M.; Devlin, G.; Hoffmann, P.; Carver, J. A. *J Biol Chem* **2008**, *283*, 9012.
(44) Jarrett, J. T.; Lansbury, P. T., Jr. *Biochemistry* **1992**, *31*, 12345.
(45) LeVine, H., 3rd; Scholten, J. D. *Methods Enzymol* **1999**, *309*, 467.
(46) Lorenzo, A.; Yankner, B. A. *Proc Natl Acad Sci U S A* **1994**, *91*, 12243.
(47) El-Agnaf, O. M.; Mahil, D. S.; Patel, B. P.; Austen, B. M. *Biochem Biophys Res Commun* **2000**, *273*, 1003.
(48) Lambert, M. P.; Barlow, A. K.; Chromy, B. A.; Edwards, C.; Freed, R.; Liosatos, M.; Morgan, T. E.; Rozovsky, I.; Trommer, B.; Viola, K. L.; Wals, P.; Zhang, C.; Finch, C. E.; Krafft, G. A.; Klein, W. L. *Proc Natl Acad Sci U S A* **1998**, *95*, 6448.
(49) Bucciantini, M.; Giannoni, E.; Chiti, F.; Baroni, F.; Formigli, L.; Zurdo, J.; Taddei, N.; Ramponi, G.; Dobson, C. M.; Stefani, M. *Nature* **2002**, *416*, 507.
(50) Caughey, B.; Lansbury, P. T. *Annu Rev Neurosci* **2003**, *26*, 267.
(51) Kayed, R.; Head, E.; Thompson, J. L.; McIntire, T. M.; Milton, S. C.; Cotman, C. W.; Glabe, C. G. *Science* **2003**, *300*, 486.
(52) Walsh, P.; Neudecker, P.; Sharpe, S. *J Am Chem Soc* **2010**, *132*, 7684.
(53) Lesne, S.; Koh, M. T.; Kotilinek, L.; Kayed, R.; Glabe, C. G.; Yang, A.; Gallagher, M.; Ashe, K. H. *Nature* **2006**, *440*, 352.
(54) Cizas, P.; Budvytyte, R.; Morkuniene, R.; Moldovan, R.; Broccio, M.; Losche, M.; Niaura, G.; Valincius, G.; Borutaite, V. *Arch Biochem Biophys* **2010**, *496*, 84.
(55) Ono, K.; Condron, M. M.; Teplow, D. B. *Proc Natl Acad Sci U S A* **2009**, *106*, 14745.
(56) Simmons, L. K.; May, P. C.; Tomaselli, K. J.; Rydel, R. E.; Fuson, K. S.; Brigham, E. F.; Wright, S.; Lieberburg, I.; Becker, G. W.; Brems, D. N.; et al. *Mol Pharmacol* **1994**, *45*, 373.
(57) Shtainfeld, A.; Sheynis, T.; Jelinek, R. *Biochemistry* **2010**, *49*, 5299.
(58) Pagel, K.; Vagt, T.; Koksch, B. *Org Biomol Chem* **2005**, *3*, 3843.
(59) Pagel, K.; Seri, T.; von Berlepsch, H.; Griebel, J.; Kirmse, R.; Bottcher, C.; Koksch, B. *Chembiochem* **2008**, *9*, 531.
(60) Hoernke, M.; Koksch, B.; Brezesinski, G. *Biophys Chem* **2010**, *150*, 64.
(61) Hamley, I. W.; Castelletto, V.; Moulton, C. M.; Rodriguez-Perez, J.; Squires, A. M.; Eralp, T.; Held, G.; Hicks, M. R.; Rodger, A. *J Phys Chem B* **2010**, *114*, 8244.

(62) Makin, O. S.; Atkins, E.; Sikorski, P.; Johansson, J.; Serpell, L. C. *Proc Natl Acad Sci U S A* **2005**, *102*, 315.
(63) Blazyk, J.; Wiegand, R.; Klein, J.; Hammer, J.; Epand, R. M.; Epand, R. F.; Maloy, W. L.; Kari, U. P. *J Biol Chem* **2001**, *276*, 27899.
(64) Meier, M.; Seelig, J. *J Mol Biol* **2007**, *369*, 277.
(65) Fraser, P. E.; Nguyen, J. T.; Surewicz, W. K.; Kirschner, D. A. *Biophys J* **1991**, *60*, 1190.
(66) Esler, W. P.; Stimson, E. R.; Ghilardi, J. R.; Vinters, H. V.; Lee, J. P.; Mantyh, P. W.; Maggio, J. E. *Biochemistry* **1996**, *35*, 749.
(67) Jarvet, J.; Damberg, P.; Danielsson, J.; Johansson, I.; Eriksson, L. E.; Graslund, A. *FEBS Lett* **2003**, *555*, 371.
(68) Balbach, J. J.; Ishii, Y.; Antzutkin, O. N.; Leapman, R. D.; Rizzo, N. W.; Dyda, F.; Reed, J.; Tycko, R. *Biochemistry* **2000**, *39*, 13748.
(69) Zagorski, M. G.; Barrow, C. J. *Biochemistry* **1992**, *31*, 5621.
(70) Hilbich, C.; Kisters-Woike, B.; Reed, J.; Masters, C. L.; Beyreuther, K. *J Mol Biol* **1991**, *218*, 149.
(71) Ma, B.; Nussinov, R. *Proc Natl Acad Sci U S A* **2002**, *99*, 14126.
(72) Serpell, L. C. *Biochim Biophys Acta* **2000**, *1502*, 16.
(73) Yankner, B. A.; Duffy, L. K.; Kirschner, D. A. *Science* **1990**, *250*, 279.
(74) Clementi, M. E.; Marini, S.; Coletta, M.; Orsini, F.; Giardina, B.; Misiti, F. *FEBS Lett* **2005**, *579*, 2913.
(75) Liu, R. T.; Zou, L. B.; Fu, J. Y.; Lu, Q. J. *Behav Brain Res* **2010**, *210*, 24.
(76) Kowall, N. W.; McKee, A. C.; Yankner, B. A.; Beal, M. F. *Neurobiol Aging* **1992**, *13*, 537.
(77) Hughes, E.; Burke, R. M.; Doig, A. J. *J Biol Chem* **2000**, *275*, 25109.
(78) Tsamaloukas, A. D.; Beck, A.; Heerklotz, H. *Langmuir* **2009**, *25*, 4393.
(79) Seelig, A.; Seelig, J. *Biochemistry* **1974**, *13*, 4839.
(80) Kooijman, E. E.; Chupin, V.; Fuller, N. L.; Kozlov, M. M.; de Kruijff, B.; Burger, K. N.; Rand, P. R. *Biochemistry* **2005**, *44*, 2097.
(81) Nagle, J. F. *Proc Natl Acad Sci U S A* **1973**, *70*, 3443.
(82) Newton, A. C. *JBC* **1995**, *270*, 28495.
(83) Kitchen, J.; Crooke, E. *Journal of Liposome Research* **1998**, *8*, 337.
(84) Cullis, P. R.; Fenske, D. B.; Hope, M. J. *Physical properties and functional roles of lipids in membranes*, 1996.
(85) Goot, F. G. V. d.; Didat, N.; Pattus, F.; Dowhan, W.; Letellier, L. *Eur. J. Biochem* **1993**, *213*, 217.
(86) Xia, W.; Dowhan, W. *Proc. Natl. Acad. Sci. USA* **1995**, *Vol. 92*, pp. 783.
(87) Hwang, D. S.; Crooke, E.; Kornberg, A. *The Journal of biological chemistry* **1990**, *Vol. 265, No. 31*, pp. 19244.
(88) Sekimizu, K.; Kornberg, A. *The Journal of Biological Chemistry* **1988**, *263, N.15*, pp. 7131.
(89) Durell, S. R.; Guy, H. R.; Arispe, N.; Rojas, E.; Pollard, H. B. *Biophys J* **1994**, *67*, 2137.
(90) Sparr, E.; Engel, M. F.; Sakharov, D. V.; Sprong, M.; Jacobs, J.; de Kruijff, B.; Hoppener, J. W.; Killian, J. A. *FEBS Lett* **2004**, *577*, 117.
(91) Muller, W. E.; Koch, S.; Eckert, A.; Hartmann, H.; Scheuer, K. *Brain Res* **1995**, *674*, 133.

(92) Nagarajan, S.; Ramalingam, K.; Neelakanta Reddy, P.; Cereghetti, D. M.; Padma Malar, E. J.; Rajadas, J. *FEBS J* **2008**, *275*, 2415.
(93) Terzi, E.; Holzemann, G.; Seelig, J. *J Mol Biol* **1995**, *252*, 633.
(94) Terzi, E.; Holzemann, G.; Seelig, J. *Biochemistry* **1997**, *36*, 14845.
(95) Terzi, E.; Holzemann, G.; Seelig, J. *Biochemistry* **1994**, *33*, 7434.
(96) Terzi, E.; Holzemann, G.; Seelig, J. *Biochemistry* **1994**, *33*, 1345.
(97) Steim, J. M.; Tourtelotte, M. E.; Reinert, J. C.; McElhaney, R. N.; Rader, R. L. *Biochemistry* **1969**, *63*, 104.
(98) Wilson, G.; Fox, F. C. *Journal of Molecular Biology* **1971**, *55*, 49.
(99) Biltonen, R. L. *J. Chem. Thermodynamics* **1990**, *22*, 1.
(100) Jones, F. P.; Tevlin, P.; Trainor, L. E. H. *J. Chem. Phys.* **1989**, *91*, 1918.

II. Aims of research

Amyloid peptide aggregation leads to plaque formation[1,2], characteristic of more than 15 neurodegenerative diseases. The smaller oligomers are known to be the most toxic species to neuron cells[3,4] however their interaction with cellular membrane is poorly understood. Biophysical studies with model membranes can provide insight into the peptide-membrane interaction with consequences for both peptide and membrane structure. The description of the amyloid fragment βAP(25-35) binding to lipid membrane is the main goal of this thesis.

Biophysical studies performed on βAP(25-35) are very few and most of them were performed more than a decade ago. βAP(25-35) random-coil to β-sheet structural transition was first reported in 1994 and was shown to be concentration-dependent and reversible[5]. The Chapter III of this thesis focuses on the reproduction of these data.

βAP(25-35) is often used as a model peptide for the full-length amyloid β peptide, βAP(1-40), because the neurotoxic and neurotrophic activities and also the aggregation behavior of these two peptides are similar. However the low solubility of βAP(25-35) constitutes a major drawback in biophysical studies. Therefore the description of the peptide-to-lipid binding requires the synthesis of new model peptides. These model peptides should aggregate in the same way as βAP(25-35) but allow the precise determination of the peptide content (Chapter IV).

In Chapter VI, the newly-designed model peptides are used for biophysical studies. The thermodynamic parameters such as enthalpy, entropy and free energy can be measured with isothermal titration calorimetry, a direct high-sensitivity technique which does not require any label. Peptide secondary structural changes

upon binding can be followed with circular dichroism experiments. Eventually solid-state nuclear magnetic resonance (NMR) gives information on membrane structure. This information should allow the complete description of amyloid peptide binding to the lipid membrane.

Phospholipids are commonly used as membrane models[6] but some of their characteristics can still show unexplained particularities. The gel-to-liquid-crystal transition of phospholipids has been widely studied and its physical features such as melting temperature, viscosity or conductivity, have been characterized[7,8]. Nevertheless 1,2-dimyristoyl-glycero-3-[phospho-(1-glycerol)], DMPG, was shown to present a transition region, intermediate between the gel and liquid-crystalline state[9,10], characterized by unusual physical properties[11-13]. The molecular structure of this intermediate phase has not been defined yet. Solid-state NMR study can help to determine DMPG structure in this transition region (Chapter X).

1. References

(1) Allsop, D.; Landon, M.; Kidd, M. *Brain Res* **1983**, *259*, 348.
(2) Lundmark, K.; Westermark, G. T.; Nystrom, S.; Murphy, C. L.; Solomon, A.; Westermark, P. *Proc Natl Acad Sci U S A* **2002**, *99*, 6979.
(3) El-Agnaf, O. M.; Mahil, D. S.; Patel, B. P.; Austen, B. M. *Biochem Biophys Res Commun* **2000**, *273*, 1003.
(4) Lambert, M. P.; Barlow, A. K.; Chromy, B. A.; Edwards, C.; Freed, R.; Liosatos, M.; Morgan, T. E.; Rozovsky, I.; Trommer, B.; Viola, K. L.; Wals, P.; Zhang, C.; Finch, C. E.; Krafft, G. A.; Klein, W. L. *Proc Natl Acad Sci U S A* **1998**, *95*, 6448.
(5) Terzi, E.; Holzemann, G.; Seelig, J. *Biochemistry* **1994**, *33*, 1345.
(6) Joergensen, K.; Mouritsen, O. G. *Biophysical Journal r* **1995**, *95* 942.
(7) Jones, F. P.; Tevlin, P.; Trainor, L. E. H. *J. Chem. Phys.* **1989**, *91*, 1918.
(8) Biltonen, R. L. *J. Chem. Thermodynamics* **1990**, *22*, 1.
(9) Riske, K. A.; Amaral, L. Q.; Döbereiner, H.-G.; Lamy, M.-T. *Biophysical Journal* **2004**, *86*, 3722.
(10) Alakoskela, J.-M. I.; Kinnunen, P. J. *Langmuir* **2007**, *23*, 4203.
(11) Heimburg, T.; Biltonen, R. L. *Biochemistry* **1994**, *33*, 9477.
(12) Riske, K. A.; Politi, M. J.; Reed, W. F.; Lamy-Freund, M. T. *Chemistry and physics of lipids* **1997**, *89*, 31.
(13) Lamy-Freund, M. T.; Riske, K. A. *Chemistry and physics of lipids* **2003**, *122*, 19.

III. Structural study of βAP(25-35)

1. Introduction

In the past years the amyloid β peptide, βAP(1-40), was extensively studied and various oligomeric species were observed in solution. The smallest oligomeric species studied are soluble and are called βAP derived diffusible ligands (ADDLs). These oligomers have an aggregation range of 2 to 24[1]. They may further aggregate to form dodecamers[2], protofibrils[1] and eventually fibrils[3]. As mentioned in the introduction, there seems to be a correlation between the secondary structure of each of these species and their toxicity[4]. However the analysis of the secondary structure of βAP(1-40) is difficult because of its low solubilization in aqueous buffers and the formation of aggregates.

A common procedure to improve the solubility of βAP(1-40) is a hexafluoroisopropanol, HFIP, pretreatment. This very polar, fluorinated alcohol favors the monomeric state of amyloid peptides in solution[5]. Other fluorinated solvents like trifluoroacetic acid produce similar solubilizing effect on amyloid aggregates[5]. The common procedure of HFIP pretreatment consists in dissolving the peptide in HFIP, and then evaporating the alcohol. The peptide can then be dissolved in buffer leading to a peptide solution free of aggregates. Other protocols try to further improve the peptide solubility by subsequent lyophilization[6], or first dissolution in ammonia and then centrifugation of the sample[7]. A different procedure is to combine peptide dissolution with centrifugation, followed by column separation and dilution of the collected fractions in buffer[8]. Most of the latter procedures are inappropriate for biophysical use, either because the amyloid peptide carries with it fluorinated solvents[9], or because the preparation protocol includes a filtration or centrifugation

step, and the peptide concentration cannot be determined precisely. HFIP treatment without any additional step is therefore currently the most suitable method for biophysical studies. Its use became common only in the past years, so the early biophysical studies on βAP(1-40) did not include any peptide pre-treatment.

Previous biophysical studies with amyloid peptides and their fragments revealed a random-coil to β-sheet transition upon increase in concentration at pH 4.0[10,11]. They aggregate as anti-parallel β-sheets at pH 7.4 before forming β-cross structures[12,13]. The structural changes undergone by the peptide and their kinetics can be influenced by environmental hydrophilicity[14] and the presence of lipids[12,15]. In many cases β-sheet formation is preceded by α-helix formation[16,17]. This structural intermediate is suspected to play a role in fibrillization by facilitating β-sheet formation[18]. The α-helix intermediate was not seen yet in βAP(25-35) fibrillization. The first part of this work focuses on the structural study of βAP(25-35) and the detailed description of the random-coil to β-sheet transition. The difficulties encountered during such a study will be discussed and the influence of the procedure used for peptide dissolution on the secondary structure evidenced.

2. Materials and Methods

The amyloid peptide βAP(25-35) with the amino-acid sequence H-GSNKGAIIGLM-OH (molecular weight of 1060.3 $g.mol^{-1}$) was bought from Bachem (H-1192). The peptide had a purity higher than 95%. 1,1,1,3,3,3-hexafluoroisopropanol (HFIP) was from Sigma-Aldrich (Schnelldorf, Germany). The buffers used were either 5 or 10 mM HEPES at pH 7.4 (Roth, Karlsruhe, Germany) or sodium acetate, AcONa at pH 4.0 (Merck, Darmstadt, Germany).

Dissolution 1: Dry peptide was dissolved in buffer at 0.8 mg/mL (472 μM, assuming that 40% of the powder is salt). It was stirred magnetically for 1-2 h to reach equilibrium between aggregates and soluble monomers. This stock solution was freshly prepared prior to the measurement. Subsequent dilutions were done in parallel from the equilibrated stock solution. The diluted solutions were also stirred for 1 h

before proceeding with the measurement. The CD signal was recorded on the equilibrated samples, starting with the low peptide concentrations. Peptide concentration was estimated from the stock solution.

Dissolution 2: Dry peptide was dissolved in pure HFIP in order to get a 1.7 mg/mL stock solution (944 μM, assuming that 40% of the powder is salt). It was vortexed and sonicated for 10 s in a water bath to ensure complete solubilization of the peptide. Each dilution was performed by drying the necessary amount of the stock solution in HFIP under a steam of nitrogen and then under high vacuum for 1 h before adding the desired buffer volume. This solution was again sonicated for 10 s to ensure complete solubilization of the peptide in buffer. Each dilution was stirred 20 min before the measurement. Peptide concentration was estimated by weight from stock solution.

Circular Dichroism

Circular dichroism measurements were performed on a Chirascan (Applied Photophysics Ltd., Leatherhead, UK) using 0.2 or 0.5 mm quartz cuvettes (Hellma, Jena, Germany). The experiments were started with 0.2 mm cuvettes but 0.5 mm cuvettes could be used at a later stage with improved instrumental settings. The bandwidth was set to 1.5 nm and the signal was recorded in 1 nm steps from 190-250 nm with an averaging time of 40 sec/point with the 0.2 mm cuvettes or 20 sec/point with the 0.5 mm cuvette. All measurements were performed at room temperature. All spectra were corrected by subtracting buffer baseline.

The output signal of the Chirascan is in millidegrees and is converted into mean residue ellipticity, $[\Theta]_{MR}$, expressed in deg. $cm^2.dmol^{-1}$ via the relation:

$$[\Theta]_{MR} = 10^5 \frac{CD}{c_{peptide}\, l\, n_{AA}} \qquad (1)$$

with $c_{peptide}$ the peptide concentration in $\mu mol.L^{-1}$, l the pathlength in cm and n_{AA} the number of amino-acids of the peptide sequence.

The secondary structure was analyzed by spectral fitting based on the linear combination of a CD spectra of peptide database[19].

3. Results

Based on the previous biophysical studies with βAP(25-35)[10,15], the dissolution procedure 1 was followed to dissolve dry βAP(25-35) in buffer at pH 7.4. At this pH, the peptide is known to adopt β-sheet secondary structure[10]. Figure 1 shows the structural changes of βAP(25-35) upon peptide dilution.

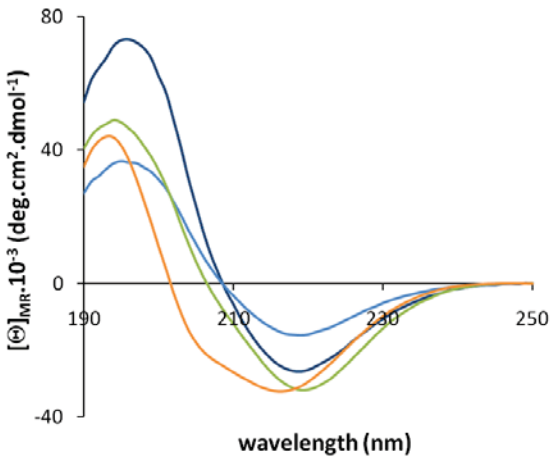

***Figure 1**: Concentration-dependent structural changes of βAP(25-35) at pH 7.4. A 500 μM βAP(25-35) stock solution was prepared in 10 mM HEPES buffer at pH 7.4 and diluted. The estimated peptide concentrations are: 25 (—), 50 (—), 75 (—) and 102 μM (—).*

Three of the spectra displayed in Figure 1 (25, 50 and 75 μM) present similar CD characteristics. The mean residue ellipticity has a minimum at 215-218 nm and a maximum around 195 nm. This experiment was repeated by the same procedure and the reproducibility was low. For similar peptide dilutions, the CD spectra were different from those shown in Figure 1 (results not shown).

The shape of the 25 μM spectrum corresponds to β-sheet features[20,21] but the signal intensity is higher, evidence for a wrong estimated peptide concentration (Equation 1). In effect the peptide concentration can only be determined by weight because the molecule does not contain a chromophore. The presence of aggregates in the stock solution induces additional error. The incorrect peptide concentration leads to a spectral simulation of poor quality. Nevertheless the spectra in Figure 1 were analyzed as described in Materials and Methods (page 19); the best fittings are shown in Table 1.

***Table 1**: Secondary structure of βAP(25-35) at pH 7.4 and 4.0. The α-helix, β-sheet, random-coil and β-turn contents are expressed as percentage of the whole peptide secondary structure. The coefficient of determination R^2 gives an indication on the quality of the fit. Only the concentrations leading to a reasonable fitting are represented here.*

	Concentration (μM)	**α-helix** (%)	**β-sheet** (%)	**random-coil** (%)	**β-turn** (%)	**R^2** /
pH 7.4	50	2	98	0	0	0.95
	75	38	62	0	0	0.85
	102	63	31	6	0	0.96
pH 4.0	62.5	38	8	54	0	0.96
	125	59	38	3	0	0.97
	250	49	8	43	0	0.80
	500	92	0	8	0	0.96

At 102 μM, the secondary structure of βAP(25-35) contains 31% β-sheet. The β-sheet component is higher at 75 μM (62%) and is further increased at 50 μM where it contributes to 98% (R^2=0.95) of βAP(25-35) secondary structure. The presence of β-sheet at physiological pH is confirmed but its proportion in the various samples studied presents surprising features compared to the previous studies performed on the peptide. In effect Terzi *et al.* showed that the more βAP(25-35) is concentrated, the more β-sheet it forms[10]. The spectral analysis in Table 1 indicates another trend: β-sheet content decreases with increasing peptide concentration.

At pH 4, Terzi showed that βAP(25-35) undergoes a reversible and concentration-dependent random-coil to β-sheet structural transition[10]. The results in Figure 2 represent the experiment performed to reproduce this transition. Dissolution procedure 1 was followed, starting from a 500 μM peptide stock solution.

The spectra at low peptide concentrations (15.5 and 62.5 μM) are characterized by minima at 197 and 220 nm. The spectral analysis (see Table 1) shows that random-coil is the dominant component at 62.5 μM where it contributes to 54% of βAP(25-35) secondary structure. α-helix represents 38% of the peptide secondary structure at 62.5 μM and the α-helix contribution increases with βAP(25-35) concentration. The 500 μM spectrum possesses clear α-helix characteristics, with minima at 208 and 222 nm and a mean residue ellipticity $[\Theta]_{208\ nm} = -35.10^3$

deg.cm^2.dmol^{-1}. The spectral analysis shows a α-helix contribution of 92%. β-sheet contribution is exclusively observed at 125 μM where it represents 38% of the CD signal. However it is not the major component in contrast to what was expected from the literature[10].

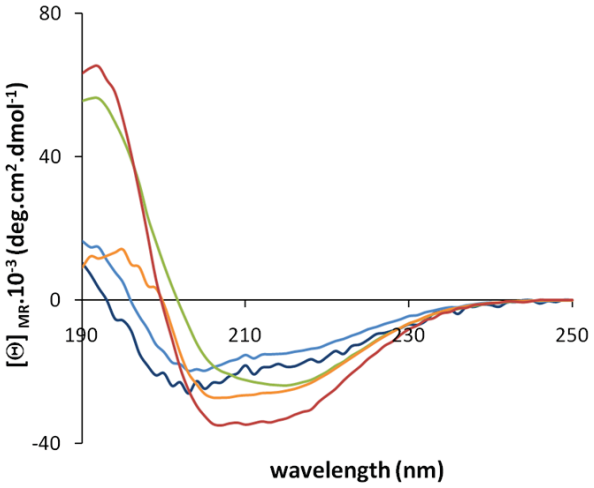

***Figure 2**: Concentration-dependent structural changes of βAP(25-35) at pH 4.0. A 500 μM βAP(25-35) stock solution was prepared in 5 mM AcONa buffer at pH 4.0 and diluted. The estimated peptide concentrations of the dilutions were: 15.5 (—), 62.5 (—), 125 (—), 250 (—) and 500 μM (—).*

a) The importance of the equilibration time in βAP(25-35) structural study

In Figure 2, the spectra at the three highest peptide concentrations (125, 250 and 500 μM) represent a α-helical structure in pH 4.0 buffer. The literature describes the α-helix secondary structure as an intermediate state in fibril formation[16,22]. It is further known that amyloid formation follows a seeding mechanism starting with a lag phase controlling nucleus formation[23,24]. Therefore increasing the equilibration time or giving supplementary energy to the system might enhance β-sheet formation. The effect of stirring, heating and lengthening of the equilibration time was therefore investigated systematically.

The CD spectrum of 500 μM amyloid peptide solution was monitored over time and is shown in Figure 3. Two stock solutions were prepared according to dissolution procedure 1. One of them was stirred for only 1 h (Figure 3A), whereas the second stock solution was stirred up to 7 h, from peptide dissolution to sample monitoring (Figure 3B). Also the second stock solution was stirred at a 6°C higher temperature to accelerate further the structural transition in the second stock solution. The CD signals

of the peptide solutions were monitored at regular intervals. The experiment was stopped when no more variation in peptide secondary structure could be observed in the second sample.

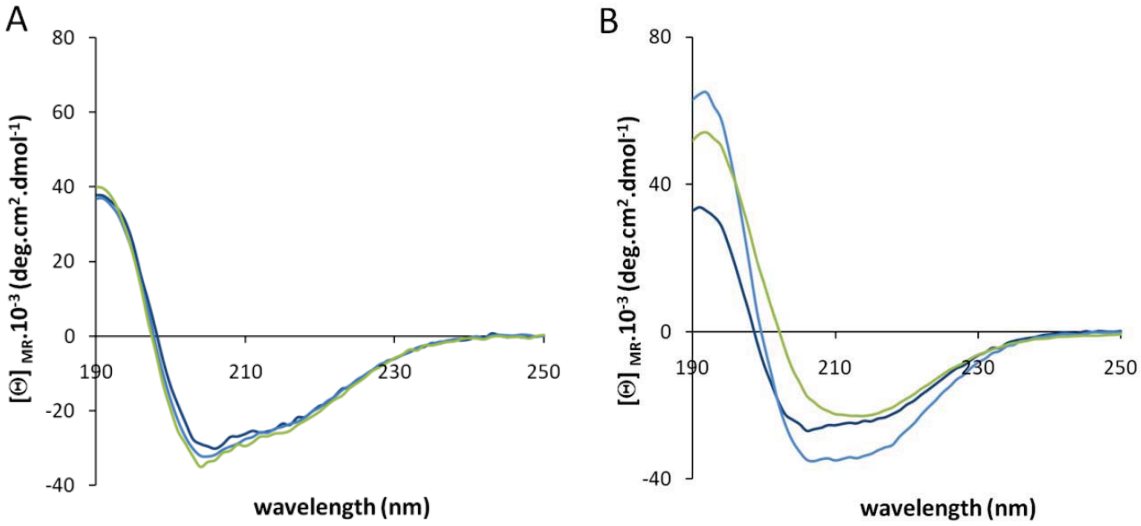

***Figure 3**: Structural changes of βAP(25-35) at pH 4.0 over time. 500 μM βAP(25-35) solution in 5 mM AcONa buffer was kept at 23°C (A) without or (B) under stirring at 29°C. The samples were measured immediately (—), 2 h (—) and 7 h (—) after peptide dissolution.*

If highly-concentrated βAP(25-35) is not continuously stirred (Figure 3A), no structural change is observed over 7 h. The peptide secondary structure remains constant, with the following contributions: 63% α-helix and 37% random-coil (R^2=0.91). β-sheet formation was observed after a 24 h waiting period (results not shown). In comparison, βAP(25-35) undergoes a clear structural transition from α-helix towards β-sheet over the same length of time upon additional stirring and heating (Figure 3B). The spectrum of βAP(25-35) after 7 h under stirring and heating is composed of 54% α-helix and 46% β-sheet (R^2=0.97). A similar experiment performed at room temperature showed a faster transition than without stirring but slower than with additional heating (results not shown). These experiments point out the influence of time, stirring, and heating in the study of amyloid peptide secondary structure.

As the structural transition can be affected by the history of the sample, the experiment shown in Figure 2 was repeated with different stirring time. Figure 4A shows the concentration-dependent structural transition of βAP(25-35) with samples measured after 30 min stirring and Figure 4B after 7 h stirring.

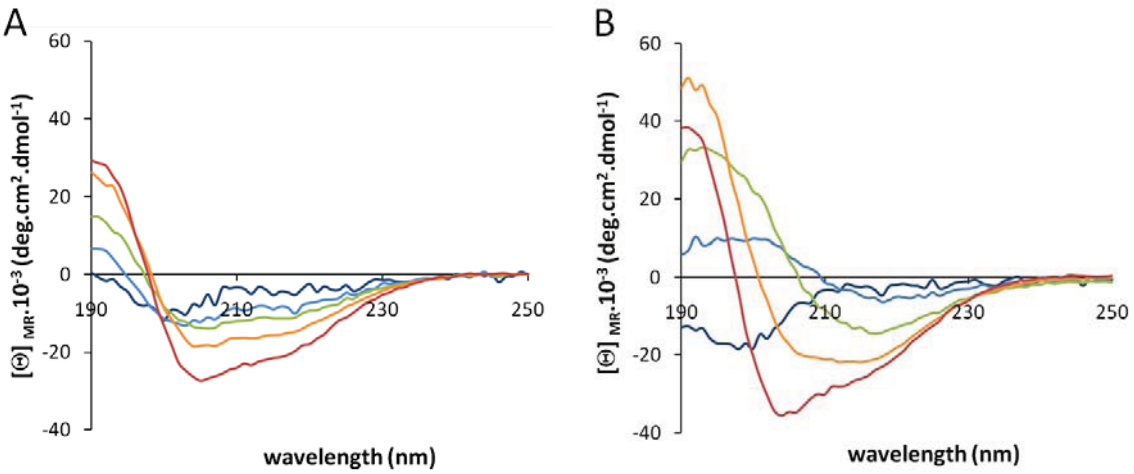

***Figure 4**: Concentration-dependent structural transition of βAP(25-35) at pH 4.0 over time under stirring. The estimated peptide concentration was 15.5 (—), 31 (—), 62.5 (—), 125 (—) and 500 μM (—) and the samples were measured (A) after 30 min or (B) after 7h of stirring.*

The comparison of Figure 4A and 4B shows that none of the sample studied has reached its final structure after 30 min equilibration. After 7h, only the two lower peptide concentrations seem to be at structural equilibrium since at 15.5 μM, random-coil is observed and at 31 μM a transition from random-coil to β-sheet occurs. Also the spectra in Figure 2 and 4A are different although the same procedure was applied. The peptide concentration was probably different in the two experiments but the peptide quantification is too inaccurate.

b) The reversibility of the random-coil to β-sheet structural transition

The previous experiments showed that the stock solution reaches β-sheet secondary structure only after several hours of stirring with additional heating. Consequently the dilutions in Figures 2 and 4 were prepared from a 500 μM stock solution of α-helix βAP(25-35) and not of β-sheet βAP(25-35), as described earlier[10]. These experiments were thus proof of a reversible α-helix to random-coil structural transition at pH 4.0, but not of a β-sheet to random-coil transition.

β-sheet reversibility to random-coil was studied next. Using dissolution procedure 1, an equilibration of 24 h was allowed for the stock solution. After this period the peptide secondary structure was mostly β-sheet. Next the stock solution was diluted and the dilutions were kept for 2h under stirring. CD spectra of selected

concentrations are represented in Figure 5. Longer stirring produced too much peptide adsorption on the vial walls.

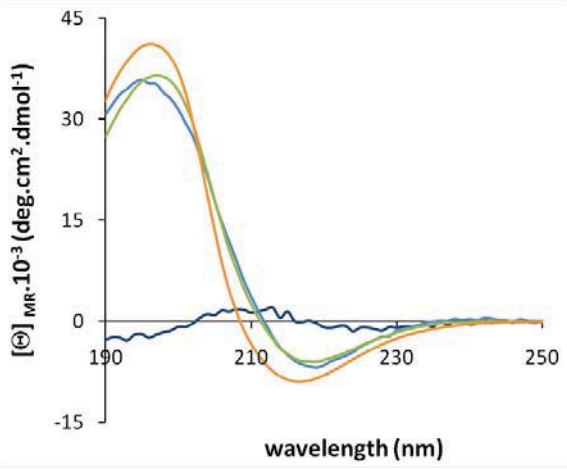

***Figure 5**: Concentration-dependent structural transition of βAP(25-35) from a 500 μM stock solution with the peptide as β-sheet at pH 4.0. The peptide concentration was estimated at 10 (—), 19 (—), 77 (—) and 308 μM (—).*

The CD spectra at 308, 77 and 19 μM are characteristic of β-sheet. The mean residue ellipticity of the 10 μM spectrum is too low to give indication on peptide secondary structure. This experiment was reproduced and β-sheet was again observed over the whole concentration range, until the signal became too weak to allow any conclusion on the structural elements.

In conclusion it seems that the major component of a diluted β-sheet stock solution is still β-sheet at pH 4.0. At low peptide concentrations where random-coil could be favored (between 15 and 30 μM, see in Figure 4 and [10]) the signal-to-noise ratio is too low. The present data provide no evidence for a β-sheet-to-random-coil transition upon dilution at pH 4.0.

c) The improvement in homogeneity of βAP(25-35) solutions with HFIP

As was mentioned previously, the estimated concentration by weight could be incorrect. Amino-acid analysis (AAA), before or after the spectroscopic measurement, can provide a precise knowledge of the peptide content of each sample. Unfortunately this facility is not available in our laboratories.

Hexafluoroisopropanol, HFIP, pretreatment was tested for preparing βAP(25-35) solutions according to dissolution procedure 2. These peptide solutions should be

free of aggregates. Each diluted solution was freshly prepared starting from a stock solution of βAP(25-35) in HFIP. After evaporation of the HFIP, each sample was diluted in buffer and stirred for 20 min prior to the spectroscopic measurement. The stirring times were therefore identical for each sample, contrary to the dissolution procedure 1. The results of the monitored CD signals of amyloid peptide dilutions at pH 7.4 and pH 4.0 are shown in Figure 6.

All spectra shown are characterized by a minimum mean residue ellipticity close to 195 nm. HFIP pretreatment favors the random-coil contribution in the secondary structure of βAP(25-35) at both pH values. The weak minimum observed at 217 nm indicates the presence of β-sheet component. The CD signals variations observed at pH 7.4 can either indicate slight conformational changes or the presence of residual aggregates in solution. At pH 4.0, the spectra can all be perfectly superimposed, no structural change occurs over the concentration range studied.

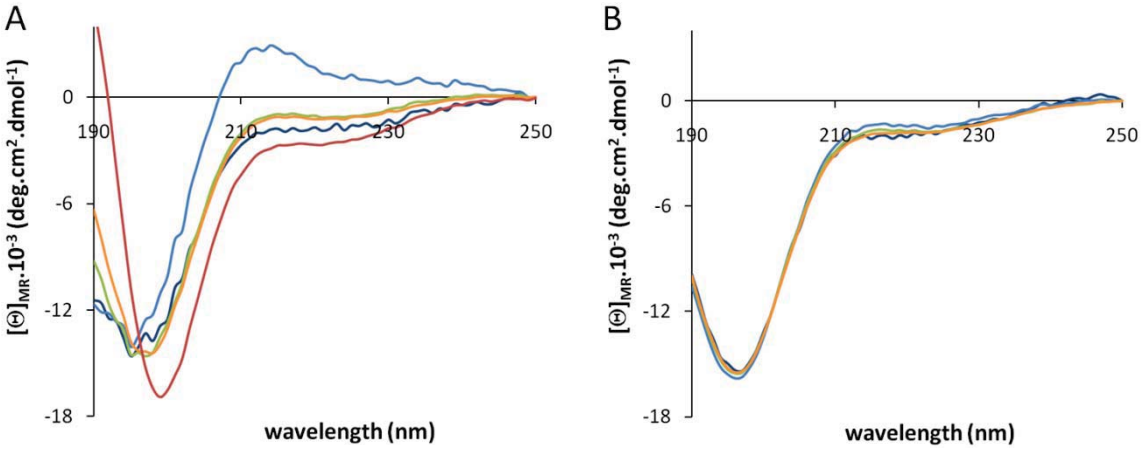

***Figure 6**: Concentration-dependent structural changes of HFIP-treated βAP(25-35) at pH 7.4 (A) and pH 4.0 (B). The estimated peptide concentration was for (A) 25 (—), 47 (—), 79 (—), 117 (—) and 141 μM (—) and for (B) 47 (—), 79 (—), 117 (—) and 141 μM (—).*

4. Discussion

This chapter points out the influence of experimental parameters on the structural properties of βAP(25-35). Stirring or heating the samples favors nucleus formation[23]. The equilibration time needed to reach a new secondary structure is therefore shortened at a given peptide concentration. A similar mechanical effect is observed for interferon γ, INF-γ, where dimers are the active form of the protein and

aggregation leads to inactivation of INFγ[25]. Stirring was shown to induce the irreversible transition from the monomeric state, mostly α-helical, to the aggregated state of INF-γ, with reduced α-helix content. Mechanical stress was investigated on βAP(1-40) to evaluate the effect of shear stress and heating on the peptide secondary structure[26]. Dunstan *et al.* showed that amyloid fibrils are formed much faster upon stirring and heating[26]. They also compared the effect of stirring with shearing in Couette flow on βAP, and concluded that shearing, rather than mixing, accelerates fibril formation. The exact mechanism leading to a decrease in the activation energy of aggregation upon shear stress is not known yet. Hill *et al.* investigated the effect of Couette flow on the aggregation of β-lactoglobulin[27]. Their experiments showed the formation of globular aggregates under shear stress. However if amyloid aggregates, formed after 24 h incubation at 80°C, are put under shear stress, they disaggregate.

The presence of aggregates in the solutions of βAP(25-35) influences the shape of the CD spectra. It was Duysens who first published in 1956 that aggregates could cause signal distortions via light scattering and optical flattening[28]. A study published in 1988 by Bastamante and Mastre[29] gave the mathematical reasons for this phenomenon. If the big aggregates have a size comparable to the light wavelength (200 nm), they invalidate Beer's law of light absorption. Therefore the absorbed light of a homogeneous sample differs from the one of an inhomogeneous sample at the same total concentration[29].

βAP solutions can be homogenized with HFIP treatment. This alcohol is able to dissolve amyloid peptide aggregates[30]. The alcohol molecules may form hydrogen bonds with water molecules close to HFIP[31]. Therefore protein aggregates are surrounded by alcohol clusters that progressively disrupt them through hydrophobic interactions. Due to less ordered water molecules in the vicinity of the peptide, short distance interactions between amino and carboxy groups of amyloid peptides are enhanced what favors α-helix stabilization[30]. This is the case when the peptide is directly dissolved in HFIP. In HFIP pretreated βAP(25-35), the alcohol molecules are evaporated and the peptide is then dissolved in aqueous buffer (dissolution procedure

2). We show that HFIP pretreatment prevents the formation of aggregates and favors random-coil formation of βAP(25-35) at both experimental pH values.

In the present study we observe the formation of α-helix as structural intermediate in the β-sheet formation of βAP(25-35) at pH 4.0. βAP(25-35) aggregation process can be extended[10] and described as follows:

A reversible random-coil to α-helix transition (see Figure 2) is followed by a α-helix to β-sheet transition (see Figure 3B, 4B and [10]). The α-helix intermediate seems to be implicated in other amyloid peptides and fragments aggregation[22,32,33]. The α-helical intermediate is also necessary for βAP(16-22) to form β-sheets from random-coil via hydrophobic and electrostatic interactions[33]. Abedini and Rayleigh proposed an aggregation process in which the initially random-coil amyloid peptides would contain an increasing α-helix component that would favor interpeptidic interactions and therefore β-sheet formation and further fibrillization[18].

5. References

(1) Walsh, D. M.; Lomakin, A.; Benedek, G. B.; Condron, M. M.; Teplow, D. B. *J Biol Chem* **1997**, *272*, 22364.
(2) Lesne, S.; Koh, M. T.; Kotilinek, L.; Kayed, R.; Glabe, C. G.; Yang, A.; Gallagher, M.; Ashe, K. H. *Nature* **2006**, *440*, 352.
(3) Lambert, M. P.; Barlow, A. K.; Chromy, B. A.; Edwards, C.; Freed, R.; Liosatos, M.; Morgan, T. E.; Rozovsky, I.; Trommer, B.; Viola, K. L.; Wals, P.; Zhang, C.; Finch, C. E.; Krafft, G. A.; Klein, W. L. *Proc Natl Acad Sci U S A* **1998**, *95*, 6448.
(4) Kayed, R.; Head, E.; Thompson, J. L.; McIntire, T. M.; Milton, S. C.; Cotman, C. W.; Glabe, C. G. *Science* **2003**, *300*, 486.
(5) Jao, S. C.; Ma, K.; Talafous, J.; Orlando, R.; Zagorski, M. G. *Amyloid: Int. J. Exp. Clin. Invest. 4* **1997**, 240.
(6) McLaurin, J.; Chakrabartty, A. *Eur J Biochem* **1997**, *245*, 355.
(7) Matsuzaki, K.; Noguch, T.; Wakabayashi, M.; Ikeda, K.; Okada, T.; Ohashi, Y.; Hoshino, M.; Naiki, H. *Biochim Biophys Acta* **2007**, *1768*, 122.
(8) Fezoui, Y.; Teplow, D. B. *J Biol Chem* **2002**, *277*, 36948.
(9) Tomaselli, S.; Esposito, V.; Vangone, P.; van Nuland, N. A.; Bonvin, A. M.; Guerrini, R.; Tancredi, T.; Temussi, P. A.; Picone, D. *Chembiochem* **2006**, *7*, 257.
(10) Terzi, E.; Holzemann, G.; Seelig, J. *Biochemistry* **1994**, *33*, 1345.
(11) Chiti, F.; Dobson, C. M. *Annu Rev Biochem* **2006**, *75*, 333.
(12) Terzi, E.; Holzemann, G.; Seelig, J. *J Mol Biol* **1995**, *252*, 633.
(13) McLaurin, J.; Franklin, T.; Chakrabartty, A.; Fraser, P. E. *J Mol Biol* **1998**, *278*, 183.
(14) Shanmugam, G.; Jayakumar, R. *Biopolymers* **2004**, *76*, 421.
(15) Terzi, E.; Holzemann, G.; Seelig, J. *Biochemistry* **1994**, *33*, 7434.
(16) Kirkitadze, M. D.; Condron, M. M.; Teplow, D. B. *J Mol Biol* **2001**, *312*, 1103.
(17) Jarvet, J.; Damberg, P.; Danielsson, J.; Johansson, I.; Eriksson, L. E.; Graslund, A. *FEBS Lett* **2003**, *555*, 371.
(18) Abedini, A.; Raleigh, D. P. *Phys Biol* **2009**, *6*, 015005.
(19) Reed, J.; Reed, T. A. *Anal Biochem* **1997**, *254*, 36.
(20) Labhardt, A. M. *J Mol Biol* **1982**, *157*, 331.
(21) Holzwarth, G.; Doty, P. *J Am Chem Soc* **1965**, *87*, 218.
(22) Andreola, A.; Bellotti, V.; Giorgetti, S.; Mangione, P.; Obici, L.; Stoppini, M.; Torres, J.; Monzani, E.; Merlini, G.; Sunde, M. *J Biol Chem* **2003**, *278*, 2444.
(23) Come, J. H.; Fraser, P. E.; Lansbury, P. T., Jr. *Proc Natl Acad Sci U S A* **1993**, *90*, 5959.
(24) Jarrett, J. T.; Lansbury, P. T., Jr. *Biochemistry* **1992**, *31*, 12345.
(25) Zlateva, T.; Boteva, R.; Salvato, B.; Tsanev, R. *Int J Biol Macromol* **1999**, *26*, 357.
(26) Dunstan, D. E.; Hamilton-Brown, P.; Asimakis, P.; Ducker, W.; Bertolini, J. *Protein Eng Des Sel* **2009**, *22*, 741.
(27) Hill, E. K.; Krebs, B.; Goodall, D. G.; Howlett, G. J.; Dunstan, D. E. *Biomacromolecules* **2006**, *7*, 10.
(28) Duysens, L. N. *Biochim Biophys Acta* **1956**, *19*, 1.
(29) Bustamante, C.; Maestre, M. F. *Proc Natl Acad Sci U S A* **1988**, *85*, 8482.
(30) Vieira, E. P.; Hermel, H.; Mohwald, H. *Biochim Biophys Acta* **2003**, *1645*, 6.
(31) Israelachvili, J. *Intermolecular and surface forces*; Academic press, 1997.

(32) Hebda, J. A.; Saraogi, I.; Magzoub, M.; Hamilton, A. D.; Miranker, A. D. *Chem Biol* **2009**, *16*, 943.
(33) Klimov, D. K.; Thirumalai, D. *Structure* **2003**, *11*, 295.

IV. Alzheimer model peptides for aggregation studies

1. Introduction

The previous chapter outlined the heterogeneity of βAP(25-35) solutions due to aggregation. The low accuracy in the determination of the peptide concentration prevents the correct evaluation of thermodynamic data. Biophysical studies therefore require the design of related model peptides. These peptides should possess similar aggregation behavior as βAP(25-35), form fibrils and allow an accurate determination of the peptide content.

Peptide concentrations can be measured precisely by UV-absorbance. This requires peptides with chromophores, such as tryptophan or tyrosine. These amino-acids have absorbance maxima at 280 and 275 nm, respectively, with the corresponding extinction coefficients ε_{Trp} = 5500 M^{-1} and ε_{Tyr} = 1490 M^{-1}. The insertion of an amino-acid such as tryptophan, Trp, in the peptide sequence will therefore facilitate the concentration determination.

The wild-type βAP(25-35) sequence is: GSNKGAIIGLM and the appropriate position for Trp insertion needs to be defined. Some amino-acids are known to be essential for peptide aggregation and membrane binding. For example, the mutation of the Asn27 to Gln27 prevents amyloid formation of βAP(25-35)[1] despite the similarity of these amino-acids. The replacement of Ala30 by Ile30 in βAP(28-35) has no effect on peptide conformation and fibril formation, whereas the mutation of Ala30 into Gly30 prevents β-sheet formation[2]. Lys28 and the C-terminal Met35 should not be modified because of the importance of electrostatic interactions in membrane binding of βAP(25-35)[3]. Mutating the C-terminal Met35 to Ala35 decreases the hydrophobicity of

βAP(25-35) and increases its toxicity[4]. Replacing or adding an amino-acid to the peptide sequence thus requires special care since peptide aggregation should not be prevented.

Only few studies included Trp in the peptide sequences and little is known about the influence of this residue on peptide aggregation[5-7]. Trp fluorescence was used to monitor fibril formation and structural changes of βAP(1-40). Fibril hydrophobicity was observed when Phe4 or Phe19 in βAP(1-40) were replaced by Trp[5]. Trp in position 4 did not alter fibril formation or kinetics, whereas the substitution at position 19 lengthened the lag phase prior to nucleus formation[5].

The effects of Trp on the peptide-membrane interaction are better described and were particularly well-investigated in the field of antimicrobial peptides. Based on Trp fluorescence, it was observed that the residue is located preferentially in the lipid-water interface[7]. The presence of Trp supports magainin toxicity[6]. Magainin is electrostatically attracted to the membrane and the preference of Trp for the lipid-water interface increases the affinity of the peptide for the membrane[8].

In order to decide on the position of the Trp insertion for βAP(25-35), the amino-acid sequences and their hydrophobicity were evaluated for the replacement of each amino-acid using the computing program TANGO[9,10]. The calculations are based on the physico-chemical properties of a peptide sequence that may influence aggregation namely hydrophobicity, energy of solvation, electrostatic interactions, and hydrogen bonding[9]. They result in the definition of a β-sheet aggregation factor which increases with the aggregation propensity. Two peptide sequences containing Trp were selected. The Trp was added at position 24 in the first peptide, named WβAP(25-35), whereas in the second peptide named, βAP(25-35)_I32W, Ile32 was replaced with Trp32. The calculated β-sheet aggregation factors of the two designed peptides, at both neutral and acidic pH, are given in Table 1 together with their sequence.

The calculation predicts a very similar aggregation behavior for WβAP(25-35) compared to the wild-type peptide; the β-sheet aggregation factors of the two peptides are identical. Trp addition at the N-terminal position does not seem to modify

the peptide aggregation behavior. In contrast, βAP(25-35)_I32W seems to have reduced aggregation tendency and may be better solubilized.

***Table 1**: Aggregation factors calculated at pH 7.4 and 4.0 for βAP(25-35), WβAP(25-35) and βAP(25-35)_I32W. Their sequence is expressed in one-letter amino-acid code. The positively-charged Lys is colored in yellow and the inserted Trp in blue.*

Sequence	Designation	Aggregation factor	
		pH 7.4	pH 4.0
	βAP(25-35)	135.6	61.3
	WβAP(25-35)	135.5	61.3
	βAP(25-35)_I32W	60.7	24.8

The ability of these two model peptides to aggregate will be investigated with light microscopy and dynamic light scattering, DLS. A fluorescence experiment with Thioflavine T will study their ability to form fibrils, a stacking of antiparallel β-sheets. The secondary structure of the designed model peptides will be characterized with circular dichroism, CD, and compared to βAP(25-35).

2. Materials and Methods

Peptides

The wild-type amyloid peptide βAP(25-35), H-GSNKGAIIGLM-OH, was bought from Bachem, Switzerland (H-1192). The solid-phase peptide synthesis of the analog βAP(25-35)_I32W, H-GSNKGAIWGLM-OH, was initially performed but the peptide was difficult to separate from its derivative containing an aspartimide (see Appendix, page 51). The analog βAP(25-35)_I32W (molecular weight of 1133 $g.mol^{-1}$) was therefore bought at Peptide 2.0 (Chantilly, USA). The analog WβAP(25-35), H-WGSNKGAIIGLM-OH, (molecular weight of 1247.5 $g.mol^{-1}$) was ordered from AnaSpec (Fremont, USA). All peptides had a purity better than 95%. 1,1,1,3,3,3-hexafluoroisopropanol (HFIP) was from Sigma-Aldrich (Schnelldorf, Germany). The buffers were either 5 or 10 mM

HEPES (Roth, Karlsruhe, Germany) at pH 7.4 or sodium acetate (AcONa, Merck, Darmstadt, Germany) at pH 4.0.

The peptides were prepared following either dissolution procedure 1 or 2 as described on pages 20-21.

Microscopic Imaging

Microsocope images were recorded with an inverted microscope Nikon Diaphot TMD equipped with a high pressure mercury lamp (DC 100W USHIO) and CF objectives (x10: Ph L, Plan 4/0.13 DL; x20: Ph 1, Plan 10/0.30 DL).

A 20 μL droplet of peptide solution was deposited on siliconized glass of 1.8 cm diameter and covered with the same glass before observation.

Ultra-violet spectroscopy

The samples were monitored on a Uvikon 860 (GOEBEL Instrumentelle Analytik, Germany) with the buffer spectrum as a reference. A 1 cm cuvette was used (Hellma, Jena, Germany). Peptide concentration was determined from the absorption measured at 280 nm using ε_{Trp} = 5500 M^{-1}. The absorption spectra of WβAP(25-35) and βAP(25-35)_I32W are shown below.

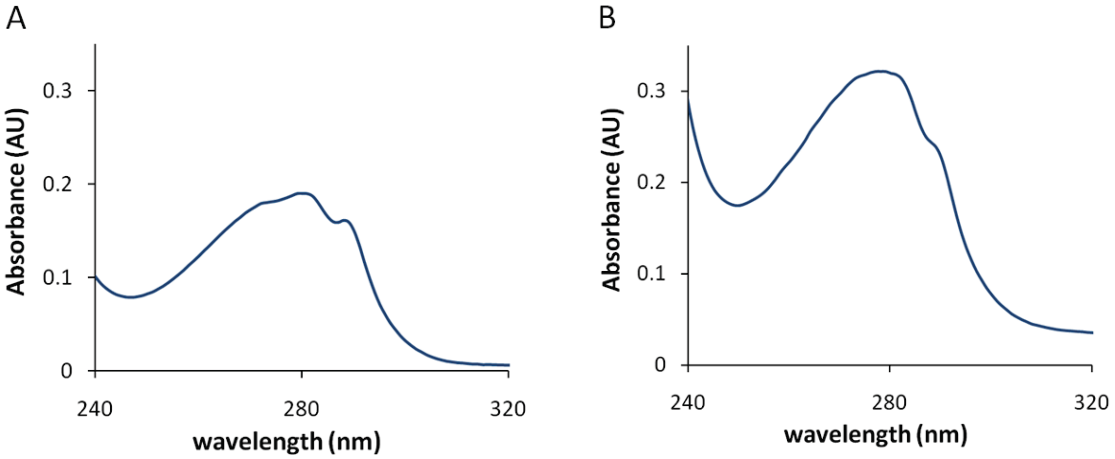

***Figure 2**: Absorbance spectra of (A) WβAP(25-35) and (B) βAP(25-35)_I32W at pH 7.4. The peptide concentration was determined from the value of the absorbance at 280 nm at 35 μM for WβAP(25-35) and at 58 μM for βAP(25-35)_I32W.*

Fluorescence

Trp is known to emit fluorescence if excited at 280 nm. The fluorescence spectra of WβAP(25-35) and βAP(25-35)_I32W are shown in Figure 1. However Trp fluorescence did not allow us to monitor peptide aggregation, therefore the procedure described thereafter was used.

The peptides were prepared in the same way as described above (Dissolution 1 or 2). To the peptide powder or dried peptide film was added 395 µL of buffer (10 mM HEPES at pH 7.4 or 10 mM AcONa at pH 4.0) and the solution was sonicated in a water bath for 10 s. The solution was transferred to a glass fluorescence cuvette (pathlength of 5mm, Hellma) and degassed with Argon. 5 µL of Thioflavine T (Th T, Sigma, Schnelldorf, Germany) was added[11]. The solution was stirred during the whole measurement. The fluorescence spectra were recorded on a Jasco fluorimeter FP-6500 (Gross-Umstadt, Germany), the bandwidth of both emission and excitation slit was 3 nm and the scanning rate 50 nm/min. Every measurement was repeated twice and the spectrum of Th T in buffer was monitored to ensure no influence of the Th T alone on the observed signal.

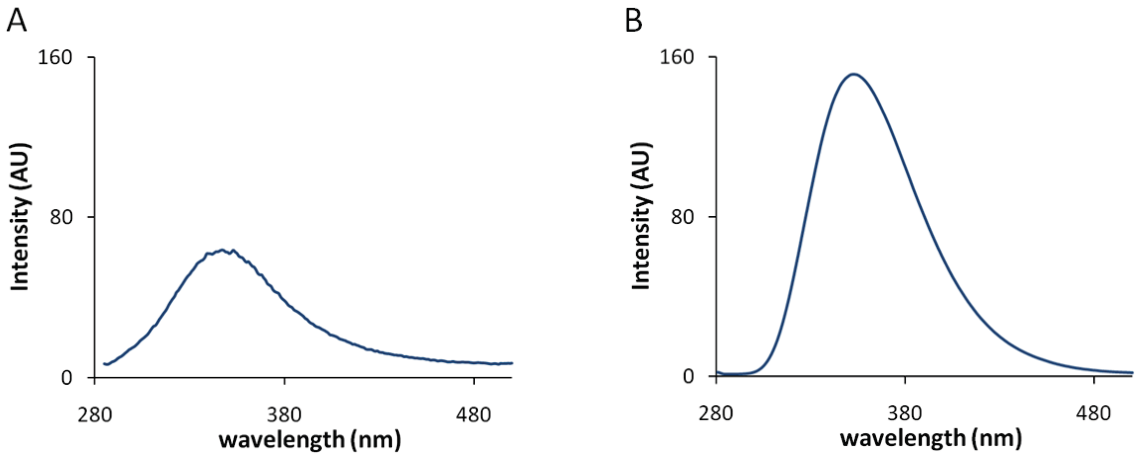

***Figure 1**: Fluorescence spectra of (A) WβAP(25-35) and (B) βAP(25-35)_I32W at pH 7.4. The peptide concentration was 45 µM for WβAP(25-35) and 98 µM for βAP(25-35)_I32W. The excitation wavelength was set at 280 nm.*

Dynamic Light Scattering measurements (DLS)

The size of the peptide aggregates were assessed by DLS on a Zetaziser (Nano Series NS, ZEN3600, Malvern Instruments Ltd, UK).

Circular Dichroism

The CD measurements were performed in the way described previously on pages 21-22.

3. Results

a) Aggregation of the model peptides

The aggregation behavior of the newly-designed model peptides can be readily observed by eye when diluting the model peptides into buffer. The dissolution of βAP(25-35) in buffer at physiological pH and at ~ 100 μM concentration leads to the formation of small oligomers, evidenced either as precipitates on the walls of the glass vial or as small flakes when gently agitating the solution. No precipitates or flakes can be detected by eye at pH 4.0 or when βAP(25-35) is pretreated with HFIP. The same simple experiment was performed with the two model peptides. The solution of βAP(25-35)_I32W appears to be clear both at pH 7.4 and 4.0, whether the peptide is pretreated with HFIP or not and no aggregates were observed by eye. This confirms the low peptide aggregation factor calculated earlier with TANGO (Table 1). In contrast, the dissolution of dry WβAP(25-35) in buffer at pH 7.4 leads to the spontaneous formation of very large aggregates. At pH 4.0 without pretreatment and also at both pH if WβAP(25-35) is pretreated with HFIP, no aggregates can be detected by eye. Visual observation agrees again with the aggregation factors in Table 1: WβAP(25-35) and βAP(25-35) have both a higher tendency to aggregate at pH 7.4 than at pH 4.0. In order to have a closer view of these aggregates, pictures of the various peptide solutions were taken under a light microscope (Figure 3).

The pictures allow an estimate of the size of the aggregates formed in the various solutions. Pretreated or not, βAP(25-35)_I32W forms only small oligomers ranging from 3 to 10 μm at both pH values (Figure 3C). In βAP(25-35) and WβAP(25-35) solutions at pH 7.4, large heterogeneous oligomers are favored. In Figure 3A, βAP(25-35) oligomers with size between 8 and 29 μm are detected. The large aggregates of WβAP(25-35) in Figure 3B are very thick and unstructured; their size varies between 22 and 110 μm. If βAP(25-35) and WβAP(25-35) are pretreated or

dissolved as powder in pH 4.0 buffer, similar aggregates to the ones observed in Figure 3C are observed (results not shown).

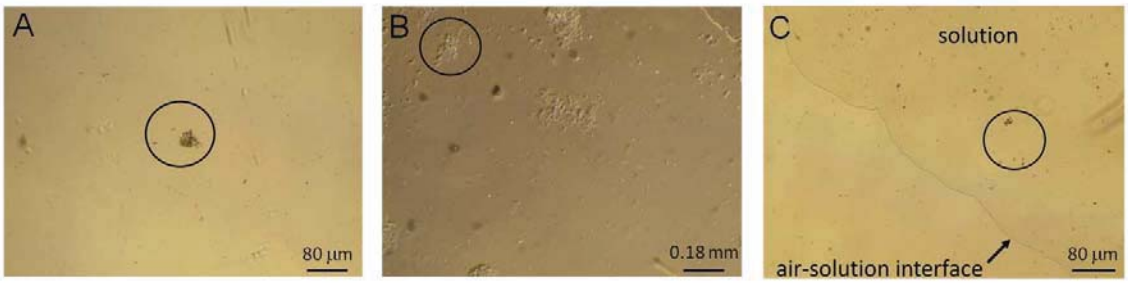

***Figure 3**: Pictures of aggregates observed for βAP(25-35), WβAP(25-35) and βAP(25-35)_I32W in solution. (A) βAP(25-35) and (B) WβAP(25-35) were prepared at 230 µM in HEPES pH 7.4 following dissolution 1. (C) βAP(25-35)_I32W at 230 µM in AcONa pH 4.0 was prepared following dissolution 2. The black circles indicate representative aggregates.*

The aggregates shown in Figure 3 are observed at 230 µM peptide concentration but the biophysical study will use HFIP-treated peptides at concentrations ranging down to 5 µM. Studies in this lower concentration range require a different technique. The appropriate technique for this purpose is dynamic light scattering (DLS) as it allows the observation of aggregates between 1 nm and 1 µm. The scattering intensity of the aggregate populations and their size are displayed in Figure 4.

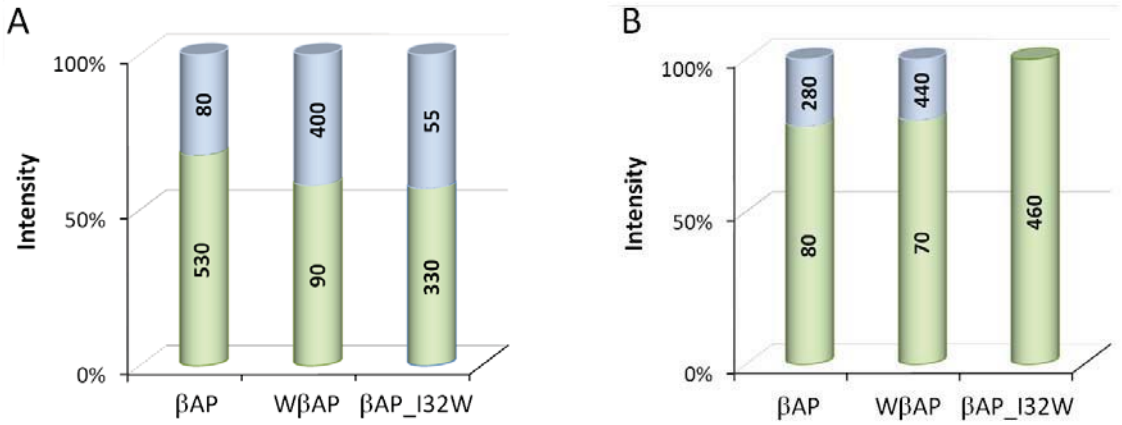

***Figure 4**: Size distribution of the aggregate populations by DLS in HFIP pretreated peptide solutions at (A) pH 7.4 and (B) pH 4.0. βAP(25-35), WβAP(25-35) and βAP(25-35)_I32W are respectively (A) at 17, 9 and 3 µM and (B) at 8, 12 and 6 µM. The major population is depicted in green and the minor population in blue. The average size (in nm) of the composing aggregates is indicated on each bar.*

βAP(25-35) is composed of two aggregate populations both at pH 7.4 and 4.0 but their proportions differ with the pH value. At pH 7.4, 530 nm particles account for 67% of the light scattering, whereas 33% intensity is due to ~ 80 nm particles. At pH 4.0, the ~ 80 nm particles are predominant (78%) and the ~ 280 nm wide particles represent only 22% of the oligomers. WβAP(25-35) forms aggregates of ~ 90 nm (58%) and ~ 400 nm (42%) size at pH 7.4. At pH 4.0, two oligomer populations of ~ 70 nm (80%) diameter and of ~ 480 nm diameter (20%) are observed. βAP(25-35)_I32W is composed of ~ 330 nm (57%) and ~ 55 nm (43%) wide particles at pH 7.4. Only one population of βAP(25-35)_I32W aggregates is observed at pH 4.0, these particle are ~ 460 nm wide. HFIP pretreatment does not lead to an exclusively monomeric solution. In most cases studied, at least two aggregate populations are observed.

The DLS experiment provides an estimate of the size reached by the amyloid oligomers in the low concentration range studied. The size of the aggregates changes over time and the big aggregates tend to sediment. Therefore it is probable that the peptide solutions are constituted by a distribution of particles with a diameter ranging from 70 to 500 nm, or even larger diameters. It seems that the aggregates of βAP(25-35) and WβAP(25-35) tend to be smaller at pH 4.0, in accordance with the aggregation factor given in Table 1. However βAP(25-35)_I32W forms bigger aggregates at pH 4.0 than at pH 7.4, which is in contrast to the TANGO predictions (see Table 1). These results show however that HFIP pretreated peptides aggregate at both pH values in this lower concentration range. The size of the measured particles is of the same order for each peptide. Only βAP(25-35)_I32W forms bigger aggregates at pH 7.4 than the other two peptides studied.

b) Fibrillization kinetics of the model peptides

The ability of the designed peptides to form fibrils was studied following the protocol detailed in Materials and Methods (see pages 39-40). The time course of fibrillization can be followed by the change of Th T fluorescence and give indications on its kinetics. This widely used benzothiazole dye binds specifically to fibrils that form anti-parallel β-sheet, without binding to monomeric or oligomeric intermediates[11]. The

binding mechanism of Th T to stacked β-sheets is not understood yet. However the fluorescence intensity is proportional to the amount of amyloid fibrils formed[11]. The excitation of Th T at 450 nm results in fluorescence emission at 482 nm. Fibrillization of each of the three peptides was followed at pH 7.4 with a peptide concentration of 230 μM. The results are shown on Figure 5.

Figure 5A shows that the fluorescence intensity of Th T bound to βAP(25-35) is higher than that induced by the two analogs. This disagrees with the imaging results (see Figure 3): the microscope pictures showed more and larger aggregates at pH 7.4 for WβAP(25-35) than for βAP(25-35) and βAP(25-35)_I32W. The magnification of the same data in Figure 5B shows that Th T bound to βAP(25-35) and WβAP(25-35) gives rise to similar fluorescence spectra. During the first 30 minutes of the experiment, a lag phase is observed and no fluorescence can be detected for both peptides. Following this waiting period, the fluorescence intensity starts to increase, indicating fibril formation. Maximum fluorescence intensity is reached after 120 and 50 min for WβAP(25-35)and βAP(25-35), respectively. After this fibrillization period, a gradual decrease of fluorescence intensity is registered until the end of the experiment (10-20% decrease).

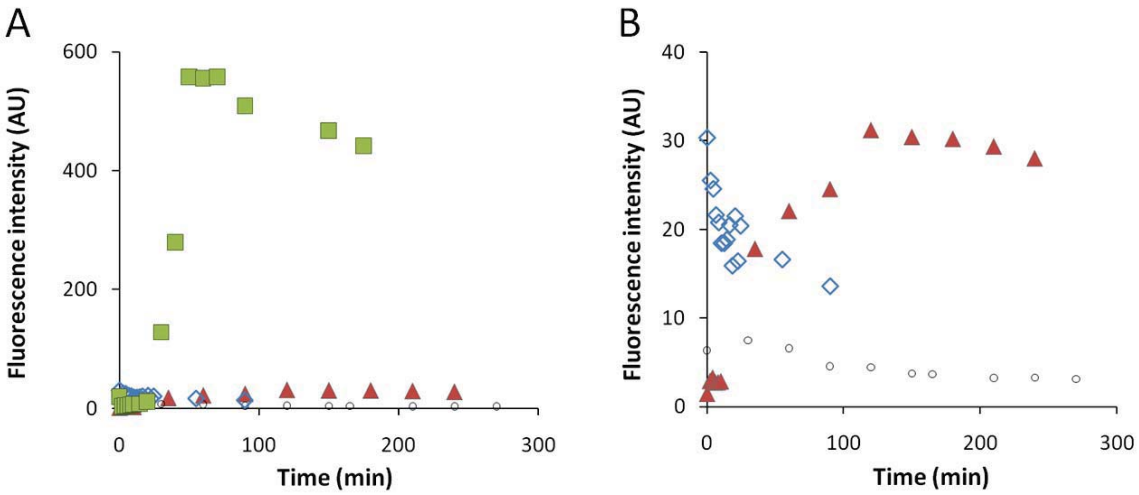

***Figure 5**: Time course of Th T fluorescence in the presence of βAP(25-35), WβAP(25-35) and βAP(25-35)_I32W at pH 7.4. (A) HFIP pretreated peptides at ~230 μM were prepared following procedure 2. The evolution of ThT fluorescence alone (○), and in presence of βAP(25-35) (■) , WβAP(25-35) (▲), or βAP(25-35)_I32W (◇) are displayed. (B) Magnification of (A) showing ThT fluorescence in the presence of the analog peptides only. The experiment was repeated and a similar behavior was observed. A representative result is shown here.*

The evolution of Th T fluorescence intensity in presence of βAP(25-35)_I32W follows another trend. It starts at the maximum fluorescence intensity and the fluorescence keeps decreasing over the measuring period; a 60% decrease in fluorescence intensity is measured. The variations of Th T fluorescence in presence of the βAP(25-35)_I32W is not characteristic of fibril formation. However the microscopy and DLS studies performed previously showed that βAP(25-35)_I32W and WβAP(25-35) aggregate (see Figure 3 and 4). The fluorescence study summarized in Figure 4 does not allow their detection, or not to the expected extent. The aggregates observed in microscopy appear not to be assemblies of β-sheet, or fibrils.

c) Secondary structure of the model peptides in aqueous solutions

The circular dichroism, CD, spectra of the two HFIP treated model peptides are displayed in Figure 6. All spectra show a minimum at 195-197 nm, characteristic of a random-coil structure. Yet the low mean residue ellipticity compared to a 100% random-coil spectrum implies the presence of another component. Details of the secondary structure can be obtained by spectral decomposition in terms of α-helix, β-sheet, random-coil and β-turn (Table 2).

***Table 2**: Secondary structure component of the WβAP(25-35) and βAP(25-35)_I32W at pH 7.4 and 4.0. α-helix, β-sheet, random-coil and β-turn contents are expressed as percentage of the whole peptide secondary structure. The coefficient of determination R^2 gives an indication on the quality of the fit and is comprised between 0 and 1. Only the concentrations leading to reasonable fitting are represented here.*

	Concentration (μM)	**α-helix** (%)	**β-sheet** (%)	**random-coil** (%)	**β-turn** (%)	**R^2** /
WβAP(25-35), HFIP pH 7.4	152	0	30	58	12	0.91
	354	0	27	61	12	0.97
WβAP(25-35), HFIP pH 4.0	93	0	26	56	18	0.93
	157	0	28	53	19	0.79
βAP(25-35)_I32W pH 7.4	69	0	32	62	6	0.97
	277	0	30	63	7	0.97
	554	0	29	60	11	0.98
βAP(25-35)_I32W pH 4.0	22	0	28	56	16	0.99
	98	0	28	57	15	0.98
	407	0	30	58	12	0.97

The secondary structure of βAP(25-35)_I32W at pH 7.4 is independent of the peptide concentration: the spectra obtained at different concentrations are identical (Figure 6C). They are constituted by about 60% random-coil and 40% β-content.

At pH 4.0, an increase in βAP(25-35)_I32W concentration induces an increase in the mean residue ellipticity (Figure 6D). A small increase of β-sheet can be observed when βAP(25-35)_I32W concentration increases (Table 2). The spectrum of βAP(25-35)_I32W at 11 μM deviates from the others at higher wavelengths, which can be attributed to a lower signal-to-noise ratio.

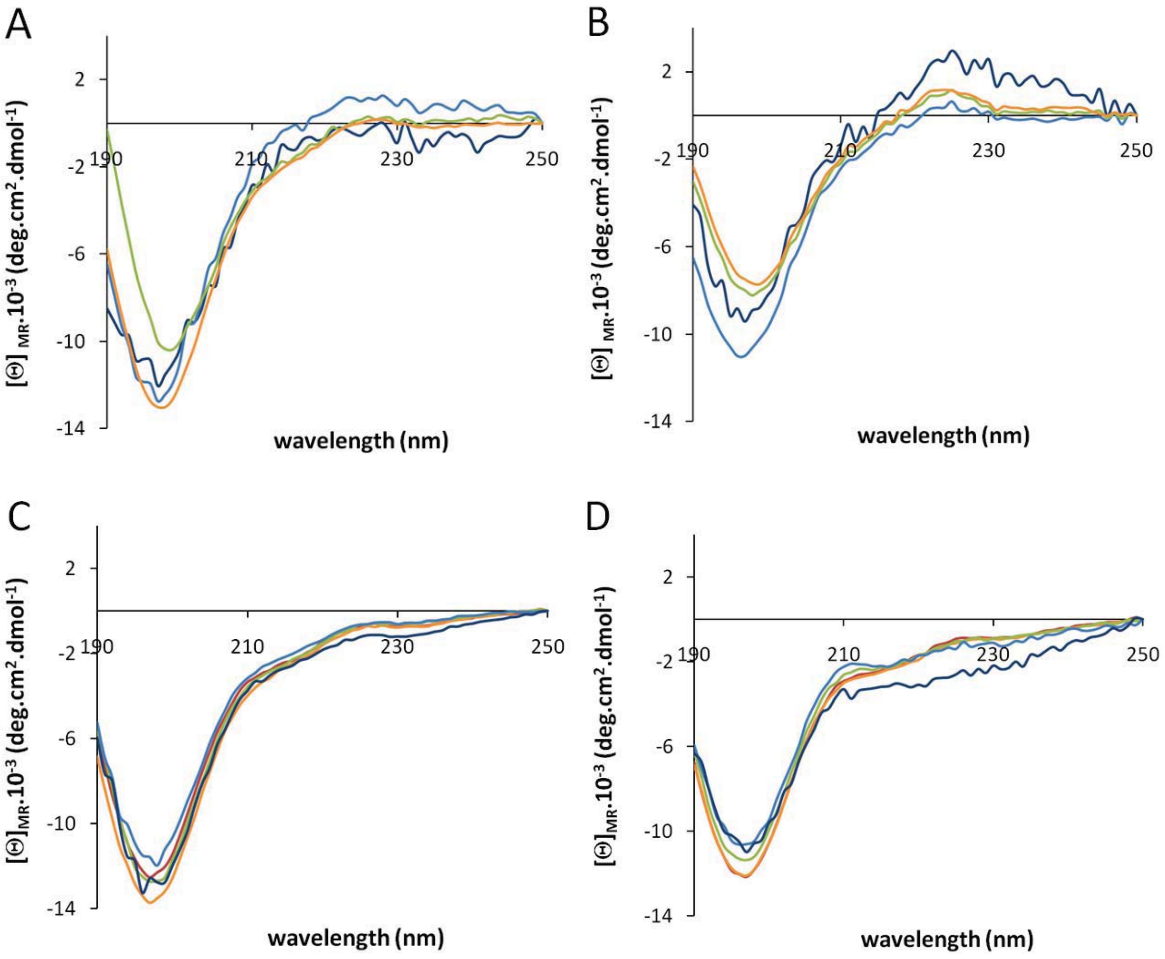

***Figure 6**: CD spectra of HFIP-pretreated WβAP(25-35) at (A) pH 7.4 and (B) pH 4.0 and non-treated βAP(25-35)_I32W at (C) pH 7.4 and (D) pH 4.0. Peptide concentration was determined from tryptophan UV absorption at 280 nm in parallel to the CD measurement.*
WβAP(25-35) was prepared following dissolution 2 in 5 mM HEPES at 37 (—), 63 (—), 152 (—), and 354 μM (—) (A) and in 5 mM AcONa at 29 (—), 93 (—), 137 (—), and 157 μM (—) (B). βAP_I32W prepared following dissolution 1 in 5 mM HEPES at 31 (—), 69 (—), 139 (—), 277 μM (—), and 554 μM (—) (C) and in 5 mM AcONa at 11 (—), 22 (—), 46 (—), 98 μM (—), and 407 μM (—) (D).

In contrast, the CD spectra of WβAP(25-35) cannot be superimposed although they are very similar (Figure 6A and B). Slight structural changes are observed on the spectra that are not reflected in the structural analysis (see Table 2). Also the signal-to-noise ratio is lower, decreasing the quality of the spectral analysis. However at pH 7.4, random-coil represents nearly 60% and β-content 40% of the whole spectra. At pH 4.0, slightly less random-coil (55%) and more β-structure (45%) are calculated. The CD signal of WβAP(25-35) at pH 4.0 is positive at 225 nm. This positive contribution is also observed at pH 7.4, and at both pH values for βAP(25-35)_I32W, but it is weaker. It can originate from the aromatic side chain of the Trp that was shown to have a contribution at 226 nm, similar to Phe[12-14].

The CD spectra of HFIP treated βAP(25-35)_I32W give similar results to non-treated βAP(25-35)_I32W (see Figure 7), what agrees with the light microscope study.

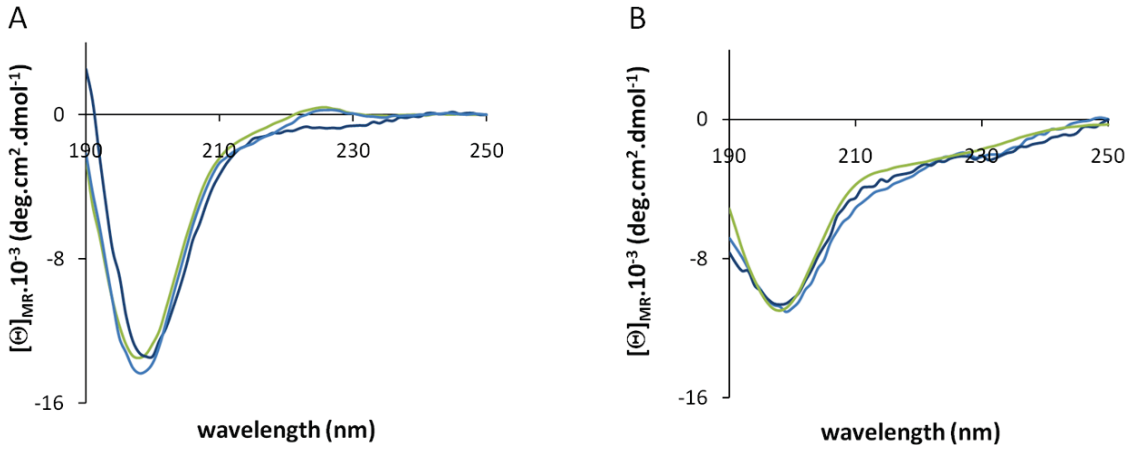

***Figure 7**: CD spectra of HFIP pretreated βAP(25-35)_I32W at (A) pH 7.4 and (B) pH 4.0. The peptide concentration was determined from Trp UV absorption at 280 nm in parallel to the CD measurement.*
βAP(25-35)_I32W was prepared following dissolution procedure 2 (A) in 5 mM HEPES at 46 (—), 67 (—) ,and 77 (—) μM and (B) in 5 mM AcONa at 81 (—), 97 (—), and 251 (—) μM .

The CD spectra prove that the aggregates observed by light microscopy (Figure 3) and DLS (Figure 4) have a β-sheet contribution of ~ 40%. The previously determined aggregation factor (Table 1) indicated a stronger tendency to aggregate at pH 7.4 than at pH 4.0 for all peptides. This trend is not observed in the CD experiments.

4. Discussion

Aggregates could be observed by eye in the peptide solutions at 230 μM and their size was evaluated with microscope imaging. It varies from 8 to 100 μm. At the lowest concentrations (μM range), the particles size measured with DLS ranged from 70 to 630 nm. These results can be compared to the aggregates sizes listed in the literature. The size of oligomeric species is reported to range from 10 to 15 nm[15], protofibrils are found with a diameter between 2.7 and 4.2 nm and a length of more than 100 nm[16], while fibrils reach several micrometers in size. In the experiments shown previously at high peptide concentration (> 100 μM), the particles observed have a similar size range as fibrils, although a fibrillar structure could not be confirmed and only unstructured aggregates were observed. In the lower concentration range (< 30 μM), the small particles detected are probably protofibrils. These DLS experiments allow to conclude that the two model peptides aggregate to a similar extent as βAP(25-35) under the same experimental conditions.

Fibrillization was studied by Th T fluorescence. Despite the presence of aggregates in both model peptides solutions (Figure 3 and 4), Th T fluorescence in presence of the model peptides was much lower than with βAP(25-35). In the case of WβAP(25-35), binding occurs but it is very weak, compared to the propensity of the model peptide to aggregate (see Figure 3B). Considering the profile of Th T fluorescence in presence of βAP(25-35)_I32W, it seems that Th T binding to this model peptide is unspecific. One of the explanations is that Th T binding to WβAP(25-35) or βAP(25-35)_I32W fibrils is hindered by the presence of Trp. It could also be that the aggregates of WβAP(25-35) or βAP(25-35)_I32W observed are amorphous and do not assemble in anti-parallel β-sheets like βAP(25-35).

Although they occur in a different fluorescence intensity range, the time course of fibrillization of WβAP(25-35) and βAP(25-35) can be compared. For both peptides, a lag phase is observed[17], followed by fibril formation. The fluorescence decrease registered at the end of the measurement is certainly due to the formation of larger aggregates. Their reduced availability in the solution[11] lowers Th T affinity for the fibrils and decreases the fluorescence intensity registered. Part of the decrease in fluorescence can also be due to photobleaching.

CD experiments show that the three peptides studied have a similar secondary structure. Therefore the aggregates of WβAP(25-35) and βAP(25-35)_I32W observed in light microscopy and DLS are probably constituted by stacked β-sheets similar to βAP(25-35). It can be concluded that the discrepancies observed between the three peptides with Th T fluorescence originate from a low affinity of the dye for the two model peptides due to the presence of Trp. Trp is slightly more polar and has a bulkier sidechain than Ile with its acyl side chain. The indole group could stick out of the stacked β-sheets and prevent Th T interaction. This hindrance is less strong if the Trp is positioned at the N-terminal end of the peptide: the inner part of the stacked β-sheet is still available for binding to Th T.

Both WβAP(25-35) and βAP(25-35)_I32W aggregate with a similar secondary structure as βAP(25-35). Due to the Trp chromophore, the concentration is accurately determined and can be excluded as a source of error. Consequently any mean residue ellipticity variation is likely to be caused by structural changes. WβAP(25-35) and βAP(25-35)_I32W are suitable model peptides to study βAP(25-35) aggregation and interaction with the lipid membrane.

5. References

(1) Ma, B.; Nussinov, R. *Biophys J* **2006**, *90*, 3365.
(2) Nagarajan, S.; Ramalingam, K.; Neelakanta Reddy, P.; Cereghetti, D. M.; Padma Malar, E. J.; Rajadas, J. *FEBS J* **2008**, *275*, 2415.
(3) Terzi, E.; Holzemann, G.; Seelig, J. *Biochemistry* **1994**, *33*, 7434.
(4) Sato, K.; Wakamiya, A.; Maeda, T.; Noguchi, K.; Takashima, A.; Imahori, K. *J Biochem* **1995**, *118*, 1108.
(5) Touchette, J. C.; Williams, L. L.; Ajit, D.; Gallazzi, F.; Nichols, M. R. *Arch Biochem Biophys* **2010**, *494*, 192.
(6) Schibli, D. J.; Epand, R. F.; Vogel, H. J.; Epand, R. M. *Biochem Cell Biol* **2002**, *80*, 667.
(7) Zhao, H.; Kinnunen, P. K. *J Biol Chem* **2002**, *277*, 25170.
(8) Oh, D.; Shin, S. Y.; Lee, S.; Kang, J. H.; Kim, S. D.; Ryu, P. D.; Hahm, K. S.; Kim, Y. *Biochemistry* **2000**, *39*, 11855.
(9) Fernandez-Escamilla, A. M.; Rousseau, F.; Schymkowitz, J.; Serrano, L. *Nat Biotechnol* **2004**, *22*, 1302.
(10) Linding, R.; Schymkowitz, J.; Rousseau, F.; Diella, F.; Serrano, L. *J Mol Biol* **2004**, *342*, 345.
(11) LeVine, H., 3rd *Arch Biochem Biophys* **1997**, *342*, 306.
(12) Holladay, L. A.; Puett, D. *Biopolymers* **1976**, *15*, 43.
(13) Holladay, L. A.; Rivier, J.; Puett, D. *Biochemistry* **1977**, *16*, 4895.
(14) Seelig, A.; Alt, T.; Lotz, S.; Holzemann, G. *Biochemistry* **1996**, *35*, 4365.
(15) Hoshi, M.; Sato, M.; Matsumoto, S.; Noguchi, A.; Yasutake, K.; Yoshida, N.; Sato, K. *Proc Natl Acad Sci U S A* **2003**, *100*, 6370.
(16) Kayed, R.; Head, E.; Thompson, J. L.; McIntire, T. M.; Milton, S. C.; Cotman, C. W.; Glabe, C. G. *Science* **2003**, *300*, 486.
(17) Come, J. H.; Fraser, P. E.; Lansbury, P. T., Jr. *Proc Natl Acad Sci U S A* **1993**, *90*, 5959.

V. Appendix: Solid-Phase Peptide Synthesis of βAP(25-35)_I32W

1. Introduction

Solid-phase peptide synthesis (SPPS) was introduced by Merrifield in 1963[1]. It consists in the successive addition of protected amino-acids onto a polymer resin, often made of cross-linked styrene and divinylbenzene. The strategy of a resin-based synthesis provides the advantage that the resin is retained by a filter, whereas non-reacted amino acids can be flushed through the filter. This results in a very rapid cycling of the synthesis steps. The steps of SPPS consist of the addition of activated and protected amino-acid onto the resin, its deprotection and subsequent coupling with the next protected amino-acid. A large choice of resins, amino acid protecting groups and activating reagents is available that afford different synthesis yields. Especially hydrophobic amino acids have a tendency to self-associate on the resin, so that reaction conditions must be optimized for each peptide of interest [2].

Various research groups describe the synthesis of a fragment or the full-length βAP(1-42). Most often, they report peptide aggregation on the resin due to the high hydrophobicity of the peptide caused by the high content in Ala, Ile, Gly, and Leu [3,4]. These interpeptidic hydrophobic attractions disturb the coupling of subsequent amino-acids by quite different means[5]. For example, on-resin aggregation influences the deprotection of the N-terminal end and thus often leads to final peptide mixtures of various lengths and compositions. Secondary reactions have been also reported for βAP(1-42), such as N-O intramolecular acyl migration[6,7] occurring especially for Ser, thus causing racemization reactions[8,9] or reactions between the coupling agents. The

work below describes a first trial of the synthesis of βAP(25-35)_I32W (amino-acid sequence GSNKGAIWGLM) and briefly proposes ways to further improve it.

2. Materials and method

a) Chemicals

Fmoc-protected L-amino-acids, Met-loaded low density (0.2-0.4 mmol/g) Wang resin together with O-Benzotriazole-N,N,N',N'-tetramethyl-uronium-hexafluoro-phosphate (HBTU) and hydroxybenzotriazol (HOBt) were bought from Nova Biochem (Merck). 1-methyl-2-pyrrolidon (NMP), N,N-diisopropylethylamine (DIEA), dimethylsulfid (DMS), tert-butyl-methylether (TBME), piperidine, acetonitrile and dichloromethane (DCM) were bought from Sigma-Aldrich (Schnelldorf, Germany). Tetrabuthylammonium iodide (TBAI), thioanisole, ethanedithiol and trifluoro acetic acid (TFA) were bought from Fluka. All solvents were of HPLC grade and were used without further purification.

b) Peptide synthesis

Solid-phase peptide synthesis of βAP(25-35)_I32W was performed on an Applied Biosystems 433A (Rotkreuz, Switzerland). Amino-acid side-chain protecting groups were: triphenylmethane (Trt) for Asn and Ser, tert-butyloxycarbonyl (Boc) for Lys and pentamethyldihydrobenzofuransulfonyl (Pbf) for Arg. A starting quantity of 0.1 mmol of resin was used, and the amino-acids were used in 10-fold excess. The Fmoc-protected amino-acids were activated with a 0.5 M HBTU/HOBt solution in DMF complemented with DIEA at 2 M in DMF. After resin rinsing, the coupled amino acids were deprotected with a 20% piperidine solution during 5 min.

After completion of the synthesis, the resin-coupled peptide was washed with DCM and dried under high vacuum. The cleavage from the resin was made by a mixture of TFA/thioanisole/ethanedithiol/H_2O/DMS/TBAI (85/5/3/3/2/2, v/v/v/v/v/v, 5 ml) under protection with Argon[10]. After 2 h, the peptide was recovered from the resin and precipitated in cold TBME. The resin was washed with ~ 2 ml of cleavage solution. The peptide in TBME was centrifuged at 6°C for 30 min and 3000 rpm,

dissolved in 5 ml H_2O and lyophilized. After lyophilization, the crude peptide was purified by reverse-phase HPLC (C8 column) and its purity was checked by analytical high-pressure liquid chromatography.

c) Purification

HPLC purification was performed on a Gilson instrument consisting of a 321 pump associated with a diode-array spectrophotometer 8452A (Hewlett Packard). A Hibar pre-packed lichrosorb column RP 8 (250 x 25 mm, 7 μm) was used, and the solvent consisted of a gradient of A: H_2O and 0.1% TFA, B: acetonitrile and 0.1% TFA. The flow rate was set to 18 ml/min and the gradient of B was chosen from 5 to 80% within 75 min[10]. The peptide sequences were detected at 230 nm, 280 nm and 300 nm, respective wavelengths of absorption of the peptide bond, Trp and Fmoc. The mass of the peptide was confirmed by MALDI-MS in a sinapinic acid matrix.

3. Results and discussion

The peptide was synthesized on a low density Wang resin. Its low grafting density resin reduced the risk for peptide aggregation. The HPLC of the crude peptide is shown in Figure 1.

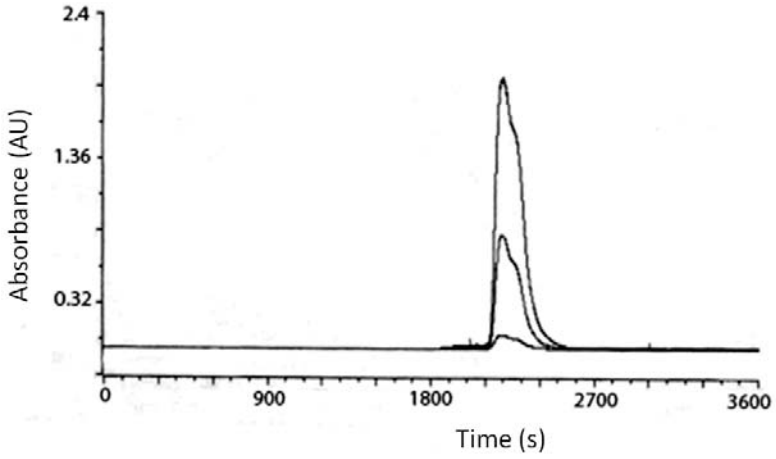

***Figure 1**: Elution profile of the synthesized peptide at 230, 280 and 330 nm. The absorbance traces are specific for Fmoc, the peptide bond and Trp (from bottom to top).*

The right-hand shoulder of the main peak suggests that at least two peptides are present that are hardly separated by HPLC. A mass spectrometry analysis helped to identify the second peptide. Figure 2 shows the mass spectra of the mixture.

MALDI confirmed the two peptides in their protonated form and as sodium adduct: βAP(25-35)_I32W has a protonated molecular weight of 1135.1 g.mol^{-1} (sodium adduct: 1157.1), and peptide X had a molecular weight of 1117.0 g.mol^{-1} (sodium adduct 1139.0). The two peptides have a m/z difference of 18 g.mol^{-1} suggesting the loss of water in the structure. This might be attributed to aspartimide formation [11] that is catalyzed by the use of strong bases in the synthesis [12,13,14]. Peptide X is thus likely composed of the desired peptide βAP(25-35)_I32W, where Asn27 underwent cyclization.

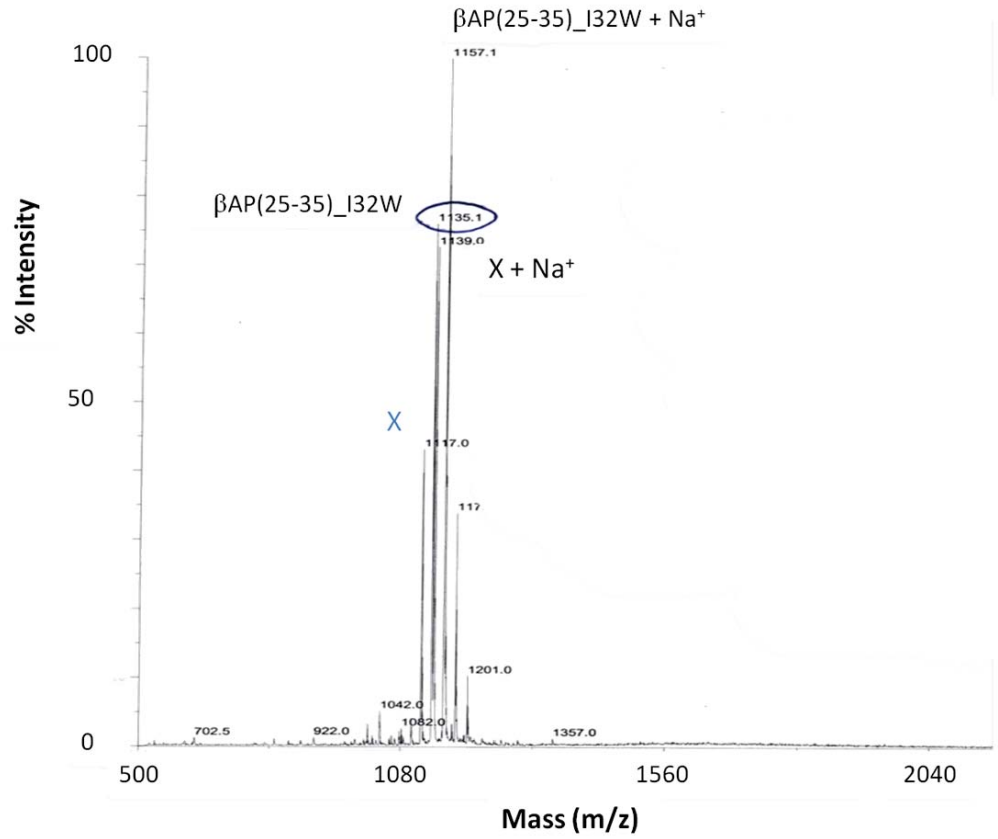

Figure 2: *MALDI mass spectra of the synthesized peptide. The expected peptide is designed as βAP(25-35)_I32W and the secondary product as X. Both peptides are present in their protonated and sodium adduct.*

In future attempts, this secondary product could be reduced by replacing piperidine by piperazine. Piperazine is a less nucleophilic deprotecting agent, but slows

down the deprotection reaction[18]. The higher peptide purity will thus be compensated by a lower total yield. Also the addition of phenols or hydroxybenzotriazole (HOBt) in the deprotecting solution[8,18,19] might buffer amines and thus might reduce the Asn cyclization. Another possibility would be to replace the Trt protecting group of the amine in γ of Asn27 by a bulkier group[20,21] that would make the nuclophilic attack of the nitrogen atom in α more difficult.

4. Conclusions

The peptide synthesis of βAP(25-35)_I32W yielded the peptide of interest to 60%, but also a derivative of it because of aspartimide formation. The HPLC separation of the two peptides appears to be difficult because of their close hydrophobicity and molecular weight. Therefore future attempts must focus on optimization of the synthesis.

5. References

(1) Merrifield, R. B. *Journal of the American Chemical Society* **1963**, *85*, 2149.
(2) Kaminski, Z. J.; Kolesinska, B.; Kolesinska, J.; Sabatino, G.; Chelli, M.; Rovero, P.; Blaszczyk, M.; Glowka, M. L.; Papini, A. M. *J Am Chem Soc* **2005**, *127*, 16912.
(3) Burdick, D.; Soreghan, B.; Kwon, M.; Kosmoski, J.; Knauer, M.; Henschen, A.; Yates, J.; Cotman, C.; Glabe, C. *J Biol Chem* **1992**, *267*, 546.
(4) Tickler, A. K.; Clippingdale, A. B.; Wade, J. D. *Protein Pept Lett* **2004**, *11*, 377.
(5) Krchnak, V.; Flegelova, Z.; Vagner, J. *Int J Pept Protein Res* **1993**, *42*, 450.
(6) Elliott, D. F. *Biochem J* **1952**, *50*, 542.
(7) Sohma, Y.; Hayashi, Y.; Skwarczynski, M.; Hamada, Y.; Sasaki, M.; Kimura, T.; Kiso, Y. *Biopolymers* **2004**, *76*, 344.
(8) Palasek, S. A.; Cox, Z. J.; Collins, J. M. *J Pept Sci* **2007**, *13*, 143.
(9) Schnolzer, M.; Alewood, P.; Jones, A.; Alewood, D.; Kent, S. B. *Int J Pept Protein Res* **1992**, *40*, 180.
(10) Nilsson, M. R.; Nguyen, L. L.; Raleigh, D. P. *Anal Biochem* **2001**, *288*, 76.
(11) Nicolàs, E.; Pedroso, E.; Giralt, E. *Tetrahedron Letters* **1989**, *30*, 497.
(12) Yamamoto, N.; Takayanagi, A.; Sakakibara, T.; Dawson, P. E.; Kajihara, Y. *Tetrahedron Letters* **2006**, *47*, 1341.
(13) Husbyn, M.; Orning, L.; Cuthbertson, A.; Fischer, P. M. *J Pept Sci* **1999**, *5*, 323.
(14) Cebrian, J.; Domingo, V.; Reig, F. *J Pept Res* **2003**, *62*, 238.
(15) Zahariev, S.; Guarnaccia, C.; Pongor, C. I.; Quaroni, L.; Cemazar, M.; Pongor, S. *Tetrahedron Letters* **2006**, *47*, 4121.
(16) Lauer, J. L.; Fields, C. G.; Fields, G. B. *Letters in Peptide Sciences* **1995**, *1*, 197.
(17) Ede, N. J.; Chen, W.; McCluskey, J.; Jackson, D. C.; Purcell, A. W. *Biomed Pept Proteins Nucleic Acids* **1995**, *1*, 231.
(18) Wade, J.; Mathieu, M.; Macris, M.; Tregear, G. *Lett. Pept. Sci.* **2000**, *7*, 107.
(19) Martinez, J.; Bodanszky, M. *Int J Pept Protein Res* **1978**, *12*, 277.
(20) Karlström, A.; Undén, A. *Tetrahedron Letters* **1996**, *37*, 4243.
(21) Offer, J.; Quibell, M.; Johnson, T. *J. Chem. Soc., Perkin Trans. 1* **1996**, 175.

VI. Amyloid β peptide interaction with the lipid membrane

1. Introduction

Amyloid peptide neurotoxicity[1,2] in Alzheimer's disease involves interaction with the lipid membrane. Small oligomers of βAP(1-40) are thought to create pores or ion channels in the membrane[3-5] but the structural evidence in support of this hypothesis is weak. Alzheimer's plaques are aggregates of βAP(1-40) to (1-42) deposited on the cellular membrane[6,7].

Terzi *et al.* showed that the interaction of βAP(1-40) and βAP(25-35) with lipid membranes induces a random-coil-to-β-sheet structural change[8,9]. The authors also studied the thermodynamics of the binding of βAP(25-35) to model membranes. They concluded that the interaction between the negatively-charged membrane and βAP was essentially electrostatic in nature because no binding between βAP(25-35) was observed in presence of high salt content.

In the following study, we use high-sensitivity titration calorimetry to study the binding of βAP(25-35), WβAP(25-35) and βAP(25-35)_I32W to model membranes at different temperatures and pH values. Special attention will be given to the effect of the inserted Trp on the binding mechanism. The changes of the secondary structure of each peptide upon binding to the lipid membrane will be followed with circular dichroism. Finally solid-state NMR experiments will be performed to investigate the structural changes of the lipid bilayer upon peptide binding.

2. Materials and Methods

Peptides

The amyloid peptide βAP(25-35) with the amino-acid sequence H-GSNKGAIIGLM-OH was bought from Bachem (H-1192). The mutant H-GSNKGAIWGLM-OH was bought at Peptide 2.0 (Chantilly, USA). The mutant H-WGSNKGAIIGLM-OH was ordered from AnaSpec (Fremont, USA). All peptides had purity higher than 95%. 1,1,1,3,3,3-hexafluoroisopropanol (HFIP) was from Sigma-Aldrich (Schnelldorf, Germany). The buffers used were either HEPES at pH 7.4 (Roth, Karlsruhe, Germany) or sodium acetate, AcONa, at pH 4.0 (Merck, Darmstadt, Germany) at 5 or 10 mM.

Unless specified differently, the peptides were prepared following dissolution procedure 2 (see Chapter III, page 21).

Lipids

1-palmitoyl-2-oleoyl-sn-glycero-3-phosphocholine (POPC, 850457C, molecular weight of 760.1 $g.mol^{-1}$), 1-palmitoyl-2-oleoyl-sn-glycero-3-[phospho-rac-(1-glycerol)] (POPG, 840457C, molecular weight of 770.9 $g.mol^{-1}$) and deuterated POPG, 1-palmitoyl(d31)-2-oleoyl-sn-glycero-3-[phospho-rac-(1-glycerol)] (860384C, molecular weight of 802.2 $g.mol^{-1}$) in chloroform were ordered from Avanti Polar Lipids (Alabaster, USA).

Small unilamellar vesicles (SUVs) of average size z = 50 nm, composed of POPC/POPG (3:1, mol/mol) were prepared as follows. The desired amount of POPC in chloroform was dried under a stream of nitrogen and then overnight under high vacuum. POPG in chloroform was added and the lipid mixture was vortexed and then dried as described for POPC. The desired amount of buffer was added and the dispersion vortexed. The multilamellar vesicles were sonified for 30 min under a stream of nitrogen (Branson sonifier S-250A equipped with a disruption horn, 200 W) until an almost clear dispersion of unilamellar vesicles was obtained.

Circular Dichroism(CD)

Circular dichroism measurements were performed on a Chirascan spectrophotometer (Applied Photophysics Ltd., Leatherhead, UK) using 0.5 mm

cuvettes (Hellma, Jena, Germany). The bandwidth was set at 1 nm, samples were measured every nanometer with an averaging time of 20 sec/point. The samples were scanned from 190 to 250 nm. All spectra were corrected by subtracting buffer baseline or the spectra of the SUVs in buffer.

The lipid vesicles prepared by the above procedure were equilibrated with peptide under stirring for 20 min before the start of the CD measurement. Results are expressed in terms of ellipticity in units of $deg.cm^2.dmol^{-1}$. The conversion into mean residue ellipticity is performed as described in the Chapter III (page 21). The secondary structure was analyzed by spectral fitting based on the linear combination of a CD spectra of peptide database[11].

Dynamic Light scattering (DLS)

The diameter of the small unilamellar vesicles (SUVs) was measured by DLS (Nano Series NS, ZEN3600, Malvern Instruments Ltd, UK) and their average size was about 50 nm at both pH values as shown in Figure 1.

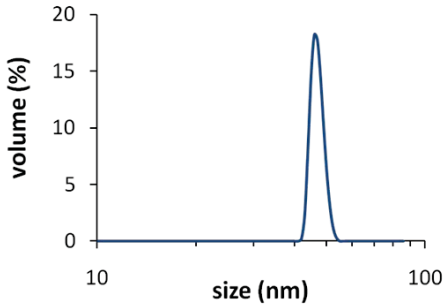

Figure 1*: Size distribution for POPC/POPG SUVs (3:1) dispersed in 10 mM HEPES buffer at pH 7.4. The average size z = 49 nm, and the peak width is 12 nm.*

This average size of POPC/POPG vesicles is larger than that of POPC SUVs with an average size z ~ 30 nm. The presence of the negatively-charged POPG molecules and the low ionic strength of the buffer solution favor a slightly larger vesicle diameter. From the size of the SUVs and assuming a bilayer thickness[10] of 4 nm, we can determine the outer membrane surface at 7855 nm^2 and the inner surface membrane at 5540 nm^2. This indicates a proportion of 59% of lipids that are accessible to the amyloid peptides for binding.

Isothermal Titration Calorimetry (ITC)

Isothermal titration calorimetry was performed with a VP ITC instrument (Microcal, Northampton, MA). The cell volume was V_{cell} = 1.4037 ml. The peptide solution and lipid dispersion were degassed under vacuum and equilibrated at the experimental temperature for 10 min before filling the cells and syringe. The heats of reaction were corrected with the heat of dilution of POPC/POPG titrated into buffer. Raw data were processed using the Origin software provided by Microcal.

Ultra-violet spectroscopy (UV)

The samples were monitored on a Uvikon 860 (GOEBEL Instrumentelle Analytik, Germany) with the buffer spectrum as a reference. A 1 cm cuvette was used (Hellma, Jena, Germany). Peptide concentration was determined from the absorption measured at 280 nm.

Solid-state Nuclear Magnetic Resonance (NMR)

Solid state phosphorus NMR experiments were performed on a Bruker Advance 400 MHz spectrometer (Bruker AXS, Karlsruhe, Germany). Spectra were recorded at 162 MHz using a pulse-acquire sequence with broadband proton decoupling and a recycle delay of 6 s. The excitation pulse length was 10 μs and 1000 FIDs were accumulated. The chemical shielding anisotropy, $\Delta\sigma$, was determined as the width at 10% of the maximum intensity of the powder type spectra.

Solid state deuterium NMR experiments were recorded at 61 MHz using a quadrupole echo sequence. The excitation pulse had a length of 5.5 μs. 20 K FIDs were accumulated with a recycle delay of 250 ms.

Preparation of NMR samples

Peptides inserted into the membrane: 80 μl (216 μM) of peptide dissolved at 1 mg/ml in HFIP, 7.5 mg (28 mM) of POPC and 250 μl (9 mM) of d_{31}-POPG at 10 mg/ml in chloroform were dried under a stream of nitrogen and then under high vacuum overnight. The film was dispersed in 10 mM HEPES in ^{2}H-depleted H_2O by vortexing in order to form multilamellar vesicles containing the peptide. 10 freeze-thaw cycles

were made to obtain homogeneous multilamellar vesicles. Each freeze-thaw cycle consists of three steps: freezing the sample at -80°C, warming it up to room temperature and vortexing it. The molar peptide-to-lipid ratio was 1:170.

Peptides adsorbed to the membrane surface: Homogeneous multilamellar vesicles were prepared with 7.5 mg (28 mM) of POPC and 250 μl (9 mM) of d_{31}-POPG at 10 mg/ml in chloroform as described in the previous paragraph (*Peptides inserted into the membrane*). Eventually 800 μM of dry peptide was added to the lipid dispersion and the mixture was vortexed. The molar peptide-to-lipid ratio was 1:50.

3. Results

a) Peptide binding to the membrane studied with ITC at pH 4.0

Two types of titrations can be performed in ITC[13,14]: either the peptide solution is injected into the lipid dispersion, or the lipid vesicles are injected into the peptide solution. In the first case, as the lipids are much in excess compared to the peptide, all peptide molecules injected will bind to the lipid vesicles provided the binding constant is large. Each injection should give the same h_i, and $h_i / \delta n_i$ will provide the enthalpy of binding, ΔH^o. This type of experiment cannot be performed in the case of the amyloid peptide. A high peptide concentration (~ 100 μM) is needed in the syringe to produce significant heat release and this would lead to aggregation before injection. Only the second type of experiment, i.e. titration of lipid vesicles into a peptide solution, could therefore be performed. Measurements were made at pH 4.0 and pH 7.4. The peptide concentration is also the limiting parameter in this type of experiment: it should not be too high, to avoid aggregation, but not too low in order to generate a significant heat release. A typical calorimetric heat flow trace obtained by titration of βAP(25-35) with the negatively-charged POPC/POPG (3:1, mol/mol) SUVs is shown in Figure 2A. The binding between βAP(25-35) and the model lipid membrane at 20°C and pH 4.0 is exothermic. At each injection, heat of reaction is released by binding of peptide to lipid. At each SUVs addition, the free peptide concentration is reduced and gives rise to lower heats of reaction, until all free peptide in the sample cell is bound. The residual heat is the heat of dilution of the lipid dispersion in the buffer.

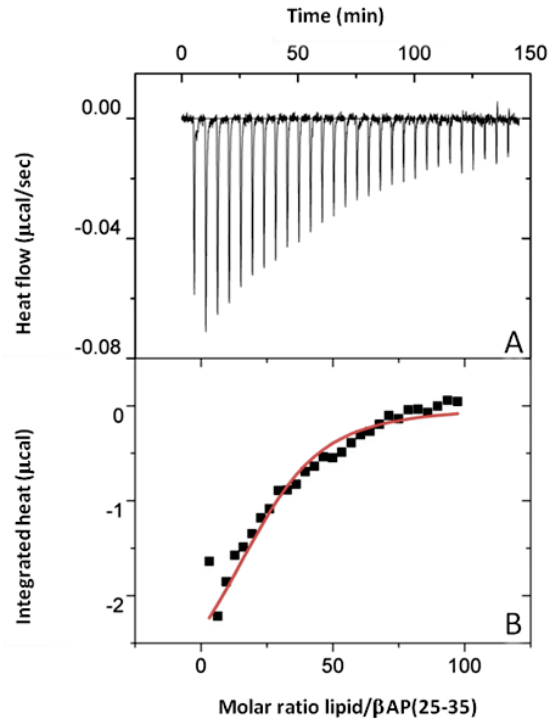

***Figure 2**: Titration of 12.3 µM βAP(25-35) in 10 mM AcONa at pH 4.0 with 5.5 mM SUVs in the same buffer. Each injection is 10 µl of POPC/POPG (3:1, mol/mol) suspension. The experiment was performed at 20°C. (A) Heat flow and (B) cumulative heat of reaction (■) as a function of the molar ratio of lipid to peptide. The theoretical binding isotherm (—) was calculated with the Gouy-Chapman theory combined with a surface partitioning equilibrium. The calculation assumes a binding constant K_o = 11 M^{-1} and a peptide effective charge z = +2.*

The molar binding enthalpy ΔH^o of amyloid peptide to POPC/POPG SUVs can be determined from the total heat released in the titration, $\sum h_i$, and the molar amount of peptide in the sample cell, n_o, according to:

$$\Delta H^0 = \frac{\sum h_i}{n_0} \qquad (1)$$

The integrated reaction heats are plotted against the molar lipid-to-peptide ratio in Figure 2B. The enthalpy of the reaction in Figure 2 is calculated according to Equation (1) with a total heat release of $\sum \Delta h_i$ = -20 µcal and assuming that the total amount of peptide in the calorimeter, n_o = 17 nmol, is bound. The calculation gives ΔH^o = -1.2 kcal.mol^{-1} (-5.0 kJ.mol^{-1}). The experiment was repeated in the temperature range of 10 to 40°C. For each temperature the enthalpy is calculated from two independent measurements. The calculated binding enthalpies ΔH^o are listed in Table 1. At all temperatures ΔH^o was measured at about -1.38 kcal.mol^{-1} (-5.8 kJ.mol^{-1}).

***Table 1**: Thermodynamic parameters for the binding of βAP(25-35), and WβAP(25-35) to SUVs composed of POPC/POPG (3:1, mol/mol) at various temperatures and pH 4.0. The data result from the average of two experiments and the standard deviation is indicated for the enthalpy and binding constant. The number of effective charges, z, is also indicated.*

	T (°C)	ΔH^0 (kcal/mol)	K_0 (M^{-1})	ΔG^0 (kcal/mol)	$T\Delta S^0$ (kcal/mol)	z /
βAP(25-35)	**10**	-1.42 ± 0.23	12 ± 0	-3.7	2.2	2
	20	-1.37 ± 0.13	11 ± 0	-3.7	2.4	2
	30	-1.36 ± 0.53	9.8 ± 0.4	-3.8	2.4	2
WβAP(25-35)	**10**	-7.18 ± 0.27	5 ± 0	-3.2	-4.0	2
	20	-2.49 ± 0.75	4 ± 0	-3.2	0.6	2
	25	-3.72 ± 0.52	4 ± 0	-3.2	-0.5	2
	30	-2.26 ± 0.42	4 ± 0	-3.3	1.0	2
	40	-3.71 ± 0.19	4.5 ± 0.7	-3.4	-0.3	2

High-sensitivity calorimetric experiments can allow the definition of a binding isotherm[15], X^i_b = f(c_f). It describes the extent of binding, X^i_b, as a function of the concentration of free peptide, c_f, at each injection of the titration. X^i_b is defined as the ratio between the molar amount of bound peptide, $n^i_{pep\ bound}$, and the molar amount of injected lipid available for binding, n^i_L, after i injections.

$$X_b^i = \frac{n_{pep,bound}^i}{n_L^i} \tag{2}$$

$n_L{}^i$ is given by the lipid concentration in the syringe, the volume of injection and the number i of injections performed. $n^i_{pep,bound}$ is determined from the experimental heats of reaction h_i as follows:

$$n_{pep,bound}^i = \frac{\sum_{i=1}^{k} h_k}{\Delta H^0 V_{cell} c_{pep}^0} \tag{3}$$

with $c_{pep}{}^o$ the total peptide concentration in the calorimeter cell and V_{cell} the volume of the calorimeter cell. The molar amount of peptide bound to the lipid membrane (Equation 3) combined with the principle of mass conservation allows the calculation of the free peptide concentration in solution. This provides the description of the binding isotherm without assuming a specific binding model. Figure 3 shows the binding isotherm corresponding to the ITC measurement of Figure 2.

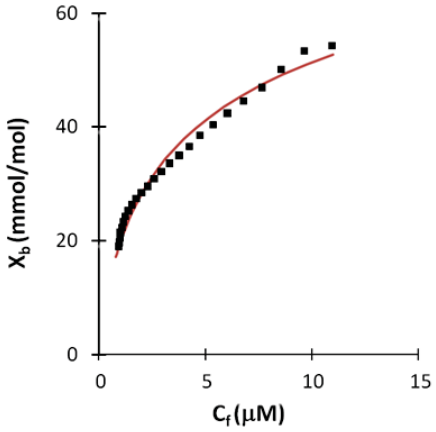

***Figure 3**: Binding isotherm of βAP(25-35) derived from the ITC experiment shown in Figure 2. The experimental extent of bound peptide per lipid of the outer monolayer (■) is plotted versus the equilibrium concentration of free peptide in solution. The theoretical binding isotherm calculated with the Gouy-Chapman theory combined with a surface partitioning equilibrium (—) is represented.*

The calculation of further thermodynamic parameters such as the binding constant or the free energy of the reaction requires the analysis of the binding isotherm. In the present context it is based on a surface partitioning model in which the peptide binding to the lipid membrane is dependent on the peptide affinity for the lipid and the concentration of peptide, c_M, found immediately above the plane of binding[16,17] according to:

$$X_b = K_0 c_M \tag{4}$$

with K_0 the intrinsic binding constant. The surface partitioning model takes into account the attraction of positively-charged peptides to the negatively-charged membrane surface. The peptide concentration at the membrane surface, c_M, is therefore higher than the peptide concentration in the bulk, c_f. The Boltzmann law expresses the electrostatic equilibrium between these two concentrations:

$$c_M = c_f e^{\left(\frac{-z_p F_0 \Psi}{RT}\right)} \tag{5}$$

where z_p is the peptide effective charge, Ψ is the membrane surface potential, F_0 is the Faraday constant and RT is the thermal energy. Ψ can be calculated from the Gouy-Chapman theory (see Appendix, page 91). It leads to the peptide concentration at the membrane surface after each lipid injection and finally to the intrinsic binding constant K_0, according to equation (4).

The binding model also assumes that the peptide does not penetrate into the membrane. Only the outside layer of the lipid membrane is accessible for peptide binding. The outer surface represents about 60% of the total amount of lipid (see Materials and Method, page 59). The model also takes into account the binding of sodium cations to the negatively-charged POPG with a Langmuir adsorption isotherm, using a binding constant of 0.6 M^{-1}. Finally at pH 4.0, an effective charge of +2 is attributed to the peptide. In effect, as the carboxyl end group is only partially protonated at acidic pH, the positive charge of the amino terminal end is not completely cancelled. The second charge is due to Lys28.

The ITC data of βAP(25-35) at each temperature were simulated with this model. As the heats of reaction were very small, not all experiments could be simulated. Only thermodynamic parameters based on a reasonable fitting are shown in Table 1.

The intrinsic binding constants K_0 of the reaction between βAP(25-35) and POPC/POPG SUVs at pH 4.0 are rather low and vary between 10 M^{-1} at 30°C and 12 M^{-1} at 20°C.

The free energy of binding ΔG^o follows from: $\Delta G^o = -RTln(55.5\ K_o)$ and has a value of ΔG^o = -3.7 kcal.mol^{-1} at 20°C (-15.5 kJ.mol^{-1}). The factor 55.5 is the molar concentration of water and corrects for the cratic contribution. The binding entropy can be derived from the second law of thermodynamics, $\Delta G^o = \Delta H^o - T\Delta S^o$ and $T\Delta S^o$ = 2.4 kcal.mol^{-1} at 20°C (10.0 kJ.mol^{-1}). The theoretical binding isotherm of the titration at 20°C is shown in Figure 3.

If the binding isotherm is expressed as a function of the free peptide concentration in the bulk, c_f, an apparent binding constant, K_{app}, is defined. The combination of equations (4) and (5) shows that K_{app} is not constant, but that it varies with the surface potential, and therefore with the progress of the titration (see Equation 6).

$$K_{app} = K_0 e^{\left(\frac{-z_p F_0 \Psi}{RT}\right)} \qquad (6)$$

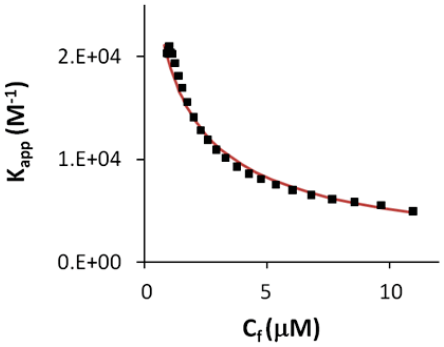

***Figure 4**: Variations of the apparent binding constant of βAP(25-35) to SUVs of POPC/POPG (3:1, mol/mol) with βAP(25-35) concentration at the membrane surface in 10 mM AcONa at pH 4.0.The change of K_{app} (■) and the best fit based on the Gouy-Chapman theory (—) are represented.*

Figure 4 shows the decrease of K_{app} with the concentration of free peptide in the cell. The apparent binding constant K_{app} varies from 4802 M^{-1} at c_f = 11.0 μM to 21096 M^{-1} at c_f = 0.8 μM at 20°C. The large difference between the apparent and intrinsic binding constants shows the importance of the electrostatic forces during the binding of βAP(25-35) to the lipid membrane.

The two designed model peptides, WβAP(25-35) and βAP(25-35)_I32W were studied in the same way at pH 4.0. The titration curve of WβAP(25-35) shows an exothermic profile, similar to the one of βAP(25-35) (see Appendix). The values of the binding enthalpy ΔH^o vary slightly around the mean binding enthalpy of -3.04 kcal.mol^{-1} (-12.7 kJ.mol^{-1}) between 20 and 40°C. These values are 2-fold higher than those measured for βAP(25-35). The intrinsic binding constants deduced after calculation with the binding model vary slightly between 4 and 5 M^{-1} (see Table 1). These values are similar to the ones observed with βAP(25-35). K_{app} varies from 4652 M^{-1} at c_f = 6.4 μM to 10040 M^{-1} at c_f = 0.9 μM at 20°C. The free energy is independent from the temperature and is close to -3.2 kcal.mol^{-1} (-13.3 kJ.mol^{-1}). The thermodynamic parameters calculated at 10°C deviate from those between 20 and 40°C. At lower temperatures, another binding mechanism could be involved.

βAP(25-35)_I32W showed an unusual ITC profile at lower temperatures. Two peaks are superimposed on the heat trace: one fast exothermic reaction followed by a slow endothermic process, as shown in Figure 5.

The calorimetric studies at higher temperatures showed exothermic profile similar to the ones observed for the binding of βAP(25-35) or WβAP(25-35). The heats of reaction were however too low to fit them with the binding model and the thermodynamic parameters could not be calculated. The ITC titrations measured between 10 and 35°C are shown in the Appendix.

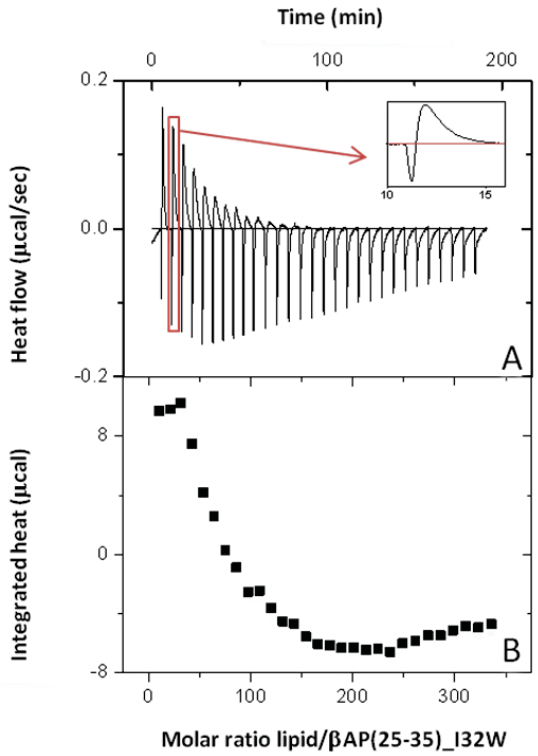

***Figure 5**: Titration of 3.7 µM βAP(25-35)_I32W in 10 mM AcON at pH 4.0 with 5.5 mM SUVs in the same buffer. Each injection is 10 µl of POPC/POPG (3:1, mol/mol) suspension. The experiment was performed at 10°C. (A) Heat flow and (B) cumulative heat of reaction (■) as a function of the molar ratio of lipid to peptide. The inset illustrates details of the heat flow during the second injection.*

b) Peptide binding to the membrane studied with ITC at pH 7.4

At pH 7.4 the ITC studies of βAP(25-35) and WβAP(25-35) showed low experimental reproducibility. Although the solutions of three HFIP-pretreated model peptides contained similar aggregate populations in DLS (Chapter IV), each sample of βAP(25-35) and WβAP(25-35) leads to a different calorimetric profile. The calorimetric study was therefore performed exclusively with βAP(25-35)_I32W at temperatures in the range of 10 to 30°C. A representative binding curve is shown in Figure 6.

Similar to the experiments at pH 4.0, the reaction is exothermic and the heats of reaction were small. No agreement was found between the experimental data and

the model, consequently the thermodynamic parameters could not be calculated. The ITC titrations are shown in the appendix.

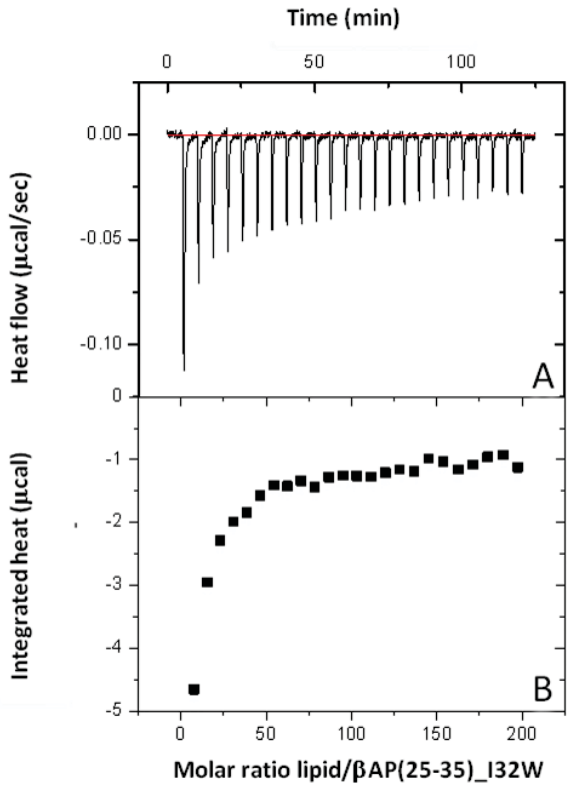

***Figure 6**: Titration of a 5.2 µM βAP(25-35)_I32W in 10 mM HEPES at pH 7.4 with 5.5 mM SUVs in the same buffer. Each injection is 10 µl of POPC/POPG (3:1, mol/mol) suspension. The experiment was performed at 30°C. (A) Heat flow and (B) cumulative heat of reaction (■) as a function of the molar ratio of lipid to peptide.*

c) Influence of the membrane surface charge on βAP_I32W binding

The difference between K_o and K_{app} observed at pH 4.0 indicates the importance of electrostatic forces in the binding of the amyloid model peptides to the lipid membrane. Thus the membrane surface charge certainly plays an important role in the binding mechanism. To investigate further the influence of the membrane surface charge, calorimetric studies were performed with βAP(25-35)_I32W and POPC/POPG SUVs and varying the amount of the negatively-charged POPG.

At pH 4.0, no heat of reaction can be measured in the calorimetric titration experiment of βAP(25-35)_I32W with neutral POPC vesicles (results not shown). This absence of binding was already observed for βAP(25-35)[9]. If the negative charge of the lipid membrane is increased (POPC/POPG 2:1, mol/mol), the binding of βAP(25-35)_I32W to the membrane leads to distinct heats of reaction. ΔH^o varies between

-8.6 kcal.mol^{-1} at 15°C and -5.9 kcal.mol^{-1} at 30°C (-36 and -24.7 kJ.mol^{-1}). The binding enthalpies of βAP(25-35)_I32W to POPC/POPG (2:1, mol/mol) at pH 4.0 are summarized in Table 2. The ITC titrations performed between 8 and 40°C are shown in the Appendix.

***Table 2**: Thermodynamic parameters for the binding of βAP(25-35)_I32W to SUVs composed of POPC/POPG (2:1, mol/mol) at various temperatures and pH 4.0. The data result from the average of at least two experiments and the standard deviation is indicated for the enthalpy and binding constant. The number of effective charges, z, is also indicated.*

T (°C)	ΔH^0 (kcal/mol)	K_0 (M^{-1})	ΔG^0 (kcal/mol)	$T\Delta S^0$ (kcal/mol)	ΔC_p (cal/mol/K)	z /
8	-8.50 ± 0.04	6.0 ± 0.7	-3.2	-5.3		2
15	-8.60 ± 0.51	4.9 ± 0.1	-3.2	-5.4	85	2
25	-7.87 ± 0.83	3.5 ± 0.1	-3.1	-4.8	R^2=0.79	2
30	-5.97 ± 0.12	3.0 ± 0	-3.1	-2.9		2
40	-6.39 ± 0.16	2.0 ± 0	-2.9	-3.5		2

The molar heat capacity change ΔC_p is determined from the variations of the binding enthalpy with the temperature[18] from $\Delta C_p = d\Delta H^o/dT$. ΔH^o increases with the temperature and the slope of the regression line shown in Figure 7 indicates ΔC_p = 85 cal.mol^{-1}.K^{-1} (356 J.mol^{-1}.K^{-1}).

The intrinsic binding constants calculated with the binding model vary between 6 M^{-1} at 8°C and 2 M^{-1} at 40°C. The free energy remains constant at a similar value to the one observed with less lipid charges ($\Delta G^o \approx$ -3.1 kcal.mol^{-1}).

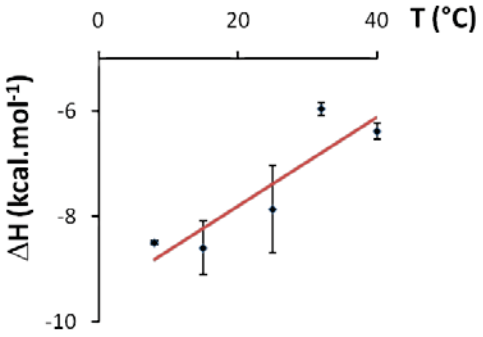

***Figure 7**: Temperature dependence of ΔH^o of βAP(25-35)_I32W binding to POPC/POPG SUVs (2:1, mol/mol) at pH 4.0. The linear regression (—) gives the relation: ΔH^o = 0.0845 T- 9.4911 (R^2 = 0.79).*

At pH 7.4, POPG is fully-charged and increases further the membrane surface charge compared to the experiments at pH 4.0. The calculated parameters are shown in Table 3.

***Table 3**: Thermodynamic parameters for the binding of βAP(25-35)_I32W to SUVs composed of POPC/POPG (2:1, mol/mol) at various temperatures and pH 7.4. The standard deviation is indicated for the enthalpy and binding constant. The number of effective charges, z, is also indicated.*

T (°C)	ΔH^0 (kcal/mol)	K_0 (M^{-1})	ΔG^0 (kcal/mol)	$T\Delta S^0$ (kcal/mol)	ΔC_p (cal/mol/K)	z /
12	-1.16 ± /	30 ± /	-4.2	3.0		1.6
15	-0.81 ± 0.10	30 ± 0	-4.3	3.4	38	1.6
20	-0.92 ± 0.06	25 ± 0	-4.2	3.3	R^2=0.73	1.6
25	-0.55 ± 0.03	15 ± 0	-4.0	3.4		1.6

Contrary to the previous experiment at pH 4.0, these ITC titrations show the release of very low heats of reaction. The binding enthalpies slightly increase from -1.2 kcal.mol^{-1} at 12°C and –0.6 kcal.mol^{-1} at 25°C (-5.0 to -2.5 kJ.mol^{-1}). The intrinsic binding constant is 5-fold higher than at pH 4.0, with K_0 = 30 M^{-1} at 12°C. The molar heat capacity is such as ΔC_p = 38 cal.mol^{-1}.K^{-1} (159 J.mol^{-1}.K^{-1}) and the free energy remains constant around -4.2 kcal.mol^{-1} (-17.5 kJ.mol^{-1}).

d) Peptide binding to the membrane studied with circular dichroism

The interaction between the negatively-charged lipids and the three amyloid model peptides was described with thermodynamic parameters at pH 4.0 for βAP(25-35) and WβAP(25-35) and at pH 4.0 and pH 7.4 with increased membrane surface charge for βAP(25-35)_I32W. Circular dichroism spectroscopy can be used to monitor the structural changes of the peptides upon lipid binding. βAP(25-35) is known to undergo lipid-induced structural transitions[9]. A circular dichroism study of the peptide bound to lipid at various temperatures will allow the correlation between the thermodynamic parameters determined previously and changes in secondary structure. A first step is to observe the effect of the temperature on the peptides without lipids. This can then be compared to the effect of the lipid binding. Figure 8

shows the variations of the secondary structure of βAP(25-35), WβAP(25-35) and βAP(25-35)_I32W at pH 4.0 from 10 to 40°C.

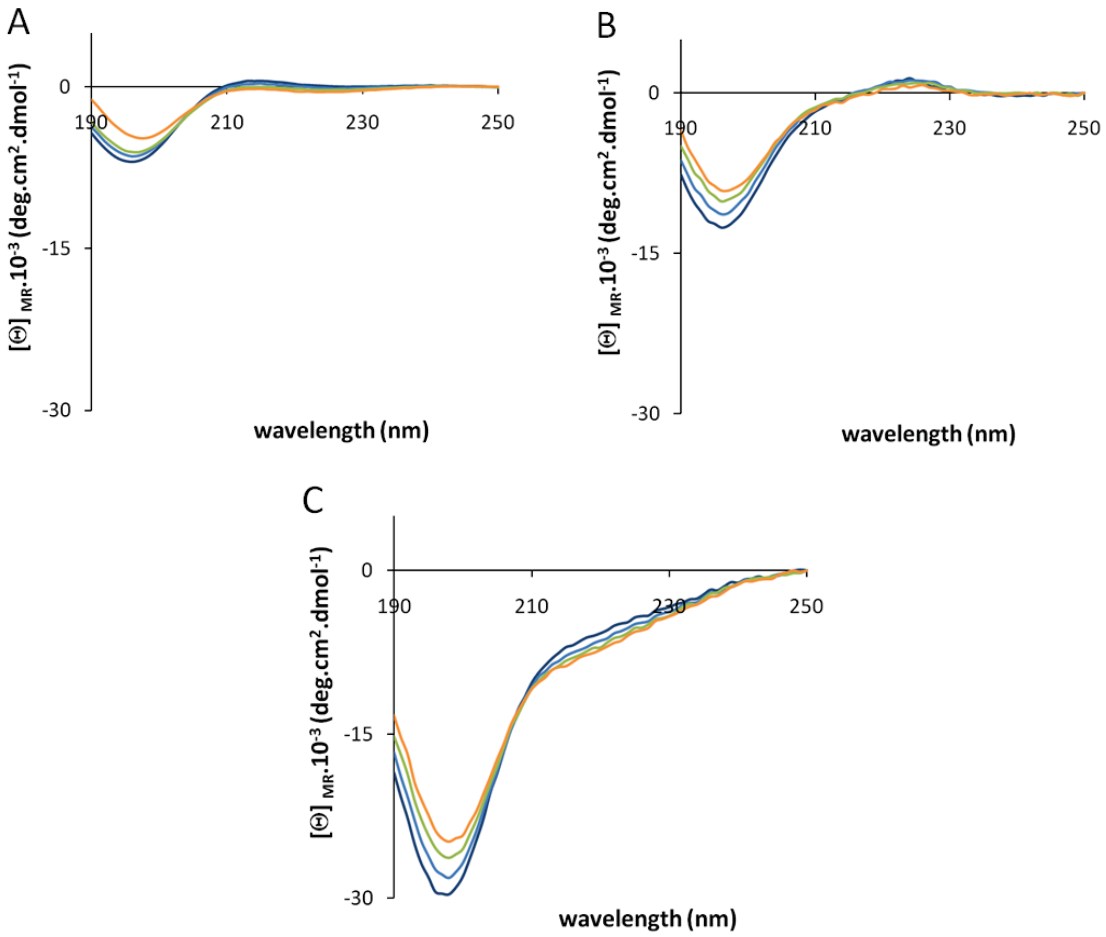

Figure 8: *Influence of the temperature on the secondary structure of the amyloid peptides in 10 mM AcONa buffer at pH 4.0. HFIP treated (A) βAP(25-35), (B) WβAP(25-35), and (C) βAP(25-35)_I32W at ~20 μM. The scans were made at 10 (—), 20 (—), 30 (—), and 40°C (—).*

The CD spectra of all three peptides at pH 4.0 have a shape characteristic of random-coil, with a minimum ellipticity at 197-198 nm that decreases with the increasing temperature. Additionally the spectra of WβAP(25-35) show contributions of the Trp24 at 225 nm[19-21]. The spectra were fitted as described previously (page 56). Although the shape of all spectra is characteristic of random-coil, the mean residue ellipticity of βAP(25-35) and WβAP(25-35) is smaller than expected for 100% random-coil ($[\theta]_{MR(197nm)}$ = -35000 deg.cm^2.dmol^{-1}). Therefore the fitting showed considerable deviation compared to the experimental data, with R^2 values comprised between 0.75 and 0.98, and can only be considered as an approximation. The fitting of βAP(25-35)_I32W is improved, with R^2 close to 0.9. The random-coil content as evaluated for

βAP(25-35), WβAP(25-35) and βAP(25-35)_I32W was 54, 57 and 89%, respectively, at 10°C. At 40°C, the random-coil contribution decreases to 49, 53 and 80%, respectively. In parallel, the β-sheet content increases from 25 to 33% for βAP(25-35) and from 25 to 31% for WβAP(25-35). Contrary to βAP(25-35) and WβAP(25-35), the secondary structure of βAP(25-35)_I32W does not contain any β-sheet component.

Figure 9 shows the variations in secondary structure of βAP(25-35), WβAP(25-35) and βAP(25-35)_I32W at pH 7.4 from 10 to 40°C.

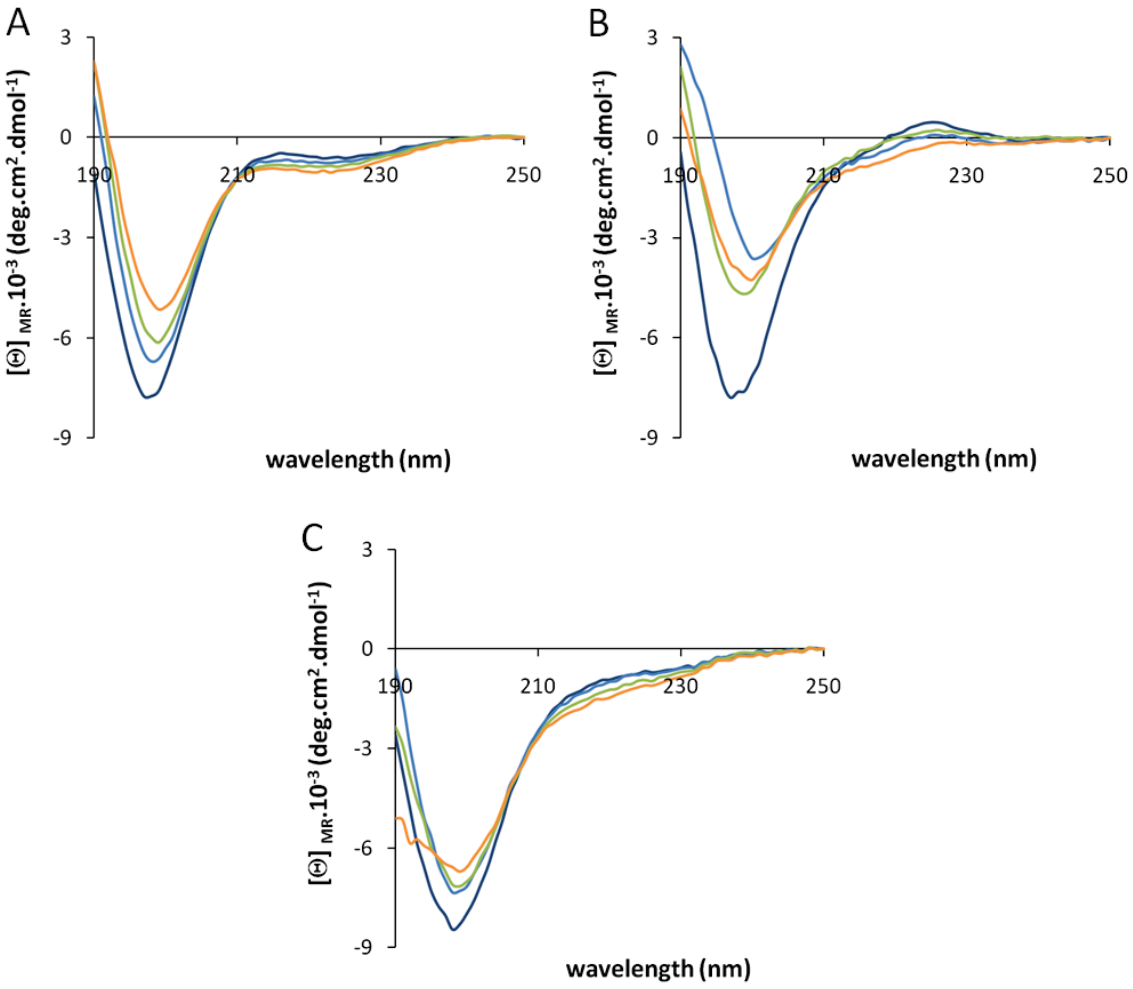

Figure 9: *Influence of the temperature on the secondary structure of the amyloid peptides in 10 mM HEPES buffer at pH 7.4. HFIP treated (A) βAP(25-35), (B) WβAP(25-35), and (C) βAP(25-35)_I32W at ~20 μM. The scans were made at 10 (—), 20 (—), 30 (—), and 40°C (—).*

At pH 7.4, the shape of the spectra contains features of random-coil, yet the mean residue ellipticity is smaller, similar to the experiment at pH 4.0. The CD spectra are also characterized by a minimum ellipticity at 197 nm. The mean residue ellipticity

tends to decrease with the increasing temperature in the case of βAP(25-35) and βAP(25-35)_I32W but this is not true for WβAP(25-35). The spectral fitting of all spectra is of poor quality (R^2 values close to 0.85) and the slight spectral changes observed in Figure 9 for βAP(25-35) and βAP(25-35)_I32W are not represented by the analysis. At 10°C, βAP(25-35) is composed of 26% β-sheet, 53% random-coil and 21% β-turn. This composition is almost unchanged at 40°C (29, 52 and 19%, respectively). The secondary structure of βAP(25-35)_I32W determined by fitting is also similar at the two temperatures, and is composed of about 32% β-sheet, 41% random-coil and 17% β-component. However an exchange between β-structure and random-coil occurs in the secondary structure of WβAP(25-35) upon temperature increase: 32% β-sheet, 41% random-coil and 17% β-turn at 10°C and 22% β-sheet, 65% random-coil and 6% β-turn at 40°C.

The peptide structural changes upon lipid binding are investigated next. The peptide-to-lipid ratio was adjusted to match the end of the calorimetric titration. This ratio varies from 1/50 to 1/100 in the calorimetric experiment (see Figure 2 and 6). In order to ensure complete peptide binding, the CD experiments were made at a peptide to lipid ratio P/L ~ 1/120. Amyloid peptide concentration and the scattering caused by the SUVs are the limiting factors in this experiment. A minimal peptide concentration of 20-30 μM is necessary for a good signal-to-noise ratio. The maximum lipid concentration used was 2.5 mM in order to minimize the scatter. CD spectra were recorded between 190 and 250 nm.

The results obtained for the structural study at acidic pH are shown in Figure 10. Bound βAP(25-35) and WβAP(25-35) have CD spectra with a shape and a minimum mean residue ellipticity close to -30000 $deg.cm^2.dmol^{-1}$, features of random-coil, yet the minimum ellipticity is slightly shifted at 200 and 203 nm, respectively. The spectra of these two bound peptides do not change with the temperature. The fitting (R^2 = 0.95 for bound βAP(25-35), and R^2 = 0.85 for bound WβAP(25-35)) confirms that both peptides are mostly in a random-coil structure, which is independent of the temperature (89% and ~ 72%, respectively). The α-helical content is 11 and 28%,

respectively. In contrast, the spectra of bound βAP(25-35)_I32W show two minima: one at 203 nm, at a mean residue ellipticity close to -13000 deg.cm^2.dmol^{-1}, and the second at 218 nm, indicating the additional contribution of β-sheet. Upon temperature increase, the mean residue ellipticity at 203 nm decreases in favor of the mean residue ellipticity at 218 nm. The spectral fitting (R^2 = 0.75) shows that at 10°C random-coil is dominant (57% against 15% α-helix and 28% β-sheet) whereas higher temperatures favor β-sheet formation (40% random-coil, 15% α-helix and 45% β-sheet at 40°C).

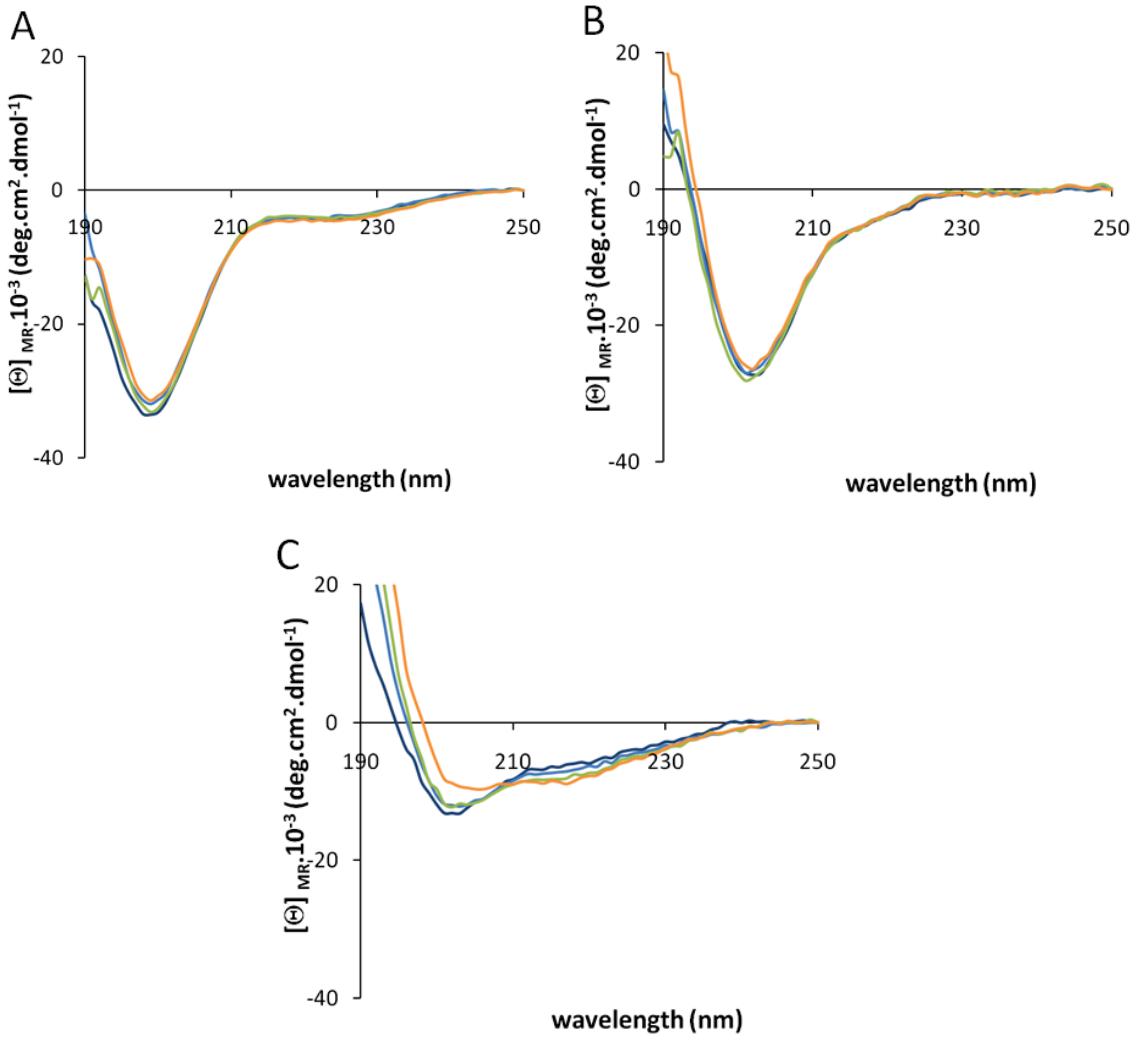

***Figure 10**: Influence of the temperature on the secondary structure of the three peptides bound to lipid at pH 4.0. HFIP treated (A) βAP(25-35), (B) WβAP(25-35), and (C) βAP(25-35)_I32W. To a peptide solution (~ 20 μM) was added POPC/POPG SUVs (3:1, mol/mol) at a 1/120 ratio. The scans were made at 10 (—), 20 (—), 30 (—), and 40°C (—).*

Figure 11 shows the structural study of the three peptides at neutral pH value. The shape of the CD spectra of bound βAP(25-35) has characteristics of random-coil

and α-helix. The spectra have a minimum at 201 nm that shifts towards 203 nm upon temperature increase, and a second minimum at 222 nm. The spectra of bound WβAP(25-35) and βAP(25-35)_I32W show a minimum at 204 nm and an additional contribution at about 219 nm. The mean residue ellipticity observed at about 204 nm for the three model peptides decreases upon temperature increase.

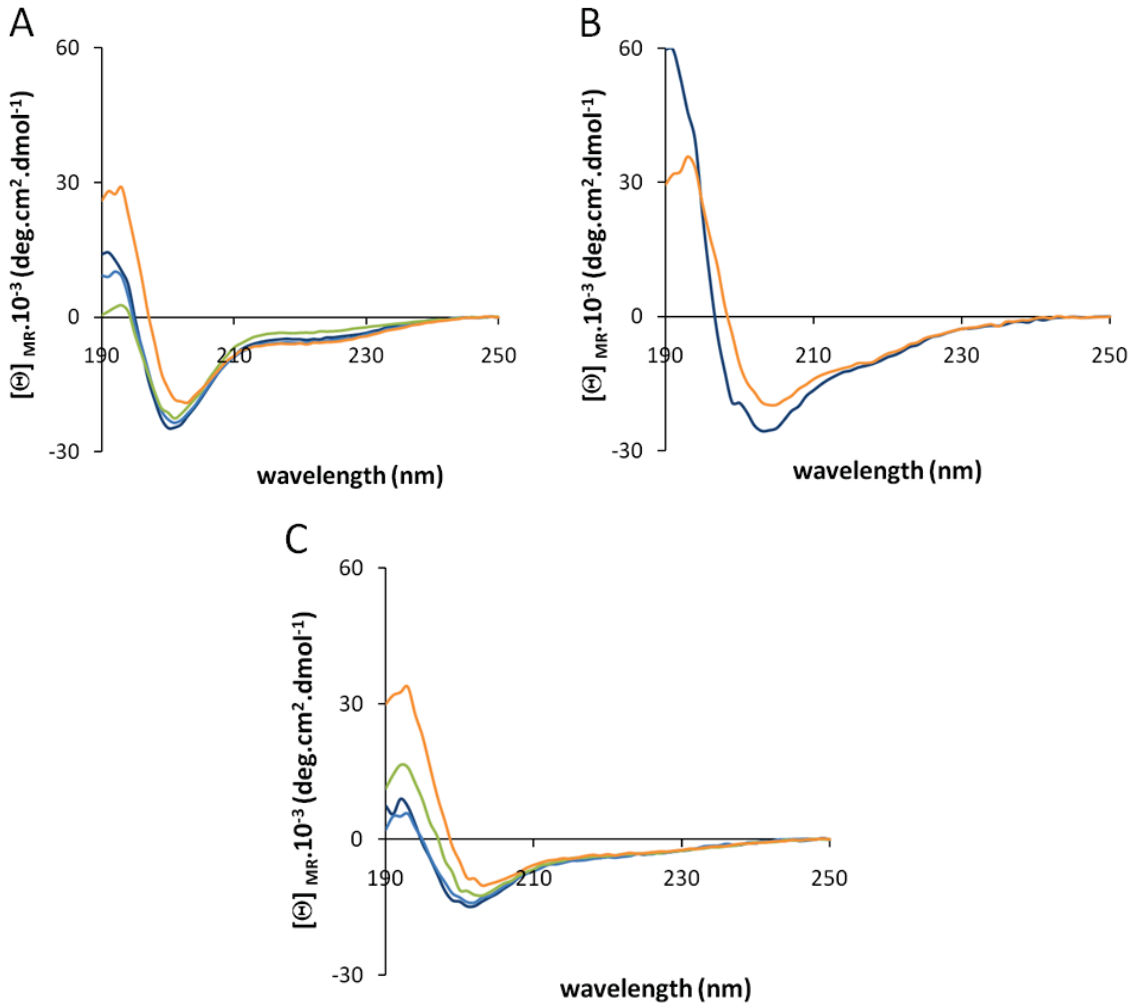

***Figure 11**: Influence of the temperature on the secondary structure of the three peptides bound to lipid at pH 7.4. HFIP treated (A) βAP(25-35), (B) WβAP(25-35), and (C) βAP(25-35)_I32W. To a peptide solution (~ 20 μM) was added POPC/POPG SUVs (3:1, mol/mol) at a 1/120 ratio. The scans were made at 10 (—), 20 (—), 30 (—), and 40°C (—).*

The spectral fitting indicates that the three bound peptides tend to increase the contribution of β-sheet in their secondary structure upon temperature increase (R^2 ~ 0.75). Random-coil is the principal structural component at low temperature (respectively for βAP(25-35), WβAP(25-35) and βAP(25-35)_I32W: 75, 55 and 64%) and

is converted into β-sheet (17, 22 and 40%) at 40°C. Only βAP(25-35)_I32W contains already 28% β-sheet at 10°C.

The comparison of the CD spectra of the peptides bound to the lipid membrane (Figure 10 and 11) with the CD signal of each unbound peptide (see Figure 8 and 9) enables to extract the effect of temperature, lipid binding and pH on the peptide secondary structure. The change in secondary structure of each peptide is summarized in Figure 12. At both pH, lipid binding has a strong influence on the secondary structure of βAP(25-35) and WβAP(25-35) since it removes or reduces β-sheet content in favor of random-coil and α-helix components. Only at pH 7.4 and 40°C, β-sheet is observed in βAP(25-35) and WβAP(25-35), but its proportion is smaller than in the unbound peptides. In contrast, the secondary structure of unbound and bound βAP(25-35)_I32W are similar at pH 7.4, whereas at pH 4.0, lipid binding induces β-structure formation in βAP(25-35)_I32W.

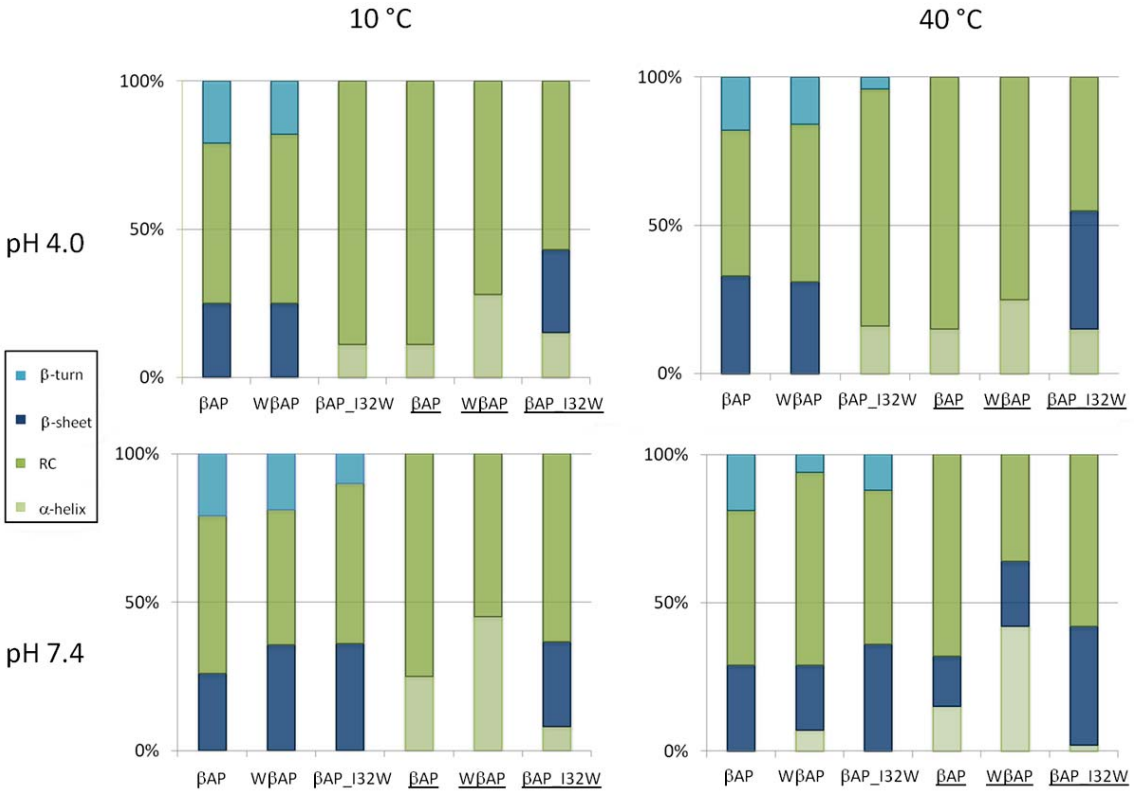

***Figure 12**: Representation of the structural content of the three amyloid model peptides at pH 7.4 or 4.0 and at 10 or 40°C. βAP(25-35), WβAP(25-35) and βAP(25-35)_I32W are represented, unbound or bound to the lipid membrane. The secondary structure considers random-coil, β-sheet, β-turn and α-helix content. It is expressed as percentage of the whole peptide structure.*

e) Peptide binding to the membrane studied with by solid-state NMR

The previous CD experiments indicate structural changes of the amyloid model peptides upon binding to the lipid membrane at both pH 7.4 and 4.0. The binding of peptide to the lipid surface can also influence the lipid phase. It can affect the membrane stability, thereby influencing the gel-to-liquid crystal transition temperature. Other effects are a change in the long-range organization of the lipid phase upon peptide association; for instance, the bilayer can be converted into a hexagonal or micellar phase[22,23]. The next step of this study focuses on lipid structure, lipid motions and phase behavior using solid-state nuclear magnetic resonance (NMR), either by looking at the phosphorus ^{31}P- or deuterium ^{2}H-NMR spectra (see Appendix, page 99). In a first type of experiment, the amyloid model peptides were co-dissolved with lipids and dried. Upon hydration the peptides inserted into the multilamellar vesicles. In a second type of experiment, the effect of the association of amyloid peptide aggregates with the preformed lipid multilamellar vesicles was investigated.

Figure 13 shows the ^{31}P-NMR spectra of the lipid vesicles after insertion of the amyloid model peptides, for temperatures between -10°C and 40°C. In this study, the peptide-to-lipid ratio was 1/170, in order to match the CD and ITC measurements performed previously. All spectra of POPC and d_{31}-POPG vesicles are characteristic of lipid bilayers either in the gel or in the liquid-crystalline state. Both POPC and d_{31}-POPG have their own specific chemical shift in the applied magnetic field. Therefore two high-intensity peaks can be distinguished at +12 and +16 ppm in the spectra of the lipid vesicles without peptide at higher temperatures (Figure 13A). This observation is also made when βAP(25-35)_I32W is inserted into the membrane (Figure 13D) at the same chemical shifts. However, if βAP(25-35) or WβAP(25-35) are inserted into the lipid membrane (Figure 13B and 13C), the high-intensity shoulders of POPC and d_{31}-POPG are merged into a broad peak at +14 and +12 ppm respectively. Furthermore in the presence of βAP(25-35), the intrinsic linewidth is much broader in the liquid-crystalline phase (Figure 13B) compared to WβAP(25-35) or βAP(25-35)_I32W. The negative curvature observed in the spectra of the pure lipid membrane (Figure 13A) at the higher temperatures could be due to insufficient lipid hydration.

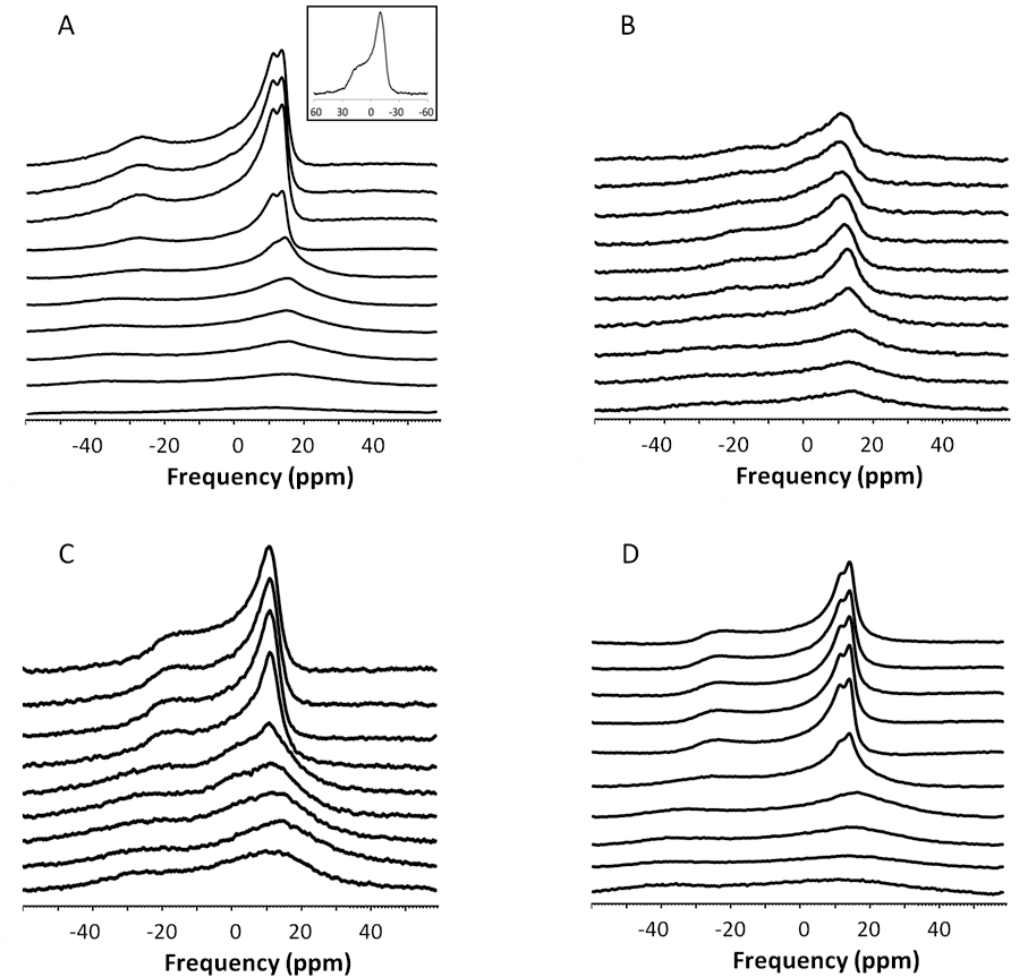

***Figure 13**: [31]P-NMR spectra of POPC/d_{31}-POPG (A) without, and with (B) βAP(25-35), (C) WβAP(25-35) and (D) βAP(25-35)_I32W inserted at a peptide-to-lipid ratio of 1/170. The amyloid model peptides and the lipid mixture were dissolved in chloroform and dried. 10 mM HEPES in deuterium-depleted water was added to give a final peptide concentration of 216 μM. The spectra were recorded from bottom to top (A) -10, -2, 0, 2, 10, 20, 30 and 40°C, (B) -10, -8, -6, -2, 0, 2,4, 6, 8, and 10°C, (C) -12, -10, -8, -6, -4, -2, 0, 2 and 4°C , (D) -10, -7, -4, -2, 0, 2, 4, 6, 8 and 10°C. The inset in A shows a theoretical bilayer spectrum.*

The anisotropic motions of the phosphate group were quantified with the chemical shielding anisotropy, $\Delta\sigma = \sigma_{\parallel} - \sigma_{\perp}$. $\Delta\sigma$ can be measured on the ^{31}P-NMR spectrum as full-width at 10% of the maximal intensity (see Appendix, page 99). Its variations with the temperature are displayed in Figure 14. Below 2°C, $\Delta\sigma$ of the pure lipid vesicles is almost constant at -77 ppm (Figure 14). At higher temperatures, the phosphate group undergoes a fast rotation and the edges of the ^{31}P-NMR spectra are better defined (see Figure 13). $\Delta\sigma$ increases to -54 ppm. The inflection point in the variations of the chemical shielding anisotropy denotes the transition temperature, T_m,

of POPC and d_{31}-POPG bilayers. It reveals a phase transition of the lipids at 2°C. This value is higher than the data available in the literature, T_m = -2°C, determined from calorimetric measurements[24,25]. When any of the model peptides is inserted into the lipid vesicles, $\Delta\sigma$ in the liquid-crystalline phase varies from -53 to -46 ppm, depending on the peptide considered. At lower temperatures, $\Delta\sigma$ is close to the value of the pure lipid bilayer when WβAP(25-35) is inserted, reaching a plateau at about -80 ppm at low temperatures. In contrast, after insertion of βAP(25-35), $\Delta\sigma$ increases to -70 ppm, whereas the insertion of βAP(25-35)_I32W induces a decrease to $\Delta\sigma$ = -90 ppm. The insertion of any of the peptides shifts T_m towards lower value. The T_m of βAP(25-35), WβAP(25-35) and βAP(25-35)_I32W determined from Figure 14 are -1, -4 and 0°C, respectively.

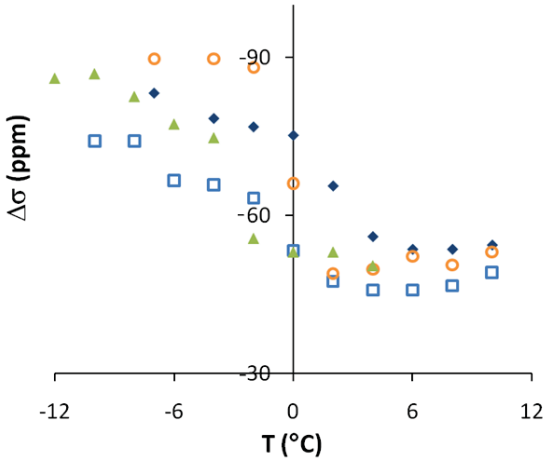

***Figure 14**: Chemical shielding anisotropy $\Delta\sigma$ of POPC/d_{31}-POPG as a function of the temperature. Amyloid model peptides were co-dissolved with lipid in organic solvent, dried, and suspended in buffer. $\Delta\sigma$ values are calculated from solid-state NMR spectra (Figure 13). $\Delta\sigma$ of POPC/d_{31}-POPG alone (◆) and with the insertion of βAP(25-35) (□), WβAP(25-35) (▲) or βAP(25-35)_I32W (○).*

Figure 15 shows the ^{2}H spectra of the lipid membrane alone and after insertion of the three amyloid peptides. The spectra result from a superposition of quadrupole splittings, $\Delta\nu_Q$, of all deuterons on the POPG lipid chain. Each deuteron gives rise to a splitting, the size of which varies with the position of the deuteron along the chain. The spectra are characteristic of lipid bilayers either in the gel or in the liquid-crystalline state. One spectrum on Figure 15B is however different from all others. A particular behavior of the acyl chains is observed at 20°C upon insertion of βAP(25-35): an

isotropic phase, or a total loss of signal, is present in addition to the bilayer phase. This isotropic phase is not observed at any other temperature.

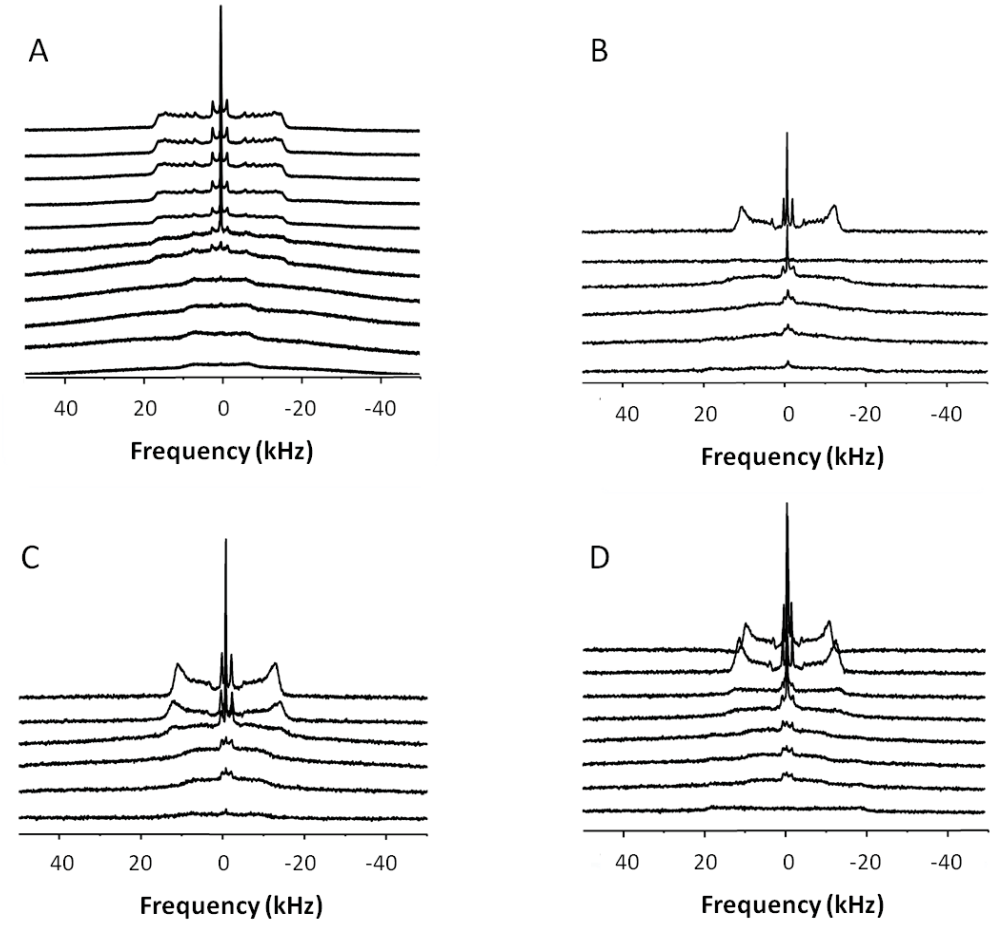

***Figure 15**: ^{2}H-NMR spectra of POPC/d_{31}-POPG (A) alone, and with (B) βAP(25-35), (C) WβAP(25-35) and (D) βAP(25-35)_I32W inserted at a peptide-to-lipid ratio of 1:170. The amyloid model peptides and the lipid mixture were dissolved in chloroform and dried. 10 mM HEPES in deuterium-depleted water was added to give a final peptide concentration of 216 μM. The spectra were recorded from bottom to top at (A) -10, -2, 0, 2, 10, 20, 30 and 40°C, (B) 0, 2, 4, 10, 20 and 30°C, (C) 0, 2, 4, 10, 20 and 30°C, (D) -10, 0, 2, 4, 10, 20, 30 and 40°C.*

The variations of the outermost quadrupole splitting with the temperature are plotted in Figure 16A. The quadrupole splitting at low temperature could not be determined for the lipid vesicle without peptide or with βAP(25-35)_I32W due to a low signal-to-noise ratio.

Above -2°C the spectra of the pure lipid membranes are characterized by $\Delta\nu_Q(CD_2)$ = 27 kHz. With any of the model peptides inserted, $\Delta\nu_Q(CD_2)$ follows similar variations and remains close to 25 kHz. Below 4°C, $\Delta\nu_Q(CD_2)$ of the vesicles containing βAP(25-35) or WβAP(25-35) reaches a plateau at 36 kHz.

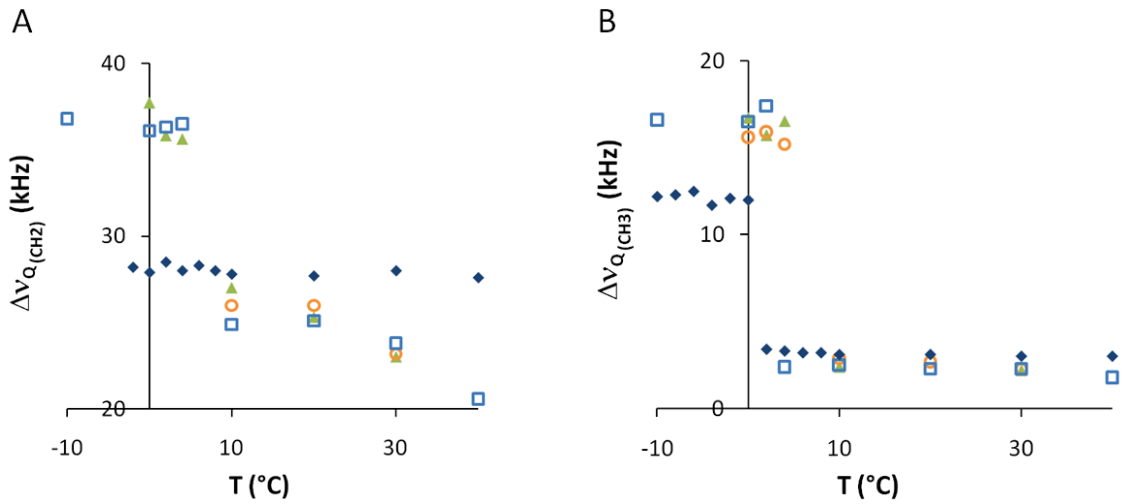

***Figure 16**: (A) Quadrupole splitting $\Delta\nu_{Q(CH2)}$ and (B) $\Delta\nu_{Q(CH3)}$ of POPC/d_{31}-POPG as a function of the temperature. Amyloid model peptides were co-dissolved with lipid in organic solvent, dried, and suspended in buffer. $\Delta\nu_Q$ are calculated from solid-state NMR spectra (Figure 15). $\Delta\nu_Q$ of POPC/d_{31}-POPG alone (◆) and with the insertion of βAP(25-35) (□), WβAP(25-35) (▲) or βAP(25-35)_I32W (○).*

The innermost quadrupole splitting observed for the spectra of Figure 15 can be assigned to the terminal CD_3 group of the acyl chain, $\Delta\nu_Q(CD_3)$. The temperature dependence of $\Delta\nu_Q(CD_3)$ is shown in Figure 16B. $\Delta\nu_Q(CD_3)$ of the pure lipid membrane reaches an upper plateau at $\Delta\nu_Q(CD_3)$ = 13 kHz below -3°C and a lower plateau at 4 kHz above this temperature. The lower plateau remains between 4 and 5 kHz also after insertion of the model peptides. In contrast, $\Delta\nu_Q(CD_3)$ increases to 15 kHz below -3°C with the three peptides inserted.

The phase transition of the pure lipid membrane can be defined at -3°C for the lipid chains, which is closer to the value reported in the literature[24,25]. The phase transition of the lipid chains of the vesicles containing βAP(25-35), WβAP(25-35) or βAP(25-35)_I32W occurs at 4°C.

Our results on peptide insertion are similar to the ones reported in the literature, based on ^{13}C or ^{31}P MAS NMR experiments[26,27] for a peptide-to-lipid ratio of typically 1/30. These previous studies did not report major change in lipid structure or phase behavior with inserted peptide. A different result was however reported for peptide bound from the aqueous phase. Our next study therefore focuses on the binding of non-treated amyloid peptide at high concentration from the aqueous phase to the membrane surface. The molar peptide-to-lipid ratio was 1/50 and the peptide

concentration of 800 μM. As shown in Chapter IV, this high concentration and the absence of HFIP-pretreatment lead to large aggregates in buffer.

Figure 17 summarizes the ^{31}P-NMR experiments performed with POPC/d_{31}-POPG membranes in presence of βAP(25-35), WβAP(25-35) or βAP(25-35)_I32W aggregates.

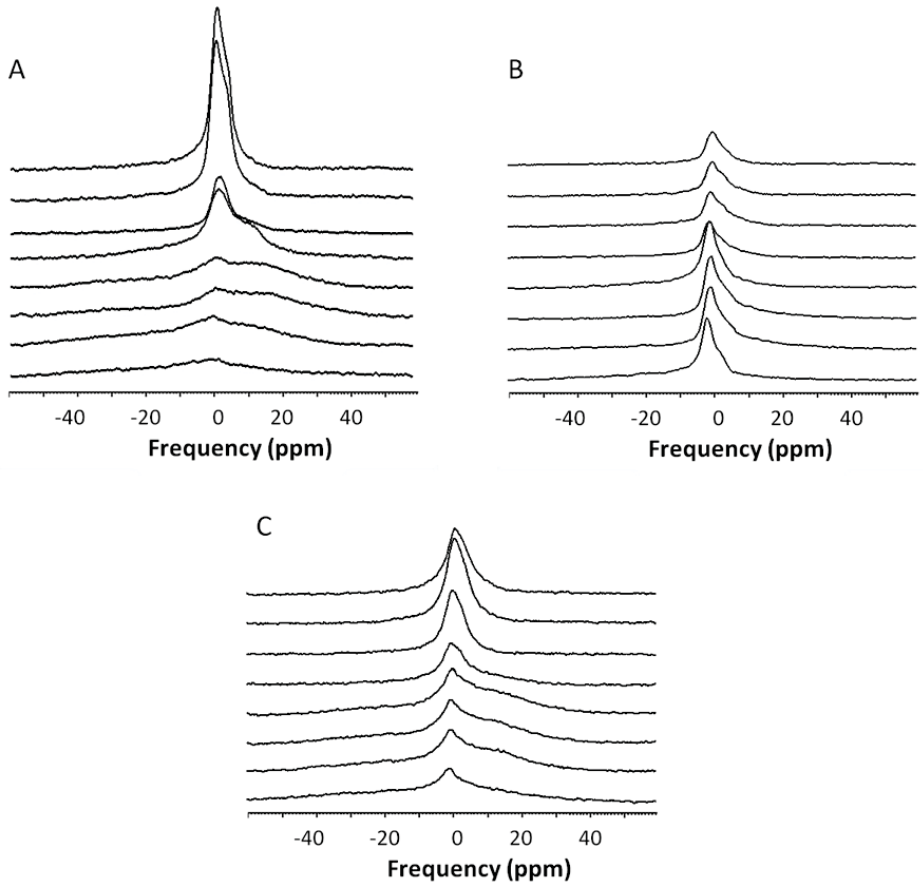

***Figure 17**: ^{31}P-NMR spectra of POPC/d_{31}-POPG associated with (A) βAP(25-35), (B) WβAP(25-35) and (C) βAP(25-35)_I32W at a peptide-to-lipid ratio of 1/50. The dry peptide powder was added to multilamellar lipid vesicles in 10 mM HEPES in deuterium-depleted water. The final peptide concentration was 800 μM. The spectra were recorded from bottom to top at -10, -2, 0, 2, 10, 20, 30 and 40°C.*

The spectra shown in Figure 17 are completely different from those obtained for the pure lipid mixture (see Figure 13A). Weak bilayer features are still observed for βAP(25-35) or βAP(25-35)_I32W (Figure 17A and 17B), however an intense isotropic line is superimposed on the bilayer spectra. The high-intensity shoulder characteristic of bilayer spectra observed at -15 ppm gradually shifts to -3 ppm upon temperature increase. In presence of WβAP(25-35) aggregates at the membrane surface (Figure 17B), no bilayer features can be observed but the signal at -3 ppm is also observed

upon temperature increase. An additional characteristic of these spectra is the decrease in intensity of the spectra with increasing temperature. Because of the superposition of different signals in each spectrum, the variations of $\Delta\sigma$ with the temperature could not be determined.

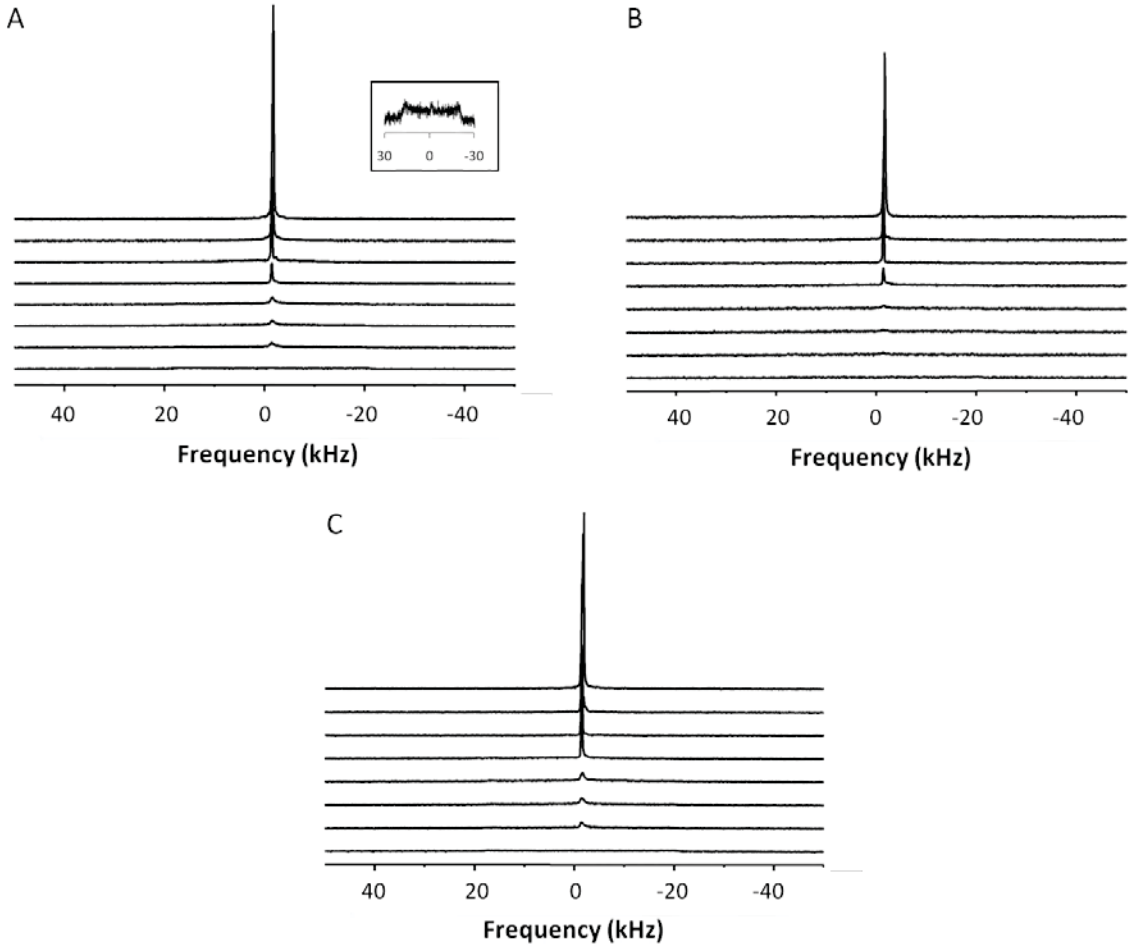

***Figure 18**: ^{2}H-NMR spectra of POPC/d_{31}-POPG associated with (A) βAP(25-35), (B) WβAP(25-35 and (C) βAP(25-35)_I32W at a peptide-to-lipid ratio of 1/50. The dry peptide powder was added to multilamellar lipid vesicles in 10 mM HEPES in deuterium-depleted water. The final peptide concentration was 800 μM. The spectra were recorded from bottom to top at -10, -2, 0, 2, 10, 20, 30 and 40°C. The inset in A shows the enlarged spectrum at -10°C.*

The results of the ^{2}H-NMR experiments of the lipid membrane in presence of peptide aggregates are shown in Figure 18. The ^{2}H-NMR spectra of the lipid membrane associated with amyloid model peptides are quite different from those observed with the inserted peptides (Figure 15).

Bilayer features are still observed at low temperatures (see inset in Figure 18A) but an intense isotropic line hides the bilayer signal at higher temperatures. The quadrupole splittings can be determined at low temperature for βAP(25-35) and

βAP(25-35)_I32W and are found to be 35 kHz, similar to the values measured with inserted peptides (Figure 16A). Above 4°C, the quadrupole splittings characteristic of a bilayer cannot be observed anymore. The abrupt change in the intensity of the central isotropic line indicates a phase transition of the peptide-associated bilayer at 4°C, which is similar to that of the vesicles containing the inserted amyloid model peptides.

4. Discussion

The data presented in this chapter provide new structural and thermodynamic input on the binding of model amyloid peptides to the lipid membrane. The CD experiments show the influence of Trp on the secondary structure of the bound peptides and prove that the lipid membrane favors the random-coil structure at low peptide concentration. Thermodynamic parameters of the peptide-to-lipid binding could be determined at pH 4.0. Eventually solid-state NMR study proved that the insertion of the model amyloid peptides increases the fluidity of the acyl chains while peptide adsorption on the membrane induces the formation of an isotropic lipid phase.

a) Peptide structural change upon binding

The CD spectra presented in this chapter provide evidence that the position of Trp influences the secondary structure of the bound amyloid model peptides. The experiments performed with HFIP-pretreated peptides indicate that βAP(25-35)_I32W is more prone to β-sheet formation upon lipid binding than βAP(25-35) and WβAP(25-35) at both pH values (see Figure 12). β-sheet formation in lipid-bound βAP(25-35)_I32W can be explained by the presence of Trp at the position 32 in the peptide sequence, since Trp is preferentially located close to the lipid carbonyl group[28]. This effect is complementary to the attraction of Lys28 for the lipid-water interface; the acyl chain of Lys is known to snorkel[28], its hydrophobic part dives into the lipid membrane while the positively-charged terminal amino group remains at the lipid-water interface. In contrast, Figure 12 shows that lipid binding at pH 7.4 and pH 4.0 causes β-structure decrease in βAP(25-35) and WβAP(25-35): the random-coil content

increases upon binding of the two peptides. It can be concluded that Trp24 does not favor β-sheet formation upon binding to the lipid membrane. However the CD spectra presented in Figure 8B and 9B show a contribution of the aromatic side-chain of Trp24 in the secondary structure[19] of WβAP(25-35) at both pH 4.0 and pH 7.4 that is not observed anymore after binding (see Figure 10B and 11B for comparison). Therefore Trp24 might also be involved in the change of secondary structure in WβAP(25-35) upon binding to the lipid membrane.

These CD experiments also provide elements to distinguish two roles of the lipid membrane on the secondary structure of βAP(25-35) and WβAP(25-35). In 1994, Terzi *et al.* studied βAP(25-35) and βAP(1-40) at a peptide concentration of 50 μM. The authors showed that the β-sheet content in these two peptides increases upon lipid addition[9] at pH 5.0. Terzi *et al.* hypothesized that both peptides were unstructured at the first stages of lipid binding. The increase in β-sheet in presence of lipid would occur either by peptide penetration in the hydrophobic part of the bilayer or by peptide aggregation at the membrane surface or by a penetration mechanism[9]. Chi *et al.* observed the crystalline ordering of βAP(1-40) at 250 nM on the lipid surface upon association with DPPG with X-rays and neutron scattering, supporting the second hypothesis of Terzi[29]. Our work validates further the aggregation hypothesis of Terzi *et al*. The CD data shown in Figure 12 show that the lipid membrane tends to unstructure βAP(25-35) and WβAP(25-35) at a peptide concentration close to 20 μM. Therefore our structural studies demonstrate that the lipid membrane unstructures low concentrated βAP(25-35) and WβAP(25-35) whereas it enhances β-sheet formation at higher peptide concentration[9]. This indicates the presence of a critical step in peptide aggregation on the membrane that is function of amyloid peptide concentration, similar to the nucleus formation in solution[30].

b) Thermodynamic characterization of the binding mechanism

At pH 4.0, the heat released during the binding of each amyloid model peptide with POPC/POPG SUVs (3:1, mol/mol) is weak and leads to constant values of ΔH^o at -1.38 and -3.04 kcal.mol^{-1} between 10 and 40°C for βAP(25-35) and WβAP(25-35),

respectively (see Table 1). This is in agreement with the previous work of Terzi *et al.*[9] who measured ΔH^o between -2 and -10 kcal.mol^{-1} (8.6 to 43 kJ.mol^{-1}) for the binding of βAP(25-35), βAP(25-35)NH_2 and βAP(25-35NLe)NH_2 to the same model membrane. The heats of reaction of βAP(25-35)_I32W with the POPC/POPG SUVs (2:1, mol/mol) are much larger at pH 4.0 and increase with the temperature (see Table 2).

The calorimetric study at pH 4.0 also shows that βAP(25-35) and WβAP(25-35) bind to the POPC/POPG (3:1, mol/mol) lipid membrane with low affinity with K_o = 11 and 4 M^{-1}, respectively (see Table 1). It is also the case for the binding of βAP(25-35)_I32W to POPC/POPG (2:1, mol/mol) lipid membrane with K_o ranging between 2 and 6 M^{-1} (see Table 2). These values of K_o calculated with the binding model are similar to those calculated by Terzi[9] for βAP(25-35), βAP(25-35)NH_2 and βAP(25-35NLe)NH_2, situated between 2 and 10 M^{-1}. The large difference shown in Figure 5 between the intrinsic and the apparent binding constants points out the importance of electrostatic forces in the binding of βAP(25-35) and WβAP(25-35) to the lipid membrane. This confirms the experiment of Terzi[9] who observed no more binding in presence of 100 mM NaCl.

The binding of βAP(25-35) to the lipid membrane at pH 4.0 is entropy-driven and peptide-to-lipid binding induces an increase in ΔS^o (see Table 1) indicating an increase in disorder. This is mostly due to the release of water from the lipid membrane surface, but the loss of secondary structure of βAP(25-35) upon binding observed by CD (see Figure 12) may also contribute. In contrast, the binding process of WβAP(25-35) to POPC/POPG SUVs (3:1, mol/mol) at pH 4.0 is enthalpy-driven, similar to the binding of βAP(25-35)_I32W to POPC/POPG SUVs (2:1, mol/mol) at the same pH value (see Table 1 and 2).

At pH 7.4, βAP(25-35)_I32W binds quickly to the POPC/POPG (2:1, mol/mol) membrane and releases little heat (see ΔH^o values in Table 3). In contrast to the experiment with βAP(25-35)_I32W at pH 4.0, but similar to the binding of βAP(25-35) at pH 4.0, the binding of βAP(25-35)_I32W is entropy-driven. ΔS^o is large and positive; $T\Delta S^o$ varies from 4.0 to 4.8 kcal.mol^{-1} (16.7 to 20.1 kJ.mol^{-1}) over the temperature range studied (from 12 to 25°C). The binding is characterized by a heat capacity change

ΔC_p = 38 cal.mol^{-1}.K^{-1}. ΔC_p is the most reliable parameter to give information on the driving forces of a binding reaction. Indeed the simple comparison of the enthalpy and entropy values is insufficient to define the binding mechanism, as was shown with the description of the nonclassical hydrophobic effect[13,31]. ΔC_p is associated with the dehydration of nonpolar surfaces[32]. In the case of a negative ΔC_p value, the binding process is mainly due to hydrophobic contributions[33]. The positive value calculated from our calorimetric titrations is unexpected, since the transfer of a hydrophobic group, i.e. the amyloid model peptide, from the aqueous phase to the hydrophobic lipid bilayer is characterized by a negative ΔC_p[34]. This slightly positive value could be due to the increased exposure of hydrophobic areas to the aqueous buffer[34]. Eventually the free energy is more favorable than at pH 4.0 with ΔG^o = -4.2 kcal.mol^{-1} (see Table 3).

c) Enthalpy-entropy compensation

The free energy of binding for all three peptides is stable around -3.3 kcal.mol^{-1} at pH 4.0 and -5.3 kcal.mol^{-1} at pH 7.4 (-13.8 and -22.2 kJ.mol^{-1}), indicating an enthalpy-entropy compensation mechanism. The compensation mechanism is represented by a linear correlation between the enthalpy ΔH^o and the entropy of reaction $T\Delta S^o$ according to Equation (7)[35]:

$$T\,\Delta S^0 = \alpha\,\Delta H^0 + T\,\Delta S_0^0 \qquad (7)$$

***Table 5**: Parameters of the equation $T\Delta S^o = \alpha\Delta H^o + T\Delta S^o_o$ for the binding of βAP(25-35), WβAP(25-35) and βAP(25-35)_I32W. The correlation is found for all binding conditions studied. The slope α, the intercept $T\Delta S_o^o$ and the correlation coefficient R^2 are summarized.*

		α /	$T\Delta S_0^0$ (kcal/mol)	R^2 /
pH 4.0	βAP(25-35)	3.55	7.24	0.98
	WβAP(25-35)	1.00	3.24	0.99
	βAP(25-35)_I32W (2:1)	0.92	2.49	0.99
pH 7.4	βAP(25-35)_I32W (2:1)	1.24	5.55	0.99

The slope α (see Table 5) indicates the extent to which enthalpy contributes to the free energy of binding, that is to say to the system stability[35]. The intercept $T\Delta S_o^o$ theoretically represents the system stability when the enthalpy is zero. In the absence

of enthalpic contribution, the entropy leads to favorable equilibrium, with $T\Delta S^{o}$ between 2.5 and 7.2 kcal.mol^{-1} (10.5 to 30.1 kJ.mol^{-1}).

d) Structure of the amyloid model peptides associated with the lipid membrane

The combination of the thermodynamic data with peptide secondary structure gives indications on the geometry of each peptide on the lipid membrane. Figure 19 shows a speculative model based on the structure of βAP(25-35) in HFIP/water (20:80, v/v)[36], for βAP(25-35) and WβAP(25-35) in Figure 19A and 19B, respectively. As the crystallization of fibril-forming peptides is difficult, no crystal structure of β-sheet βAP(1-40) or any of his model peptides are available. Therefore the β-sheet structure of βAP(25-35)_I32W in Figure 19C is based on the crystal structure of α-synuclein[37].

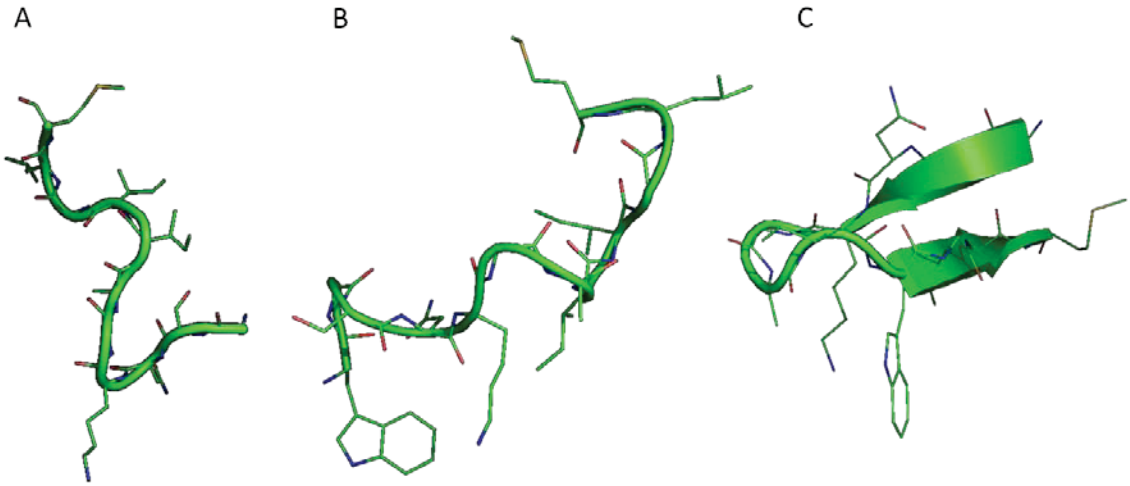

***Figure 19**: Representation of a possible geometry of (A) βAP(25-35), (B) WβAP(25-35) and (C) βAP(25-35)_I32W in their bound state. The lipid membrane surface would be at the bottom of the peptides in order to interact with the side chain of Lys28 and Trp32 or Trp24. The original crystal structures[36,37] were modified with PyMol. The side-chains of the amino-acids are represented in the most favorable conformation that matches our ITC and CD data. The snorkeling of the Lys acyl chain could not be represented with PyMol.*

The binding of βAP(25-35), WβAP(25-35) and βAP(25-35)_I32W is controlled by the electrostatic attraction of Lys28 to the negatively-charged POPG headgroup. Bound βAP(25-35) is unstructured; the only knowledge regarding peptide geometry is therefore the snorkeling of the acyl side-chain of Lys28 in the lipid membrane[38] (see Figure 19A).

The additional Trp in the sequence of WβAP(25-35) and βAP(25-35)_I32W also influences the binding mechanism as the side-chain of this residue can insert into the membrane[28]. The peptide chain of WβAP(25-35) could be aligned partially parallel to the lipid membrane surface to allow the insertion of the indole group of Trp24 and the snorkeling[38] of the side-chain of Lys28 inserted into the lipid membrane surface (see Figure 19B).

Binding to the lipid membrane induces β-sheet of βAP(25-35)_I32W. The side-chains of Lys28 snorkels[38] and that of Trp32 inserts into the apolar environment of the lipid membrane. A possible structure is therefore shown in Figure 19C. The β-sheet formed by βAP(25-35)_I32W on the surface could include a three-amino-acid long loop, from Gly29 to Ile31.

e) Structure of the lipid membrane upon peptide insertion or binding

The insertion of the three amyloid model peptides into the membrane leaves the lipid bilayer intact, similar to βAP(1-40)[8]. In effect, the large quadrupole splitting of ~ 27 kHz and the chemical shielding anisotropy of -50 ppm at high temperature are characteristic values for a lipid bilayer[39-41] and are similar to the results found for pure POPC/d_{31}-POPG lipid bilayers (see Figure 14 and 16). The lipid membranes with inserted model peptides have melting transitions close to those of the pure lipid membrane. The d_{31}-POPG acyl chains melt at T_m = 4°C (see Figure 16A), slightly above the pure lipid membrane (T_m = -3°C). In contrast, the lipid headgroups suggest an even higher transition temperature of 2 to 6°C (see Figure 14).

Below T_m, the lipid chains become more rigid and the quadrupole splittings are small (see Figure 16). Also the quadrupole splittings of the lipid membrane with the model peptides, $\Delta\nu_Q(CD_2)_{pep}$ and $\Delta\nu_Q(CD_3)_{pep}$, are smaller than the splittings of the pure lipid membrane, $\Delta\nu_Q(CD_2)_{lipid}$, in the gel phase: the insertion of peptide in the lipid membrane stiffens further the acyl chains. Above T_m, $\Delta\nu_Q(CD_3)_{pep}$ and $\Delta\nu_Q(CD_2)_{pep}$ become smaller with the increasing temperature in the presence of amyloid model peptides whereas both splittings remain constant in the lipid membrane without peptide. $\Delta\nu_Q(CD_2)_{pep}$ is 10% smaller than $\Delta\nu_Q(CD_2)_{lipid}$ at 10°C and becomes 25% smaller

at 40°C in presence of peptides. The difference is even larger for $\Delta\nu_Q(CD_3)_{pep}$: it is 19% smaller than $\Delta\nu_Q(CD_3)_{lipid}$ at 10°C and 40% smaller at 40°C. This observation indicates a higher mobility in the liquid-crystalline phase of the lipid chains in presence of amyloid peptides. These variations of quadrupole splittings are similar for all three peptides and to our knowledge, have never been observed in the past. In effect the insertion of cytochrome *c* oxidase in a $d_{9,10}$-1,2-dioleoyl-*sn*-glycero-3-phosphocholin membrane did not induce any major change in the quadrupole splittings[42] measured with ^{2}H-NMR. Similarly the insertion of a cationic amphiphilic peptide in DMPC membranes with perdeuterated acyl chains did not lead to any perturbation of the quadrupole splittings[43].

The chemical shielding anisotropy $\Delta\sigma$ of the lipid membrane in presence of βAP(25-35) or WβAP(25-35) is smaller than $\Delta\sigma_{lip}$ of the pure lipid membrane both in the gel phase and in the liquid-crystalline phase (see Figure 14). In presence of βAP(25-35)_I32W, $\Delta\sigma$ is larger than $\Delta\sigma_{lip}$ below T_m but becomes smaller above T_m. Upon temperature increase the difference between $\Delta\sigma$ of the lipid membrane in presence of any of the three amyloid model peptides and $\Delta\sigma_{lip}$ decreases; $\Delta\sigma$ is 15% smaller than $\Delta\sigma_{lip}$ at 6°C and only 10% smaller at 12°C. The insertion of the amyloid model peptides into the lipid membrane slightly increases the mobility of the lipid headgroups, however this mobility decreases with the increasing temperature, in contrast to the acyl chains. Similarly to our results, Bokvist *et al.*[26] showed a decrease in the motions of the lipid headgroups of membranes with βAP(1-40) inserted.

The presence of amyloid peptide aggregates on the membrane surface leads to important structural modifications of both the lipid headgroups and acyl chains. Although the bilayer structure is present in both ^{2}H- and ^{31}P-NMR spectra (see Figure 16 and 17), an additional isotropic peak is observed after association of aggregates of βAP(25-35), WβAP(25-35) or βAP(25-35)_I32W with the lipid membrane. This isotropic phase is favored by high temperatures and the bilayer features cannot be observed anymore. Additional DSC experiments in crucible would allow the observation of distinct phase transitions of the POPC/POPG membrane in presence of amyloid peptide aggregates at the low temperature range required.

A modification of the lipid membrane structure upon amyloid peptide association was already reported in the literature. A change of the structure and dynamics of a DMPC/DMPS lipid bilayer upon βAP(25-35) association was shown by Buchsteiner *et al*[44]. The authors used neutron diffraction to prove the disordering of the lipid and the increase in lipid mobility and lateral diffusion. Other evidence from membrane structural changes was reported by Demuro *et al.* who showed the ability of βAP(1-42) to release calcein from human neuroblastoma cell[45]. The DSC study performed by Del Mar *et al.* on DMPG vesicles associated with βAP(1-40) at pH 7.4, showed an additional shoulder in the calorimetric profile compared to DMPG alone[46], and was taken as evidence for the formation of a new lipid phase.

5. References

(1) Yankner, B. A.; Duffy, L. K.; Kirschner, D. A. *Science* **1990**, *250*, 279.
(2) Clementi, M. E.; Marini, S.; Coletta, M.; Orsini, F.; Giardina, B.; Misiti, F. *FEBS Lett* **2005**, *579*, 2913.
(3) Wong, P. T.; Schauerte, J. A.; Wisser, K. C.; Ding, H.; Lee, E. L.; Steel, D. G.; Gafni, A. *J Mol Biol* **2009**, *386*, 81.
(4) Mirzabekov, T.; Lin, M. C.; Yuan, W. L.; Marshall, P. J.; Carman, M.; Tomaselli, K.; Lieberburg, I.; Kagan, B. L. *Biochem Biophys Res Commun* **1994**, *202*, 1142.
(5) Kagan, B. L.; Azimov, R.; Azimova, R. *J Membr Biol* **2004**, *202*, 1.
(6) Allsop, D.; Landon, M.; Kidd, M. *Brain Res* **1983**, *259*, 348.
(7) Welander, H.; Franberg, J.; Graff, C.; Sundstrom, E.; Winblad, B.; Tjernberg, L. O. *J Neurochem* **2009**, *110*, 697.
(8) Terzi, E.; Holzemann, G.; Seelig, J. *Biochemistry* **1997**, *36*, 14845.
(9) Terzi, E.; Holzemann, G.; Seelig, J. *Biochemistry* **1994**, *33*, 7434.
(10) Lewis, B. A.; Engelman, D. M. *J Mol Biol* **1983**, *166*, 211.
(11) Reed, J.; Reed, T. A. *Anal Biochem* **1997**, *254*, 36.
(12) Hahn, E. L. *Physical Review* **1950**, *80*.
(13) Seelig, J.; Ganz, P. *Biochemistry* **1991**, *30*, 9354.
(14) Beschiaschvili, G.; Seelig, J. *Biochemistry* **1992**, *31*, 10044.
(15) Seelig, J.; Nebel, S.; Ganz, P.; Bruns, C. *Biochemistry* **1993**, *32*, 9714.
(16) Wenk, M. R.; Seelig, J. *Biophys J* **1997**, *73*, 2565.
(17) Wieprecht, T.; Dathe, M.; Schumann, M.; Krause, E.; Beyermann, M.; Bienert, M. *Biochemistry* **1996**, *35*, 10844.
(18) Cooper, A. *Curr Opin Chem Biol* **1999**, *3*, 557.
(19) Seelig, A.; Alt, T.; Lotz, S.; Holzemann, G. *Biochemistry* **1996**, *35*, 4365.
(20) Holladay, L. A.; Puett, D. *Biopolymers* **1976**, *15*, 43.
(21) Holladay, L. A.; Rivier, J.; Puett, D. *Biochemistry* **1977**, *16*, 4895.
(22) Killian, J. A.; Salemink, I.; de Planque, M. R.; Lindblom, G.; Koeppe, R. E., 2nd; Greathouse, D. V. *Biochemistry* **1996**, *35*, 1037.
(23) May, S.; Ben-Shaul, A. *Biophys J* **1999**, *76*, 751.
(24) Swaney, J. B. *J Biol Chem* **1980**, *255*, 8791.
(25) Fleming, B. D.; Keough, K. M. *Can J Biochem Cell Biol* **1983**, *61*, 882.
(26) Bokvist, M.; Lindstrom, F.; Watts, A.; Grobner, G. *J Mol Biol* **2004**, *335*, 1039.
(27) Ravault, S.; Soubias, O.; Saurel, O.; Thomas, A.; Brasseur, R.; Milon, A. *Protein Sci* **2005**, *14*, 1181.
(28) de Planque, M. R.; Kruijtzer, J. A.; Liskamp, R. M.; Marsh, D.; Greathouse, D. V.; Koeppe, R. E., 2nd; de Kruijff, B.; Killian, J. A. *J Biol Chem* **1999**, *274*, 20839.
(29) Chi, E. Y.; Ege, C.; Winans, A.; Majewski, J.; Wu, G.; Kjaer, K.; Lee, K. Y. *Proteins* **2008**, *72*, 1.
(30) Come, J. H.; Fraser, P. E.; Lansbury, P. T., Jr. *Proc Natl Acad Sci U S A* **1993**, *90*, 5959.
(31) Huang, C. H.; Charlton, J. P. *Biochemistry* **1972**, *11*, 735.
(32) Baldwin, R. L. *Proc Natl Acad Sci U S A* **1986**, *83*, 8069.
(33) Gomez, J.; Hilser, V. J.; Xie, D.; Freire, E. *Proteins* **1995**, *22*, 404.
(34) Wieprecht, T.; Apostolov, O.; Beyermann, M.; Seelig, J. *J Mol Biol* **1999**, *294*, 785.
(35) Rekharsky, M. V.; Inoue, Y. *Chem Rev* **1998**, *98*, 1875.
(36) D'Ursi, A. M.; Armenante, M. R.; Guerrini, R.; Salvadori, S.; Sorrentino, G.; Picone, D. *J Med Chem* **2004**, *47*, 4231.

(37) De Genst, E. J.; Guilliams, T.; Wellens, J.; O'Day, E. M.; Waudby, C. A.; Meehan, S.; Dumoulin, M.; Hsu, S. T.; Cremades, N.; Verschueren, K. H.; Pardon, E.; Wyns, L.; Steyaert, J.; Christodoulou, J.; Dobson, C. M. *J Mol Biol* **2010**, *402*, 326.
(38) Strandberg, E.; Killian, J. A. *FEBS Lett* **2003**, *544*, 69.
(39) Seelig, A.; Seelig, J. *Biochemistry* **1974**, *13*, 4839.
(40) Seelig, A.; Seelig, J. *Biochim Biophys Acta* **1975**, *406*, 1.
(41) Davis, J. H. *Biophys J* **1979**, *27*, 339.
(42) Tamm, L. K.; Seelig, J. *Biochemistry* **1983**, *22*, 1474.
(43) Roux, M.; Neumann, J. M.; Hodges, R. S.; Devaux, P. F.; Bloom, M. *Biochemistry* **1989**, *28*, 2313.
(44) Buchsteiner, A.; Hauss, T.; Dante, S.; Dencher, N. A. *Biochim Biophys Acta* **2010**, *1798*, 1969.
(45) Demuro, A.; Mina, E.; Kayed, R.; Milton, S. C.; Parker, I.; Glabe, C. G. *J Biol Chem* **2005**, *280*, 17294.
(46) Del Mar Martinez-Senac, M.; Villalain, J.; Gomez-Fernandez, J. C. *Eur J Biochem* **1999**, *265*, 744.

VII. Appendix: Gouy-Chapman theory

As was detailed in the Chapter VI (see p.60), Boltzman's law describes the electrostatic equilibrium between the peptide concentration close to the membrane, c_M, with the concentration of free peptide in the bulk solution, c_f, considering the surface potential Ψ_0 at the membrane surface.

$$c_M = c_f e^{\left(\frac{-z_p F_0 \Psi_0}{RT}\right)} \tag{5}$$

The membrane potential Ψ_0 cannot be measured directly. However it is related to the membrane surface charge density σ which, in turn, can be expressed as a function of the extent of binding X_b. The Gouy-Chapman theory[1,2] provides the relation between Ψ_0 and σ according to:

$$\sigma^2 = 2000\varepsilon_0\varepsilon_r RT\sum_i c_i\left(e^{-\frac{z_i\psi_0 F_0}{RT}} - 1\right) \tag{8}$$

with z_i the signed valency of the i^{th} species in the bulk phase and c_i its concentration. ε_0 is the permittivity of the free space, ε_r the dielectric constant of the aqueous phase[3,4], RT the thermal energy and F_0 the Faraday constant.

The membrane surface charge density can be independently determined from the extent of binding with the relation derived by Seelig and Beschiaschvili[5]:

$$\sigma = \left(e_0 / A_L\right)\frac{-X_L^0\left(1 - X_{Na}\right) + z_{pep}X_b}{1 + \left(\frac{A_{pep}}{A_L}\right)X_b} \tag{9}$$

A_L is the surface area of lipid (A_L = 68 Å for POPC and POPG[6,7]), A_{pep} is the peptide surface area and can be estimated with surface activity measurements[8], z_{pep} is the peptide effective charge, X_{Na} the mole fraction of bound sodium anions, X^o_L the

mole fraction of charged lipids, X_b the mole fraction of bound peptide. As A_{pep} is between 50 and 150 Å for most peptides, the correction term for peptide penetration into the membrane $A_{pep}/A_L\ X_b$ is small compared to unity and can been neglected for molecules which do not penetrate into the membrane.

The above relationships (Equations (5), (8) and (9)) together with the law of mass conservation make it possible to calculate the surface potential Ψ_0 and the peptide concentration at the membrane surface c_M for each value of bound peptide X_b. These equations together with the ones described in the Chapter VI will be used to find the best fit to the data obtained from ITC measurement.

1. References

(1) Gouy, G. *Journal de Physique* **1910**, 457.
(2) Chapman, J. C. *Philosophical Magazine* **1913**, *25*, 475.
(3) Grahame, D. C. *Chem Rev* **1947**, *41*, 441.
(4) McLaughlin, S. *Annu Rev Biophys Biophys Chem* **1989**, *18*, 113.
(5) Beschiaschvili, G.; Seelig, J. *Biochemistry* **1990**, *29*, 10995.
(6) Altenbach, C.; Seelig, J. *Biochemistry* **1984**, *23*, 3913.
(7) Evans, R. W.; Williams, M. A.; Tinoco, J. *Biochem J* **1987**, *245*, 455.
(8) Seelig, J.; Nebel, S.; Ganz, P.; Bruns, C. *Biochemistry* **1993**, *32*, 9714.

VIII. Appendix: solid-state NMR

Solid-state nuclear magnetic resonance (ssNMR) investigates the anisotropic motions of a nucleus in a magnetic field and provides information on the nucleus environment. Phosphorus, deuterium and carbon NMR are the most common methods in lipid membrane studies. In phosphorus and carbon ssNMR, anisotropic chemical shift and heteronuclear dipolar coupling give rise to line broadening, whereas in deuterium ssNMR anisotropic motions are easily detected. The principle of the ssNMR techniques used in this work, ^{31}P- and ^{2}H-NMR, are briefly detailed thereafter.

1. ^{31}P-NMR

The natural abundance of ^{31}P is 100%, and phosphorus NMR is a conventional method to study the orientation and structure of the phospholipid headgroups. In the case of a single crystal, the phosphate groups have a unique orientation with respect to the crystal axes. As all phosphates are aligned in the same direction, they give rise to the same sharp phosphorus resonance[1]. Due to the anisotropy of the electron density around the phosphorus atom, the chemical shielding of the applied magnetic field depends on the orientation of the phosphorus nuclei. Therefore upon rotation of the crystal in the magnetic field, these resonances will shift their position with respect to a fixed reference signal. The complete rotation pattern of a single crystal leads to the determination of the principal components (σ_{11}, σ_{22}, σ_{33}) of the chemical shielding tensor[1] (see Figure 1). The orientation of the chemical shielding tensor determined with phosphoethanolamine crystal is usually taken as a reference for the other phospholipids.

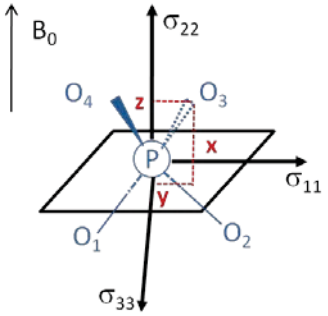

***Figure 1**: Orientation of the chemical shielding tensor in the molecular frame of the phosphate segment. O_1 connects the phosphate group with the backbone and O_2 with the head group residue. O_3 and O_4 represent the nonesterified oxygens. Reproduced from [1].*

In the case of an oriented bilayer, the phosphate groups rotate around the bilayer normal, leading to a partial averaging of the shielding tensor. This averaged tensor is axially symmetric and has two principal components, $\sigma_{\parallel}$ and $\sigma_{\perp}$ (see Figure 2).

In the case of a powder type sample, each microdomain has a different orientation with respect to the applied magnetic field. If averaged over time, each of these orientations has a defined probability. The superposition of the phosphorus resonances combined with their probability produces the observable spectrum (see Figure 2).

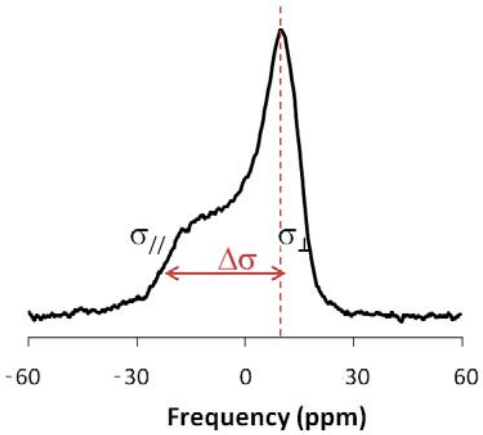

***Figure 2**: ^{31}P-NMR spectra of bilayers of dimyristoyl-phosphatidylglycerol (DMPG) at 30°C.The chemical shielding anisotropy $\Delta\sigma$ is directly measured from the distance between the low- and high-field shoulders.*

$\Delta\sigma$ is measured in the ^{31}P-NMR spectrum as the distance between the low- and the high-field shoulder (see Figure 2), $\Delta\sigma = \sigma_{\parallel} - \sigma_{\perp}$. It results from the averaging of the

chemical shielding tensor and is a measure of the orientation and average fluctuations of the phosphate headgroup. Unsonicated phospholipid bilayers in a magnetic field typically have a ^{31}P NMR powder chemical shielding anisotropy of $\Delta\sigma = -50$ ppm.

2. ^{2}H-NMR

Deuterium NMR observes the fluctuations of the labeled phospholipid chains via deuteron resonance frequencies with respect to the applied magnetic field. The deuterium spectrum consists of an isotropic line in the case of rapid isotropic motions. In the case of anisotropic motions each deuteron gives rise to a doublet due to the quadrupole moment of the deuterium nucleus.

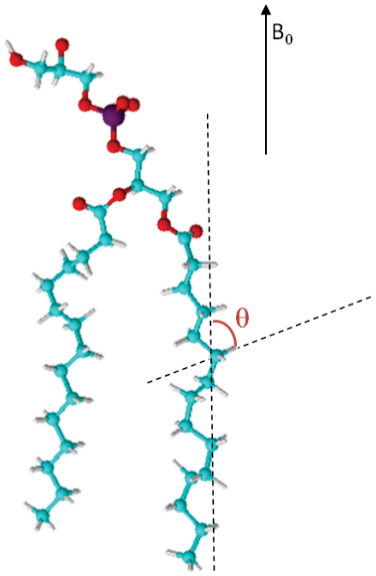

***Figure 3**: Dimyristoylphosphatidyglycerol molecule in a magnetic field B_0. The C-D bond orientation is defined with the angle θ with respect to the bilayer normal.*

The doublet spacing, also named quadrupole splitting $\Delta\nu_Q$, depends on the degree of anisotropy of the powder-type sample and on the orientation of the C-D bond vector according to[2]:

$$\pm \Delta\nu_Q = \frac{3}{4}\frac{e^2qQ}{h}S_{CD}$$

with e^2qQ/h the quadrupole coupling constant and S_{CD} the order parameter of the C-D bond. This latter is expressed as function of the angle between the bilayer normal and the C-D bond (see Figure 3) as follows:

$$S_{CD} = \frac{1}{2}\left(3\cos^2\theta - 1\right)$$

As an example[3], a bilayer in the gel phase has an order parameter S_{CD} = -0.4. The C-D bond order parameter is correlated to the molecular order parameter with the relation:

$$S_{mol} = -2\,S_{CD}$$

The quadrupole splitting can be directly measured on the ^{2}H-NMR spectrum, as shown in Figure 4. The spectrum observed is the superposition of quadrupole splittings of each deuteron present in the lipid chain.

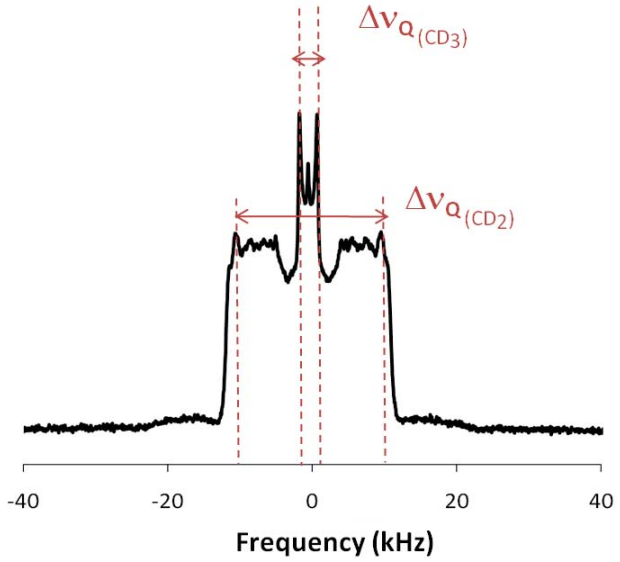

Figure 4: *^{2}H-NMR spectra of POPC/d_{31}-POPG bilayer. The quadrupole splittings represented in red originate from the terminal deuterons on the lipid chain ($\Delta\nu_{Q(CD3)}$) or from the closest deuterons to the phosphate headgroup ($\Delta\nu_{Q(CD2)}$).*

3. References

(1) Seelig, J. *Biochim Biophys Acta* **1978**, *515*, 105.
(2) Seelig, J. *Q Rev Biophys* **1977**, *10*, 353.
(3) Seelig, A.; Seelig, J. *Biochemistry* **1974**, *13*, 4839.

IX. Appendix: ITC titrations

The thermodynamic parameters, given in Table 1, 2, 3 and 4 of the Chapter VI, result from the fitting of the experimental data with the surface partitioning model combined with the Gouy-Chapman theory. All titrations are shown in the following section.

The title of each subsection indicates the peptide titrated, the pH and the molar POPC-to-POPG ratio. The peptides titrated were βAP(25-35), WβAP(25-35) or βAP(25-35)_I32W. The titrations were performed in 10 mM HEPES buffer at pH 7.4 or in 10 mM AcONa buffer at pH 4.0. The lipid system was POPC/POPG either at a ratio of 3:1 or 2:1, mol/mol. The SUVs were prepared as described in Chapter VI (Materials and Methods).

Each titration shows the same information. The upper figure represents the heat flow. The lower figure shows the cumulative heat of reaction as a function of the lipid-to-peptide molar ratio. The values on the right-hand side are the integrated heats of reaction in μcal for each lipid injection. In the lower figure, additional data are given: the peptide concentration c_{pep} in the sample cell, the lipid concentration c_{lip} in the syringe, the temperature T of the cells during the titration, the values of the enthalpy ΔH^o, free energy ΔG^o, entropy ΔS^o and intrinsic binding constant K_o of the reaction. The last indication in italic is the name of the file where the raw data are stored.

The injection volume of all titrations shown is 10 μl.

1. WbAP(25-35) titrations with POPC/POPG SUVs (3:1) at pH 4.0

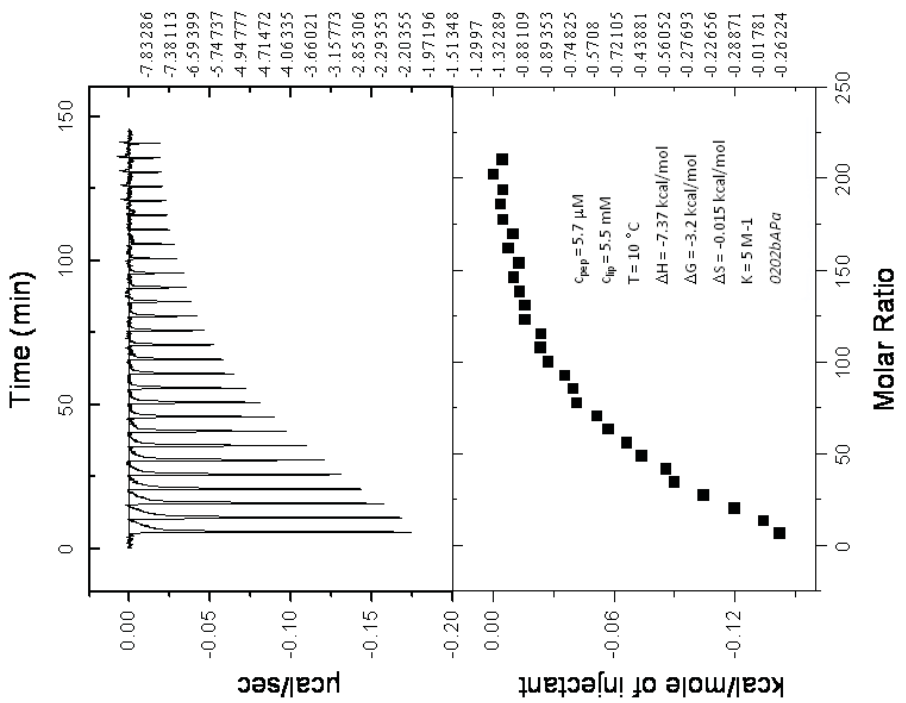

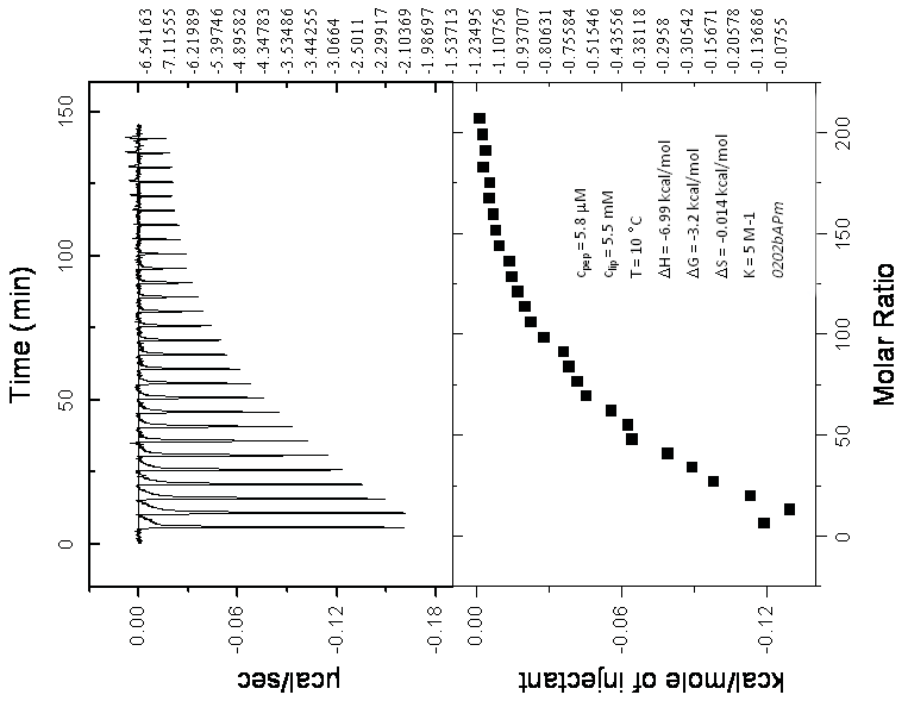

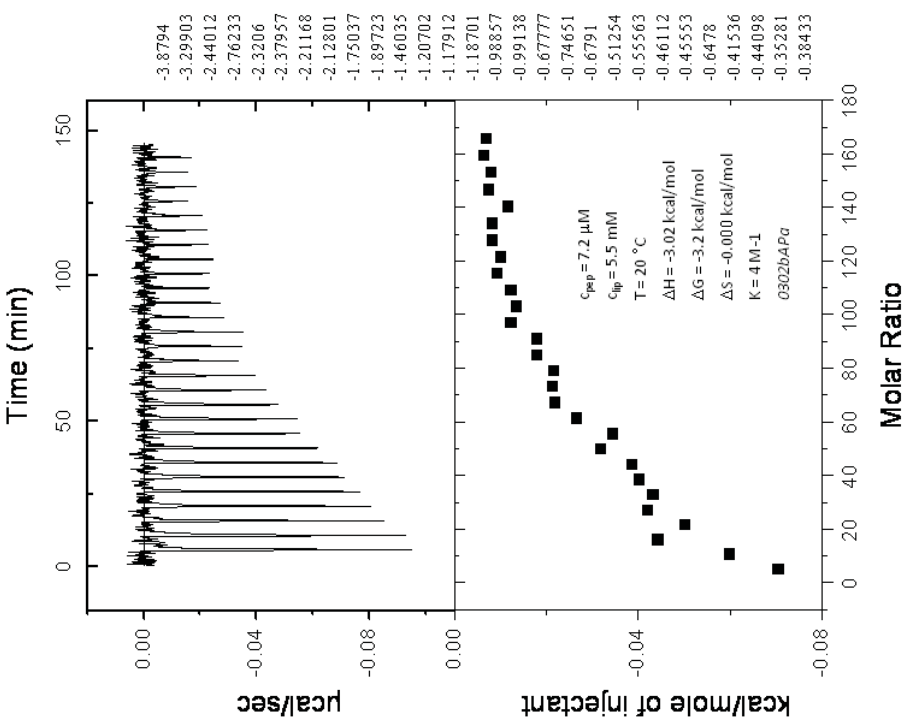
-3.8794
-3.29903
-2.44012
-2.76233
-2.3206
-2.37957
-2.21168
-2.12801
-1.75037
-1.89723
-1.46035
-1.20702
-1.17912
-1.18701
-0.98857
-0.99138
-0.67777
-0.74651
-0.6791
-0.51254
-0.55563
-0.46112
-0.45553
-0.6478
-0.41536
-0.44098
-0.35281
-0.38433
Time (min)
µcal/sec
kcal/mole of injectant
Molar Ratio
c_{pep} = 7.2 µM
c_{lip} = 5.5 mM
T = 20 °C
ΔH = -3.02 kcal/mol
ΔG = -3.2 kcal/mol
ΔS = -0.000 kcal/mol
K = 4 M-1
0302bAPa

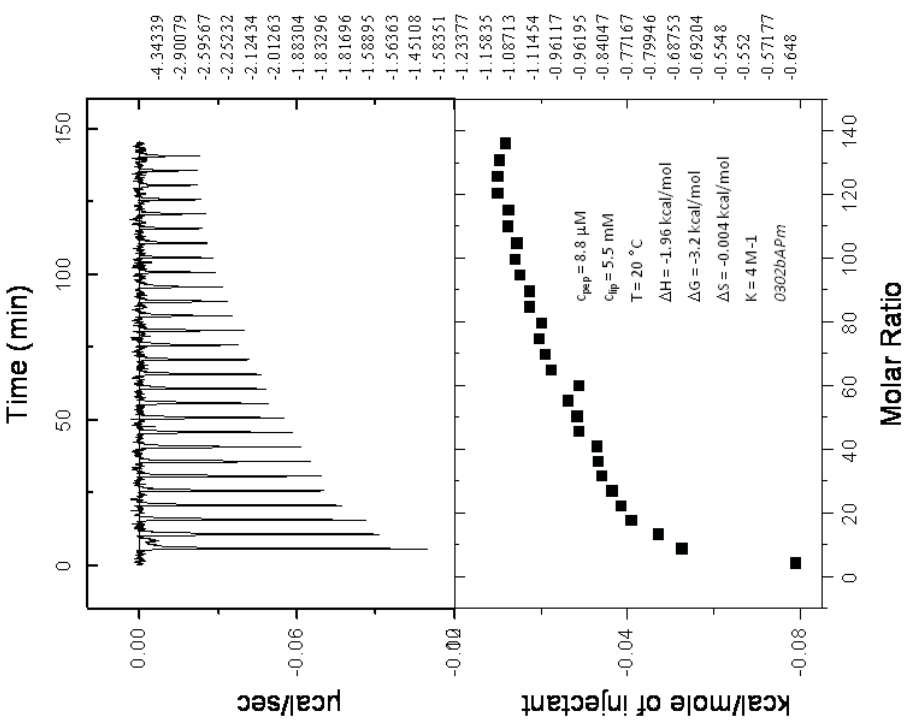
-4.34339
-2.90079
-2.59567
-2.25232
-2.12434
-2.01263
-1.88304
-1.83296
-1.81696
-1.58895
-1.56363
-1.45108
-1.58351
-1.23377
-1.15835
-1.08713
-1.11454
-0.96117
-0.96195
-0.84047
-0.77167
-0.79946
-0.68753
-0.69204
-0.5548
-0.552
-0.57177
-0.648
Time (min)
µcal/sec
kcal/mole of injectant
Molar Ratio
c_{pep} = 8.8 µM
c_{lip} = 5.5 mM
T = 20 °C
ΔH = -1.96 kcal/mol
ΔG = -3.2 kcal/mol
ΔS = -0.004 kcal/mol
K = 4 M-1
0302bAPm

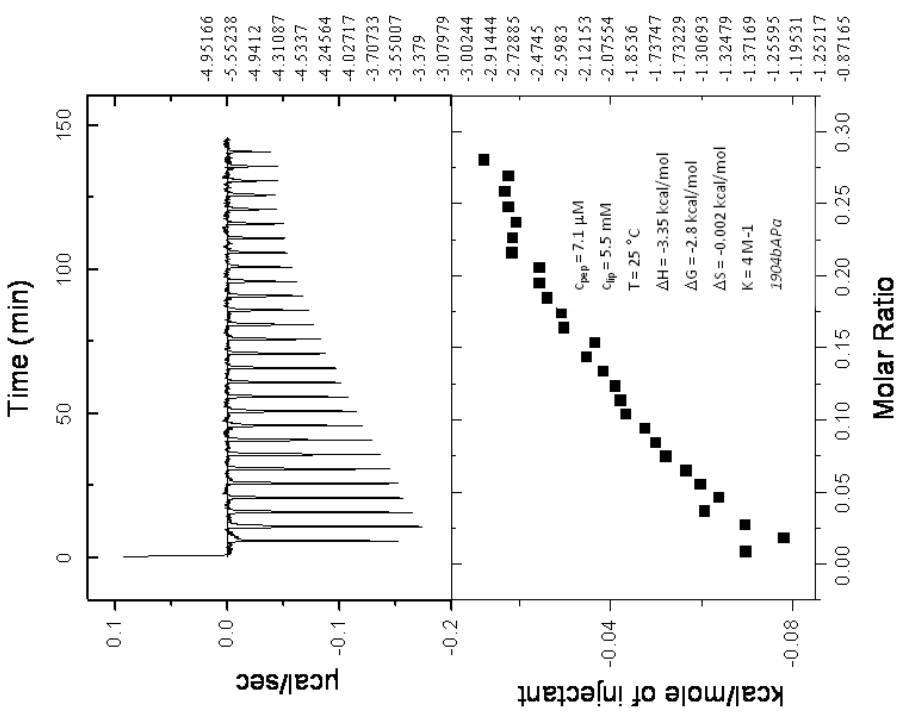
-4.95166
-5.55238
-4.9412
-4.31087
-4.5337
-4.24564
-4.02717
-3.70733
-3.55007
-3.379
-3.07979
-3.00244
-2.91444
-2.72885
-2.4745
-2.5983
-2.12153
-2.07554
-1.8536
-1.73747
-1.73229
-1.30693
-1.32479
-1.37169
-1.25595
-1.19531
-1.25217
-0.87165
Time (min)
0
50
100
150
0.1
0.0
-0.1
-0.2
µcal/sec
0.00
0.05
0.10
0.15
0.20
0.25
0.30
-0.04
-0.08
kcal/mole of injectant
Molar Ratio
cpep = 7.1 µM
citp = 5.5 mM
T = 25 °C
ΔH = -3.35 kcal/mol
ΔG = -2.8 kcal/mol
ΔS = -0.002 kcal/mol
K = 4 M-1
1904bAPa

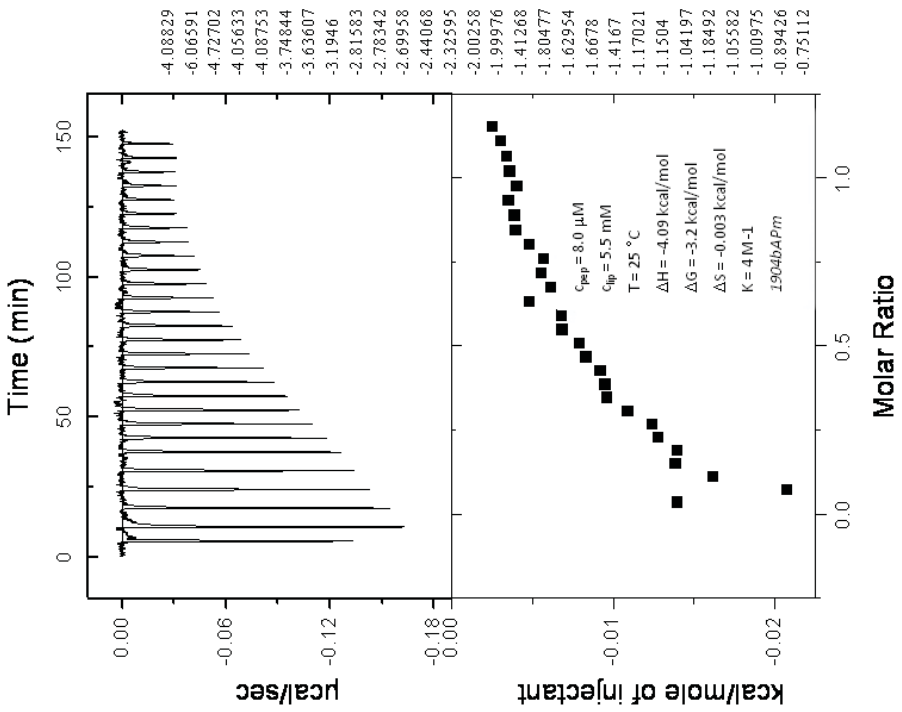
-4.08829
-6.06591
-4.72702
-4.05633
-4.08753
-3.74844
-3.63607
-3.1946
-2.81583
-2.78342
-2.69958
-2.44068
-2.32595
-2.00258
-1.99976
-1.41268
-1.80477
-1.62954
-1.6678
-1.4167
-1.17021
-1.1504
-1.04197
-1.18492
-1.05582
-1.00975
-0.89426
-0.75112
Time (min)
0
50
100
150
0.00
-0.06
-0.12
-0.18
µcal/sec
0.00
-0.01
-0.02
kcal/mole of injectant
0.0
0.5
1.0
Molar Ratio
cpep = 8.0 µM
citp = 5.5 mM
T = 25 °C
ΔH = -4.09 kcal/mol
ΔG = -3.2 kcal/mol
ΔS = -0.003 kcal/mol
K = 4 M-1
1904bAPm

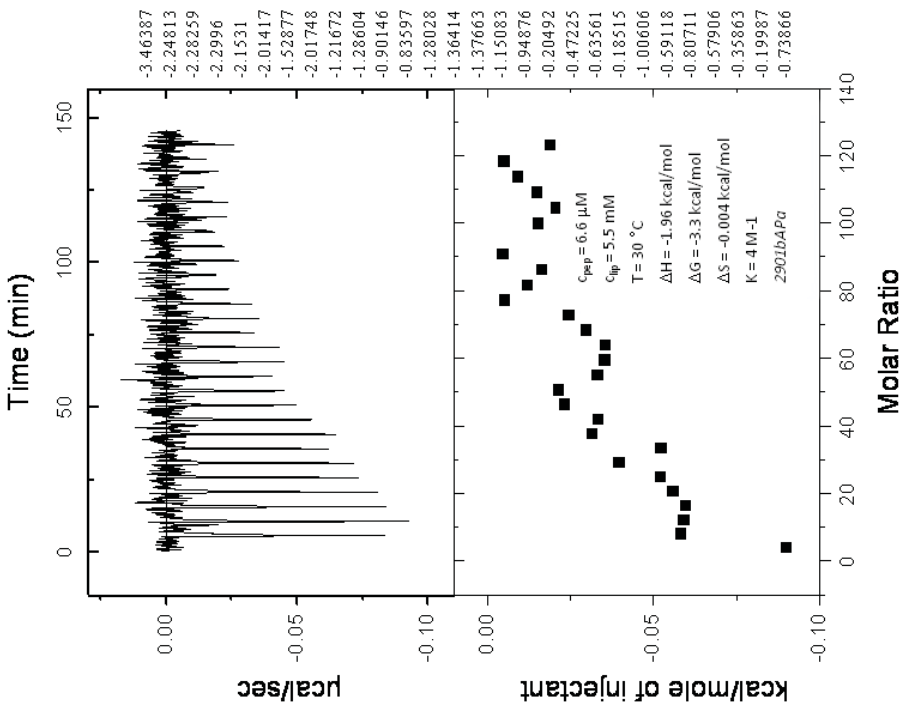
Time (min)
µcal/sec
kcal/mole of injectant
Molar Ratio
c_{pep} = 6.6 µM
c_{itp} = 5.5 mM
T = 30 °C
ΔH = -1.96 kcal/mol
ΔG = -3.3 kcal/mol
ΔS = -0.004 kcal/mol
K = 4 M-1
291bAPa
-3.46387
-2.24813
-2.28259
-2.2996
-2.1531
-2.01417
-1.52877
-2.01748
-1.21672
-1.28604
-0.90146
-0.83597
-1.28028
-1.36414
-1.37663
-1.15083
-0.94876
-0.20492
-0.47225
-0.63561
-0.18515
-1.00606
-0.59118
-0.80711
-0.57906
-0.35863
-0.19987
-0.73866

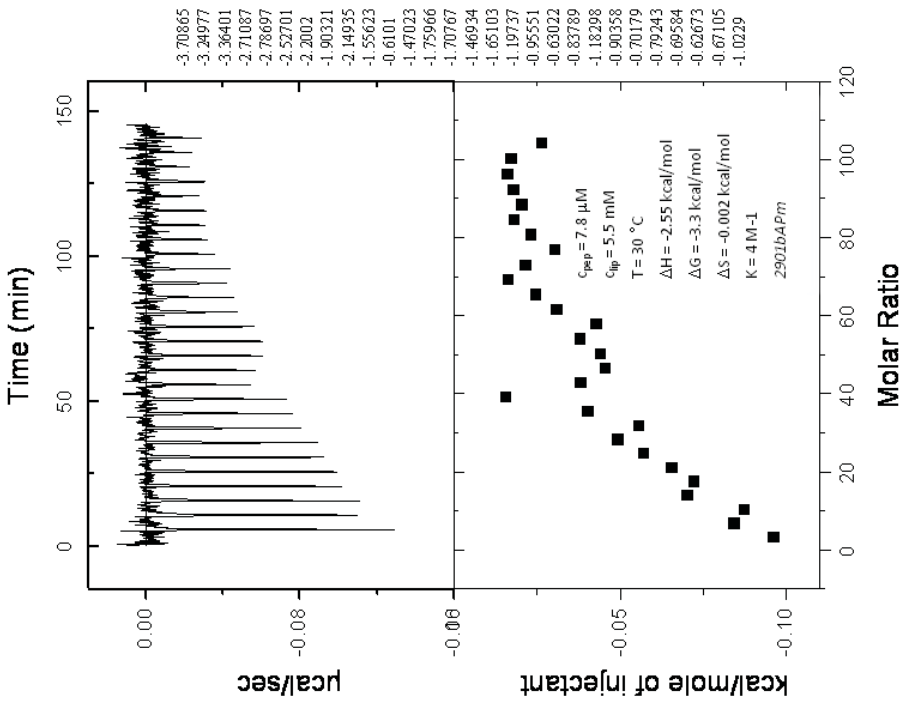
Time (min)
µcal/sec
kcal/mole of injectant
Molar Ratio
c_{pep} = 7.8 µM
c_{itp} = 5.5 mM
T = 30 °C
ΔH = -2.55 kcal/mol
ΔG = -3.3 kcal/mol
ΔS = -0.002 kcal/mol
K = 4 M-1
291bAPm
-3.70865
-3.24977
-3.36401
-2.71087
-2.78697
-2.52701
-2.2002
-1.90321
-2.14935
-1.55623
-0.6101
-1.47023
-1.75966
-1.70767
-1.46934
-1.65103
-1.19737
-0.95551
-0.63022
-0.83789
-1.18298
-0.90358
-0.70179
-0.79243
-0.69584
-0.62673
-0.67105
-1.0229

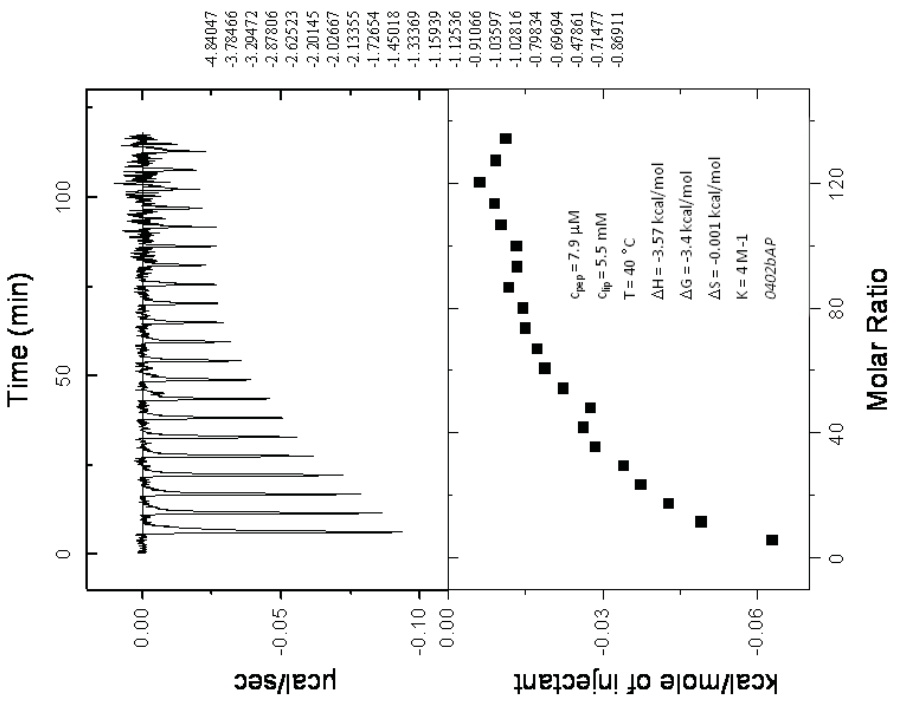
-4.84047
-3.78466
-3.29472
-2.87806
-2.62523
-2.20145
-2.02667
-2.13355
-1.72654
-1.45018
-1.33369
-1.15939
-1.12536
-0.91066
-1.03597
-1.02816
-0.79834
-0.69694
-0.47861
-0.71477
-0.86911
Time (min)
0
50
100
0.00
-0.05
-0.10
µcal/sec
0.00
-0.03
-0.06
kcal/mole of injectant
0
40
80
120
Molar Ratio
cpep = 7.9 µM
citp = 5.5 mM
T = 40 °C
ΔH = -3.57 kcal/mol
ΔG = -3.4 kcal/mol
ΔS = -0.001 kcal/mol
K = 4 M-1
0402bAP

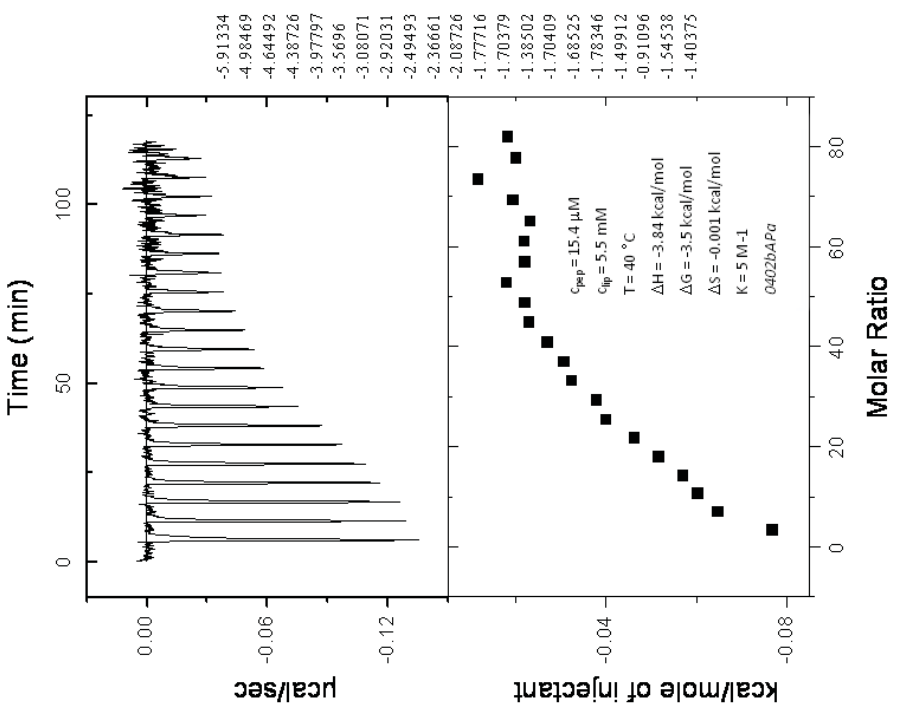
-5.91334
-4.98469
-4.64492
-4.38726
-3.97797
-3.5696
-3.08071
-2.92031
-2.49493
-2.36661
-2.08726
-1.77716
-1.70379
-1.38502
-1.70409
-1.68525
-1.78346
-1.49912
-0.91096
-1.54538
-1.40375
Time (min)
0
50
100
0.00
-0.06
-0.12
µcal/sec
0.00
-0.04
-0.08
kcal/mole of injectant
0
20
40
60
80
Molar Ratio
cpep = 15.4 µM
citp = 5.5 mM
T = 40 °C
ΔH = -3.84 kcal/mol
ΔG = -3.5 kcal/mol
ΔS = -0.001 kcal/mol
K = 5 M-1
0402bAPa

2. βAP(25-35) titrations with POPC/POPG SUVs (3:1) at pH 4.0

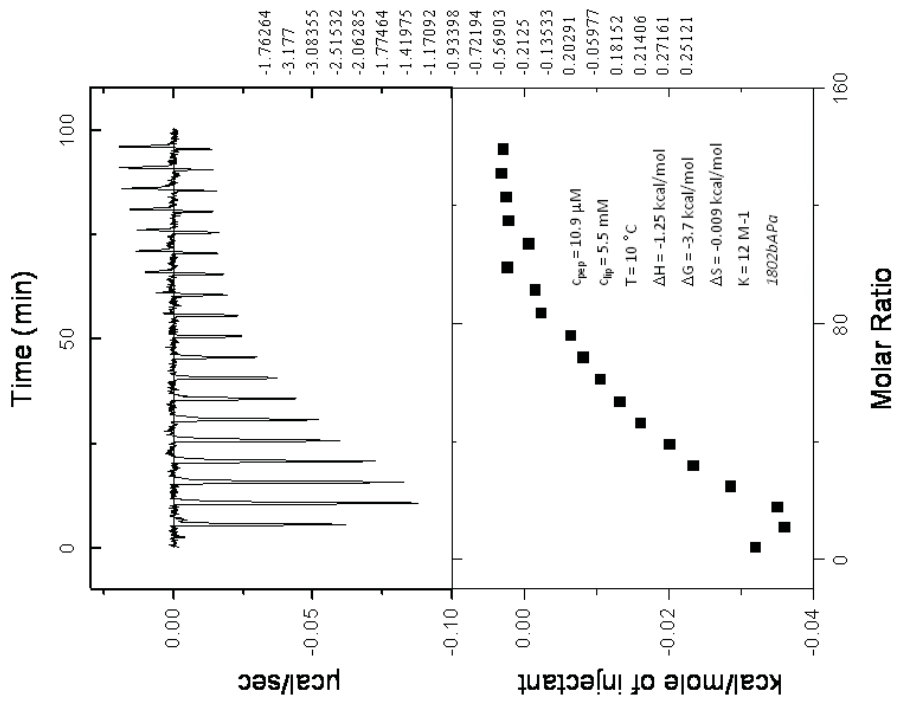

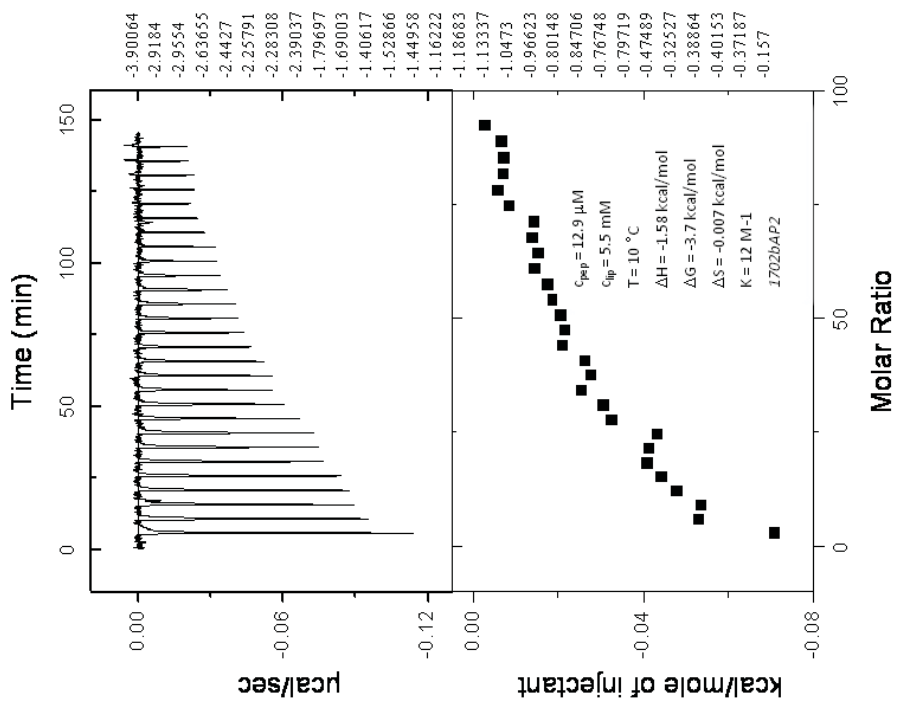

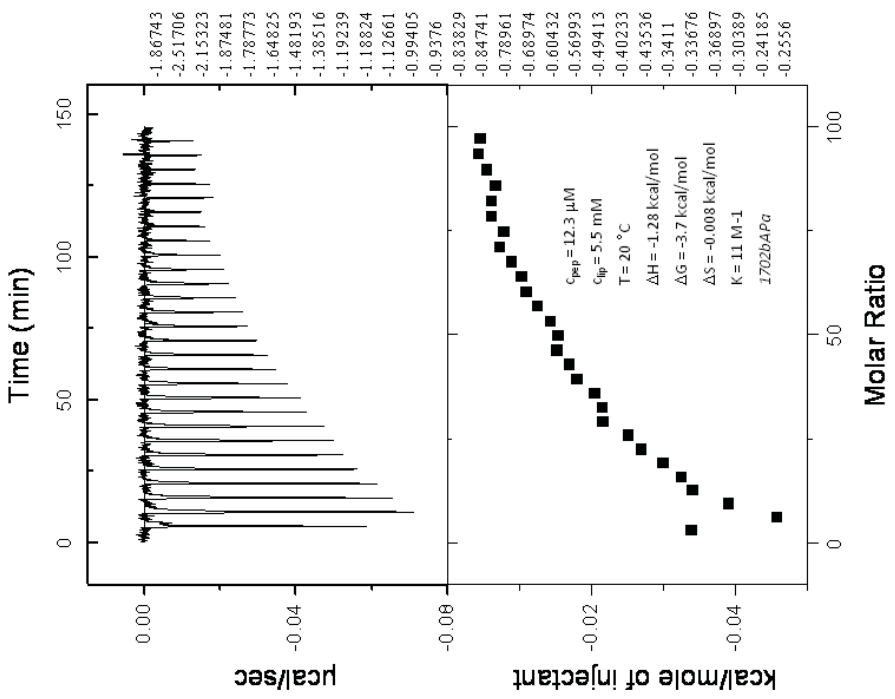
Time (min)
µcal/sec
kcal/mole of injectant
Molar Ratio
c_{pep} = 12.3 µM
c_{ip} = 5.5 mM
T = 20 °C
ΔH = -1.28 kcal/mol
ΔG = -3.7 kcal/mol
ΔS = -0.008 kcal/mol
K = 11 M-1
1702bAPa
-1.86743
-2.51706
-2.15323
-1.87481
-1.78773
-1.64825
-1.48193
-1.38516
-1.19239
-1.18824
-1.12661
-0.99405
-0.9376
-0.83829
-0.84741
-0.78961
-0.68974
-0.60432
-0.56993
-0.49413
-0.40233
-0.43536
-0.3411
-0.33676
-0.36897
-0.30389
-0.24185
-0.2556

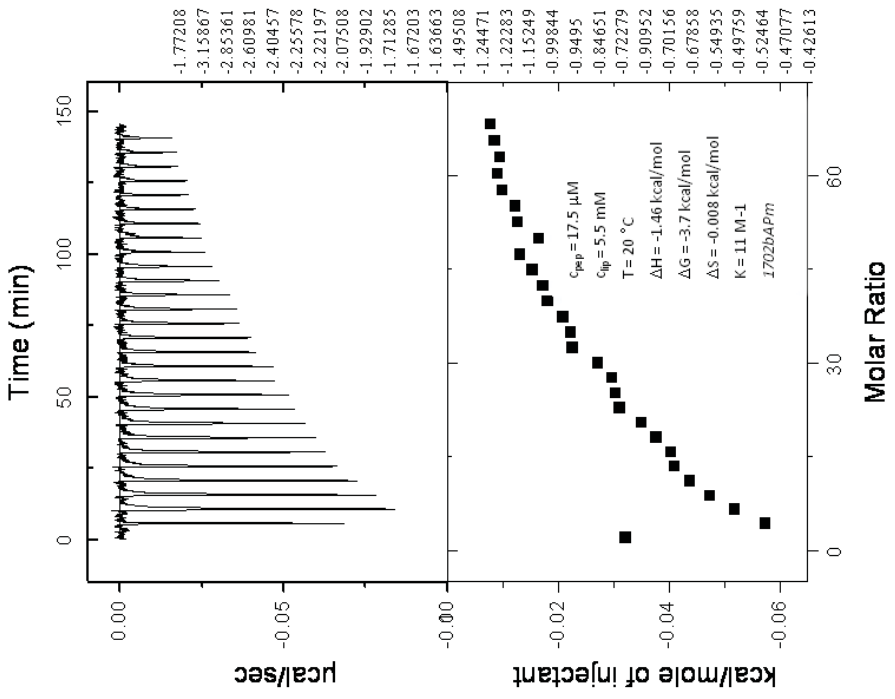
Time (min)
µcal/sec
kcal/mole of injectant
Molar Ratio
c_{pep} = 17.5 µM
c_{ip} = 5.5 mM
T = 20 °C
ΔH = -1.46 kcal/mol
ΔG = -3.7 kcal/mol
ΔS = -0.008 kcal/mol
K = 11 M-1
1702bAPm
-1.77208
-3.15867
-2.85361
-2.60981
-2.40457
-2.25578
-2.22197
-2.07508
-1.92902
-1.71285
-1.67203
-1.63663
-1.49508
-1.24471
-1.22283
-1.15249
-0.99844
-0.9495
-0.84651
-0.72279
-0.90952
-0.70156
-0.67858
-0.54935
-0.49759
-0.52464
-0.47077
-0.42613

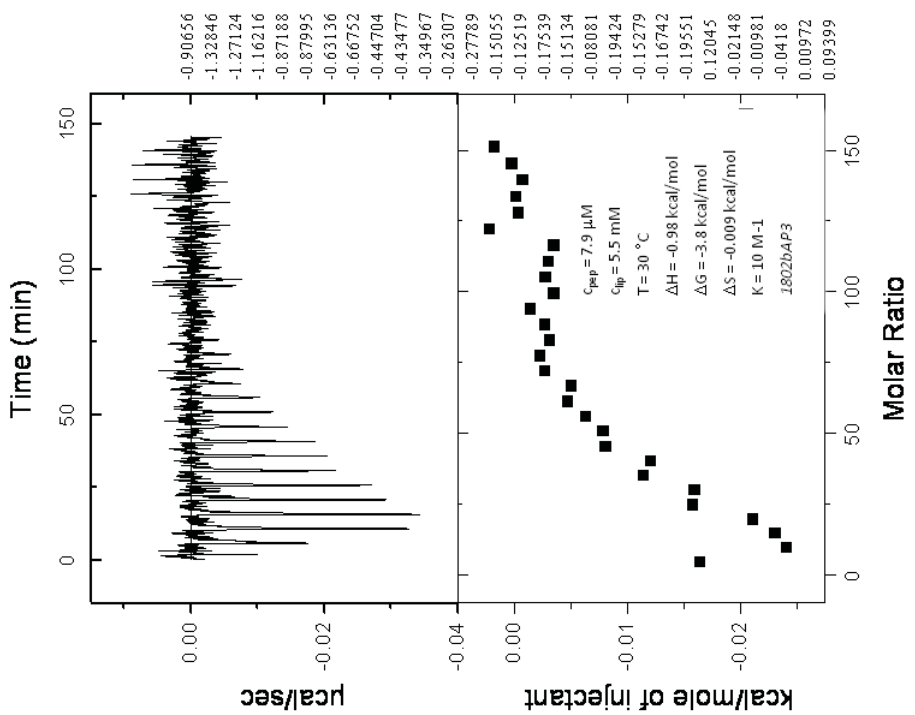
Time (min)
µcal/sec
kcal/mole of injectant
Molar Ratio
c_{pep} = 7.9 µM
c_{tip} = 5.5 mM
T = 30 °C
ΔH = -0.98 kcal/mol
ΔG = -3.8 kcal/mol
ΔS = -0.009 kcal/mol
K = 10 M-1
1802bAP3

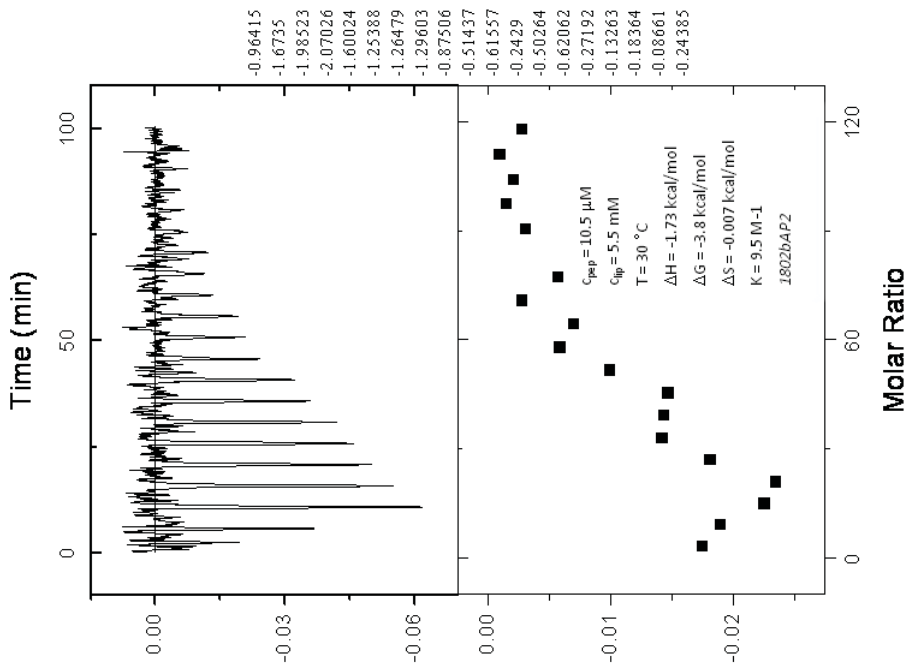
Time (min)
Molar Ratio
c_{pep} = 10.5 µM
c_{tip} = 5.5 mM
T = 30 °C
ΔH = -1.73 kcal/mol
ΔG = -3.8 kcal/mol
ΔS = -0.007 kcal/mol
K = 9.5 M-1
1802bAP2

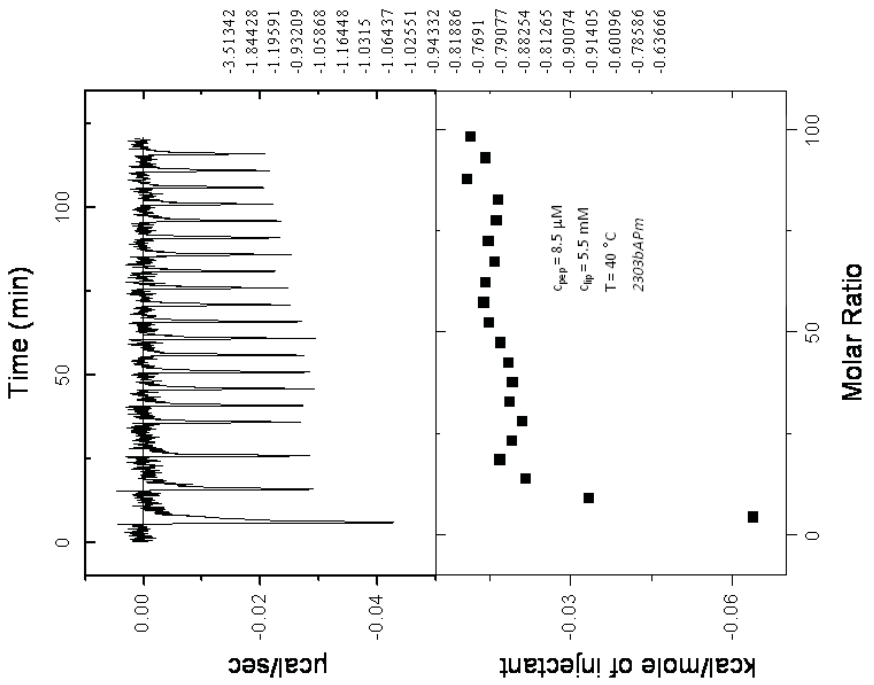
-3.51342
-1.84428
-1.19591
-0.93209
-1.05868
-1.16448
-1.0315
-1.06437
-1.02551
-0.94332
-0.81886
-0.7691
-0.79077
-0.88254
-0.81265
-0.90074
-0.91405
-0.60096
-0.78586
-0.63666
Time (min)
µcal/sec
kcal/mole of injectant
Molar Ratio
c_{PEP} = 8.5 µM
c_{Mg} = 5.5 mM
T = 40 °C
2303bAPm

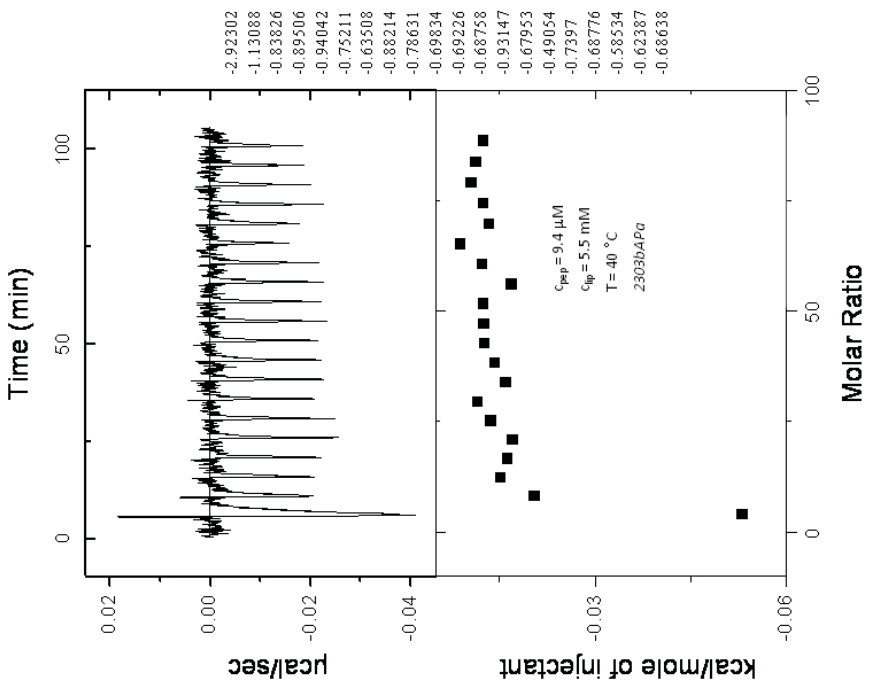
-2.92302
-1.13088
-0.83826
-0.89506
-0.94042
-0.75211
-0.63508
-0.88214
-0.78631
-0.69834
-0.69226
-0.68758
-0.93147
-0.67953
-0.49054
-0.7397
-0.68776
-0.58534
-0.62387
-0.68638
Time (min)
µcal/sec
kcal/mole of injectant
Molar Ratio
c_{PEP} = 9.4 µM
c_{Mg} = 5.5 mM
T = 40 °C
2303bAPa

3. βAP(25-35)_I32W titrations with POPC/POPG SUVs (3:1) at pH 4.0

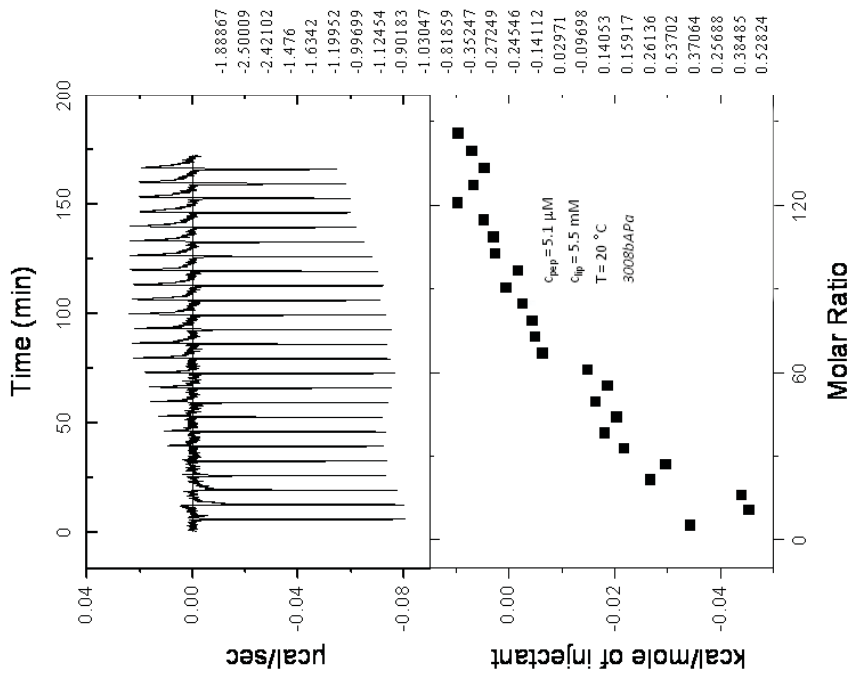

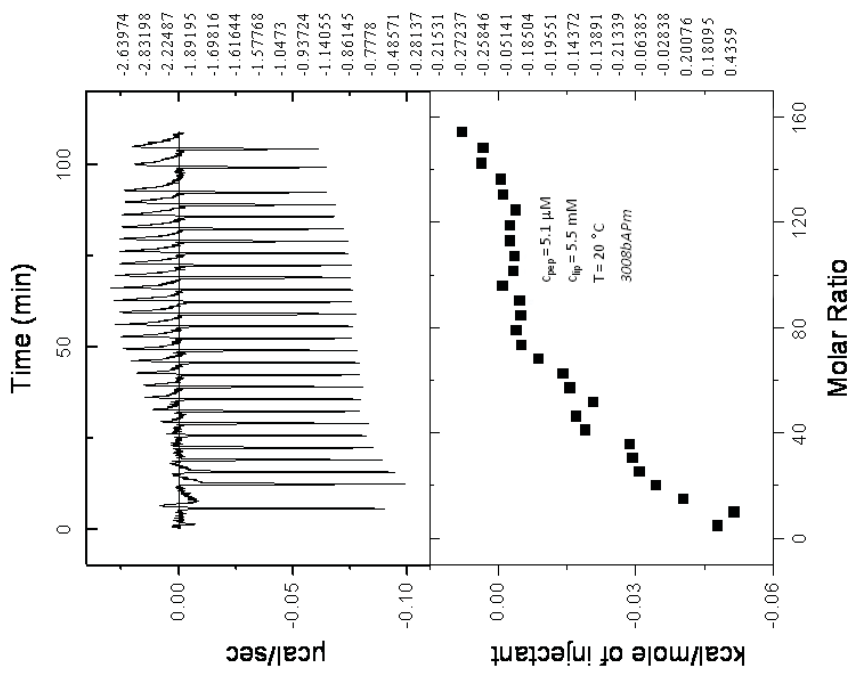

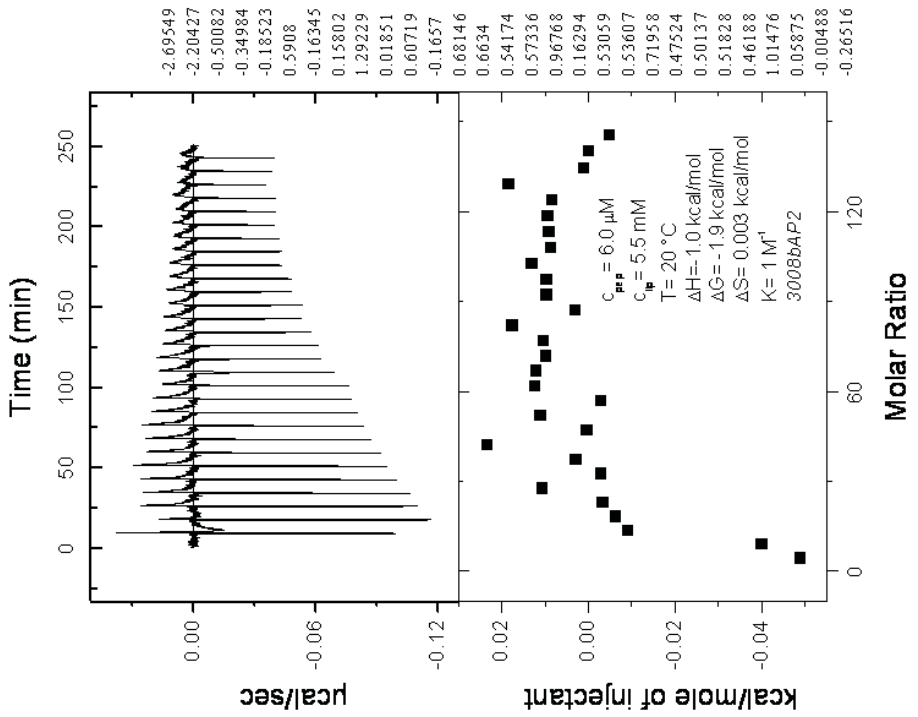
Time (min)
0
50
100
150
200
250
µcal/sec
0.00
-0.06
-0.12
kcal/mole of injectant
0.02
0.00
-0.02
-0.04
Molar Ratio
0
60
120
-2.69549
-2.20427
-0.50082
-0.34984
-0.18523
0.5908
-0.16345
0.15802
1.29229
0.01851
0.60719
-0.1657
0.68146
0.6634
0.54174
0.57336
0.96768
0.16294
0.53059
0.53607
0.71958
0.47524
0.50137
0.51828
0.46188
1.01476
0.05875
-0.00488
-0.26516
c_pep = 6.0 µM
c_lip = 5.5 mM
T= 20 °C
ΔH=-1.0 kcal/mol
ΔG= - 1.9 kcal/mol
ΔS= 0.003 kcal/mol
K= 1 M-1
3008bAP2

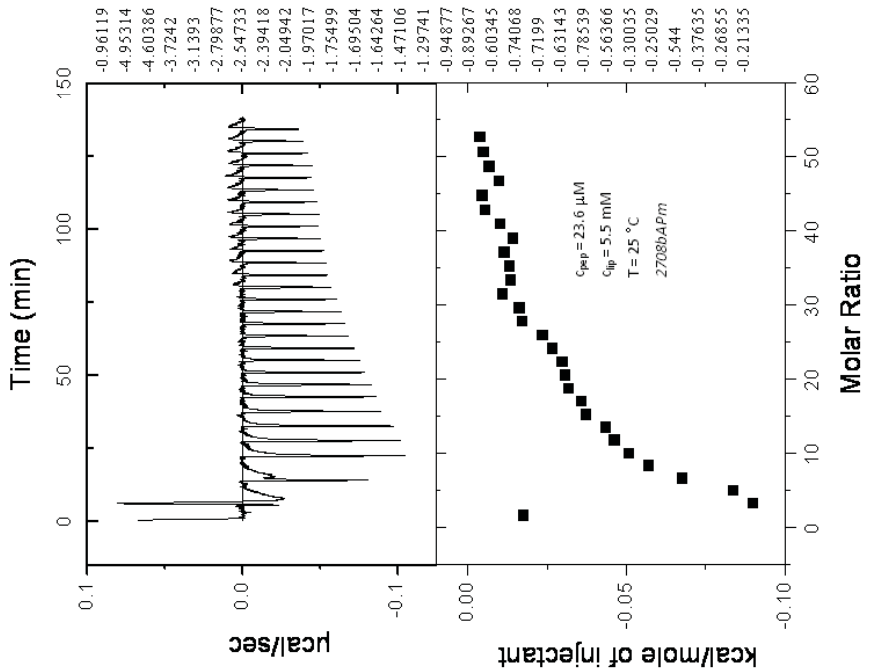
Time (min)
µcal/sec
kcal/mole of injectant
Molar Ratio
c_{pep} = 23.6 µM
c_{lip} = 5.5 mM
T = 25 °C
2708bAPm

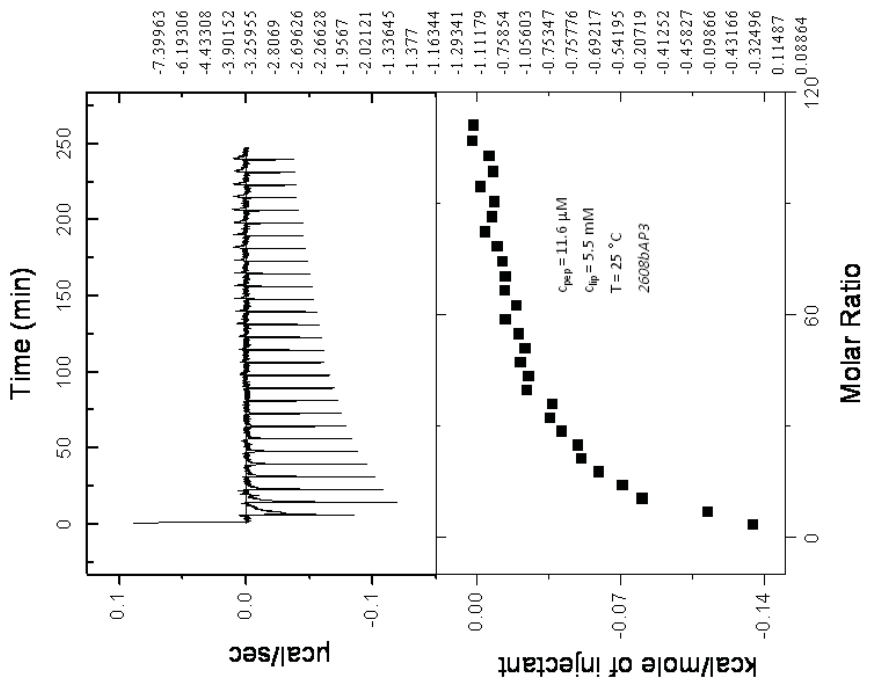
Time (min)
µcal/sec
kcal/mole of injectant
Molar Ratio
c_{pep} = 11.6 µM
c_{lip} = 5.5 mM
T = 25 °C
2608bAP3

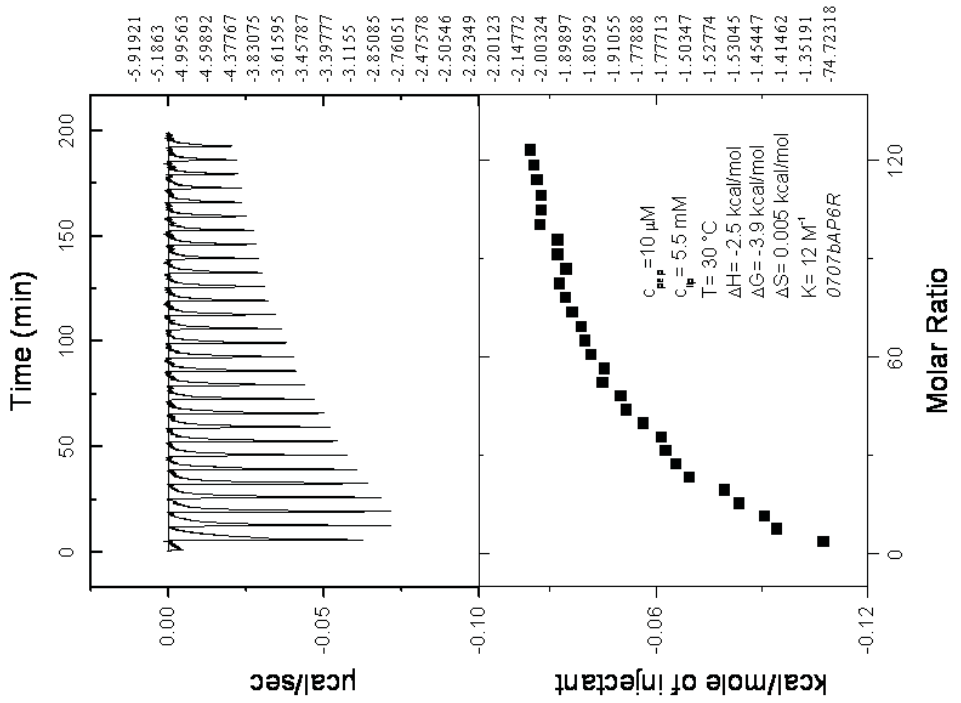
-5.91921
-5.1863
-4.99563
-4.59892
-4.37767
-3.83075
-3.61595
-3.45787
-3.39777
-3.1155
-2.85085
-2.76051
-2.47578
-2.50546
-2.29349
-2.20123
-2.14772
-2.00324
-1.89897
-1.80592
-1.91055
-1.77888
-1.77713
-1.50347
-1.52774
-1.53045
-1.45447
-1.41462
-1.35191
-74.72318
Time (min)
0
50
100
150
200
0.00
-0.05
-0.10
µcal/sec
-0.12
-0.06
kcal/mole of injectant
0
60
120
Molar Ratio
c = 10 µM
c = 5.5 mM
T= 30 °C
ΔH= -2.5 kcal/mol
ΔG= -3.9 kcal/mol
ΔS= 0.005 kcal/mol
K= 12 M-1
0707bAP6R

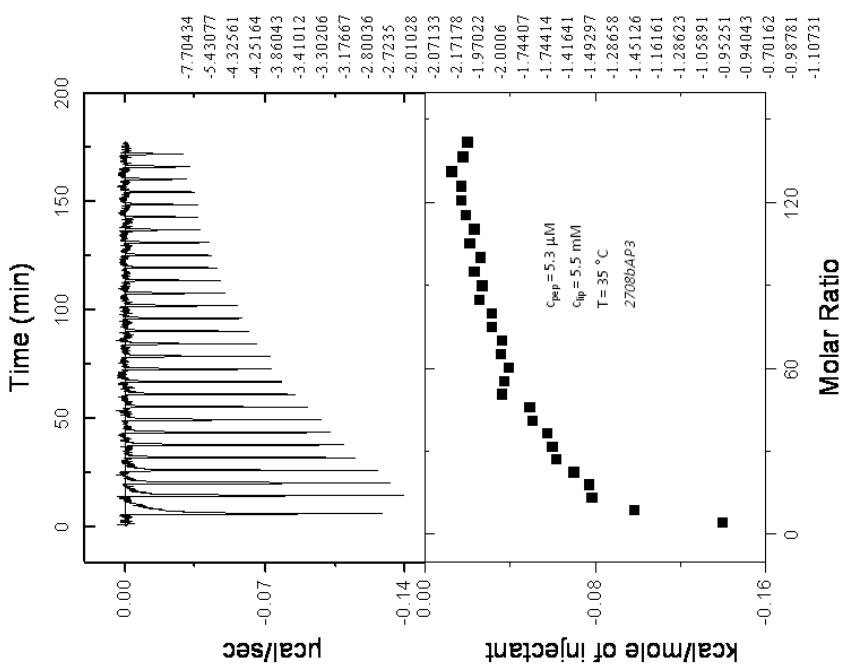
Time (min)
µcal/sec
kcal/mole of injectant
Molar Ratio
c_{Pep} = 5.3 µM
c_{Hp} = 5.5 mM
T = 35 °C
2708bAP3
-7.70434
-5.43077
-4.32561
-4.25164
-3.86043
-3.41012
-3.30206
-3.17667
-2.80036
-2.7235
-2.01028
-2.07133
-2.17178
-1.97022
-2.0006
-1.74407
-1.74414
-1.41641
-1.49297
-1.28658
-1.45126
-1.16161
-1.28623
-1.05891
-0.95251
-0.94043
-0.70162
-0.98781
-1.10731

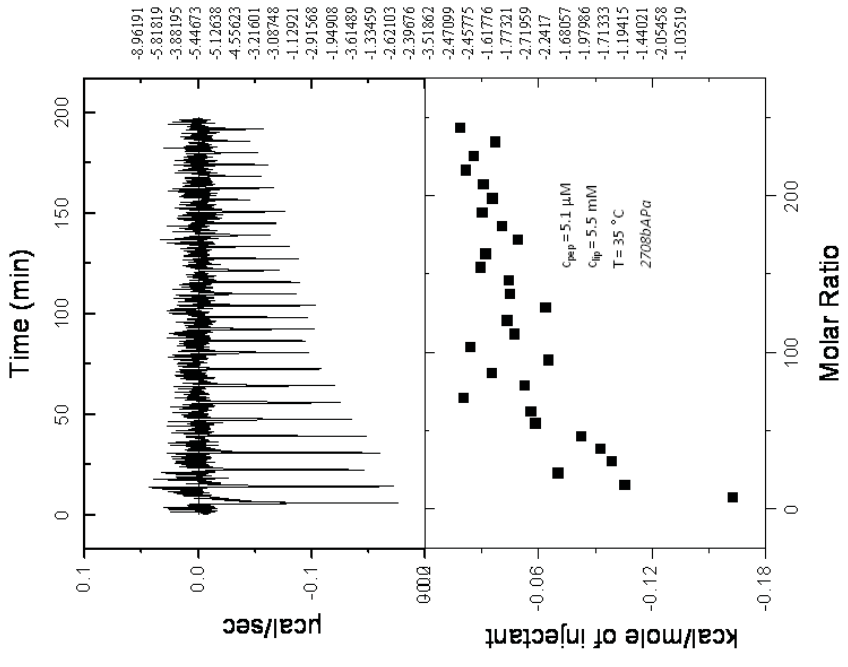
Time (min)
µcal/sec
kcal/mole of injectant
Molar Ratio
c_{Pep} = 5.1 µM
c_{Hp} = 5.5 mM
T = 35 °C
2708bAPa
-8.96191
-5.81819
-3.88195
-5.44673
-5.12638
-4.55623
-3.21601
-3.08748
-1.12921
-2.91568
-1.94908
-3.61489
-1.33459
-2.62103
-2.39676
-3.51862
-2.47099
-2.45775
-1.61776
-1.77321
-2.71959
-2.2417
-1.68057
-1.97986
-1.71333
-1.19415
-1.44021
-2.05458
-1.03519

4. βAP(25-35)_I32W titrations with POPC/POPG SUVs (3:1) at pH 7.4

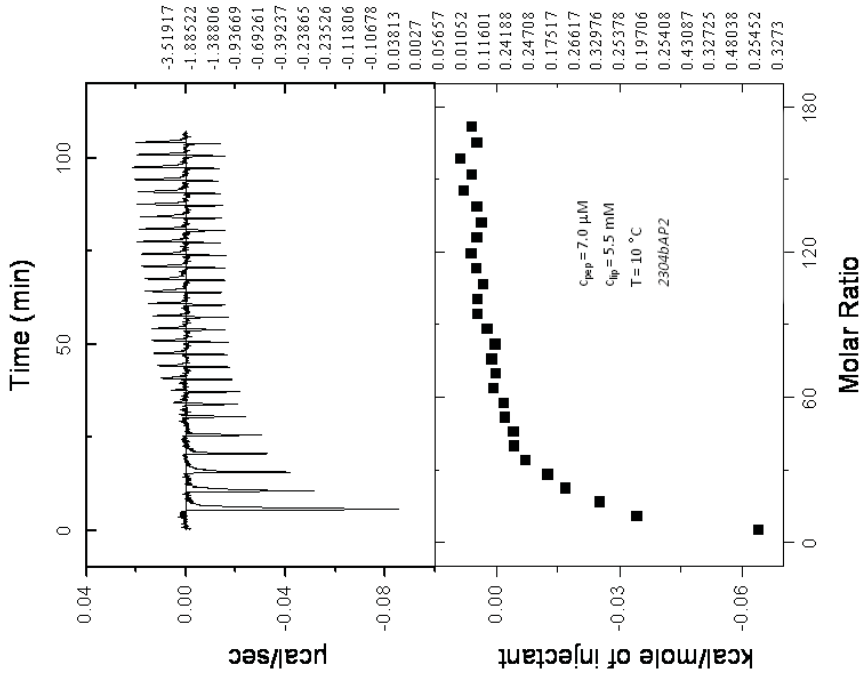

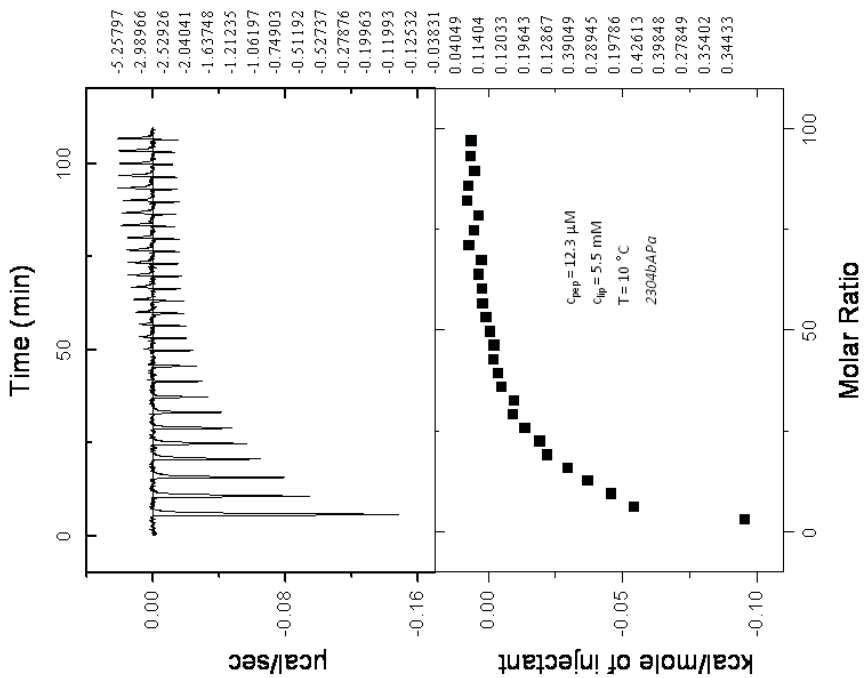

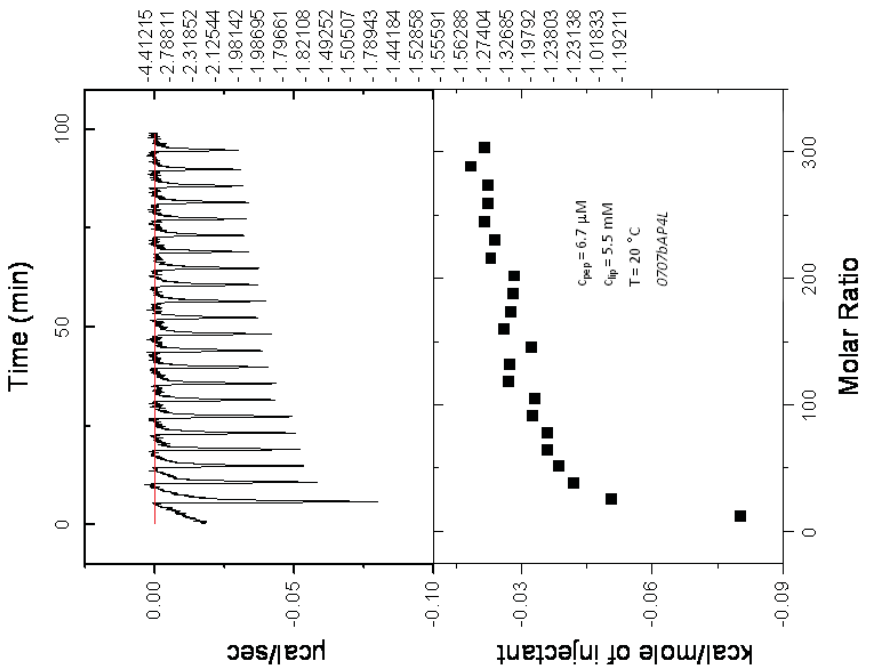
Time (min)
µcal/sec
kcal/mole of injectant
Molar Ratio
-4.41215
-2.78811
-2.31852
-2.12544
-1.98142
-1.98695
-1.79661
-1.82108
-1.49252
-1.50507
-1.78943
-1.44184
-1.52858
-1.55591
-1.56288
-1.27404
-1.32685
-1.19792
-1.23803
-1.23138
-1.01833
-1.19211
c_{pep} = 6.7 µM
c_{lip} = 5.5 mM
T = 20 °C
0707bAP4L

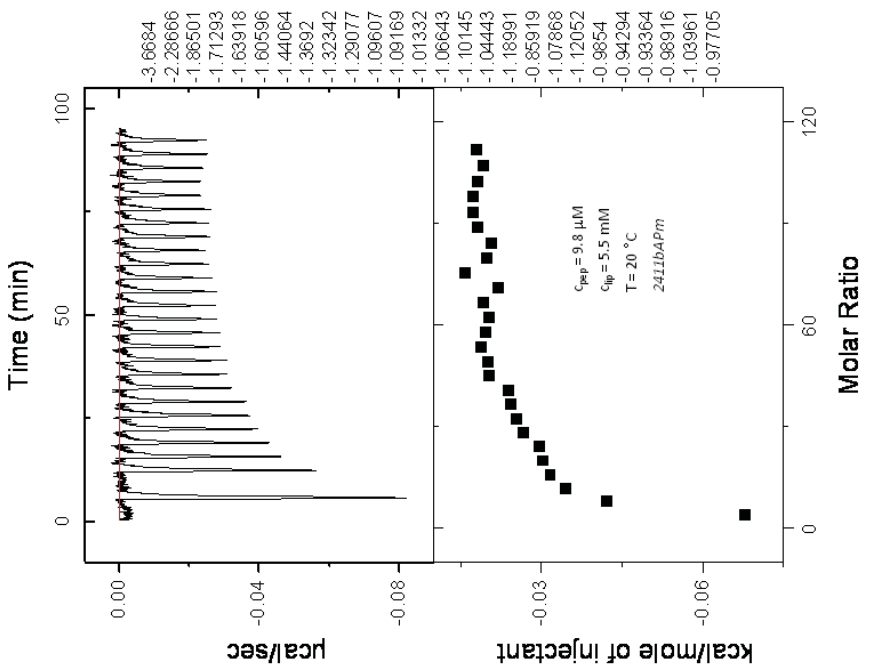
Time (min)
µcal/sec
kcal/mole of injectant
Molar Ratio
-3.6684
-2.28666
-1.86501
-1.71293
-1.63918
-1.60596
-1.44064
-1.3692
-1.32342
-1.29077
-1.09607
-1.09169
-1.01332
-1.06643
-1.10145
-1.04443
-1.18991
-0.85919
-1.07868
-1.12052
-0.9854
-0.94294
-0.93364
-0.98916
-1.03961
-0.97705
c_{pep} = 9.8 µM
c_{lip} = 5.5 mM
T = 20 °C
2411bAPm

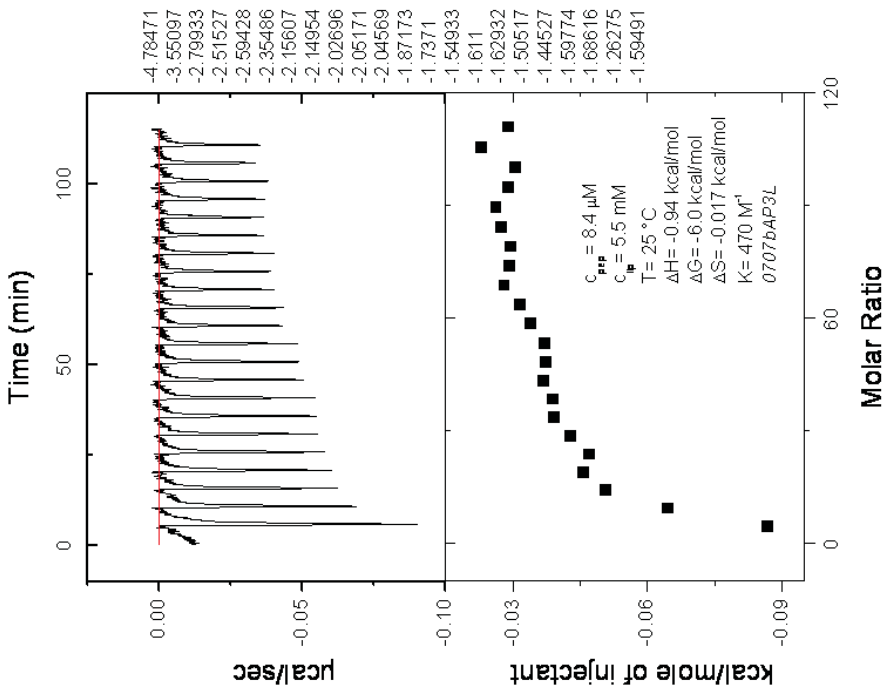
-4.78471
-3.55097
-2.79933
-2.51527
-2.59428
-2.35486
-2.15607
-2.14954
-2.02696
-2.05171
-2.04569
-1.87173
-1.7371
-1.54933
-1.611
-1.62932
-1.50517
-1.44527
-1.59774
-1.68616
-1.26275
-1.59491
Time (min)
0
50
100
0.00
-0.05
-0.10
µcal/sec
-0.03
-0.06
-0.09
kcal/mole of injectant
0
60
120
Molar Ratio
c = 8.4 µM
c = 5.5 mM
T= 25 °C
ΔH= -0.94 kcal/mol
ΔG= -6.0 kcal/mol
ΔS= -0.017 kcal/mol
K= 470 M-1
0707bAP3L

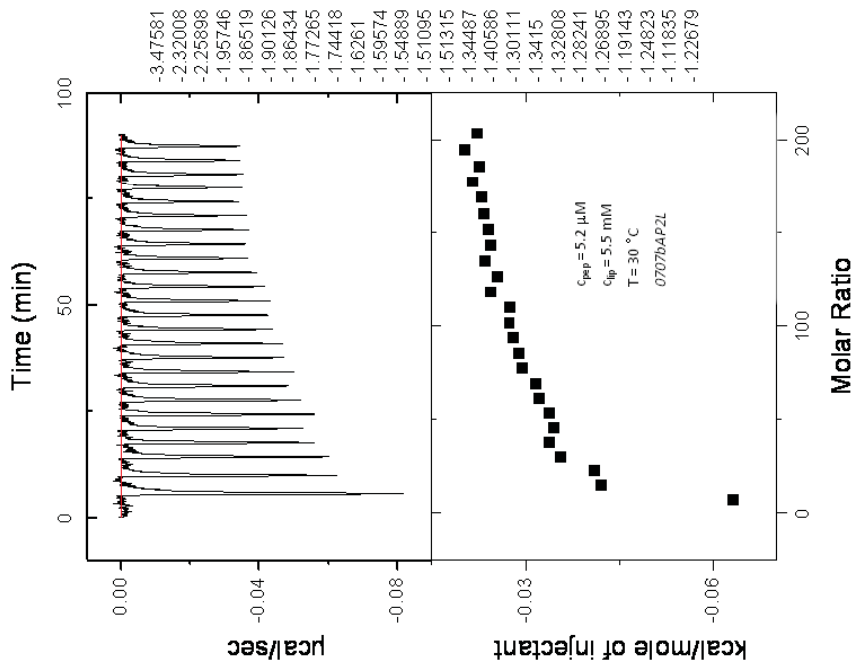
Time (min)
µcal/sec
kcal/mole of injectant
Molar Ratio
c_{pep} = 5.2 µM
c_{lip} = 5.5 mM
T = 30 °C
0707bAP2L

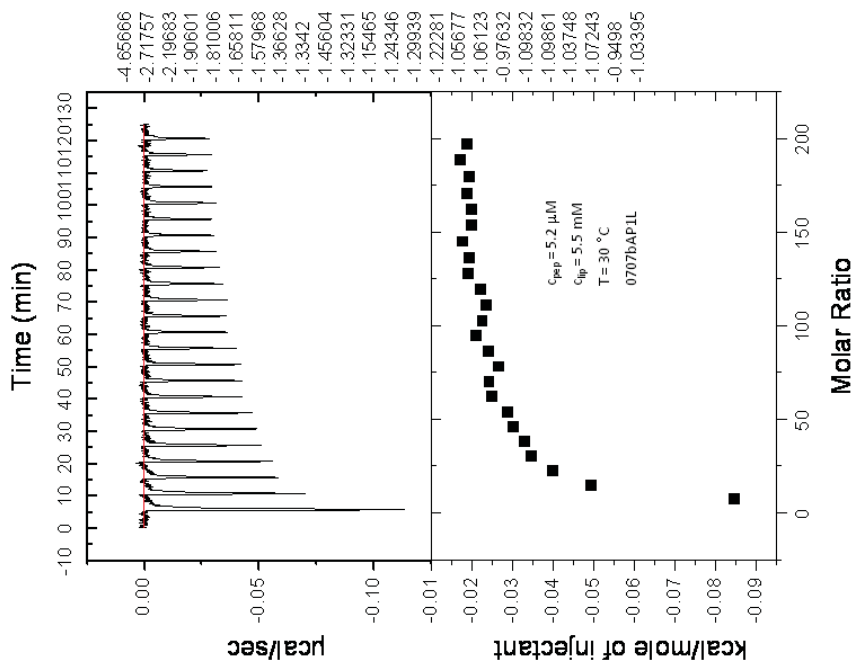
Time (min)
µcal/sec
kcal/mole of injectant
Molar Ratio
c_{pep} = 5.2 µM
c_{lip} = 5.5 mM
T = 30 °C
0707bAP1L

5. βAP(25-35)_I32W titrations with POPC/POPG SUVs (2:1) at pH 4.0

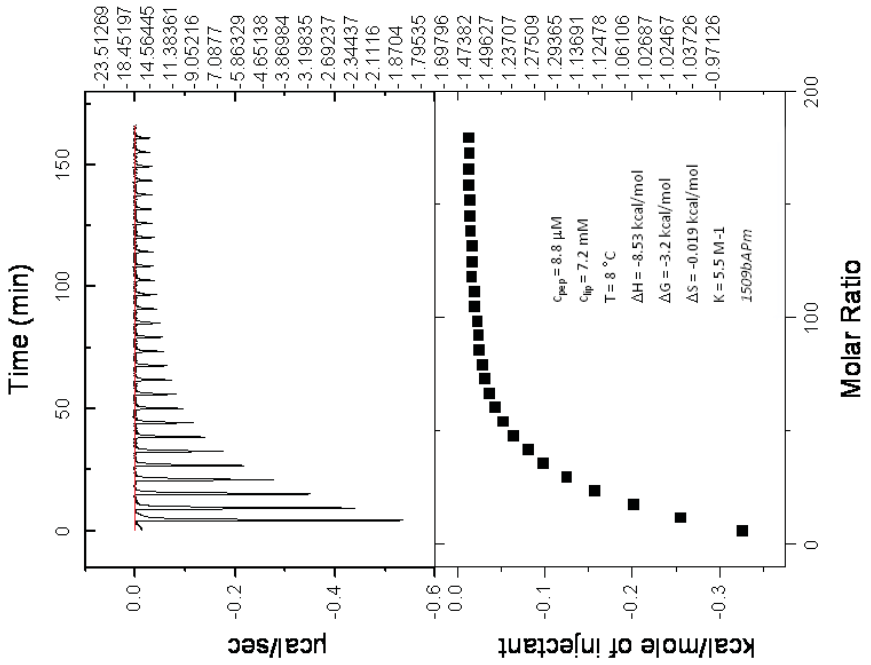

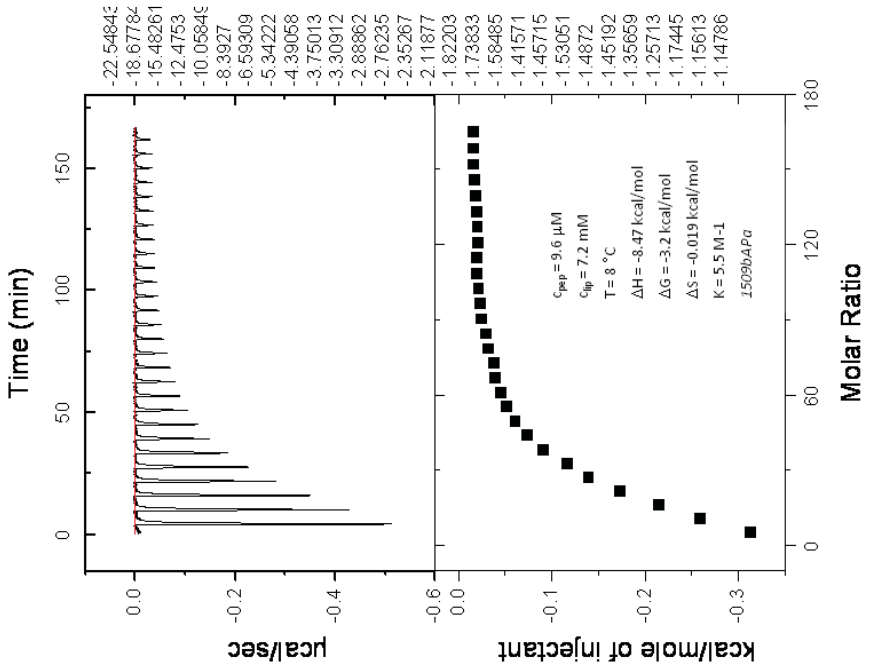

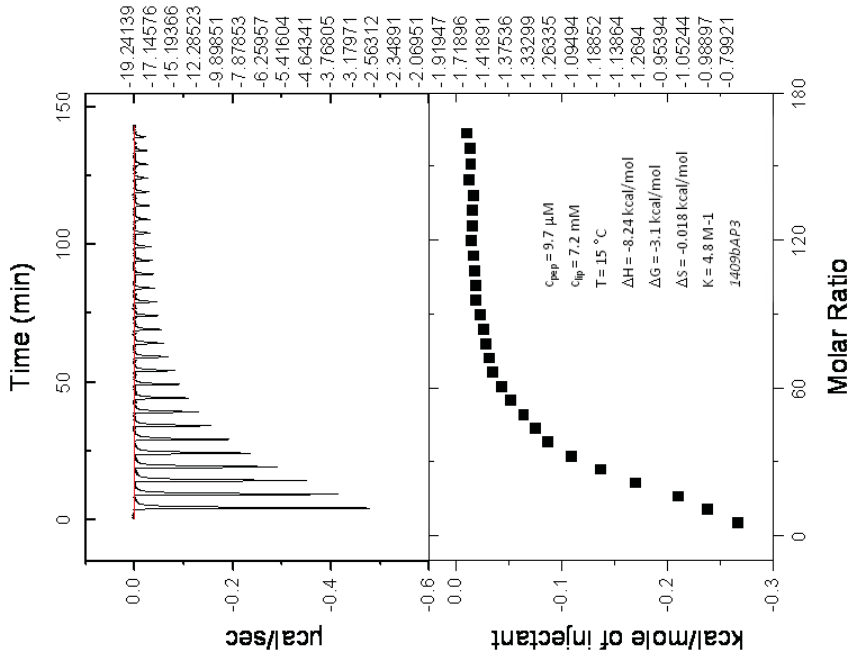
Time (min)
µcal/sec
kcal/mole of injectant
Molar Ratio
c_{pep} = 9.7 µM
c_{ip} = 7.2 mM
T = 15 °C
ΔH = -8.24 kcal/mol
ΔG = -3.1 kcal/mol
ΔS = -0.018 kcal/mol
K = 4.8 M-1
1409bAP3

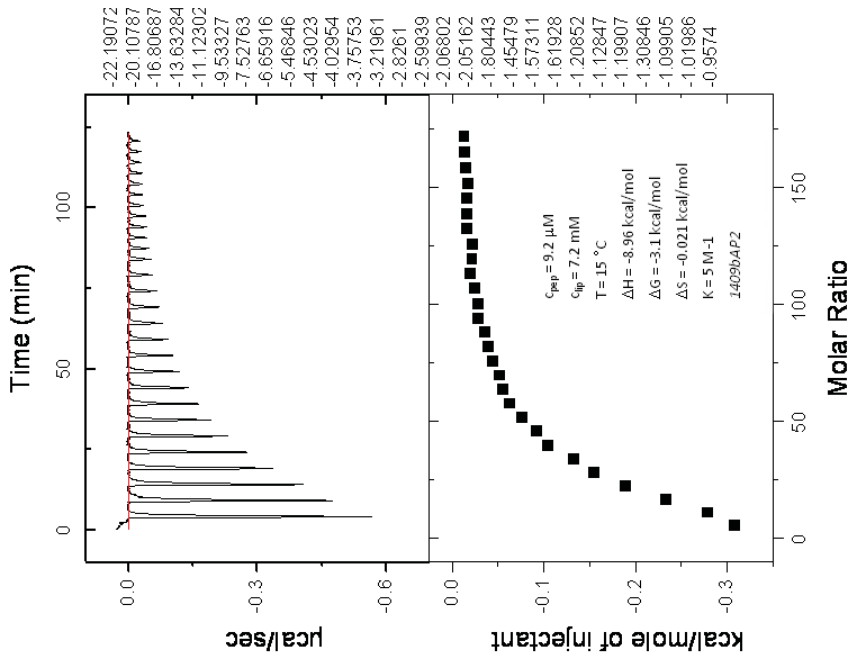
Time (min)
µcal/sec
kcal/mole of injectant
Molar Ratio
c_{pep} = 9.2 µM
c_{ip} = 7.2 mM
T = 15 °C
ΔH = -8.96 kcal/mol
ΔG = -3.1 kcal/mol
ΔS = -0.021 kcal/mol
K = 5 M-1
1409bAP2

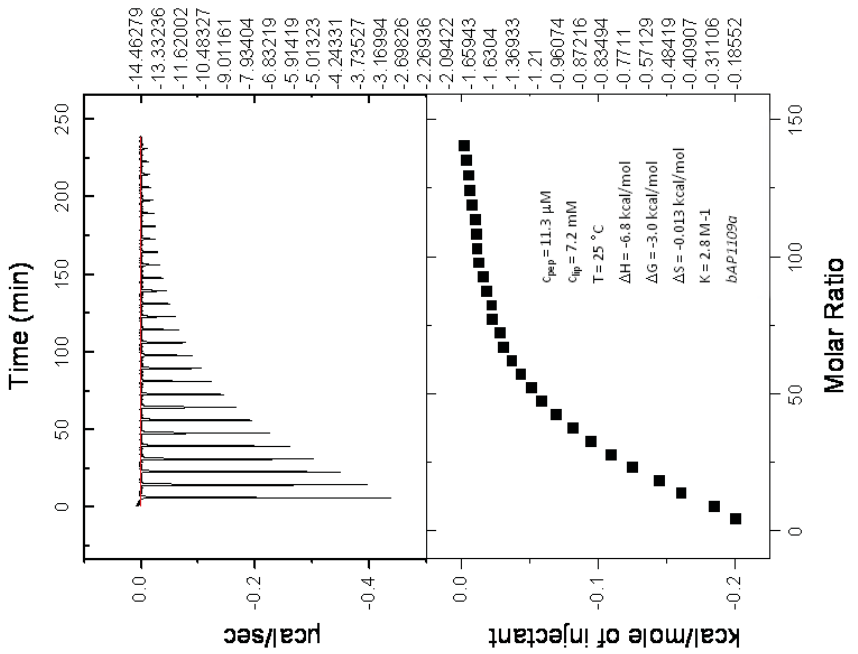
Time (min)
µcal/sec
kcal/mole of injectant
Molar Ratio
-14.46279
-13.33236
-11.62002
-10.48327
-9.01161
-7.93404
-6.83219
-5.91419
-5.01323
-4.24331
-3.73527
-3.16994
-2.69826
-2.26936
-2.09422
-1.65943
-1.6304
-1.36933
-1.21
-0.96074
-0.87216
-0.83494
-0.7711
-0.57129
-0.48419
-0.40907
-0.31106
-0.18552
cpep = 11.3 µM
citp = 7.2 mM
T = 25 °C
ΔH = -6.8 kcal/mol
ΔG = -3.0 kcal/mol
ΔS = -0.013 kcal/mol
K = 2.8 M-1
bAP1109a

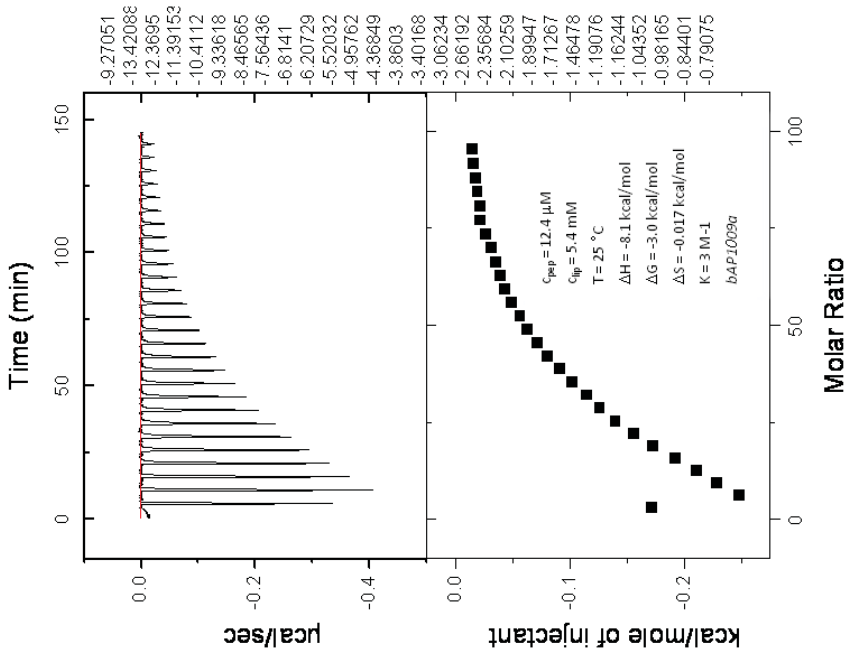
Time (min)
µcal/sec
kcal/mole of injectant
Molar Ratio
-9.27051
-13.42088
-12.3695
-11.39153
-10.4112
-9.33618
-8.46565
-7.56436
-6.8141
-6.20729
-5.52032
-4.95762
-4.36849
-3.8603
-3.40168
-3.06234
-2.66192
-2.35684
-2.10259
-1.89947
-1.71267
-1.46478
-1.19076
-1.16244
-1.04352
-0.98165
-0.84401
-0.79075
cpep = 12.4 µM
citp = 5.4 mM
T = 25 °C
ΔH = -8.1 kcal/mol
ΔG = -3.0 kcal/mol
ΔS = -0.017 kcal/mol
K = 3 M-1
bAP1109a

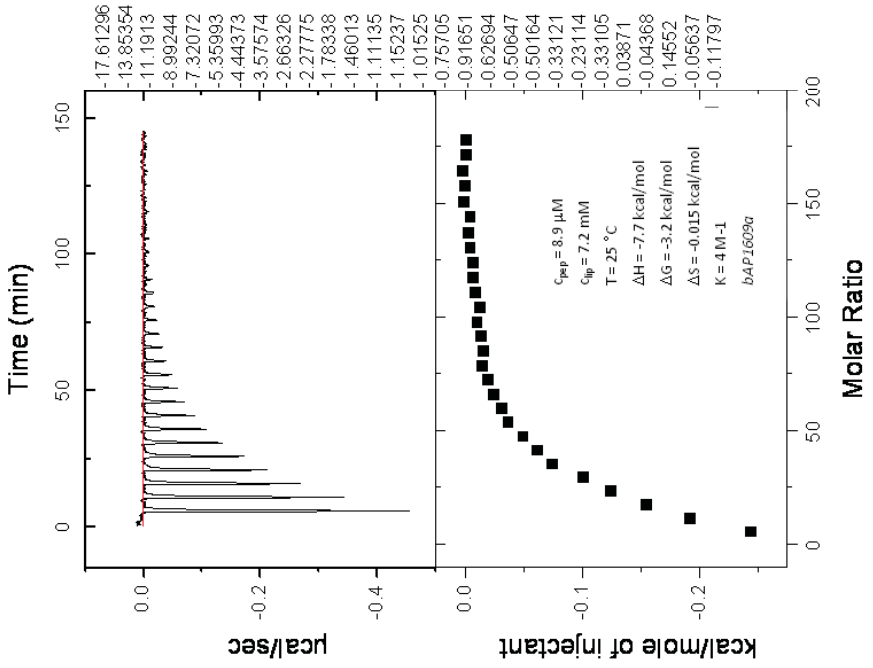
-17.61296
-13.85354
-11.1913
-8.99244
-7.32072
-5.35993
-4.44373
-3.57574
-2.66326
-2.27775
-1.78338
-1.46013
-1.11135
-1.15237
-1.01525
-0.75705
-0.91651
-0.62694
-0.50647
-0.50164
-0.33121
-0.23114
-0.33105
0.03871
-0.04368
0.14552
-0.05637
-0.11797
Time (min)
µcal/sec
kcal/mole of injectant
Molar Ratio
c_{pep} = 8.9 µM
c_{lip} = 7.2 mM
T = 25 °C
ΔH = -7.7 kcal/mol
ΔG = -3.2 kcal/mol
ΔS = -0.015 kcal/mol
K = 4 M-1
bAP1609a

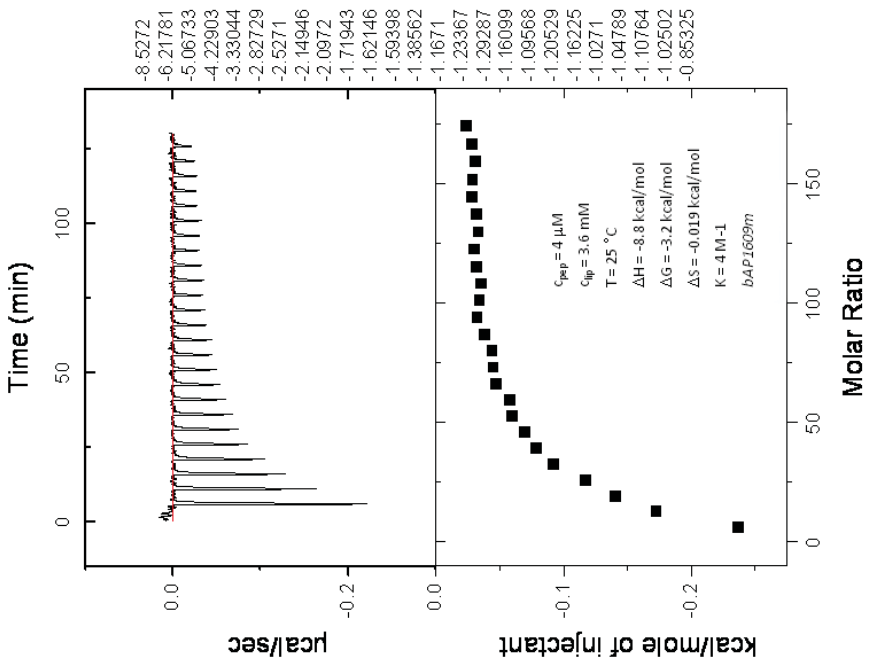
-8.5272
-6.21781
-5.06733
-4.22903
-3.33044
-2.82729
-2.5271
-2.14946
-2.0972
-1.71943
-1.62146
-1.59398
-1.38562
-1.1671
-1.23367
-1.29287
-1.16099
-1.09568
-1.20529
-1.16225
-1.0271
-1.04789
-1.10764
-1.02502
-0.85325
Time (min)
µcal/sec
kcal/mole of injectant
Molar Ratio
c_{pep} = 4 µM
c_{lip} = 3.6 mM
T = 25 °C
ΔH = -8.8 kcal/mol
ΔG = -3.2 kcal/mol
ΔS = -0.019 kcal/mol
K = 4 M-1
bAP1609m

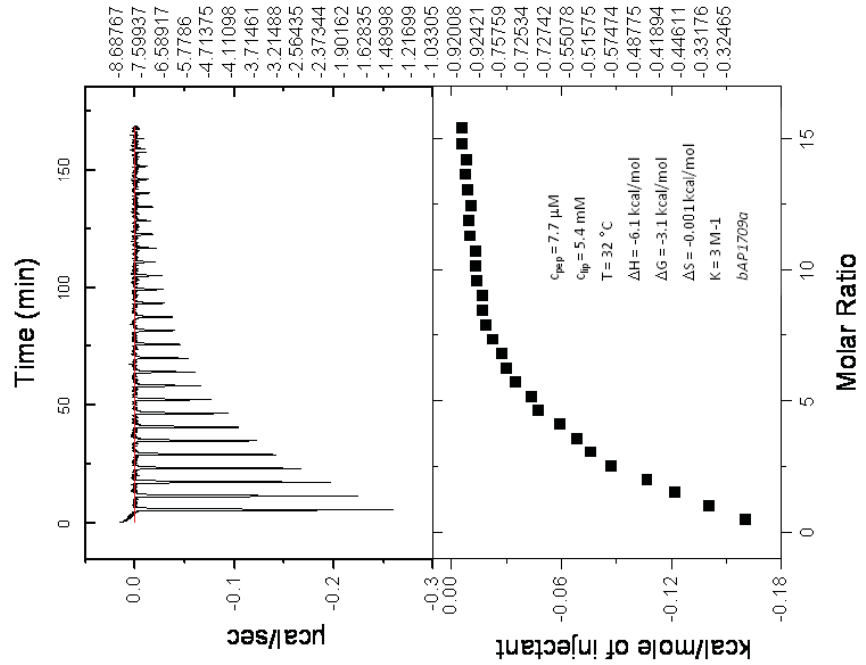
Time (min)
µcal/sec
kcal/mole of injectant
Molar Ratio
c_{pep} = 7.7 µM
c_{tip} = 5.4 mM
T = 32 °C
ΔH = -6.1 kcal/mol
ΔG = -3.1 kcal/mol
ΔS = -0.001 kcal/mol
K = 3 M-1
bAP1709a

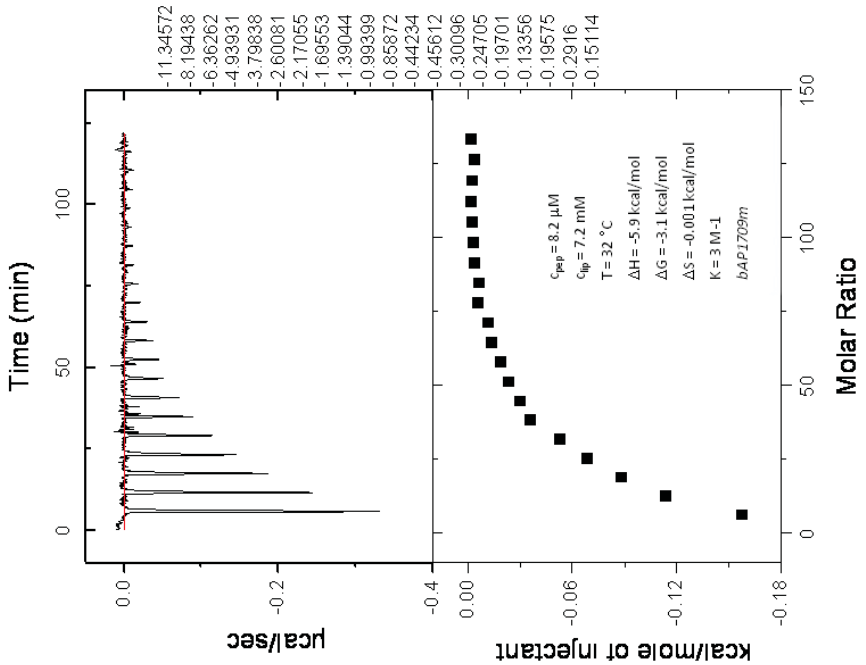
Time (min)
µcal/sec
kcal/mole of injectant
Molar Ratio
c_{pep} = 8.2 µM
c_{tip} = 7.2 mM
T = 32 °C
ΔH = -5.9 kcal/mol
ΔG = -3.1 kcal/mol
ΔS = -0.001 kcal/mol
K = 3 M-1
bAP1709m

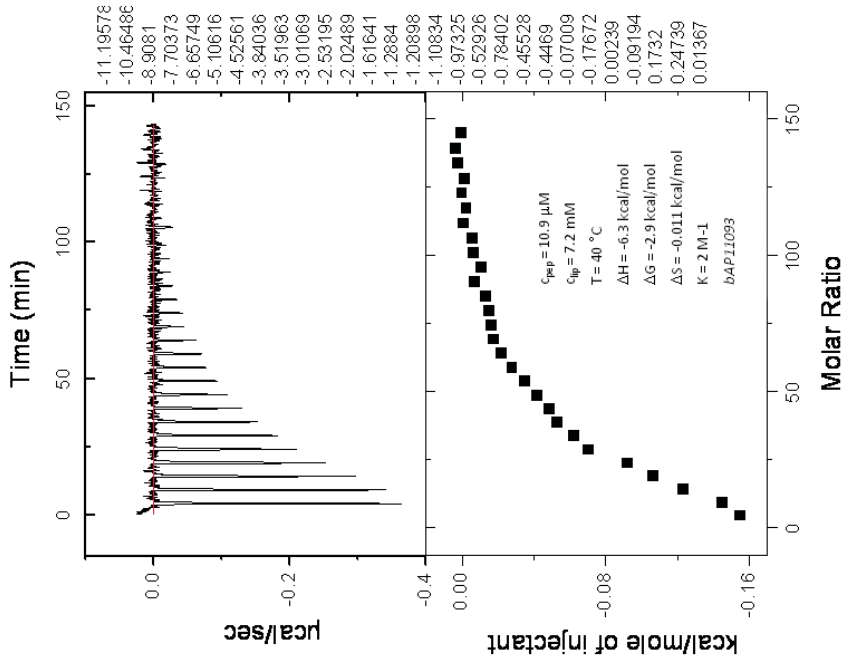
Time (min)
µcal/sec
kcal/mole of injectant
Molar Ratio
c_{cell} = 10.9 µM
c_{titr} = 7.2 mM
T = 40 °C
ΔH = -6.3 kcal/mol
ΔG = -2.9 kcal/mol
ΔS = -0.011 kcal/mol
K = 2 M-1
bAP11093

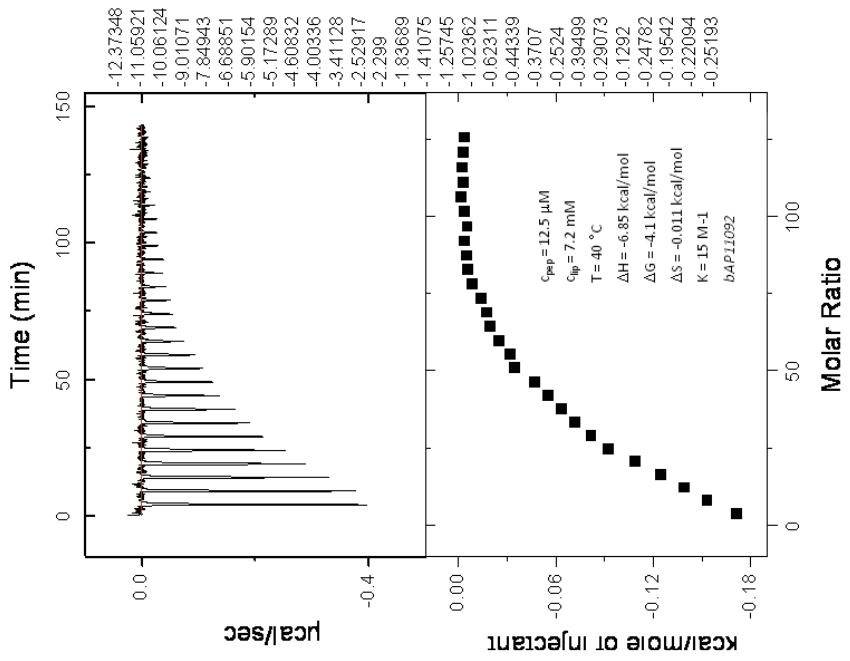
Time (min)
µcal/sec
kcal/mole of injectant
Molar Ratio
c_{cell} = 12.5 µM
c_{titr} = 7.2 mM
T = 40 °C
ΔH = -6.85 kcal/mol
ΔG = -4.1 kcal/mol
ΔS = -0.011 kcal/mol
K = 15 M-1
bAP11092

6. βAP(25-35)_I32W titrations with POPC/POPG SUVs (2:1) at pH 7.4

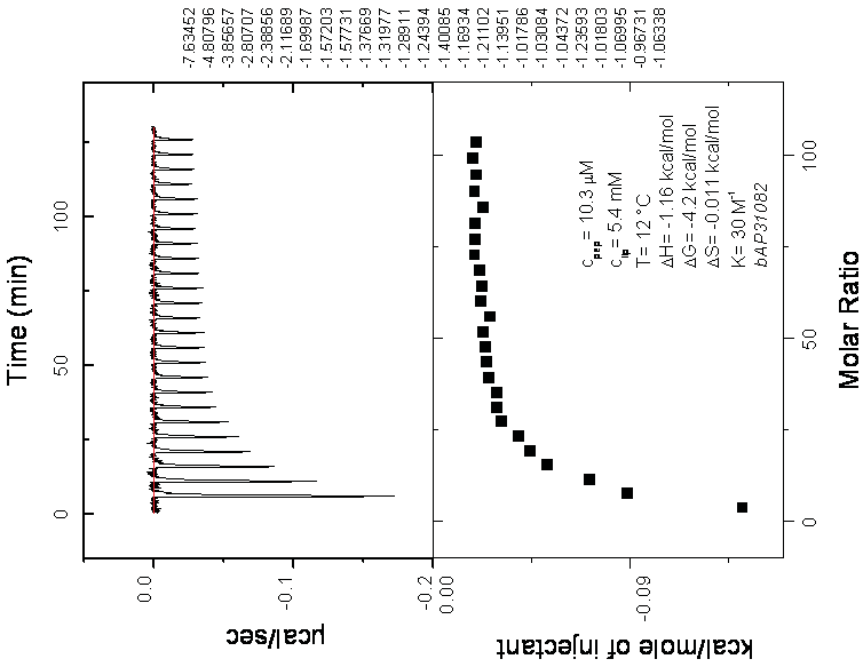

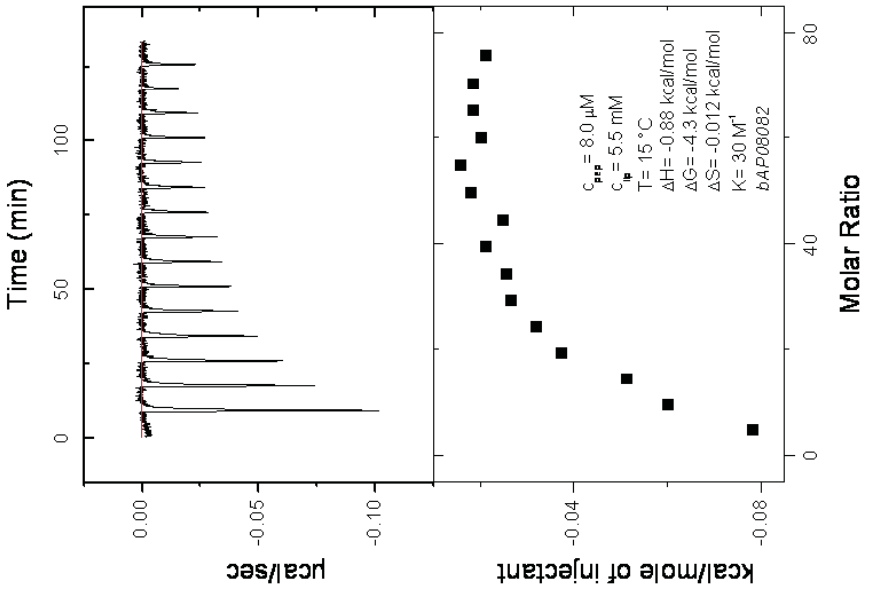
Time (min)
0
50
100
0.00
-0.05
-0.10
µcal/sec
kcal/mole of injectant
-0.04
-0.08
0
40
80
Molar Ratio
c_{PEP} = 8.0 µM
c_{Ip} = 5.5 mM
T= 15 °C
ΔH= -0.88 kcal/mol
ΔG= -4.3 kcal/mol
ΔS= -0.012 kcal/mol
K= 30 M^{-1}
bAP08082

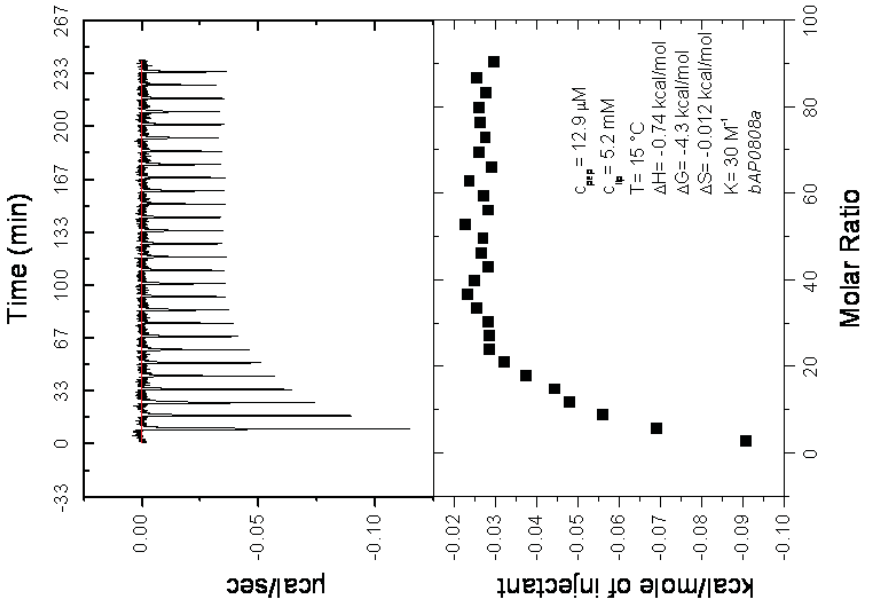
Time (min)
-33
0
33
67
100
133
167
200
233
267
0.00
-0.05
-0.10
µcal/sec
kcal/mole of injectant
-0.02
-0.03
-0.04
-0.05
-0.06
-0.07
-0.08
-0.09
-0.10
0
20
40
60
80
100
Molar Ratio
c_{PEP} = 12.9 µM
c_{Ip} = 5.2 mM
T= 15 °C
ΔH= -0.74 kcal/mol
ΔG= -4.3 kcal/mol
ΔS= -0.012 kcal/mol
K= 30 M^{-1}
bAP0808a

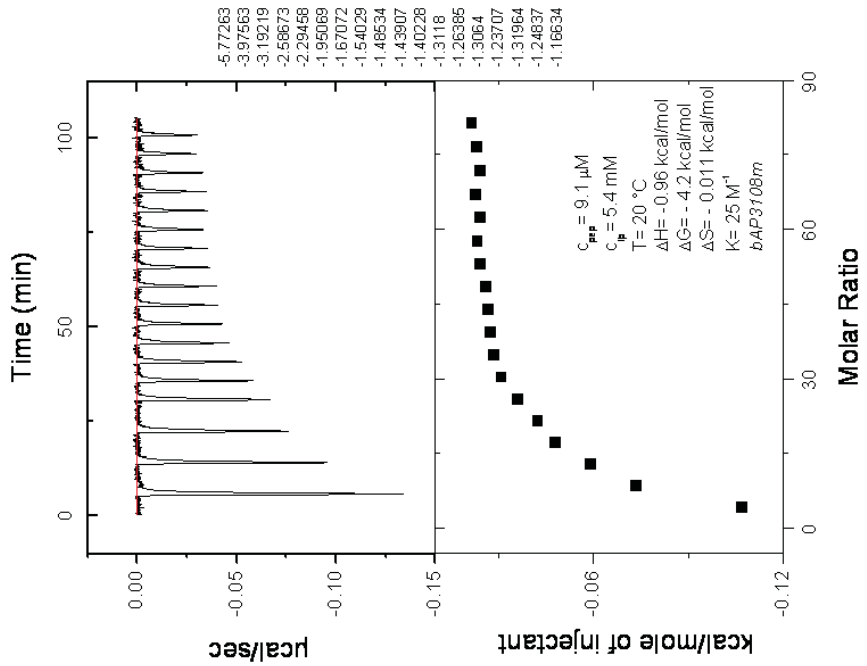
-5.77263
-3.97563
-3.19219
-2.58673
-2.29458
-1.95069
-1.67072
-1.54029
-1.48534
-1.43907
-1.40228
-1.3118
-1.26385
-1.3064
-1.23707
-1.31964
-1.24837
-1.16634
Time (min)
0
50
100
0.00
-0.05
-0.10
-0.15
µcal/sec
0
30
60
90
-0.06
-0.12
kcal/mole of injectant
Molar Ratio
c_{PEP} = 9.1 µM
c_{Ip} = 5.4 mM
T= 20 °C
ΔH= -0.96 kcal/mol
ΔG= - 4.2 kcal/mol
ΔS= - 0.011 kcal/mol
K= 25 M^{-1}
bAP3108m

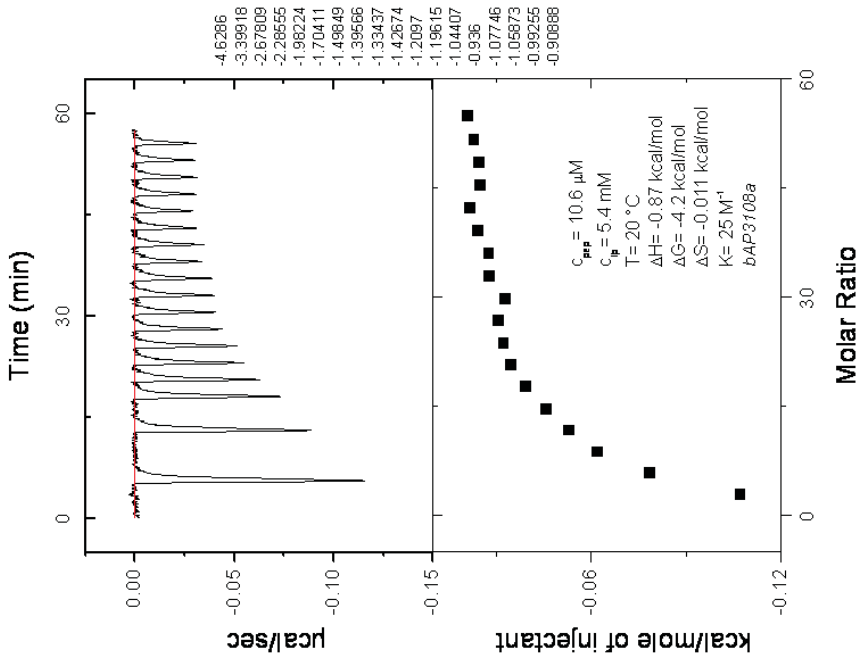
-4.6286
-3.39918
-2.67809
-2.28555
-1.98224
-1.70411
-1.49849
-1.39566
-1.33437
-1.42674
-1.2097
-1.19615
-1.04407
-0.936
-1.07746
-1.05873
-0.99255
-0.90888
Time (min)
0
30
60
0.00
-0.05
-0.10
-0.15
µcal/sec
0
30
60
-0.06
-0.12
kcal/mole of injectant
Molar Ratio
c_{PEP} = 10.6 µM
c_{Ip} = 5.4 mM
T= 20 °C
ΔH= -0.87 kcal/mol
ΔG= -4.2 kcal/mol
ΔS= -0.011 kcal/mol
K= 25 M^{-1}
bAP3108a

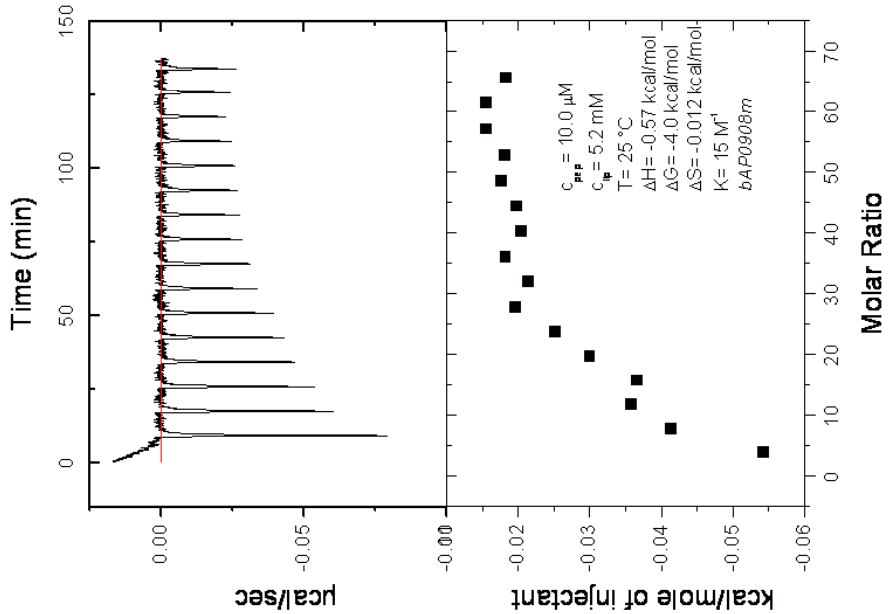
Time (min)
0
50
100
150
0.00
-0.05
µcal/sec
-0.00
-0.02
-0.03
-0.04
-0.05
-0.06
kcal/mole of injectant
0
10
20
30
40
50
60
70
Molar Ratio
c_{prp} = 10.0 µM
c_{lig} = 5.2 mM
T= 25 °C
ΔH= -0.57 kcal/mol
ΔG= -4.0 kcal/mol
ΔS= -0.012 kcal/mol
K= 15 M^{-1}
bAP0908m

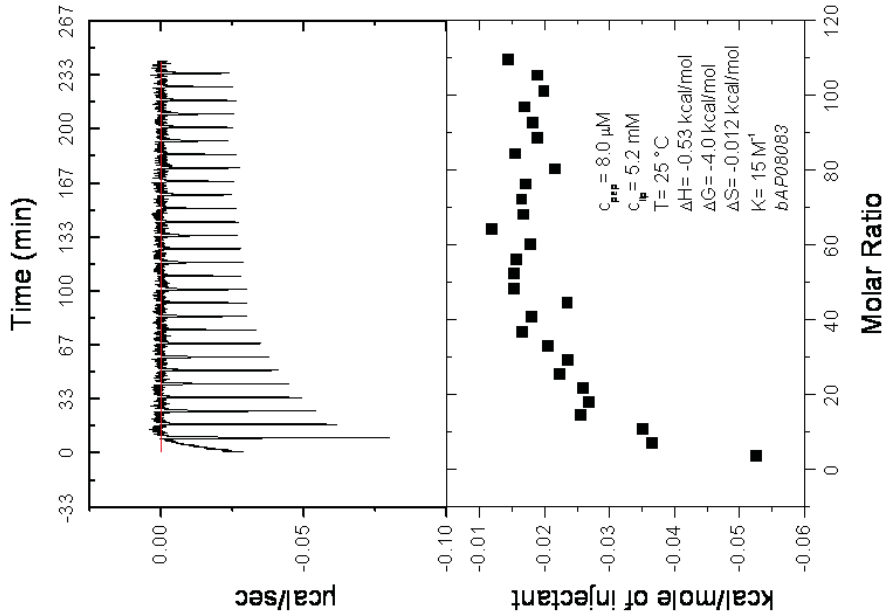
Time (min)
-33
0
33
67
100
133
167
200
233
267
0.00
-0.05
µcal/sec
-0.10
-0.01
-0.02
-0.03
-0.04
-0.05
-0.06
kcal/mole of injectant
0
20
40
60
80
100
120
Molar Ratio
c_{prp} = 8.0 µM
c_{lig} = 5.2 mM
T= 25 °C
ΔH= -0.53 kcal/mol
ΔG= -4.0 kcal/mol
ΔS= -0.012 kcal/mol
K= 15 M^{-1}
bAP08083

Manuscript accepted for publication in *Langmuir*.

X. Thermal Phase Behavior of DMPG Bilayers in Aqueous Dispersions as revealed by ^{2}H- and ^{31}P- NMR †

Caroline Loew[1], Karin A. Riske[2], M. Teresa Lamy[3], and Joachim Seelig[1]*

[1]Biozentrum, University of Basel, Div. of Biophysical Chemistry, Klingelbergstrasse 50/70, CH-4056 Basel, Switzerland

[2]Departamento de Biofísica, Universidade Federal de São Paulo, R. Pedro de Toledo, 669 9° andar, São Paulo, Brazil

[3]Instituto de Física, Universidade de São Paulo, CP 66318, CEP 05314-970, São Paulo, SP, Brazil

*To whom correspondence should be addressed:

Tel. +41-61-267 2190, Fax. +41-61-267 2189, e-mail: joachim.seelig@unibas.ch

† Supported by the Swiss National Science Foundation Grant # 31003A-129701

1. Abstract

The synthetic lipid 1,2-dimyristoyl-*sn*-3-phosphoglycerol (DMPG), when dispersed in water/NaCl exhibits a complex phase behavior caused by its almost unlimited swelling in excess water. Using deuterium (^{2}H)- and phosphorus (^{31}P)-NMR we have studied the molecular properties of DMPG/water/NaCl dispersions as a function of lipid and NaCl concentration. We have measured the order profile of the hydrophobic part of the lipid bilayer with deuterated DMPG while the orientation of the phosphoglycerol headgroup was deduced from the ^{31}P-NMR chemical shielding anisotropy. At temperatures >30 °C we observe well-resolved ^{2}H- and ^{31}P-NMR spectra not much different from other liquid crystalline bilayers. From the order profiles it is possible to deduce the average length of the flexible fatty acyl chain. Unusual spectra are obtained in the temperature interval of 20 °C to 25 °C, indicating one or several phase transitions. The most dramatic changes are seen at low lipid concentration and low ionic strength. Under these conditions and at 25 °C the phosphoglycerol headgroup rotates into the hydrocarbon layer and the hydrocarbon chains show larger flexing motions than at higher temperatures. The orientation of the phosphoglycerol headgroup depends on the bilayer surface charge and correlates with the degree of dissociation of DMPG-Na^{+}. The larger the negative surface charge the more rotates the headgroup towards the non-polar region.

2. Introduction

Phosphatidylglycerol (PG) is one of the predominant biological lipids and has been found to occur in higher plants, algae, bacteria and, to a lesser extent, in animal tissue. PG is negatively charged at physiological pH with an apparent pK of the phosphate group of pK = 2.9 - 5.5.[1,2] ^{2}H- and ^{31}P- NMR as well as neutron diffraction have been used to deduce the conformation and dynamics of PG bilayers. [3-6] The phosphoglycerol headgroup was found to be oriented at about 30° to the membrane surface making the negatively charged phosphate group easily accessible to cations, present in the bulk aqueous phase. The influence of Ca^{2+} on membranes composed of synthetic 1-palmitoyl-2-oleoyl-*sn*-glycero-3-phosphoglycerol (POPG) and natural PG

isolated from *E.coli*, either in pure form or mixed with neutral 1-palmitoyl-2-oleoyl-*sn*-glycero-3-phosphocholine (POPC), was also investigated with ^{2}H- and ^{31}P-NMR.[7] The binding of Ca^{2+} leads to a considerable increase in the transition temperature of the gel-to-liquid crystal phase transition. The conformation of the phospholipid headgroups changes upon Ca^{2+} binding and NMR can be used to deduce the binding isotherm. Nevertheless, a headgroup orientation essentially parallel to the membrane surface is maintained.

Among the synthetic phosphatidylglycerols 1,2-dimyristoyl-*sn*-glycero-3-phospo-*rac*-glycerol (DMPG) has received particular attention because of its unusual phase properties. It appears to form single bilayers when dissolved in water at low lipid and low salt concentration.[8] DMPG-Na^{+} has been claimed to dissolve as a monomer with a solubility coefficient of ~4.6 x 10^{-5} M at 25 °C ([9], figure 2). Multilamellar bilayer dispersions of DMPG-Na^{+} show an almost unlimited uptake of water due to electrostatic repulsion of juxtaposed bilayers.[10] In early studies of DMPG-Na^{+} differential scanning calorimetry (DSC) revealed a gel-to-liquid crystal transition at 24 °C with a transition enthalpy of ΔH = 6.8 – 7.0 kcal/mol.[11,12] Subsequently, an additional pre-transition at 13 – 15 °C with a smaller enthalpy of ΔH ~ 0.6 kcal/mol was detected.[13-20] The molecular basis of the pre-transition is a realignment of the extended hydrocarbon chains in gel-state. A pre-transition and a gel-to-liquid crystal main transition are also typical for neutral phosphatidyl cholines.[21,22] For example, bilayers of 1,2-dimyristoyl-*sn*-glycero-3-phosphocholine (DMPC) in excess water exhibit a pre-transition and a main transition with very similar parameters as those of DMPG-Na^{+} in 0.1 M NaCl. However, in addition to pretransition and main transition DMPG-Na^{+} displays an even more complex phase behavior at low salt content [8,23,24] which was described as "the solution phase containing monomer or micelle, the two bilayer phases (gel and liquid crystal) and the three morphologically distinct bilayer states [jelly, unilamellar vesicles (LUV) and multilamellar vesicle (MLV)]".[8] Most remarkable and different from other phospholipids is the jelly-like state of DMPG-Na^{+} at low lipid and low salt concentration which has a completely transparent structure of high viscosity.[14] Freeze-fracture studies of DMPG in distilled water showed particles with morphologies different from bilayer vesicles. It was concluded that "the lipid appears visually to 'dissolve' in distilled water".[24]

These initial observations stimulated a series of further investigations to characterize the phase diagram of DMPG-Na^{+} in detail and to elucidate the lipid packing in the different phases. DMPG-Na^{+} dispersions require careful attention to the exact quantitative composition of the system such as lipid concentration, the presence of salt/buffer, pH and temperature.[25,26] This is quite different compared to zwitterionic lipids where a small excess of water is usually sufficient to establish unambiguous physical conditions. Of particular interest is DMPG-Na^{+} at low lipid concentration and low ionic strength. The molecular picture associated with the phase transition region is that of "uncorrelated bilayers in which in-plane correlated cavities/pores open on the membrane surface, giving rise to mesoscopic correlation".[19,27] This model is supported by fluorescence measurements suggesting "open (tattered)" bilayer sheets in the transition region.[28]

The purpose of the present study is to investigate the unusual phase behavior of DMPG-Na^{+} dispersions with deuterium (^{2}H) and phosphorus (^{31}P) NMR. These methods allow a clear distinction between bilayer and non-bilayer phases.[29,30] Four different regions will be considered, characterized either by high or low lipid concentration and both measured at either high or low NaCl concentration.

3. Methods

Solid-State NMR. Solid state NMR experiments were performed on a Bruker Avance 400MHz spectrometer (Bruker AXS, Karlsruhe, Germany).

Solid-state ^{31}P-NMR spectra were recorded at 162 MHz using a pulse-acquire sequence with broadband proton decoupling (WALTZ-16) and a recycle delay of 6s. The excitation pulse length was 3μs and 1000 FIDs were accumulated. The chemical shielding anisotropy, $\Delta\sigma$, was determined by a simulation of the spectra.[30]

Solid state ^{2}H-NMR experiments were recorded at 61 MHz using the quadrupole echo technique. The excitation pulse had a length of 5.5 μs. 8 K FIDs were accumulated with a recycle delay of 250 ms.

Differential Scanning Calorimetry. A Microcal VP-DSC microcalorimeter with a scan rate of 45 °C/h and a cell volume of 0.5 mL was used for the low lipid content samples (~ 20 mg/mL = 27 mmol/kg lipid, using a molecular weight of DMPG-Na^+ = 688 g/mol plus 3 H_2O). The samples were scanned in the range of 10 to 60 °C. As a control, pure buffer was measured as baseline. The Microcal Origin software was used for data evaluation. Each DSC measurement was reproduced at least twice.

Mass Spectrometry. Thin-Layer Chromatography. After the NMR experiments the stability of the lipid was checked with mass spectrometry and thin layer chromatography. The mass of the lipid at low ionic strength was assessed by Voyager-DE Pro mass spectrometer (Applied Biosystems; Foster City, U.S.A.). The lipid was run on a TLC plate (Fluka) in a dichloromethane/methanol/water mixture (70/26/4) and was exposed to iodine vapor. In both assays no differences to fresh DMPG were detected.

Sample preparation. 1,2-Dimyristoyl-*sn*-glycero-3-phospho-*rac*-glycerol (DMPG, molecular weight 688.4 $g.mol^{-1}$) and 1,2-dimyristoyl-d_{54}-*sn*-glycero-3-phospho-*rac*-glycerol in chloroform (d_{54}-DMPG, molecular weight of 743.2 $g.mol^{-1}$) were purchased from Avanti Polar Lipids (Alabaster, USA).

Two types of buffers were used. *Low ionic strength buffer* composed of 10 mM Hepes, pH 7.4, 2 mM NaCl, or *high ionic strength buffer* 10 mM Hepes, 100 mM NaCl, pH 7.4. For deuterated lipid samples the buffer was made with deuterium-depleted water.

Non-deuterated NMR samples. 50 mg of DMPG as a powder was dispersed in 250 µL of buffer to produce the *high lipid content* sample molality (270 mmol/kg). 13.7 mg of DMPG as a powder was dispersed in 400 µL of buffer to produce the *low lipid content* sample (50 mmol/kg). Multilamellar vesicles were formed by vortexing the dispersion. 10 freeze-thaw cycles were made to obtain homogeneous multilamellar vesicles. Each freeze-thaw cycle consisted of three steps: freezing the sample to -80 °C, warming it up to room temperature and vortexing it.

Deuterated NMR sample. 19 mg of DMPG as a powder and 6 mg of d_{54}-DMPG in chloroform were dried under a stream of nitrogen and then under high vacuum overnight. The film was dispersed in 250 µL of buffer to produce the *high lipid content* sample (143 mmol/kg). 10.3 mg of DMPG as a powder and 3.5 mg of d_{54}-DMPG in chloroform were dried under a stream of nitrogen and then under high vacuum overnight. The film was dispersed in 400 µL of buffer to produce the *low lipid content* sample (50 mmol/kg DMPG). Multilamellar vesicles were formed by vortexing the dispersion. 10 freeze-thaw cycles were made to obtain homogeneous multilamellar vesicles.

4. Results

DMPG Suspensions at High Lipid Content. In a first series of experiments DMPG-Na^{+} was dispersed at a lipid molality of 270 mmol/kg in 100 mM NaCl, 10 mM Hepes, pH 7.4. ^{31}P-NMR spectra were recorded in the range of 15 °C to 50 °C and are shown in figure 1 for temperatures above (1A) and below (1B) the phase transition. The spectra are characteristic of multilamellar lipid bilayers. The anisotropic motion of the phosphate group can be quantitated by the chemical shielding anisotropy, $\Delta\sigma$, measured as the distance between the low- and high-field shoulders of the ^{31}P-NMR spectrum [31] (indicated by arrows in 1B).

Figure 1 compares the experimental spectra (black lines) with theoretical simulations (red lines). At 20 °C (fig. 1B), that is, for the viscous gel-phase the agreement between theory and experiment is excellent. The chemical shielding anisotropy is $\Delta\sigma$ = -45.5 ppm and the shape of the spectrum corresponds to a random distribution of bilayers ("powder-type spectrum"). Above the phase transition temperature (25 °C, fig 1A) the experimental spectrum has excess intensity at the high-field shoulder, suggesting a magnetically induced alignment for about 20% of the bilayers such that the planes of the oriented domains are parallel to the B0 field.32 As all bilayers carry a negative surface charge the electrostatic repulsion between adjacent bilayers is strong, leading to an increase in the intermembrane distance. Consequently, more water can be imbibed between juxtaposed bilayers facilitating the

motion and reorientation of the bilayers in a strong magnetic field. Magnetic alignment has first been reported for Eschericia coli lipids containing about 20 % PG and for a mixture of synthetic phosphatidylethanolamine and phosphatidylglycerol, both containing cis-unsaturated fatty acids.32 It has also been observed by 2H-and 31P-NMR for phospholipid bilayers consisting of a 40:60 mixture of N-palmitoylsphingomyelin and 1,2-dimyristoyl-sn-glycero-3-phosphocholine.33 The present data represent the first observation of magnetic alignment for a phospholipid with 2 saturated fatty acyl chains and a phosphoglycerol headgroup. Magnetic alignment is additional evidence for a lamellar structure as other structures such as micelles or cubic phases cannot be magnetically ordered for symmetry reasons.

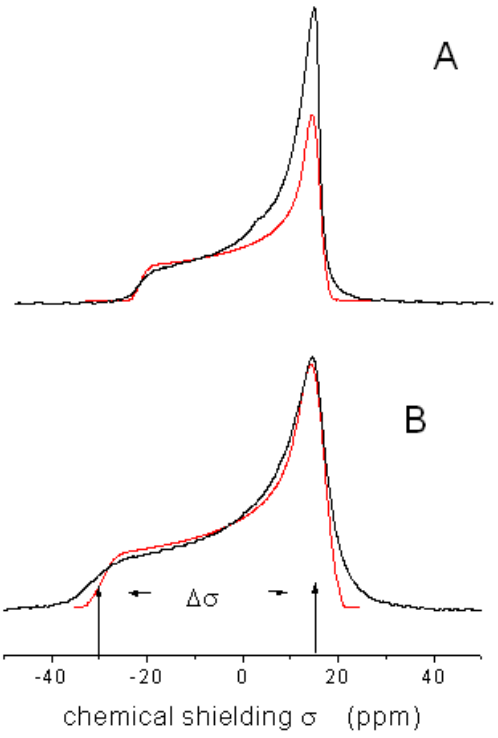

Figure 1: *^{31}P-NMR spectra of DMPG-Na^{+} bilayers at high lipid and high salt concentrations DMPG-Na^{+} at a molality of 270 mmol/kg was dispersed in buffer composed of 100 mM NaCl, 10 mM Hepes, pH 7.4 (A) 25 °C, (B) 20 °C. Black line: experimental spectrum; red line: simulation according to [29].*

The temperature dependence of the chemical shielding anisotropy, Δσ, is shown in figure 2A (♦) and reveals a phase transition at 23 °C. Above this temperature the bilayer is in the liquid-crystalline state and the chemical shielding anisotropy is

almost constant with $\Delta\sigma$ = -37 ppm at 23 °C and -36 ppm at 50 °C. Below T_c = 23 °C the bilayer is in a gel-like state and $\Delta\sigma$ decreases rapidly to -50 ppm. In parallel, the rate of reorientation of the phospholipid headgroup slows down.

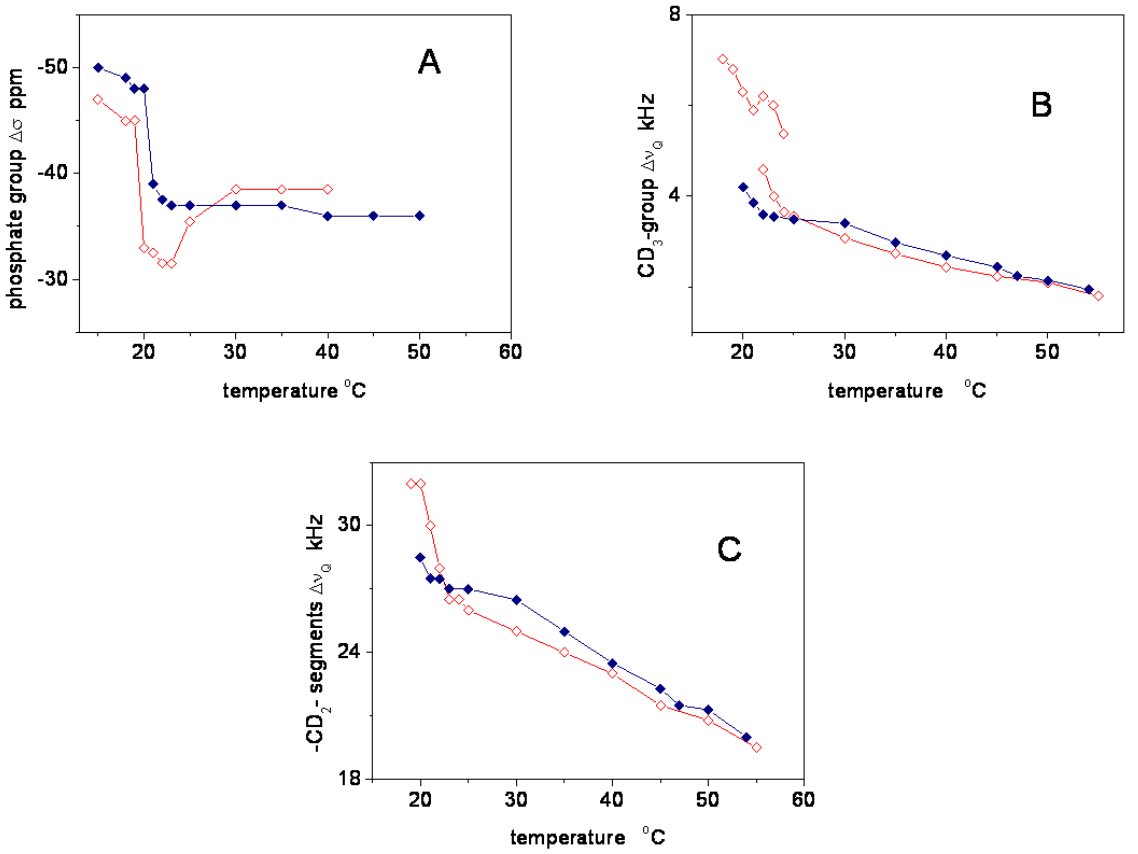

Figure 2: *^{31}P- and ^{2}H-NMR anisotropy parameters of DMPG-Na^{+} bilayers at a lipid molality of 270 mmol/kg*
(♦) 100 mM NaCl, 10 mM Hepes, pH 7.4. (◊) 2 mM NaCl, 10 mM Hepes, pH 7.4. (A) ^{31}P-NMR chemical shielding anisotropy Δσ; (B) quadrupole splitting, $\Delta\nu_Q$, of the terminal -CD_3 groups. At low ionic strength 2 separate quadrupole splittings are observed in the transition region, (C) quadrupole splitting, $\Delta\nu_Q$, of -CD_2-groups located close to the lipid-water interface, giving rise to the maximum splitting.

A different picture was obtained for ^{31}P-NMR spectra measured at the same high lipid molality of 270 mmol/kg but at *low ionic strength* (2 mM NaCl, 10 mM Hepes, pH 7.4). Figure 3A compares ^{31}P- NMR spectra in the range of 19 °C to 23 °C.

Two features are notable. (i) At 20 °C the spectrum is a superposition of 2 spectra indicating the *coexistence of two bilayer phases*. This appears to be an equilibrium situation as exactly the same spectrum is obtained after 5 hrs of equilibration at this temperature. (ii) The spectra at 21 °C and higher temperatures are

consistent with a single phase but are again characterized by an increased intensity of the high-field shoulder. Spectral simulations reveal that about 20% of the total lipid material is magnetically aligned.

The temperature dependence of the chemical shielding anisotropy, $\Delta\sigma$, at low ionic strength is included in figure 2A (◊). Compared to spectra at 100 mM NaCl the transition region is broader and extends from 20 °C to 24 °C. Unexpectedly, the size of $\Delta\sigma$ goes through a distinct minimum in this temperature interval indicating an unusual change in orientation of the phosphoglycerol headgroup (cf. Discussion).

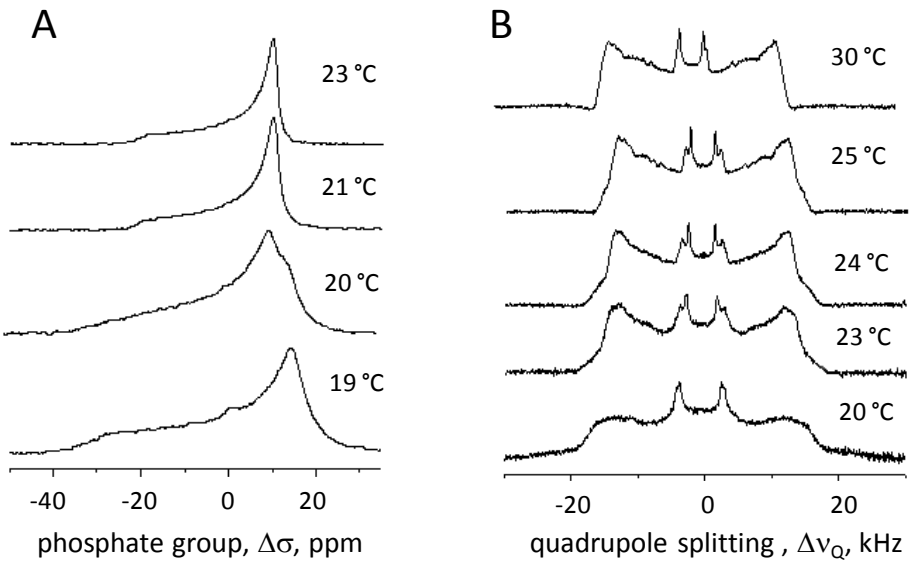

***Figure 3**: ^{31}P- and ^{2}H-NMR spectra of DMPG -Na^{+} lipid bilayers at high lipid content but low ionic strength buffer*
(A) ^{31}P-NMR 50 mg of DMPG-Na^{+} was dispersed in 250 µL of low ionic strength buffer (10 mM Hepes, 2 mM NaCl, pH 7.4) (lipid molality 270 mmol/kg). (B) ^{2}H-NMR 6 mg perdeuterated of d_{54}-DMPG-Na^{+} and 19 mg of DMPG were dispersed in 100 µL of the same buffer as in (A) (lipid molality 340 mmol/kg).

The hydrophobic part of the bilayer was monitored with ^{2}H-NMR using DMPG-Na^{+} with 2 perdeuterated myristic acid chains and mixed with non-deuterated DMPG-Na^{+} at a 1:3 (deuterated/non-deuterated) molar ratio. ^{2}H-NMR spectra of lipid bilayers at low ionic strength are shown in figure 3B providing independent evidence for the co-existence of two different bilayer phases in the transition region. The spectra arise from a superposition of the time-averaged quadrupole splittings of all deuterated chain segments. The size of the quadrupole splitting varies along the chain. An unambiguous assignment can be made for the high-intensity, innermost splitting which

comes from the terminal -CD_3 groups of both chains. Figure 3B reveals *two* CD_3-splittings in the transition region with separations of $\Delta\nu_Q$ ~ 3 kHz and 6.5 kHz. As the temperature is raised from 22 °C to 24 °C, the intensity of the 3 kHz splitting increases at the expense of the 6.5 kHz splitting, confirming the co-existence of 2 bilayer phases. Figure 2B summarizes the temperature dependence of $\Delta\nu_Q$(-CD_3) for both high and low NaCl concentrations. Very similar quadrupole splitting are measured for DMPG membranes suspended in 100 mM NaCl (♦) or 2 mM NaCl (◊). An increase in the quadrupole splitting occurs when the temperature is lowered below 24 °C. The gel-to-liquid phase transition of the perdeuterated DMPG-Na^+ is about 1 °C higher than that of the non-deuterated lipid because of stronger van-der-Waals interactions. Figure 2B shows 2 splittings for the CD_3-groups in the phase transition region.

The ordering of the hydrocarbon chains can be deduced from the edges of the deuterium NMR spectra (fig. 3B). The quadrupole splittings range between 19 kHz at 55 °C and 32 kHz at 20 °C. They reflect the anisotropic motion of those -CD_2- segments, which are located near the lipid-water interface.[33] Figure 2C summarizes the temperature dependence of the $\Delta\nu_Q$ (-CD_2-). Again, very similar quadrupole splittings are observed at 100 mM NaCl (♦) and 2 mM NaCl (◊). The increase in $\Delta\nu_Q$(-CD_2-) at about 24 °C reflects the phase transition region. However, even below the phase transition the fatty acyl chains are not extended in the all-trans conformation as a much larger quadrupole splittings of ~60 kHz would be expected. The experimental observations yield only ~32 kHz, indicating considerable chain flexing motions.

We observed thixotropy for samples which contained perdeuterated DMPG at high lipid concentration and high ionic strength. Freshly prepared samples showed typical bilayer ^{2}H- and ^{31}P-NMR spectra up to the highest temperature (50 °C). When NMR-sample tube was then taken out of the NMR spectrometer and was slightly shaken it became completely transparent. Re-insertion into the NMR spectrometer produced only isotropic lines, indicating an increased fluidity. Bilayer-type spectra returned only after months of storage at low temperature.

DMPG Suspensions at Low Lipid Content. The thermodynamic phase transitions of DMPG-Na^+ suspensions at *low lipid content* (molality ≤ 50 mmol/kg) and *high salt*

concentration have been investigated with DSC by several groups.[15,16,19,25,28] For samples dispersed at ≥ 100 mM NaCl the DSC scans reveal a pre-transition at 13-14 °C and a gel-to-liquid crystal transition at ~23 °C as confirmed in figure 4A for a sample used in the present NMR experiment.

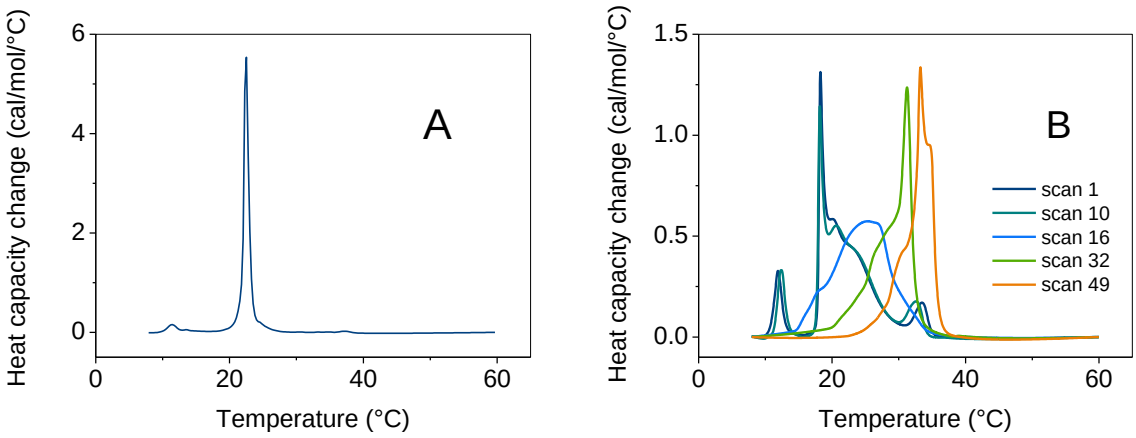

***Figure 4**: DSC thermograms of DMPG-Na^{+} suspensions*
(A) Low lipid concentrations, high ionic strength. 20.3 mg DMPG suspended in 1 mL at 100 mM NaCl, 10 mM Hepes, pH 7.4 (lipid molality 27.4 mmol/kg). The scan rate was 45 °C/h. 35 scans were performed yielding identical thermograms. (B) Low lipid concentration, low ionic strength. 19.8 mg DMPG dispersed in 1 mL buffer (2 mM NaCl, 10 mM Hepes, pH 7.4) (lipid molality 27 mmol/kg). 49 scans were obtained over a period of 5 days.

The ^{2}H- and ^{31}P-NMR spectra of such bilayers are not shown as they are similar to those in figure 1. However, their NMR anisotropy parameters are reported in figure 5. Most obvious is the change in the ^{31}P-NMR chemical shielding anisotropy (5A,●) from -39 ppm at 22 °C to -48 ppm at 20 °C. The phase transition occurs at the same temperature as found for the *high lipid* and *high salt* concentration (5A, ♦). The same phase transition is also observed in the ^{2}H-NMR spectra, not so much by a change in the quadrupole splitting but by a distinct line broadening.

The most unusual properties are observed for DMPG-Na^{+} samples at *low lipid content* and *low salt* concentrations. The DSC diagram displays a broad transition region between 17 to 35 °C with several peaks, the intensity of which changes with consecutive scans (fig. 4B).[34] The transition enthalpy remains, however, constant at 6.1 ± 0.2 kcal/mol.

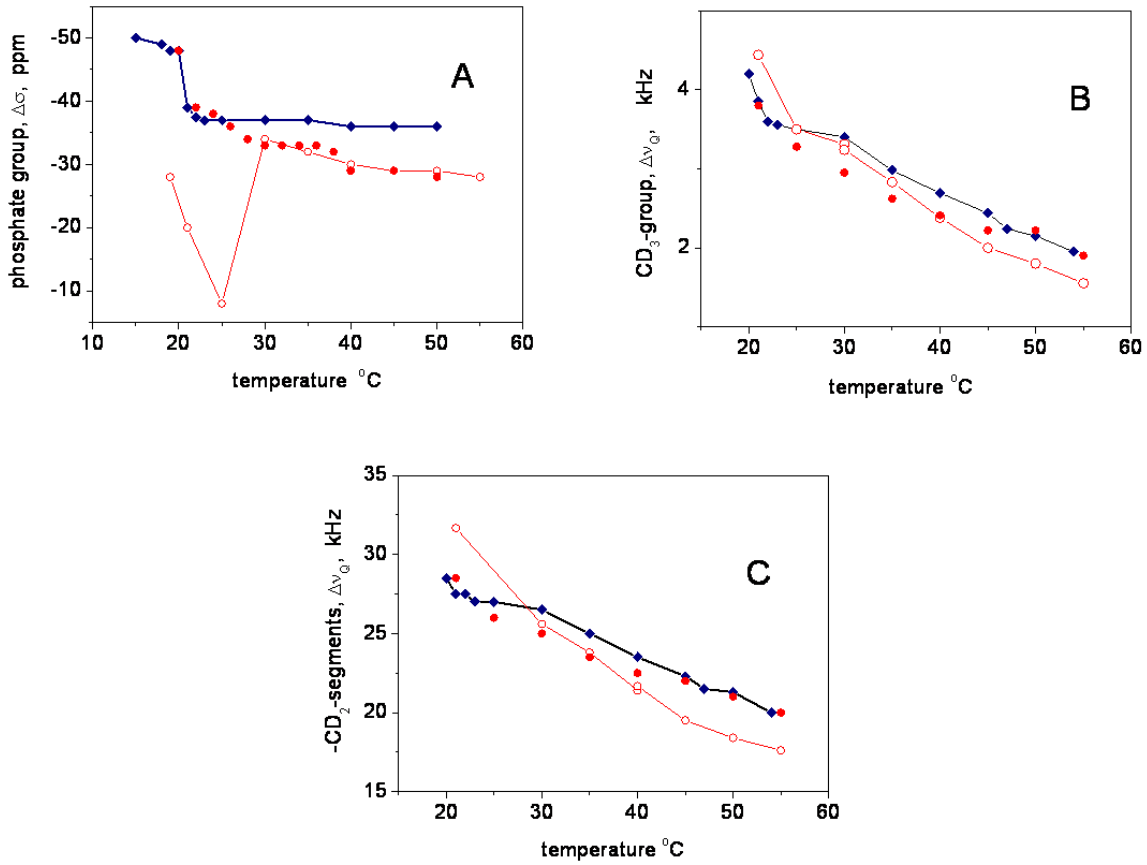

Figure 5: *^{31}P- and ^{2}H-NMR anisotropy parameters at low lipid molalities (lipid molality ≤ 50 mmol/kg)*

The lipid molality was typically 30 mmol/kg. (●) 100 mM NaCl, 10 mM Hepes, pH 7.4. (○) 2 mM NaCl, 10 mM Hepes, pH 7.4. (♦) repeats the data of figure 1 obtained at high lipid concentration and 100 mM NaCl. (A) ^{31}P-NMR. Phosphorus chemical shielding anisotropy Δσ. (B) ^{2}H-NMR. Quadrupole splitting of the terminal CD_3 groups. (C) ^{2}H-NMR. $\Delta\nu_Q$ of the largest splitting of the CD_2-groups.

The corresponding ^{31}P- and ^{2}H-NMR spectra (50 mmol/kg DMPG-Na^+, 2 mM NaCl, 10 mM Hepes, pH 7.4) are displayed in figures 6 and 7, respectively. Above the phase transition, at 30 and 35 °C, both ^{31}P- and ^{2}H-NMR show bilayer spectra of lipid membranes in the liquid-crystalline state. The ^{31}P-NMR spectrum at 35 °C also contains an isotropic component which increases in intensity as the temperature is raised even further.

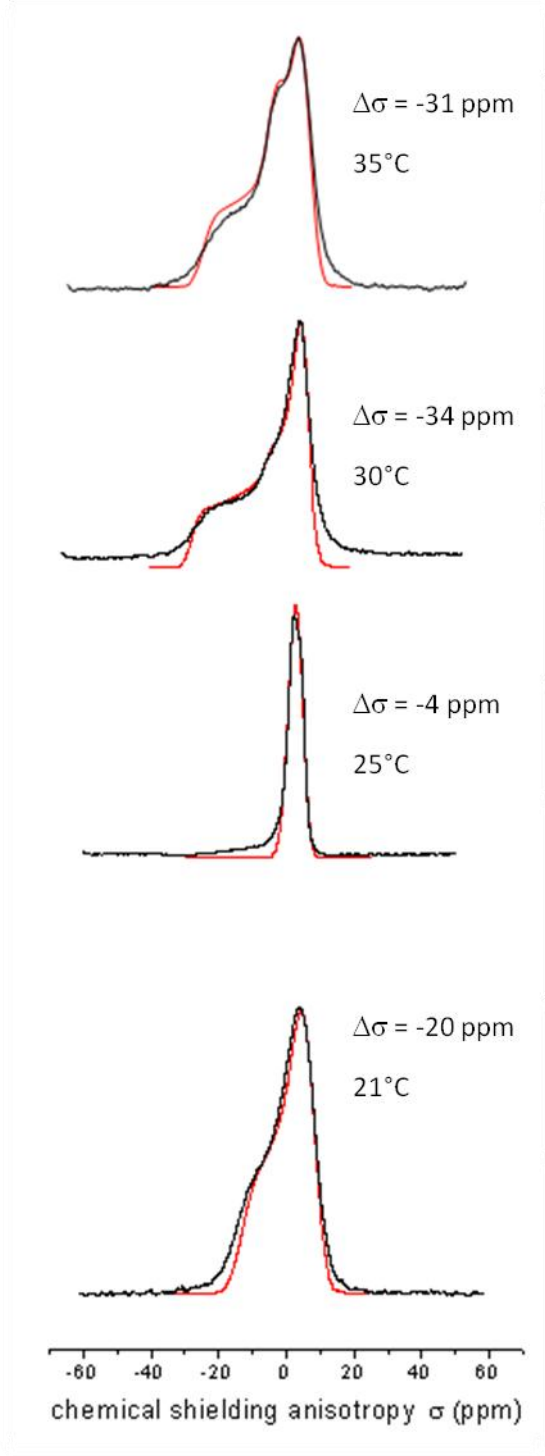

Figure 6: *^{31}P-NMR spectra of non-deuterated DMPG at low lipid content in low ionic strength buffer at different temperatures*
13.7 mg of DMPG was dispersed in 400 µL of low ionic strength buffer (2 mM NaCl, 2 mM Hepes, pH 7.4) (lipid molality 46.2 mmol/kg). The red lines are the spectral simulations. The 35 °C spectrum contains a small contribution from an isotropic line.

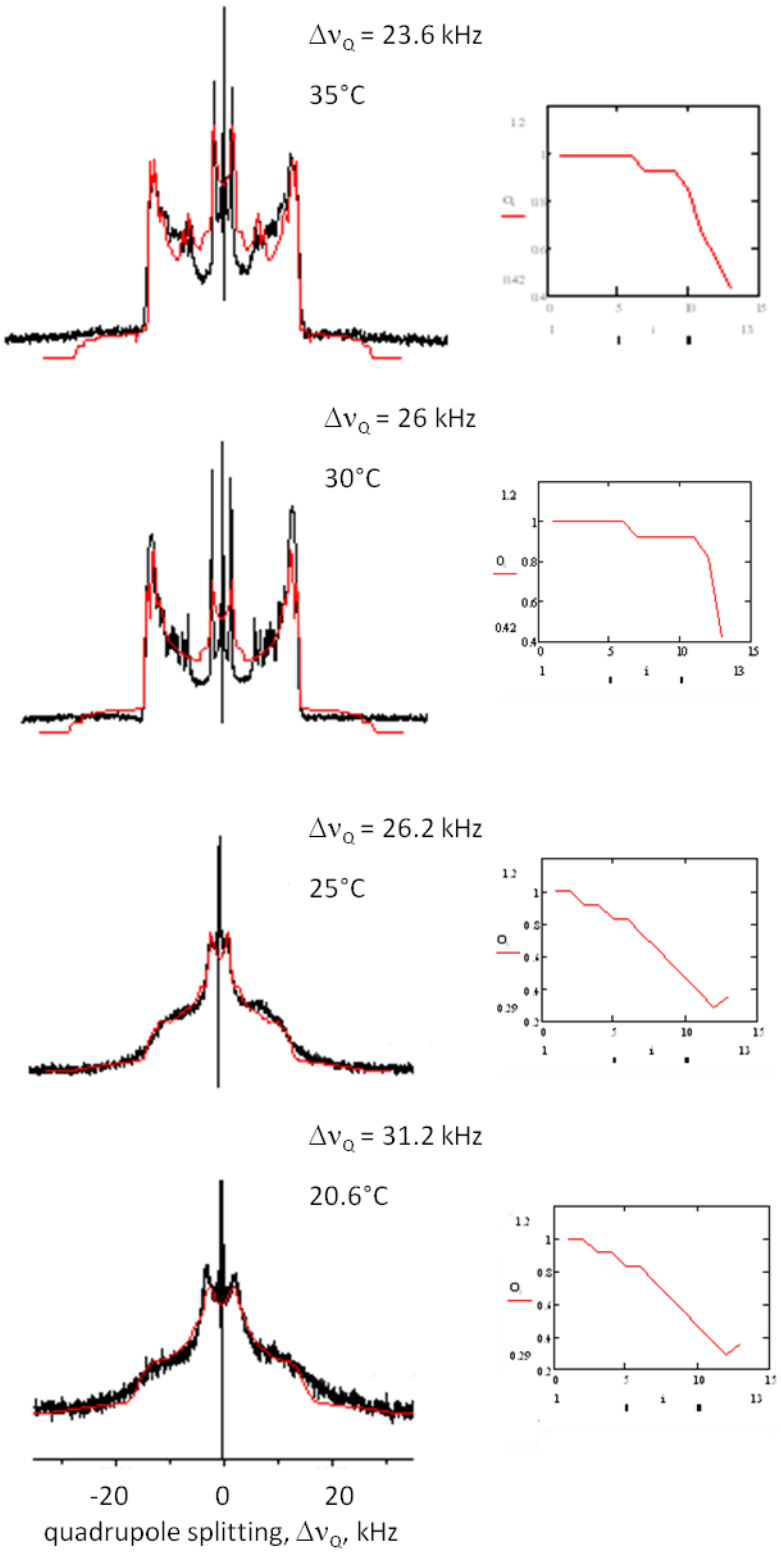

Figure 7: *^{2}H NMR spectra of deuterated DMPG at low lipid content in low ionic strength at different temperatures*
10.3 mg of DMPG and 3.5 mg of d_{54}-DMPG was dispersed in 400 µL of low ionic strength buffer (2 mM NaCl, 10 mM Hepes, pH 7.4) (lipid molality 46.5 mmol/kg). The red line represents the spectral simulation assuming a distribution of quadrupole splitting. The inserts represents the normalized order profiles used for the simulation.

Unusual ^{31}P- and ^{2}H-NMR spectra are however obtained between 20 and 25 °C. Such spectra have hitherto not been observed for bilayer systems. In particular, the ^{31}P-NMR spectrum at 25 °C consists of a narrow resonance, similar to that predicted for an isotropic phase. This is however contradicted by the ^{2}H-NMR spectrum at the same temperature which documents an anisotropic motion of the hydrocarbon chains (fig. 7). The narrow ^{31}P-NMR resonance is thus caused by a specific orientation of the phosphoglycerol headgroup with respect to the bilayer normal. If the temperature is further lowered to 21 °C, the ^{31}P-NMR spectrum becomes similar in shape to the 35 °C spectrum albeit with a Δσ of only -20 ppm. The temperature dependence of Δσ is shown in figure 5A (○). The dip in Δσ is even more pronounced than reported in figure 2A (◊) for high lipid, but low salt concentration.

The unusual behavior of the DMPG-Na^{+} headgroup is also reflected in the ^{2}H-NMR spectra of the deuterated hydrocarbon chains. At 35 °C and 30 °C (fig. 7) the spectra correspond to normal bilayers with the classical order profile and well-resolved resonances. In contrast, at 25 °C and 20.6 °C, the spectra show no individual resonances (except for the terminal CD_3-groups). They are characterized by a completely different order profile which is caused by a continuous distribution of gradually decreasing quadrupole splittings. Figure 5 summarizes the quadrupole splittings of the methyl groups (5B, ○) and the maximum splitting of the –CD_2-segments (5C, ○). The size and the temperature dependence of these splittings are not much different from those obtained at high salt concentration (●). The main difference is thus the shape of the order profiles.

After measuring at high temperatures the NMR-samples were taken out of the probe-head and turned upside-down several times. By this procedure the samples became completely transparent both at low and high ionic strength. The ^{31}P-NMR of these samples showed an isotropic line with Lorentzian lineshape and full-width-at-half height (FWHH) 850 Hz. The corresponding ^{2}H-NMR spectrum was also isotropic but composed of 2 lorentzians of FWHH = 280 Hz and 3000 Hz. As there are 24 deuterons in CD_2 segments and 3 in the CD_3 terminal we assign the sharp resonance to the CD_3 groups, the broader one to the CD_2 groups.

When the sample was stored for several months at 4 °C, a bilayer spectrum was partially recovered.

5. Discussion

The most characteristic property of phospholipids, which distinguishes this class of molecules from all other biomolecules, is their polymorphic behavior. Depending on the physiological conditions such as temperature, ion concentration, pH etc. structurally different mesophases can be formed. Gel-to-liquid-crystal phase transitions of the most abundant natural lipids usually occur below 0 °C and have not been investigated extensively. In contrast, phase transitions of synthetic lipids with 2 saturated chains are characterized by distinctly higher transition temperatures. Among these, the anionic 1,2-dimyristoyl-*sn*-glycero-3-phosphoglycerol has attracted particular attention as its phase diagram exhibits rather unusual features and is clearly more complex than that of its zwitterionic analog 1,2-dimyristoyl-*sn*-glycero-3-phosphocholine. In the present study we use NMR methods to deduce both the long-range organization and the dynamic molecular conformation of DMPG-Na^{+} under a variety of conditions. Not all phase transitions detected with DSC and other methods are accessible to NMR. NMR is well suited for liquid-crystalline material but in solids the NMR lines become too broad to provide useful information in the present context.

Order profiles of the hydrocarbon chains. The quadrupole splittings, $\Delta\nu_Q$, derived from the ^{2}H-NMR spectra describe the average conformation and fluctuations of the flexible hydrocarbon chains. An unambiguous assignment of the resonances is only possible with selectively labeled lipids [33]. For the perdeuterated hydrocarbon chains studied here we assume a sequential decrease in the size of the quadrupole splitting starting from the headgroup region with the largest splitting towards the bilayer interior with the smallest $\Delta\nu_Q$. The quadrupole splitting, $\Delta\nu_Q$, can be translated into a molecular order parameter, S_{CD}, according to

$$\Delta\nu_Q = \pm\frac{3}{4}\frac{e^2qQ}{h}S_{CD}$$

where (e^2qQ/h) = 167 kHz is the quadrupole coupling constant and $\Delta\nu_Q$ is the most intense splitting in powder-type spectra. A maximum quadrupole splitting of 26.2 kHz, as observed at 30 °C for the ^{2}H-NMR spectrum in figure 7, corresponds to S_{CD} = - 0.21. The negative sign follows from measurements of related systems.[29] The inserts in figure 7 show the *relative* order profiles necessary to simulate the experimental ^{2}H-

NMR spectra. To facilitate the comparison the order profiles are normalized such that S = 1 is assigned to the largest splitting in the spectrum. In the liquid-crystalline state (spectra at 30 °C and 35 °C), the order profiles show constant order parameters for the first 10 chain segments, but decrease rapidly for the last 4 segments as the tail of the hydrocarbon chain gains more motional freedom in the bilayer interior. This type of order profile has been observed for many other bilayers. However, unusual and not observed so far in bilayer structures are the order profiles of DMPG-Na^{+} in the region of the phase transition (spectra at 25 °C and 21 °C). The ^{31}P-NMR spectra (figure 6) provide evidence that the headgroups are still in a highly fluid environment. Nevertheless, it is not possible with ^{2}H-NMR to resolve individual quadrupole splitting of the hydrocarbon chains as the order profile decreases more rapidly than observed at higher temperatures (e.g. 30 °C). The envelope of the quadrupole splittings can be simulated by the order profile shown as inserts. Each segment adds approximately the same incremental contribution to chain flexing which leads to a more rapid decrease in S. The plateau region observed at 30 °C and 35 °C is replaced by a continuous decrease of the order parameter at 25 °C and 21 °C.

Knowledge of the order profile allows a determination of the average or projected length, <L>, of the fatty acyl chain according to

$$\langle L(n) \rangle \text{ Å} = 1.25 \left(\frac{n}{2} - \sum_{i=}^{n} S_{CD}^{(i)} \right)$$

where n is the number of chain segments.[33,35] For a rigid all-*trans* chain, rotating rapidly around its long axis $S_{CD}^{(i)}$ = -0.5 for all segments. The maximum length of a myristic acid chains (12C-C segments, neglecting the CO-CH_2 segment) is thus 15 Å. In contrast, in the liquid-crystalline state the average (or projected) chain length is distinctly reduced due to the flexing motions produced by *trans-gauche* rotations around the carbon-carbon single bonds. Based on the order profiles shown in figure 7 we determine a chain length of L(12) = 11.2 Å at 30 °C for the liquid-crystalline bilayer region and L(12) = 10.8 Å at 25 °C in the transition region. The latter result is quite surprising as a phase transition to lower temperature usually produces chain stiffening. For DMPG-Na^{+} at low salt concentration the opposite is observed. Immediately below the main transition the hydrocarbon chains adopt an even more coiled conformation.

Shorter hydrocarbon chains require a larger chain cross section as the volume remains constant. The increase in chain-chain spacing has distinct consequences for the orientation of the phosphoglycerol headgroup.

Molecular structure of DMPG headgroup in the bilayer phase. The analysis of the ^{31}P- NMR spectra provides quantitative insight into the orientation of the phosphoglycerol headgroup. The quantitative analysis leads to the molecular structure shown in figure 8 for DMPG at low lipid concentration and low ionic strength. Using the crystal structures obtained for 1,2-dimyristoyl-*sn*-glycero-3-phosphocholine [36], DMPG [37], and glycerylphosphocholine [38] it is possible to explain the NMR data in terms of a dynamic model [39], in which the glycerol headgroup fluctuates rapidly between two mirror-like conformations. The torsion and bond angles of the headgroup segments used in figure 8 are identical to those given in reference.[39] The change in the headgroup orientation and, in turn, $\Delta\sigma$ is brought about exclusively by the C_2-C_3-O-P torsion angle, i.e. the rotation around the C_3-O bond (C_2-C_3 $\triangleq$ carbon atoms of the glycerol backbone) (cf. atom labeling in figure 8). Figure 8 describes the two extreme situations observed in this study. Figure 8A corresponds to the 30 °C spectrum in figure 6 with $\Delta\sigma$ = -34 ppm; figure 8B displays the headgroup orientation at 25 °C with $\Delta\sigma$ = -4 ppm. The arrow represents the orientation of a virtual dipole between the P-atom and the terminal OH group at 30 °C. Its orientation is left unchanged in 8B to better illustrate the movement of the glycerol headgroup. At 30 °C the phosphoglycerol dipole makes an angle α_{dipole} ~ 12° with the bilayer surface. As the temperature is reduced to 25 °C, the headgroup moves closer to the hydrocarbon layer such that the oxygen-end points into the hydrocarbon interior with α_{dipole} = -16°. As the temperature is further lowered to 21 °C, the headgroup moves back towards the water phase and its dipole is almost exactly parallel to the bilayer surface with α_{dipole} = 2°.

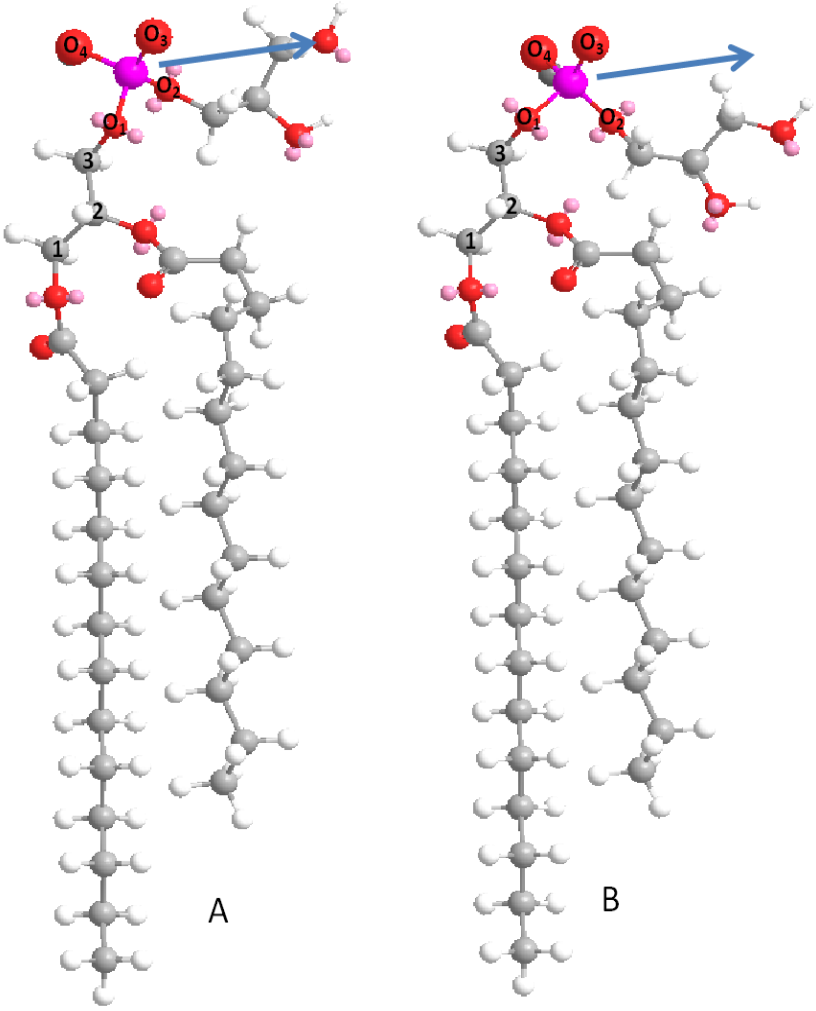

***Figure 8**: Orientation of the phosphoglycerol headgroup*
The figure shows the change in orientation of the phosphoglycerol headgroup as the temperature changes from 30 °C (A) with Δσ = -34 ppm to 25 °C (B) with Δσ = -4 ppm. The torsion angles are those listed in reference [39] for the NMR experiment with glycerylphosphocholine. The variation in Δσ can be explained by a ~30 ° rotation around the C(3)-O_1 axis of the C(2)-C(3)-O_1-P segment, which connects the headgroup with the glycerol backbone. For convenience the hydrocarbon chains are left in the rigid all-trans-conformation, even though the order profiles of figure 7 provide evidence for extensive segmental fluctuations perpendicular to the bilayer normal. The blue arrow in (A) connects the P-atom with the terminal glycerol-oxygen atom and is only introduced to guide the eye. Its orientation is not changed in (B) to better indicate the movement of the glycerol headgroup.

The unusual movement of the PG headgroup is caused exclusively by a change of the C_2-C_3-O-P torsion angle and is correlated with a change in the membrane surface charge. For the zwitterionic phosphatidylcholine it is known that the polar headgroup is sensitive to the surface charge (molecular voltmeter concept).[40,41] In neutral POPC bilayers the P-N dipole makes an angle of 23° with the bilayer surface and Δσ ≈ -50 ppm. The addition of cationic molecules to the bilayer surface moves the N-

tip of the dipole into the aqueous phase, the insertion of anionic molecules induces the opposite rotation. It appears that the same physical principle can be invoked to explain the movement of the glycerol headgroup of DMPG-Na^+. Conductivity measurements have shown that the electrical conductivity of DMPG-Na^+ dispersions at low ionic strength goes through a pronounced maximum in the temperature interval of 15-40 °C.[34,42] Model calculations reveal that the degree of Na^+ dissociation of DMPG-Na^+ bilayers changes from α_{ion} = 0.27 at 21 °C (Δσ = -20 ppm), to α_{ion} = 0.33 at 25 °C (Δσ = -4ppm) to α_{ion} = 0.16 (Δσ = -34 ppm) at 30 °C. Including the result for neutral POPC as α_{ion} = 0 (Δσ = -50 ppm) we obtain an approximately linear relationship between Δσ (and, in turn, α_{dipole}) and the membrane surface charge. The direction of the change is the same as observed for phosphatidylcholine. The larger the negative surface charge, the closer the glycerol headgroup to the hydrocarbon layer. As the choline residue has a positively charged $-\overset{+}{N}(CH_3)_3$ endgroup while the glycerol residue is neutral with an OH terminal, the identical reaction of both residues to negative charge suggests that the main interaction occurs close to the phosphate group. Molecular dynamics calculations are performed at present to provide a more detailed insight.

Phase properties of DMPG bilayers. A large series of experiments has led to the conclusion that DMPG dispersions at low lipid and low salt concentrations give rise to fragmented structures or tattered bilayer sheets.[19,23,34] This would produce an almost isotropic motion of lipid molecules in the rim region and give rise to isotropic NMR spectra. However, deuterium-and phosphorus-NMR spectra with bilayer characteristics were observed even under these conditions. The temperature interval between 20 and 30°C showed bilayer-like long-range order but with short-range order different from classical bilayers. The order profile indicated a more disordered hydrocarbon region and the lipid headgroups were found to move closer to the bilayer interior. Above 30°C the NMR spectra had the typical fluid-like bilayer signature with disordered hydrocarbon chains, below 20° the characteristics of extended hydrocarbon chains in the gel-state were observed. At a high lipid concentration but low-salt, the deuterium NMR spectra revealed the coexistence of two lipid bilayers, in agreement

with earlier EPR studies.[43] These data could always be reproduced if freshly prepared lipid samples were used for the experiments. Unusual phase properties were however observed upon prolonged heating of the NMR samples to 55°C. This generated NMR signals characteristic of an isotropic motion of lipids. The bilayer signal could only be recuperated if the samples were stored for several months at 4°C and then warmed up again. In agreement with earlier reports [24] this suggests that temperatures below 10 and above 50°C can produce metastable states which may not easily return to thermodynamic equilibrium situations.

In conclusion, the NMR data have shown that DMPG-Na^{+} aqueous dispersions display bilayer-like structures under all conditions measured. Micellar structures were not observed. At low salt concentrations and at temperatures between 20 to 25 °C the phosphocholine headgroup rotates closer to the hydrophobic part. The extent of rotation can be linearly correlated with the negative membrane surface charge, that is, the extent of ionization of DMPG-Na^{+}.

6. References

(1) Sacre, M. M.; Tocanne, J. F. *Chemistry and physics of lipids* **1977**, *18*, 334.
(2) Watts, A.; Harlos, K.; Maschke, W.; Marsh, D. *Biochimica et biophysica acta* **1978**, *510*, 63.
(3) Wohlgemuth, R.; Waespe-Sarcevic, N.; Seelig, J. *Biochemistry* **1980**, *19*, 3315.
(4) Gally, H. U.; Pluschke, G.; Overath, P.; Seelig, J. *Biochemistry* **1981**, *20*, 1826.
(5) Borle, F.; Seelig, J. *Biochimica et biophysica acta* **1983**, *735*, 131.
(6) Mischel, M.; Seelig, J.; Braganza, L. F.; Buldt, G. *Chemistry and physics of lipids* **1987**, *43*, 237.
(7) Borle, F.; Seelig, J. *Chemistry and physics of lipids* **1985**, *36*, 263.
(8) Gershfeld, N. L.; Stevens, W. F., Jr.; Nossal, R. J. *Faraday discussions of the Chemical Society* **1986**, 19.
(9) Gershfeld, N. L. *Biochemistry* **1989**, *28*, 4229.
(10) Loosley-Millman, M. E.; Rand, R. P.; Parsegian, V. A. *Biophysical journal* **1982**, *40*, 221.
(11) van Dijck, P. W.; Ververgaert, P. H.; Verkleij, A. J.; van Deenen, L. L.; de Gier, J. *Biochimica et biophysica acta* **1975**, *406*, 465.
(12) Findlay, E. J.; Barton, P. G. *Biochemistry* **1978**, *17*, 2400.
(13) Salonen, I. S.; Eklund, K. K.; Virtanen, J. A.; Kinnunen, P. K. *Biochimica et biophysica acta* **1989**, *982*, 205.
(14) Heimburg, T.; Biltonen, R. L. *Biochemistry* **1994**, *33*, 9477.
(15) Zhang, Y. P.; Lewis, R. N.; McElhaney, R. N. *Biophysical journal* **1997**, *72*, 779.
(16) Schneider, M. F.; Marsh, D.; Jahn, W.; Kloesgen, B.; Heimburg, T. *Proceedings of the National Academy of Sciences of the United States of America* **1999**, *96*, 14312.
(17) Riske, K. A.; Amaral, L. Q.; Lamy-Freund, M. T. *Biochimica et biophysica acta* **2001**, *1511*, 297.
(18) Pabst, G.; Danner, S.; Karmakar, S.; Deutsch, G.; Raghunathan, V. A. *Biophysical journal* **2007**, *93*, 513.
(19) Riske, K. A.; Amaral, L. Q.; Lamy, M. T. *Langmuir* **2009**, *25*, 10083.
(20) McMullen, T. P.; Lewis, R. N.; McElhaney, R. N. *Biochimica et biophysica acta* **2009**, *1788*, 345.
(21) Chapman, D.; Williams, R. M.; Ladbrooke, B. D. *Chemistry and physics of lipids* **1967**, *1*, 445.
(22) Small, D. M. In *Handbook of Lipid Research 4*; Plenum Press: New York, 1986, p 475.
(23) Epand, R. M.; Hui, S. W. *FEBS letters* **1986**, *209*, 257.
(24) Epand, R. M.; Gabel, B.; Epand, R. F.; Sen, A.; Hui, S. W.; Muga, A.; Surewicz, W. K. *Biophysical journal* **1992**, *63*, 327.
(25) Riske, K. A.; Döbereiner, H. G.; Lamy-Freund, M. T. *J Phys Chem B* **2002**, *106*, 239.
(26) Lamy-Freund, M. T.; Riske, K. A. *Chemistry and physics of lipids* **2003**, *122*, 19.
(27) Riske, K. A.; Amaral, L. Q.; Dobereiner, H. G.; Lamy, M. T. *Biophysical journal* **2004**, *86*, 3722.
(28) Alakoskela, J. M.; Kinnunen, P. K. *Langmuir* **2007**, *23*, 4203.
(29) Seelig, J. *Quarterly reviews of biophysics* **1977**, *10*, 353.
(30) Seelig, J. *Biochimica et biophysica acta* **1978**, *515*, 105.
(31) Niederberger, W.; Seelig, J. *J Amer Chem Soc* **1976**, *98*, 3704.
(32) Seelig, J.; Borle, F.; Cross, T. A. *Biochimica et biophysica acta* **1985**, *814*, 195.
(33) Seelig, A.; Seelig, J. *Biochemistry* **1974**, *13*, 4839.
(34) Barroso, R. P.; Riske, K. A.; Henriques, V. B.; Lamy, M. T. *Langmuir* **2010**, *26*, 13805.
(35) Schindler, H.; Seelig, J. *Biochemistry* **1975**, *14*, 2283.
(36) Pearson, R. H.; Pascher, I. *Nature* **1979**, *281*, 499.
(37) Pascher, I.; Sundell, S.; Harlos, K.; Eibl, H. *Biochimica et biophysica acta* **1987**, *896*, 77.
(38) Sundaralingam, M. *Annals of the New York Academy of Sciences* **1972**, *195*, 324.

(39) Seelig, J.; Gally, G. U.; Wohlgemuth, R. *Biochimica et biophysica acta* **1977**, *467*, 109.
(40) Seelig, J.; Macdonald, P. M.; Scherer, P. G. *Biochemistry* **1987**, *26*, 7535.
(41) Scherer, P. G.; Seelig, J. *Biochemistry* **1989**, *28*, 7720.
(42) Riske, K. A.; Politi, M. J.; Reed, W. F.; LamyFreund, M. T. *Chemistry and physics of lipids* **1997**, *89*, 31.
(43) Riske, K. A.; Fernandez, R. M.; Nascimento, O. R.; Bales, B. L.; Lamy-Freund, M. T. *Chemistry and physics of lipids* **2003**, *124*, 69.

XI. Appendix: Thermal phase behavior of DMPG

Lipid bilayers generally adopt two packing geometries depending on the temperature. At temperatures below the melting temperature, T_m, they are in the highly ordered gel phase. At temperatures higher than T_m, the lipids are in the liquid crystalline phase. DMPG, in contrast to most other phospholipids, does not have a single melting temperature, but shows a more elaborate phase diagram at low ionic strength. The structure adopted by DMPG in this temperature range is unusual and was studied in the previous manuscript (Chapter X).

1. DMPG at high lipid content

A particularly prominent feature of DMPG is its change in optical appearance at high lipid content with the temperature. This is true for DMPG both at high and low ionic strength. Figure 1 shows the sample of DMPG at high lipid content and low ionic strength. At 10°C, DMPG looks milky and opaque. At room temperature, the formation of white cloud-like structures is observed in the lipid dispersion. At 50°C the mixture becomes completely transparent and jelly-like.

The change in optical appearance is not the only unusual feature of DMPG. After the upwards temperature scan, if the NMR sample at high lipid content is gently shaken, it becomes transparent and fluid: it shows very low viscosity under gentle agitation. This applies for the samples at high lipid content, both in low or high ionic strength, if they are kept a few hours at high temperature (~ 50°C) and then gently shaken.

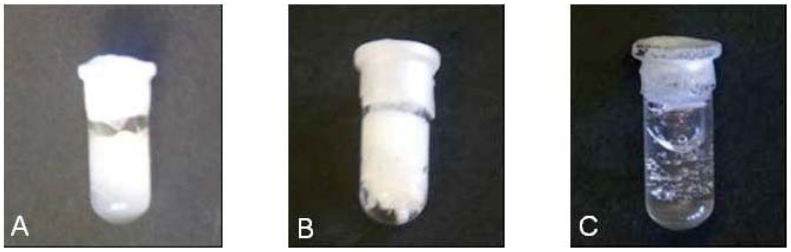

***Figure 1**: DMPG at high lipid content (290 mM) dispersed in low ionic strength buffer (10mM HEPEs, 2mM NaCl, pH7.4). The temperature of the sample is (A) 10, (B) 25 and (C) 50°C, respectively.*

This particular effect was further investigated. The ^{2}H-NMR spectra of a sample at high lipid content and low ionic strength is shown in Figure 2. The freshly prepared sample was measured at high temperature (40-55°C) with ^{2}H-NMR and the recorded spectra are shown at the bottom of Figure 2. At the end of these measurements, the sample was transparent and fluid. The sample was still transparent after two weeks of storage at 8°C. This transparent sample was measured with ^{2}H-NMR and led to isotropic peaks. They are shown at the top of Figure 2.

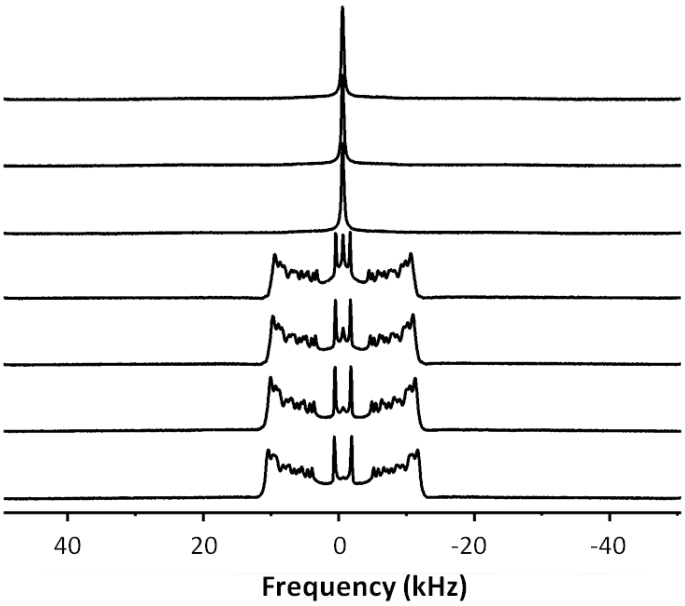

***Figure 2**: ^{2}H-NMR spectra of DMPG at high lipid concentration and low ionic strength at different temperatures. 290 mM DMPG/d_{54}-DMPG (3:1, mol/mol) was dispersed in low ionic strength buffer (2 mM NaCl, 10 mM HEPEs, pH 7.4).*
Temperature from bottom to top: 40, 45, 50 and 55°C, the sample was measured again after 2 weeks at 15, 18, and 19°C.

The isotropic phase was studied further with a freshly-prepared sample at high lipid content and high ionic strength. The sample was first measured in the gel and in the liquid-crystal phase with ^{2}H-NMR (Figure 3A).

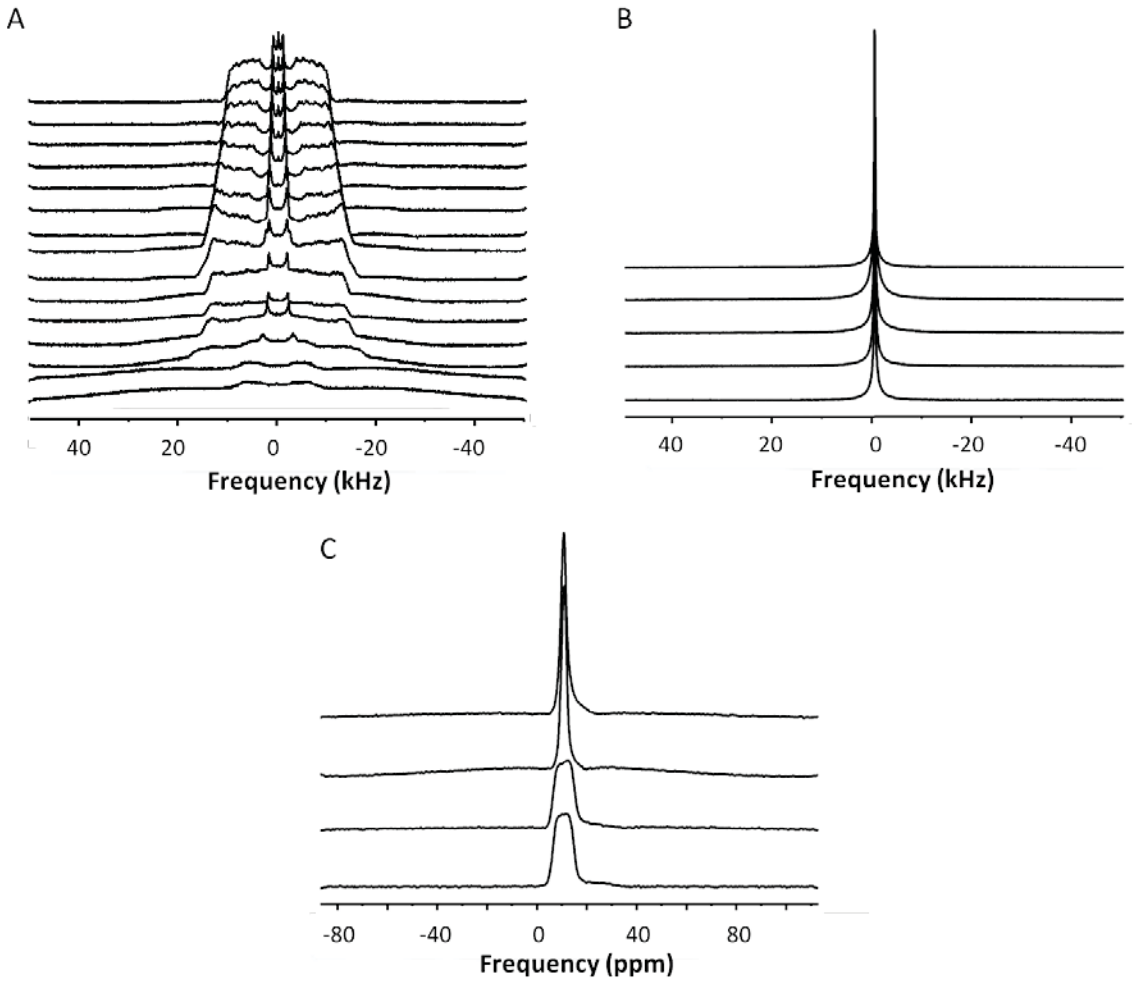

***Figure 3**: (A, B) ^{2}H- and (C) ^{31}P-NMR spectra of DMPG at high lipid concentration and high ionic strength at different temperatures. 290 mM DMPG/d_{54}-DMPG (3:1, mol/mol) was dispersed in high ionic strength buffer (100 mM NaCl, 10 mM HEPEs, pH 7.4).*
Temperature from bottom to top: (A) 15, 18, 19, 20, 21, 22, 23, 24, 25, 30, 35, 40, 45, 50, 54°C, (B) 20, 25, 30, and 35°C, (C) 22, 40, 55, and 25°C.

At the end of the experiments at high temperature (Figure 3A), the sample was transparent and fluid, as described at high lipid content and low ionic strength. The isotropic phase was studied with ^{2}H-NMR after two weeks (Figure 3B), and with ^{31}P-NMR after three weeks of storage at 8°C (Figure 3C). The sharp line observed in ^{2}H-NMR is paralleled by a broader peak in ^{31}P-NMR at low temperature. Upon

temperature increase the broad peak also converts into a sharp isotropic line in ^{31}P-NMR.

2. DMPG at low lipid content

At low lipid content, the samples have a different optical appearance in contrast to the sample at high lipid content. DMPG at low lipid content in high ionic strength looks turbid at room temperature and becomes transparent at high temperatures, similarly to the samples at high lipid content. In contrast, DMPG at low lipid content and low ionic strength is transparent at all temperatures. Figure 4 shows the samples at low lipid content and high or low ionic strength at room temperature.

Figure 4*: DMPG at low lipid content (50 mM) in (left) high and (right) low ionic strength at room temperature.*

A solid-state NMR study at low lipid content was performed at high and low ionic strength. Figure 5 shows the recorded ^{31}P and ^{2}H spectra. For this study, four distinct samples were freshly prepared. The spectra of the sample at high ionic strength (see Figure 5A and C) are typical for a lipid bilayer. The spectra at low ionic strength (see Figure 5B and D) have unusual characteristics and are discussed in the manuscript (Chapter X).

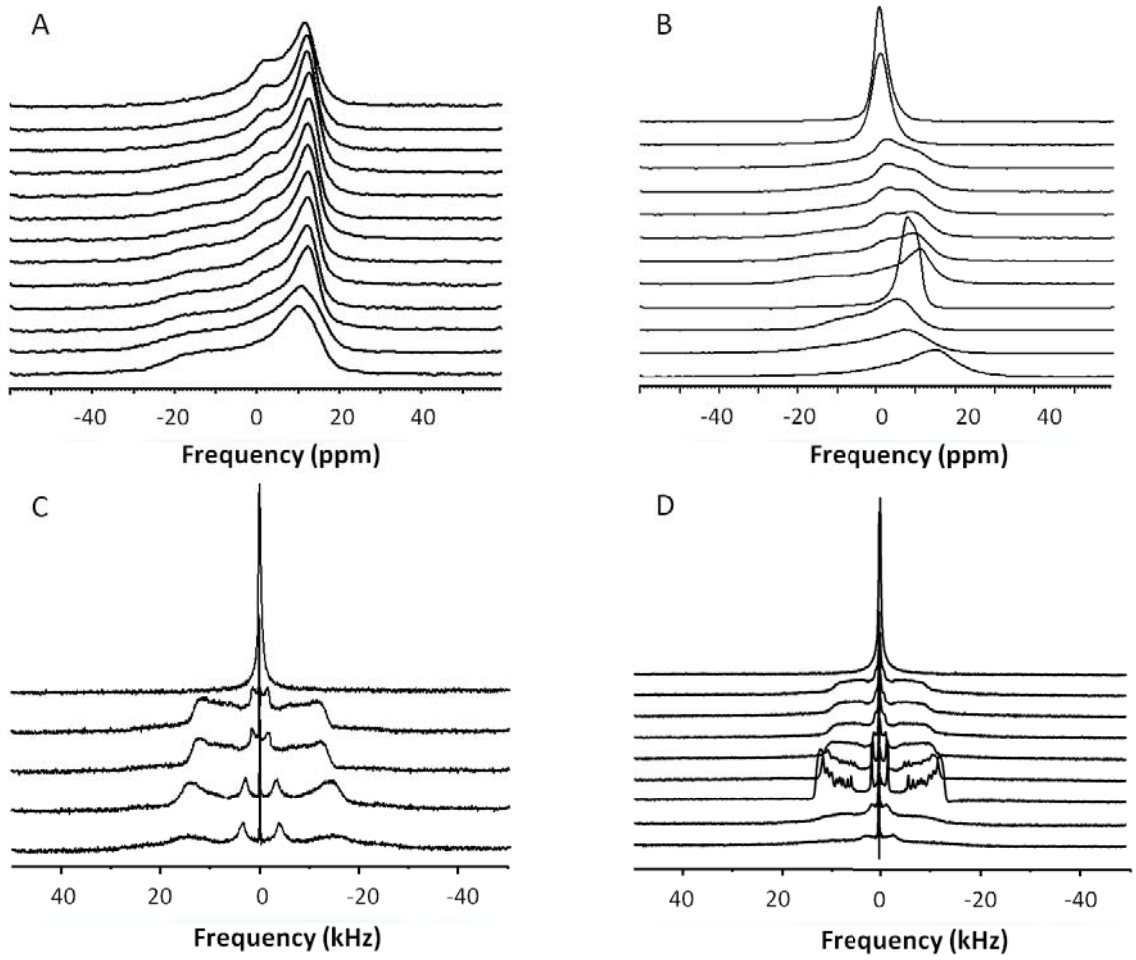

***Figure 5**: ^{31}P- (A, B) and ^{2}H-NMR (C, D) spectra of DMPG at low lipid concentration and at different temperatures. 50 mM (A) DMPG or (C) DMPG/d_{54}-DMPG (3:1, mol/mol) was dispersed in high ionic strength buffer (100 mM NaCl, 10 mM HEPEs, pH 7.4). 50 mM (B) DMPG or (D) DMPG/d_{54}-DMPG (3:1, mol/mol) was dispersed in low ionic strength buffer (2 mM NaCl, 10 mM HEPEs, pH 7.4).*
Temperature from bottom to top: (A) 22, 24, 26, 28, 30, 32, 34, 36, 38, 40, 45, 50, 55°C, (B) 17, 19, 21, 25, 30, 35, 40, 45, 50, 55, sample taken out of the probe head and measured at 20, and 31°C, (C) 20, 22, 24, 26°C, sample heated up to 55°C, taken out of the probe head and measured at 20°C, (D) 21, 25, 30, 35, 40, 45, 50, 55°C, sample taken out of the probe head and measured at 20°C after 2 weeks.

The interesting feature observed in the NMR spectra (Figure 5) is that the samples at low lipid content and low or high ionic strength show thixotropy, similarly to the samples at high lipid content. If they are gently shaken after the experiments at high temperature and measured again, the spectra show an isotropic line (see the two upper spectra in Figure 5B, the top spectrum in Figure 5C, and the top spectrum in Figure 5D).

It was observed that the isotropic phase could be reached by prolonged heating of the sample after the freeze-thaw procedure. For this purpose the sample was heated above the melting transition, at 50°C, and vortexed. Successive cycles of heating at 50°C and vortexing were repeated until the sample becomes transparent.

The stability of the isotropic phase was investigated over time in a sample at low lipid content and low ionic strength. This sample did not contain deuterated lipid in order to eliminate the possibility of a particular interaction due to the deuterons on both acyl chains of DMPG. It was successively heated at 50°C and vortexed in order to reach directly the isotropic phase, as described in the previous paragraph. The ^{31}P-NMR spectra of the non-deuterated sample are show in Figure 6.

The isotropic phase is observed also in the non-deuterated sample at low lipid content and low ionic strength. The intensity of the isotropic line increases with the temperature and a slight shift in the frequencies is observed, from 1 to 3 ppm (see Figure 6A). After one month of storage at 8°C, a broader peak is superimposed on the isotropic line (see Figure 6B). Furthermore the several phases observed in the DMPG system have properties that change over time, even 11 months after the dispersion of DMPG in buffer (see Figure 6C).

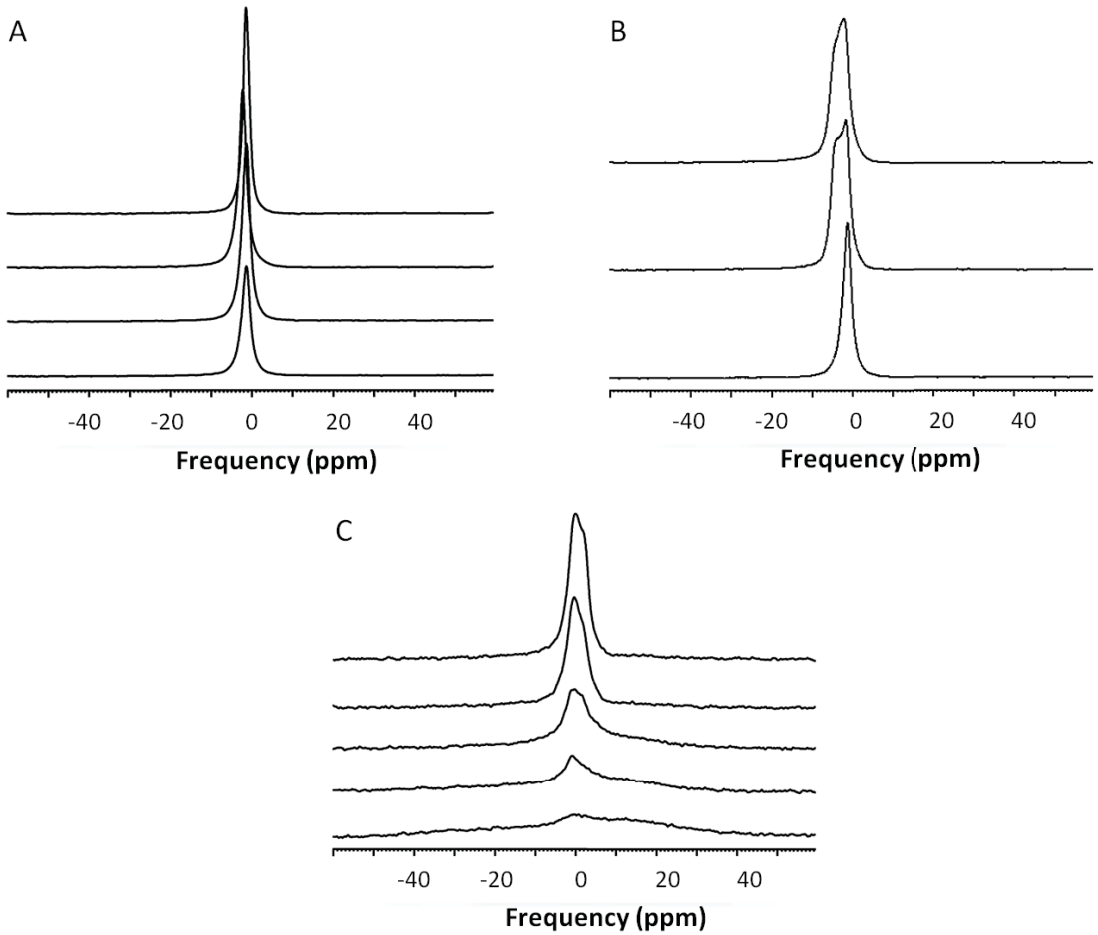

***Figure 6**: ^{31}P-NMR spectra of DMPG at low lipid concentration and low ionic strength at different temperatures and after different storage periods. 50 mM DMPG was dispersed in low ionic strength buffer (2 mM NaCl, 10 mM HEPEs, pH 7.4).The sample was successively heated at about 50°C and vortexed. This heat-vortex cycle was repeated until the sample was transparent.*
(A) Fresh sample measured from bottom to top at 23, 23, 13, and 33°C. (B) The sample was measured at 23°C immediately, and at 25°C after 30 and 37 days, from bottom to top. (C) Sample stored 11 months at 8°C and then measured at 0, 5, 10, 15, and 20°C, from bottom to top.

Repeating this experiment with a freshly-prepared non-deuterated sample leads to similar but not identical results. Figure 7A shows the ^{31}P-NMR spectra of a second sample at low lipid content and low ionic strength. This sample was prepared in order to reach directly the isotropic phase, as described above. After a few months at 8°C, the sample is not completely transparent anymore but it contains a few white clouds that disappear under vortexing. The ^{31}P-NMR spectra of this aged sample are shown in Figure 7B. The phase properties of the DMPG system changed within 3 months.

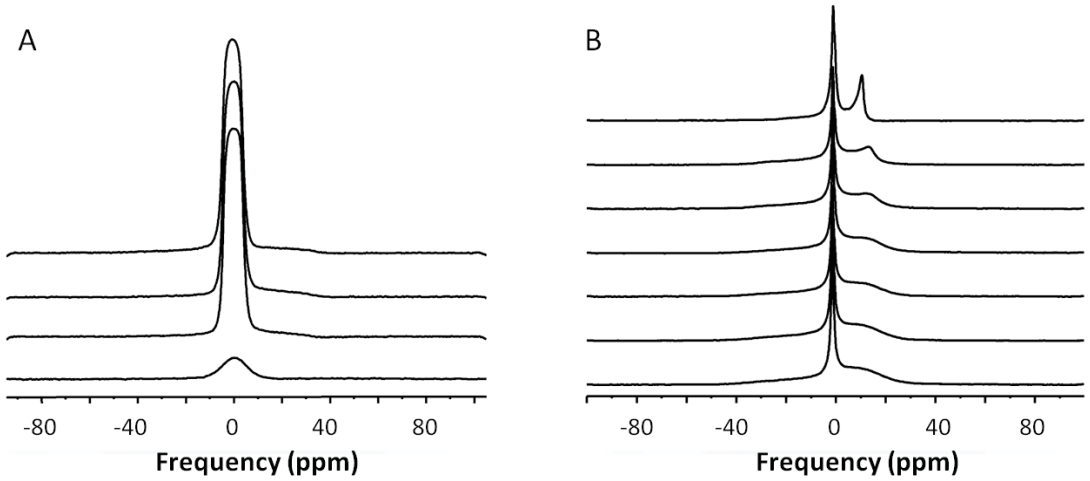

***Figure 7**: ^{31}P-NMR spectra of DMPG at low lipid concentration and low ionic strength at different temperatures. 50 mM DMPG was dispersed in low ionic strength buffer (2 mM NaCl, 10 mM HEPEs, pH 7.4). The sample was successively heated at about 50°C and vortexed. This heat-vortex cycle was repeated until the sample was transparent.*
(A) Condition from bottom to top: the sample was measured at 25°C, after 45 days it was measured at -15, 5 and 2°C. (B) after 3 months, temperature from bottom to top: 15, 20, 25, 30, 35, 40 and 50°C.

Another unusual feature of DMPG at low lipid content and low ionic strength is the continuous shift of the phase transition observed in the calorimetric profile (Chapter X, Figure 4D). This shift could be due to degradation of the sample due to hydrolysis, for example, as mentioned in the manuscript. Therefore the integrity of the sample was checked by mass spectrometry (MALDI-TOF) by comparing a freshly prepared sample with a sample used in a series of DSC scans. The results are shown in Figure 8.

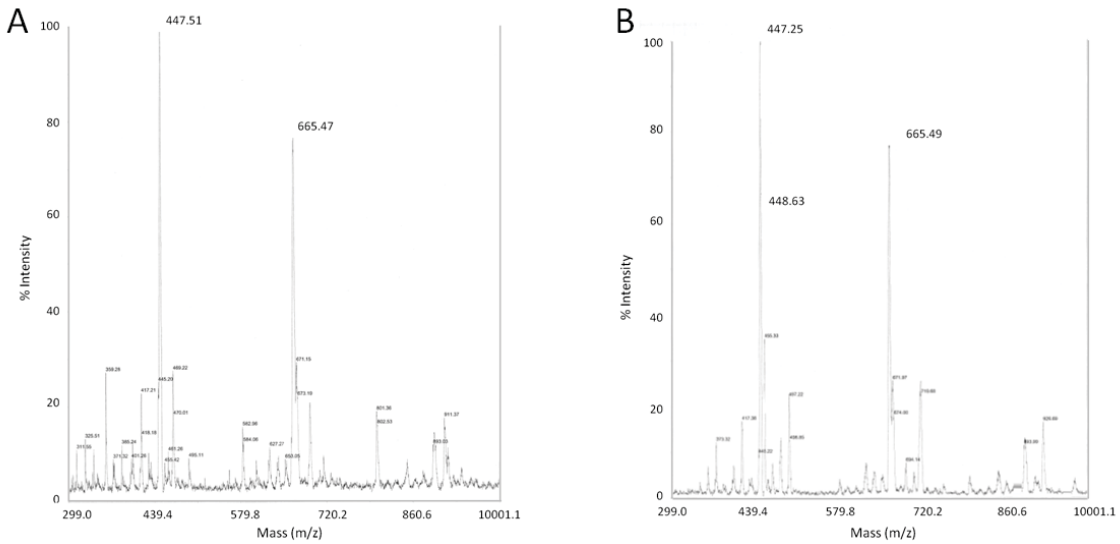

***Figure 8**: Mass spectra of (A) freshly prepared DMPG or (B) DMPG at the end of the DSC scans. The mass at 666 g.mol^{-1} represents DMPG without the sodium cation and the one at 447 g.mol^{-1} represents the matrix (sinapinic acid).*

The two mass spectra are similar and do not show a major product other than DMPG or the matrix. The lipid sample is not decomposed and the shift observed in the calorimetric profile is only due to variations in the lipid phase transition.

Additional solid-state NMR spectra and their description are presented thereafter (Figure 9-14).

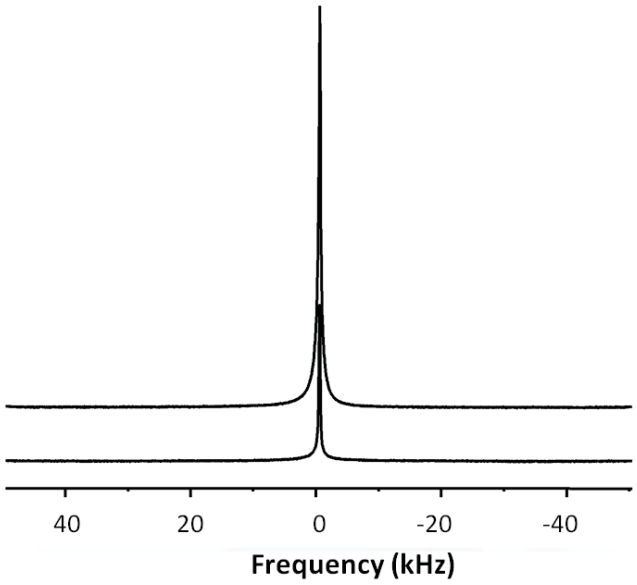

***Figure 9**: ^{2}H-NMR spectra of DMPG at high lipid content and high ionic strength. 290 mM DMPG/d_{54}-DMPG (3:1, mol/mol) was dispersed in high ionic strength buffer (100 mM NaCl, 10 mM HEPEs, pH 7.4). The ^{2}H-NMR spectra of the fresh sample are shown in Figure 3A. At the end of the measurements at high temperature, the sample was transparent and fluid. Figure 9 shows the spectra of the same sample recorded 6 weeks later.*
Temperature from bottom to top: 25 and 45°C.

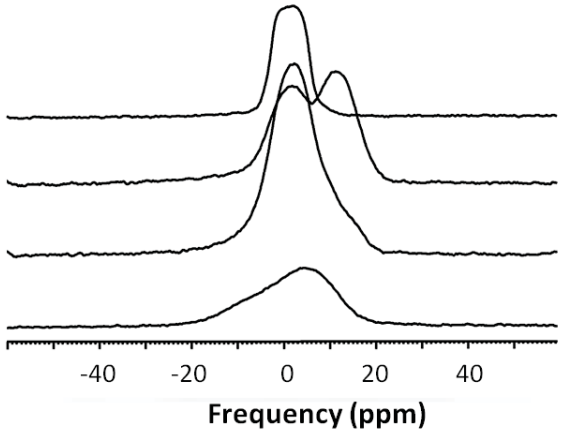

***Figure 10**: ^{31}P-NMR spectra of DMPG at low lipid content and low ionic strength. 50 mM DMPG/d_{54}-DMPG (3:1, mol/mol) was dispersed in low ionic strength buffer (2 mM NaCl, 10 mM HEPEs, pH 7.4).*
Temperature from bottom to top: 21, 30, 40, 55°C.

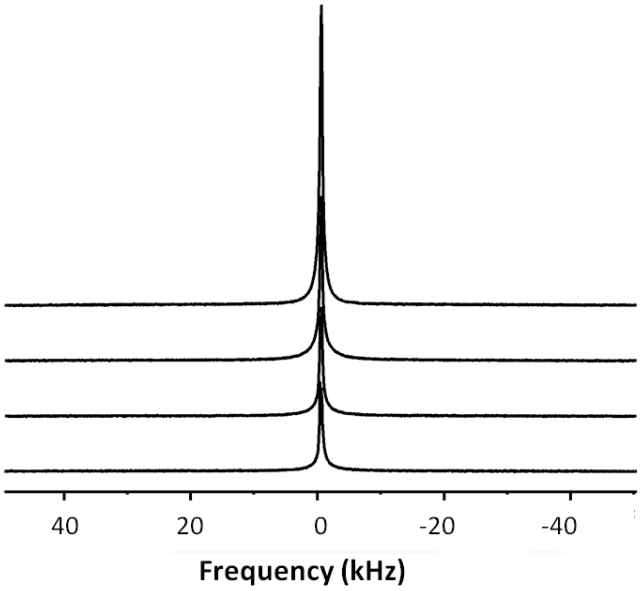

***Figure 11**: ^{2}H-NMR spectra of DMPG at low lipid content and low ionic strength. 50 mM DMPG/d_{54}-DMPG (3:1, mol/mol) was dispersed in low ionic strength buffer (2 mM NaCl, 10 mM HEPEs, pH 7.4). The ^{2}H-NMR spectra of the fresh sample are shown in Figure 5D. At the end of the measurements at high temperature, the sample was transparent and fluid. Figure 11 shows the spectra measured from this transparent and fluid sample.*
Temperature from bottom to top: 10, 20, 30 and 40°C.

If the sample is kept at high temperature in the probe head, the isotropic phase can be reached as well but the line is less sharp. Figure 12-14 show examples at high lipid content and low ionic strength (Figure 12 and 13), and at low lipid content and high ionic strength (Figure 14).

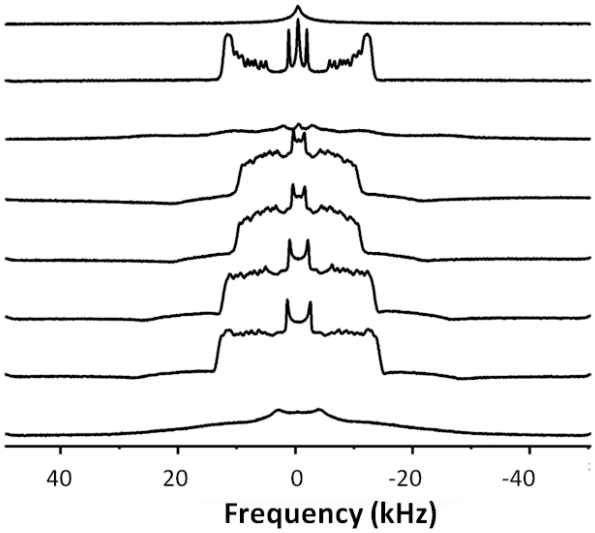

***Figure 12**: ^{2}H-NMR spectra of DMPG at high lipid content and low ionic strength. 290 mM DMPG/d_{54}-DMPG (3:1, mol/mol) was dispersed in low ionic strength buffer (2 mM NaCl, 10 mM HEPEs, pH 7.4).*
Temperature from bottom to top: 20, 25, 30, 50, 55, 25, 56, sample let at 55°C and measured after 12 h at 25°C. The sample remains in the probe head during this whole series of measurements.

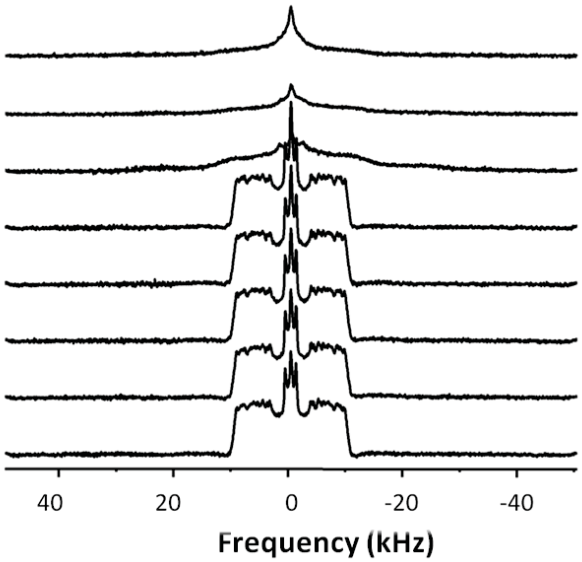

***Figure 13**: ^{2}H-NMR spectra of DMPG at high lipid content and low ionic strength. 290 mM DMPG/d_{54}-DMPG (3:1, mol/mol) was dispersed in low ionic strength buffer (2 mM NaCl, 10 mM HEPEs, pH 7.4).*
Temperature from bottom to top: 60, 60, 60, 60, 60, 25, 25 and 25°C. The sample remains in the probe head during this whole series of measurements.

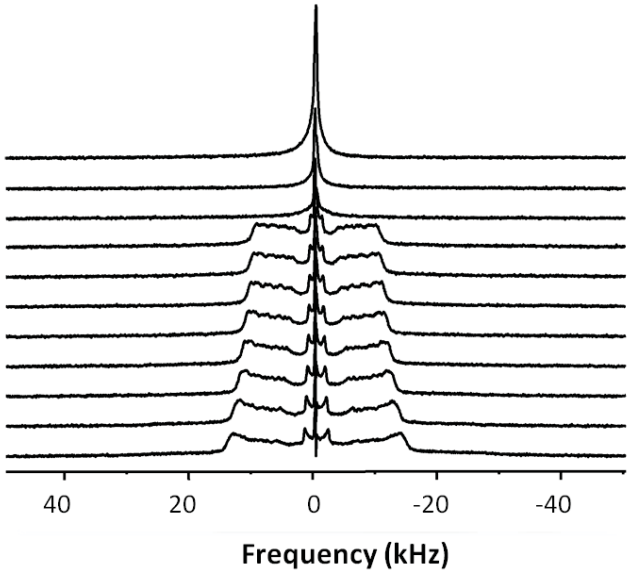

***Figure 14**: ^{2}H-NMR spectra of DMPG at low lipid content and high ionic strength. 50 mM DMPG/d_{54}-DMPG (3:1, mol/mol) was dispersed in high ionic strength buffer (100 mM NaCl, 10 mM HEPEs, pH 7.4).*
Temperature from bottom to top: 21, 25, 30, 35, 40, 45, 50, 55, 19, 17, and 25°C.The sample remains in the probe head during this whole series of measurements.

XII. Summary

The aim of this work was to characterize the structural modifications of model β-amyloid peptides and the lipid membrane upon binding. The first step of this thesis was to reproduce the random-coil to β-sheet structural transition of βAP(25-35). It appeared that additional energy, brought by stirring or heating, acts as a catalyst of the structural transition. Also the presence of inhomogeneous aggregates of βAP(25-35) in the solution influences the CD spectra and thereby the analysis of the peptide secondary structure. This work points out the experimental factors that can strongly influence βAP(25-35) secondary structure and make biophysical studies difficult. In this study, an α-helical intermediate was observed for the first time in the random-coil to β-sheet transition of βAP(25-35).

βAP(25-35) has no chromophore and the quantification of the peptide content was difficult, in particular under conditions of aggregation. Amyloid model peptides were therefore synthesized. The insertion of Trp either at position 24 or 32 of βAP(25-35) resulted in two analog peptides, WβAP(25-35) and βAP(25-35)_I32W. They form aggregates in aqueous buffers at micromolar peptide concentrations, similar to βAP(25-35). HFIP pretreatment homogenizes WβAP(25-35) solutions at physiological and acidic pH values. The aggregates of βAP(25-35)_I32W are small and no effect of HFIP pretreatment was observed. Aggregates with sizes ranging from 60 to 600 nm are measured with dynamic light scattering for the three pretreated peptides. Nevertheless fibril formation of the two analogs could not be observed with Thioflavin T fluorescence, in contrast to βAP(25-35). The presence of Trp in WβAP(25-35) and βAP(25-35)_I32W seems to hinder the binding of the fluorescent dye. Our work opens

new possibilities in the design of amyloid model peptides that can facilitate structural and thermodynamic studies.

CD spectroscopy showed that the presence and position of Trp influences the secondary structure of the free and the lipid-bound amyloid model peptides. The lipid membrane favors the random-coil structure of βAP(25-35) and WβAP(25-35) at low peptide concentration. This shows the dual role of the membrane which can enhance β-sheet content in the peptide structure at higher peptide concentrations. Thermodynamic parameters of the peptide-to-lipid binding could be determined at pH 4.0. In addition, we demonstrated with solid-state NMR that the insertion of the amyloid model peptides into the lipid membrane influences the fluidity of the lipid acyl chains. In contrast, the association of aggregated amyloid model peptides from the aqueous phase with the lipid membrane leads to the formation of an isotropic phase. This phenomenon is reported here for the first time and might be correlated with the toxicity of the amyloid peptide on the neuronal cells.

The NMR study of DMPG at high lipid content proved that DMPG is in a bilayer state at low and high salt content. At high ionic strength, the phase transition occurs at 24°C. At low ionic strength, two distinct bilayer phases are observed on the NMR spectra; they are characterized by a broad phase transition between 20 and 24°C. The results obtained at low lipid content and high ionic strength are similar to those at high lipid content: bilayer features are observed on the whole temperature range and the gel-to-liquid-crystal transition occurs at 23°C, as proved with DSC and NMR data. At low lipid content and low ionic strength, bilayer characteristics are also observed on the whole temperature range in the ^{2}H-NMR spectra. In contrast, during the phase transition, an isotropic line is observed in the ^{31}P-NMR spectra. Spectral fitting indicated that at low ionic strength, the phase transition is characterized by enhanced motions of the acyl chains and a change in the orientation of the phosphoglycerol headgroup. In addition, we observed thixotropy in all samples upon prolonged heating, independently of the lipid or salt content.

XIII. Acknowledgments

This work was carried out from November 2007 until April 2011 in the laboratory of Prof. Dr. Joachim Seelig in the Department of Biophysical Chemistry at the Biozentrum of Basel University.

In a first place, I wish to thank my supervisor Prof. Dr Joachim Seelig, as main contributor of my work. The time spent in his research group was a fabulous opportunity to broaden my knowledge in biophysics and lipid science. His great experience and knowledge in this field was of great value to me.

I would also like to acknowledge the work of Prof. Dagmar Klostermeier as a referee of this thesis and thank her for reading and evaluating this thesis.

Many lab colleagues guided me during my PhD work and shared their acquired knowledge. Their valuable advice enabled me to solve problems and incited me to question my work. Gabriela Klocek, André Ziegler and Andreas Beck, thank you for this.

I also want to thank Matthias Meier for introducing me to solid-state NMR and Mathias Zwick for his help on microscopic imaging.

My other labmates contributed to transforming the working hours in an extremely enjoyable time. I want to thank especially Päivi Äanisma and Samantha Perspicace. Our lunches together were full of laughs and interesting exchanges that made my days in the Biozentrum very pleasant. Additional thanks go to Therese Schulthess for her company, technical help and availability in uncountable occasions. A special thank to Michael Hayley with made the first one year and a half very lively and cheerful.

I am grateful to my other present and former lab colleagues for the pleasant working atmosphere: Susanna Notz, Andreas Bruns, Estefania Egido de Frutos, Cinzia Esposito, Sarah Güthe, Götz Kohler, Xiao-Chun Li-Blatter, Christine Magg, Koji Mochizuki, Christian Müller, Rita Müller, Reto Sauder, Fabian Zehender, and Andreas Zumbühl. Special thanks to the colleagues of “the other side of the floor”.

I am indebted to Leo Faletti and Simon Saner who solved numerous technical problems.

Je tiens à remercier tout particulièrement mes parents, Géraldine, Hervé, Arthur et Charlotte. Votre soutien sans faille, vos conseils, vos encouragements et votre amour m’ont bien souvent donné le courage de me surpasser. Les moments passés ensemble ont été un excellent remède contre mes chutes de moral et mes doutes. Cette thèse n’aurait pas vu le jour sans vous. Merci de tout coeur.

Manuel, du warst immer da, genau wenn ich dich gebraucht habe. Ich danke dir dafür.

XVI. Curriculum Vitae

Caroline Loew born October 5th, 1983 in Mulhouse, France

Education

11/2007-04/2011 **PhD thesis** in Biophysics, Biozentrum Basel, Switzerland
Biophysical Chemistry , Prof. Dr. Joachim Seelig
The interaction of β-amyloid model peptides with lipid membranes

02/2007-07/2007 **M. Sc thesis** in Chemistry and Physical-Chemistry
Laboratoires de Recherches Servier, Croissy-sur-Seine, France
Biophysical and biochemical characterization of autotaxin and its interaction with some of its substrates and inhibitors

09/2005-06/2007 **M. Sc and engineering studies** in Chemistry and Physical-Chemistry
Ecole Nationale Supérieure de Chimie de Paris, France

09/2004-06/2005 **Erasmus student** in Chemistry and Physical-Chemistry
Imperial College of London, United Kingdom

09/2002-06/2004 **Bachelor studies** in Science and Technologies
Université Louis Pasteur de Strasbourg, France

Publications

Thermal Phase Behavior of DMPG Bilayers in Aqueous Dispersions as revealed by ^{2}H- and ^{31}P- NMR, C. Loew, K. Riske, M.T. Lamy, J. Seelig, *Langmuir*, accepted for publication

Comprehensive Kinetic Screening of Palladium Catalysts for Heck Reactions, D.G. Blackmond, T. Schultz, J.S. Mathew, C. Loew, T. Rosner, A. Pfaltz, *Synlett Letter,* **2006,** *1*, pp 1-5

Near-UV molar absorptivities of acetone, alachlor, metolachlor, diazinon and dichlorvos in aqueous solution, V. Feigenbrugel, C. Loew, S. Le Calvé, P. Mirabel, *Journal of Photochemistry and Photobiology A:Chemistry*, **2005**, *174*, pp 76-81